Neuroglial Coupling and the Cerebral Metabolism of Monocarboxylates as Detected by ^{13}C Nuclear Magnetic Resonance

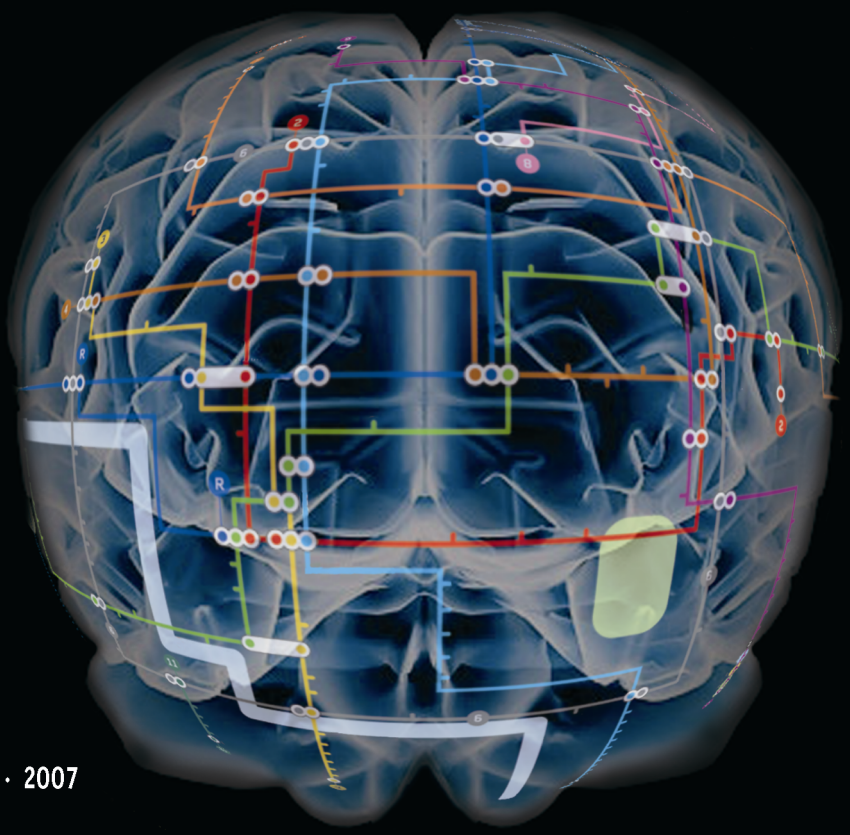

TIAGO
BRANDÃO
RODRIGUES

UNIVERSIDADE DE COIMBRA · 2007

Neuroglial Coupling and the Cerebral Metabolism of Monocarboxylates as Detected by ^{13}C Nuclear Magnetic Resonance

Tiago Brandão Rodrigues

2007

The studies presented in this thesis were carried out at the Institute of Biomedical Research "Alberto Sols", Higher Council for Scientific Research/Autonomous University of Madrid, Madrid, Spain and the Department of Biochemistry, the NMR Center and the Center for Neuroscience and Cell Biology, Faculty of Sciences and Technology, University of Coimbra, Coimbra, Portugal. This thesis was supported in part by a fellowship from the Foundation for Science and Technology, Portugal.

Print and Bound Version:

Cover design: Javier Pérez

With special thanks to: Inês Violante, Javier Pérez, Ricardo Uña

Printed by: *p. g. m.*, Madrid, Spain

ISBN: 978-989-95492-0-3

CD-ROM Version:

Cover design: Javier Pérez

ISBN: 978-989-95492-1-0

Universidade de Coimbra
Faculdade de Ciências e Tecnologia
Departamento de Bioquímica

Neuroglial Coupling and the Cerebral Metabolism of Monocarboxylates as Detected by ^{13}C Nuclear Magnetic Resonance

Dissertation presented to obtain a Ph.D. degree in Biochemistry, speciality in Molecular Biophysics, at the Departament of Biochemistry, Faculty of Sciences and Technology, University of Coimbra

Dissertação apresentada para prestação de provas de Doutoramento em Bioquímica, especialidade de Biofísica Molecular, no Departamento de Bioquímica, Faculdade de Ciências e Tecnologia, Universidade de Coimbra

Tiago Brandão Rodrigues

2007

Supervised by:
Sebástián Cerdán, Ph.D.
Carlos F.C.G. Geraldes, D.Phil.

Para os meus queridos avós

Para os meus pais, sempre presentes

Para a minha Patrícia

"Creio que foi o sorriso,
o sorriso foi quem abriu a porta."

Eugénio de Andrade, *in* "O Sorriso"
do livro "O Outro Nome da Terra" (1988)

Contents

Abbreviations

AAC	ATP translocators
AAT	Aspartate aminotransferase (EC 2.6.1.1)
Ac	Acetate
AcCoA	Acetyl coenzyme A
ADP	Adenosine diphosphate
AGC	Aspartate/glutamate exchanger
ANLS	Astrocyte to neuron lactate shuttle
Asp	Aspartate
ATP	Adenosine triphosphate
ATT	Alanine aminotransferase (EC 2.6.1.2)
BBB	Blood brain barrier
BCA	Bicinchoninic acid
BSA	Bovine serum albumin
(^{13}C)	refers to labeling with ^{13}C in any position of a specified metabolite
(^{14}C)	refers to labeling with ^{14}C in any position of a specified metabolite
CAC	Carnitine carrier
Cho	Choline
CIC	Citrate/malate exchanger
CL	Citrate lyase (EC 4.1.3.6)
CMR_{glc}	Cerebral metabolic rate of glucose
CNS	Central nervous system
CoA	Coenzyme A
CPD	Composite pulse decoupling
Cr	Creatine
CS	Citrate synthase (EC 2.3.3.1)
DAPI	4'-6-diaminodino-2-phenylindol

DIC	Dicarboxylate exchanger
DMEM	Dulbecco's modified Eagle's medium;
D_1R	Dopamine D_1 receptor
D_2R	Dopamine D_2 receptor
EC	Enzyme commission number
(^{18}F)	refers to labeling with ^{18}F in any position of a specified metabolite
FAD	Flavin adenine dinucleotide, oxidized form
$FADH_2$	Flavin adenine dinucleotide, reduced form
FBS	Fetal bovine serum
FDG	(^{18}F)-2-deoxyglucose
FFA	Free fatty acids
fMRI	Functional magnetic resonance imaging
GABA	γ-aminobutyric acid
GAPDH	Glyceraldehyde 3-phosphate dehydrogenase (EC 1.2.1.12)
GDP	Guanosine diphosphate
GFAP	Glial fibrillary acidic protein
Glc (or GLC)	Glucose
Gln (or GLN)	Glutamine
GlnC4d	Doublet resonances of cerebral glutamine C4
Glu (or GLU)	Glutamate
GluC4d	Doublet resonances of cerebral glutamate C4
GLUT	Glucose transporter
Glx	Glutamine and/or glutamate
GS	Glutamine synthetase (EC 6.3.1.2)
GTP	Guanosine triphosphate
(^{2}H)	refers to labeling with ^{2}H in any position of a specified metabolite
HEPES	N-[2-hydroxyethyl]piperazine-N'-[2-ethanesulfonic acid]
HS	Horse serum

IDH	Isocitrate dehydrogenase (EC 1.1.1.42)
IgG	Immuno gamma globulin
Ino (or mI)	*Myo*-inositol
J	Homonuclear or heteronuclear scalar coupling constant
α-KG	α-ketoglutarate
KHB	Krebs-Henseleit buffer
K_i	Inhibition constant
K_m	Michaelis-Menten constant
Lac (or LAC)	Lactate
LDH	Lactate dehydrogenase (EC 1.1.1.27)
L-DOPA	3,4-dihidroxyphenyl-l-alanine
Mal	Malate
MCF	Mitochondrial carrier family proteins
MCT	Monocarboxylate transporter
MDH	Malate dehydrogenase (EC 1.1.1.37)
ME	Malic enzyme (EC 1.1.1.40)
mI (or Ino)	*Myo*-inositol
mRNA	Messenger ribonucleic acid
MSO	Methionine sulfoximine
NAA	N-acetyl aspartic acid
NAD^+	Nicotinamide adenine dinucleotide, oxidized form
NADH	Nicotinamide adenine dinucleotide, reduced form
$NADP^+$	Nicotinamide adenine dinucleotide phosphate, oxidized form
NADPH	Nicotinamide adenine dinucleotide phosphate, reduced form
NMR	Nuclear magnetic resonance
NTP	Nucleotide triphosphate
(^{15}O)	refers to labeling with ^{15}O in any position of a specified metabolite
OAA	Oxaloacetate

OGC	α-ketoglutarate-malate exchanger
ORC	Ornithine carrier
PB	Phosphate buffer
PBS	Phosphate buffered saline
PC	Pyruvate carboxylase (EC 6.4.1.1)
PCr	Phosphocreatine
PDE	Phosphodiesters
PDHC	Pyruvate dehydrogenase complex (EC 1.2.4.1)
PEP	Phosphoenolpyruvate
PET	Positron emission tomography
Pg	Cytosolic pyruvate pool originated from glucose
PGK	Phosphoglycerate kinase (EC 2.7.2.3)
P_i	Inorganic phosphate
PiC	Phosphate exchanger
PME	Phosphomonoesters
Pp	Cytosolic pyruvate pool originated from extracellular pyruvate or lactate
ppm (or PPM)	Parts per million
PyC	Pyruvate carrier
Pyr (or PYR)	Pyruvate
RSA	Radioactive specific activities
SD	Standard deviation
SEM	Standard error of the mean
SLC	Solute carrier protein coding genes
TCA	Tricarboxylic acid cycle
TCAg	Glial tricarboxylic acid cycle
TCAn	Neuronal tricarboxylic acid cycle
TFA	Trifluoroacetic acid
TSP	2, 2´, 3, 3´-tetradeutero trimethylsilyl propionate sodium salt

UCP	Mitochondrial uncoupling proteins
$\mathbf{V}_{cycle}$	Glutamine cycle flux
$\mathbf{V}_{max}$	Maximum reaction rate
vol	Volume
$\mathbf{V}_{TCAg}$	Astroglial tricarboxylic acid cycle flux
$\mathbf{V}_{TCAn}$	Neuronal tricarboxylic acid cycle flux
$\mathbf{V}_{x}$	Global α-ketoglutarate/glutamate exchange
WB	Wide bore
WT	Wild type
Δ_1	Geminal isotopic shift
Δ_2	Two bonds vicinal isotopic shift
Δ_3	Three bonds vicinal isotopic shift

Summary

Strict coupling of energy metabolism and neurotransmission with cellular function and cerebral regionalization is mandatory for an adequate operation of the Central Nervous System. Despite decades of work, the classical neurochemical approaches proved limited in unravelling the coupling mechanisms involved in these complex interactions. The combination of several frontier methodologies, including imaging and spectroscopy by Magnetic Resonance methods, is currently contemplated as a more powerful alternative.

Intra- and intercellular pyruvate and lactate metabolisms play an important role in the metabolic coupling of neurons and glial cells. However, the directionality of intra- and intercellular monocarboxylate exchange, the role of neuronal and glial redox states and monocarboxylate compartmentation and the relationship of these variables with neurotransmission, remain crucial and insufficiently understood aspects. In this thesis, I address the cerebral metabolism of pyruvate and lactate, its intra- and extracellular compartmentation, its relationship to the neuronal and glial tricarboxylic acid cycles of neurons and glial cells, and how all these processes are integrated *in vivo* and *in vitro* into a functionally operating unit during glutamatergic neurotransmission. To this end I combined the classical neurochemical approach, including conventional biochemical assays, with more recent developments such as ^{13}C and (^{13}C,^{2}H) Nuclear Magnetic Resonance (NMR) techniques. I emphasize how these novel approaches have modified the earlier interpretations of neuroglial coupling during glutamatergic neurotransmission.

In **chapter 1,** I begin with a general description of brain energy metabolism, including the main pathways of cerebral energetics and the experimental approaches used for these studies. I review the vital roles of pyruvate and lactate in the neuronal and glial cells, providing an updated revision of the cerebral energetics, integrating previous proposals. I address in more detail NMR Spectroscopy methods, in order to allow later a better understanding and discussion of the results presented. On these grounds, I show that modern NMR methods acquire vital importance for the understanding of the neuroglial coupling during glutamatergic, GABAergic or even serotoninergic neurotransmissions.

Chapters 2 and 3 present new methodologies to investigate lactate recycling between extracellular space and the cytosolic pool of pyruvate through the monocarboxylate transporters of the plasma membrane and the lactate dehydrogenase isozymes of C6 glioma cells. In chapter 2, two novel ^{1}H NMR approaches are presented to characterize the recycling process, one of them based in a specific lactate editing sequence. In chapter 3, a novel (^{13}C,^{2}H) NMR approach was also formulated to address alternatively this question. In these experiments, C6 glioma cells were incubated in Krebs-Henseleit buffer containing 50% $^{2}H_2O$ and (3-^{13}C) lactate. Samples of

incubation medium were collected at different time points and analyzed by ^{13}C NMR to determine the kinetics of deuteration of (3-^{13}C) lactate. The use of ^{13}C NMR spectroscopy to detect deuteration in the ^{13}C labeled precursor proved to be a powerful technique to study hydrogen turnover, providing complementary information to the traditional ^{13}C NMR methods routinely used to investigate carbon turnover. Additionally, several experiments were done with different mixtures of labeled substrates, demonstrating that the deuteration process that allows the study of this lactate recycling is redox sensitive and that glycolysis is a redox controlled process.

Chapter 4 presents our novel hypothesis describing the metabolic coupling between neuronal and glial cells in the brain during neurotransmission. The results obtained in the previous chapters provide the basis to this new theory, including the presence of subcellular compartmentation of pyruvate and monocarboxylate recycling through the plasma membrane of both neurons and glial cells. We describe the mechanisms underlying this Redox Switch/Redox Coupling hypothesis, as well as its kinetic properties, in primary cultures of cortical neurons and astrocytes from rat brain. With these results we delineated a revised interpretation of the mechanisms underlying metabolic coupling, compatible also with the subcellular compartmentation of monocarboxylates and glutamate, as well as with the redox switch and monocarboxylate recycling through the plasma membrane. The proposed redox shuttles may couple the activity of glycolytic and oxidative environments, providing a general mechanism of intra- and intercellular coupling supporting universally metabolic heterogeneity in cells.

Gene targeting technology has become recently a valuable tool for the understanding of some specific neurodegenerative diseases and Magnetic Resonance Spectroscopy is a very appropriate technique to characterize these transgenic mice models. **Chapter 5** combines ^{13}C NMR spectroscopy and gene targeting techniques to investigate glutamatergic neurotransmission and glutamate-glutamine cycle in brain extracts of D_1 or D_2 dopamine receptors deficient mice. We complemented our experimental design using a pharmacological approach based on reserpine, a dopamine depleting drug, and also on L-DOPA, the basis of the clinical antiparkinsonian treatment. Additional behavioural and c-Fos expression tests were used to investigate in more detail the dopamine receptor subtype that mediates the communication between both neurotransmission systems. Together, our results indicate that the lack of dopamine or D_1 dopamine receptors, but not D_2 receptors, results in increased glutamatergic activity. Our data reveal that the D_1 dopamine receptor subtype is the main mediator of the metabolic interactions between glutamatergic and dopaminergic neurotransmissions.

Resumo

O adequado funcionamento do Sistema Nervoso Central requer uma integração precisa do metabolismo energético e da neurotransmissão entre os diversos tipos celulares involvidos, assim como a sua distribuição precisa entre as diferentes regiões cerebrais. Apesar de décadas de trabalho, os métodos da neuroquímica clássica provaram ser muito limitadas na clarificação dos mecanismos de acoplamento envolvidos nestas complexas interacções. A combinação de várias metodologias, incluindo métodos de imagem e de espectroscopia por Ressonância Magnética, contempla-se mais recentemente como uma alternativa mais robusta.

O metabolismo do piruvato e do lactato intra- e extracelular tem um papel importante no acoplamento metabólico de neurónios e células gliais. No entanto, a direccionalidade dos intercâmbios intra- e intercelular de monocarboxilatos, o papel dos estados redox neuronais e gliais e a compartimentação intracelular dos monocarboxilatos, assim como a relação destas variáveis com a neurotransmissão continuam ainda a ser aspectos insuficientemente compreendidos. Nesta tese, pretende-se avaliar o metabolismo do piruvato e do lactato, a sua compartimentação intra- e extracelular, a sua relação aos ciclos dos ácidos tricarboxílicos neuronais e gliais, bem como a interligação desta rede de processos numa unidade funcional durante a neurotransmissão glutamatérgica, tanto *in vivo* como *in vivo*. Com vista a alcançar este objectivo, combinam-se abordagens da neuroquímica clássica, como os ensaios enzimáticos convencionais, com os mais recentes avanços tecnológicos, como sejam as técnicas de Ressonância Magnética Nuclear (RMN) de ^{13}C e de (^{13}C,^{2}H). Neste trabalho destaca-se como estas novas abordagens modificam as interpretações tradicionais do acoplamento neuroglial durante a neurotransmissão glutamatérgica.

No **capítulo 1,** inicia-se com uma descrição geral do metabolismo energético cerebral, descrevendo as principais vias metabólicas da energética cerebral e as abordagens experimentais utilizadas nestes estudos. Em concreto, resumem-se os papéis fundamentais do piruvato e do lactato nas células neuronais e gliais, apresentando-se uma actualizada revisão do funcionamento da energética cerebral, integrando as propostas apresentadas anteriormente. Foi dado especial ênfase na explicação da Espectroscopia por RMN, com o objectivo de possibilitar ao leitor uma adequada compreensão e discussão dos resultados apresentados. Neste contexto, os métodos modernos de RMN adquirem uma importância fulcral para a compreensão do acoplamento neuroglial durante as neurotransmissões glutamatérgica, GABAérgica, e mesmo serotoninérgica.

Os **capítulos 2 e 3** apresentam novas metodologias para estudar a reciclagem de monocarboxilatos entre o espaço extracelular e o citosólico, através dos transportadores de monocarboxilatos da membrana plasmática e da lactato desidrogenase de células de glioma C6. O capítulo 2 descreve duas novas abordagens de RMN de ^{1}H para caracterizar este processo de reciclagem, sendo uma

delas baseada numa sequência específica de edição de RMN de ^{1}H para lactato. Por outro lado, no capítulo 3 desenvolveu-se também uma nova técnica de RMN de (^{13}C,^{2}H), com o intuito de resolver, de forma alternativa, esta questão. Para este fim, incubaram-se células de glioma C6 em tampão Krebs-Henseleit, contendo 50% $^{2}H_2O$ e (3-^{13}C) lactato. Recolheram-se, a diferentes tempos de incubação, amostras do meio, analisando-se por RMN de ^{13}C, com o objectivo de determinar a cinética de deuteração de (3-^{13}C) lactato. A utilização da Espectroscopia de RMN de ^{13}C para detectar deuteração nos precursores marcados com ^{13}C demonstrou ser uma técnica muito robusta para o estudo dos intercâmbios de hidrogénio, fornecendo informação complementar à RMN de ^{13}C tradicional, utilizada de forma rotineira para elucidar os intercâmbios de carbono. Adicionalmente, várias experiências foram realizadas com diferentes combinações de compostos marcados, demonstrando-se que o processo de deuteração que permite o estudo da reciclagem de lactato é sensível às condições redox, e que a glicólise é também um processo modulado pelo estado redox.

O **capítulo 4** inclui a nossa nova hipótese de acoplamento metabólico entre as células neuronais e gliais no cérebro. Os resultados obtidos nos capítulos prévios proporcionam a base para esta nova interpretação, que inclui a presença da compartimentação sub-celular do piruvato e da reciclagem de monocarboxilatos através da membrana plasmática, tanto de neurónios como de células gliais. Descrevem-se também os mecanismos que estão na base da hipótese Interruptor Redox/Acoplamento Redox, assim como as suas propriedades cinéticas, em culturas primárias de neurónios corticais e de astrócitos de cérebro de rato. Com estes resultados, pudemos construir uma interpretação revista do acoplamento metabólico, sendo compatível com a compartimentação sub-celular de piruvato, lactato e glutamato, com o interruptor redox e com a reciclagem de monocarboxilatos através da membrana plasmática. Por fim, os *shuttles* redox propostos podem acoplar a actividade dos ambientes oxidativos e glicolíticos, fornecendo um mecanismo geral para o acoplamento intra- e intercelular que sustentam a heterogeneidade metabólica nas células.

A tecnologia associada à manipulação de genes tem-se tornado recentemente uma valiosa ferramenta para a compreensão de algumas doenças neurodegenerativas específicas, sendo a Espectroscopia por RMN uma das técnicas mais apropriadas para a caracterização fenotípica destes modelos de ratos transgénicos. O **capítulo 5** combina a Espectroscopia por RMN de ^{13}C e as técnicas associadas à manipulação de genes para investigar a neurotransmissão glutamatérgica e o ciclo glutamina-glutamato, em extractos cerebrais de ratos deficientes nos receptores dopamina D_1 ou D_2. Complementamos o nosso protocolo experimental usando uma abordagem farmacológica baseada na administração de reserpina, um fármaco que reduz a quantidade disponível de dopamina, e de L-DOPA, que constitui a base de tratamentos clínicos anti-parkinsonianos. Ampliamos a nossa abordagem com testes de comportamento e de expressão de c-Fos adicionais para caracterizar com

maior profundidade o sub-tipo de receptores de dopamina que medeia a comunicação entre ambos sistemas de neurotransmissão. Os nossos resultados indicam que a falta de dopamina ou a ausência de receptores D_1 (mas não de receptores D_2) produz um aumento na actividade glutamatérgica. Estes resultados associam claramente o receptor D_1 da dopamina na regulação das interacções metabólicas entre as neurotrasmissões glutamatérgica e dopaminérgica.

Sumario

El funcionamiento adecuado del Sistema Nervioso Central requiere una integración precisa del metabolismo energético y de la neurotransmisión entre los diversos tipos celulares involucrados, así como su distribución precisa entre las diferentes regiones cerebrales. A pesar del trabajo realizado durante décadas, los métodos de neuroquímica clásica resultan muy limitados en la clarificación de los mecanismos de acoplamiento involucrados en estas complejas interacciones. La combinación de varias metodologías, incluyendo métodos de imagen y de espectroscopia por Resonancia Magnética, se contempla más recientemente como una alternativa más robusta.

El metabolismo del piruvato y del lactato intra- y extracelular adquiere un papel importante en el acoplamiento metabólico de neuronas y de células gliales. Sin embrago, la direccionalidad de los intercambios intra- e intercelular de monocarboxilatos, el papel de los estados redox neuronales y gliales y la compartimentación de los monocarboxilatos, así como la relación de estas variables con la neurotransmisión permanecen aún como aspectos insuficientemente comprendidos. En esta tesis proponemos evaluar el funcionamiento del metabolismo de piruvato y de lactato, su compartimentación intra- y extracelular, su relación con los ciclos de los ácidos tricarboxílicos neuronales y gliales, y entender como se integran todos estos procesos en una unidad funcional durante la neurotransmisión glutamatérgica *in vivo* e *in vitro*. Para alcanzar este objetivo, hemos combinado abordajes de la neuroquímica clásica, como los ensayos enzimáticos convencionales, con los más recientes avances, como son las técnicas de Resonancia Magnética Nuclear (RMN) de ^{13}C y de (^{13}C,^{2}H). En este trabajo, destacamos como estos nuevos abordajes han modificado las interpretaciones tradicionales del acoplamiento neuroglial durante la neurotransmisión glutamatérgica.

En el **capítulo 1**, se presenta una descripción general del metabolismo energético cerebral, describiendo las principales rutas metabólicas de la energética cerebral y las técnicas experimentales utilizadas en estos estudios. En particular, se resúmen las funciones fundamentales del piruvato y del lactato en las células neuronales y gliales, presentándose una revisión actualizada del funcionamiento de la energética cerebral, integrando las propuestas presentadas con anterioridad. Se ha concedido un énfasis especial a la explicación de la Espectroscopia por RMN, con el objetivo de hacer posible al lector una adecuada comprensión y discusión de los resultados presentados. En este contexto, los modernos métodos de RMN adquieren una importancia central para la comprensión del acoplamiento neuroglial durante las neurotransmisiones glutamatérgica, GABAérgica, e incluso serotoninérgica.

Los **capítulos 2 y 3** presentan nuevas metodologías para estudiar el reciclaje de monocarboxilatos entre el espacio extracelular y el citosólico, a través de los transportadores de

monocarboxilatos de la membrana plasmática y de lactato deshidrogenasa en células de glioma C6. El capitulo 2 describe dos nuevos abordajes de RMN de ^{1}H para caracterizar este proceso de reciclaje, uno de ellos basado en una secuencia específica de edición de RMN de ^{1}H para lactato. Por otro lado, en el capítulo 3, desarrolla una nueva técnica de RMN de (^{13}C,^{2}H) con el objetivo de resolver, de forma alternativa, esta cuestión. Con este fin, se incubaron células de glioma C6 en tampón Krebs-Henseleit, conteniendo 50% $^{2}H_2O$ y (3-^{13}C) lactato. A diferentes tiempos de incubación, se recogieron muestras del medio, y se analizaron por RMN de ^{13}C, con objetivo de determinar la cinética de deuteración de (3-^{13}C) lactato. La utilización de la Espectroscopia de RMN de ^{13}C para detectar deuteración en los precursores marcados con ^{13}C ha demostrado ser una técnica muy robusta para el estudio de los intercambios de hidrogeno, proporcionando información complementaria a la RMN de ^{13}C tradicional, que se utiliza de forma rutinaria para dilucidar los intercambios de carbono. Adicionalmente, se realizaron varios experimentos con diferentes combinaciones de compuestos marcados, demostrando que el proceso de deuteración que permite el estudio del reciclaje de lactato es sensible al estado redox, y que la glucólisis es también un proceso modulado por el estado redox.

El **capítulo 4** incluye nuestra nueva hipótesis de acoplamiento metabólico entre las células neuronales y gliales en el cerebro. Los resultados obtenidos en los capítulos previos proporcionan la base para esta nueva interpretación, que incluye la presencia de la compartimentación subcelular de piruvato y del reciclaje de monocarboxilatos a través de la membrana plasmática, tanto de neuronas como de células gliales. Se describen también los mecanismos que constituyen la base de la hipótesis Interruptor Redox/Acoplamiento Redox, así como sus propiedades cinéticas en cultivos primarios de neuronas corticales y de astrocitos de cerebro de rata. Con estos resultados, pudimos construir una interpretación revisada del acoplamiento metabólico neuroglial, compatible con la compartimentación subcelular de piruvato, lactato y glutamato, con el interruptor redox y con el reciclaje de monocarboxilatos a través de la membrana plasmática. Finalmente, las lanzaderas redox propuestas pueden acoplar la actividad de los ambientes oxidativos y glucolíticos, ofreciendo un mecanismo general para el acoplamiento intra- e intercelular que sustenta la heterogeneidad metabólica en las células.

La tecnología asociada a la manipulación de genes se ha convertido recientemente en una valiosa herramienta para la comprensión de algunas enfermedades neurodegenerativas específicas, siendo la Espectroscopia por RMN una de las técnicas más apropiadas para la caracterización fenotípica de estos modelos de ratones transgénicos. El **capítulo 5** combina la Espectroscopia por RMN de ^{13}C y las técnicas asociadas a la manipulación de genes para investigar la neurotransmisión glutamatérgica y el ciclo glutamina-glutamato en extractos cerebrales de ratones con deficiencias en

los receptores dopamina D_1 o D_2. Complementamos nuestro protocolo experimental utilizando un abordaje farmacológico basado en la administración de reserpina, un fármaco que reduce la cantidad disponible de dopamina, y de L-DOPA, que proporciona la base de tratamientos clínicos anti-parkinsonianos. Hemos ampliado este abordaje con estudios de comportamiento y de expresión de c-Fos adicionales para caracterizar con mayor profundidad el subtipo de receptores de dopamina que median la comunicación entre ambos sistemas de neurotransmisión. Nuestros resultados indican que la falta de dopamina o la ausencia de receptores D_1 (pero no de receptores D_2) produce un aumento en la actividad glutamatérgica. Estos resultados asocian claramente el receptor D_1 de la dopamina con la regulación de las interacciones metabólicas entre las neurotransmisiones glutamatérgica e dopaminérgica.

Brain Energy Metabolism

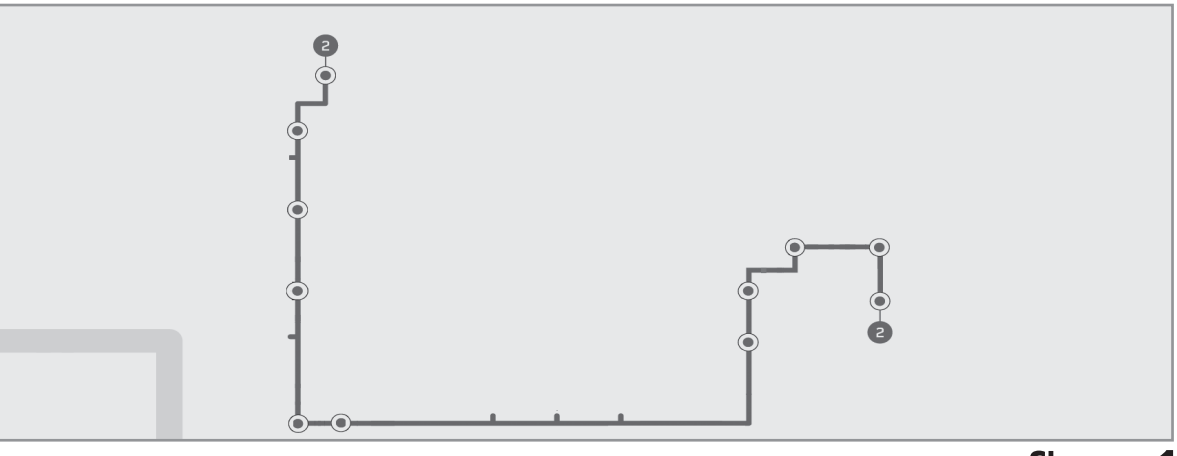

Chapter 1

1. General Introduction

The brain is metabolically the most active organ of the economy. Adequate cerebral physiology depends on the continuous supply of sufficient amounts of glucose and oxygen from the blood. Consequently, limitations in the delivery of these two vital substrates cause most physiopathological responses. Briefly, an adult human brain of 1400 g consumes approximately 55 mg of glucose.min^{-1} and produces 110 mg of pyruvate.min^{-1} approximately. Oxidation of these pyruvate molecules requires ca. 49 mL of O_2.min^{-1}. This indicates that approximately 20% of the total oxygen used by the adult body is consumed by the brain, an organ accounting for only 2% of the total body weight (Nicholls 2007; Okada and Lipton 2007).

Pyruvate plays a pivotal role in the metabolism of Central Nervous System (CNS), linking the anaerobic and aerobic portions of glucose catabolism and providing the carbon skeletons that couple the vital energy exchange between neurons and astrocytes (Denton and Halestrap 1979; Sokoloff 1989; Sokoloff 1992). Pyruvate is known to be an essential nutrient for neural cells in culture and has important neuroprotective actions, contributing also the building blocks for many anabolic activities in the brain (Desagher *et al.* 1997; Izumi *et al.* 1997; Matsumoto *et al.* 1994). Among these functions, pyruvate oxidation entails vital bioenergetic importance for appropriate cerebral performance, having a pronounced influence on the general physiology of the individual (Dienel 2002).

The cerebral metabolism of pyruvate, and that of its precursor glucose, has been reviewed several times. Classical approaches involved the use of radioactive isotopes or optical methods which required the isolation and purification of the enzymes or transport systems involved to investigate their *in vitro* kinetics (Bachelard 1989; Clark and Lai 1989; Siesjo 1982; Sokoloff 1989). This reductionist approach provided fundamental information on the operation of the CNS, despite the limitations brought by the minute amounts of proteins present in neural tissues and by the fact that its use is restricted to cerebral extracts or *post mortem* biopsies.

The impressive development during the past three decades of powerful non-invasive tools for studying the human brain has had a tremendous impact on our ability to investigate and understand brain function. Positron Emission Tomography (PET) with (^{18}F)-2-deoxyglucose (FDG) was the first technique used to investigate *non invasively* cerebral glucose uptake in animals and man with moderate resolution (Wienhard 2002). Similarly, functional Magnetic Resonance Imaging (fMRI) allowed indirectly the investigation of the hemodynamic and blood oxygenation changes associated with sensory or motor stimulation (Heeger and Ress 2002). Despite their importance, FDG uptake or fMRI provide no information on the pathways and metabolic interactions underlying the cerebral activation process, implying that further advances in this field would necessarily rely on

the implementation of additional methods.

From this perspective, genome cloning and sequencing techniques, as well as the development of novel ^{13}C Nuclear Magnetic Resonance (NMR) strategies have overcome many of the limitations of the traditional approaches. In particular, sequencing of the human and mouse genomes has provided a comprehensive view of the different isoforms of enzymes and transporters present in the brain, without the need to isolate and purify the corresponding proteins (Consortium 2001; Consortium 2002). However, the genomic methods do not allow the investigation of the function and *in vivo* performance of the genes sequenced or cloned. In this respect ^{13}C NMR, and more recently (^{13}C,^{2}H) NMR, technologies have become more helpful, providing the quantitative assessment of transport steps, metabolic fluxes and subcellular compartmentation of glycolysis, pyruvate oxidation and tricarboxylic acid (TCA) cycle in a plethora of neural systems ranging from primary cell cultures to the intact rodent or human brain (Cerdán 2003; Gruetter *et al.* 2003; Morris and Bachelard 2003; Shulman *et al.* 2004).

Several recent reviews complement and extend the information presented here (De Meirleir 2002; García-Espinosa *et al.* 2004; Gruetter 2002; Magistretti and Pellerin 1999; Rodrigues and Cerdán 2007; Rothman *et al.* 2003; Schurr 2002).

2. Overview of Pyruvate Metabolism

Figure 1.1 provides a general overview of pyruvate oxidation in the brain and its interactions with other cerebral metabolic pathways. Pyruvate oxidation involves: (i) the transport of glucose or monocarboxylate precursors through the blood brain barrier (BBB) and the plasma membrane of neural cells, (ii) the production of cytosolic pyruvate and reducing equivalents through the glycolytic pathway, (iii) the transport of cytosolic pyruvate and reducing equivalents to the mitochondrial matrix by the carriers of the inner mitochondrial membrane and finally, (iv) the terminal oxidation of pyruvate in the mitochondrial TCA cycle.

Glucose and monocarboxylates are transported through the plasma membrane through the family of glucose and monocarboxylate transporters (Figure 1.1, processes 1 and 2) (Dwyer *et al.* 2002; Halestrap and Meredith 2004; Palmieri 2004). Glycolytic pyruvate production from glucose in the cytosol generates two molecules of NADH and ATP (Dienel 2002) (process 3). Cytosolic pyruvate may then be transaminated to alanine by alanine aminotransferase (ATT, process 4), reduced to lactate by lactate dehydrogenase (LDH, process 5), or transported to the mitochondrial matrix (process 6) and oxidized (processes 7-16) (Denton and Halestrap 1979). Under normoxic

conditions, the mitochondrial respiratory chain is able to reoxidize completely the reducing equivalents (NADH and $FADH_2$) generated in aerobic glycolysis and TCA cycle (process 18). Since the mitochondrial membrane is impermeable to NADH, the transfer of cytosolic reducing equivalents through the inner mitochondrial membrane requires the operation of specific shuttle mechanisms (processes 20-22) (Palmieri 1994; Palmieri *et al.* 1996). Oxygen limitations in hypoxic

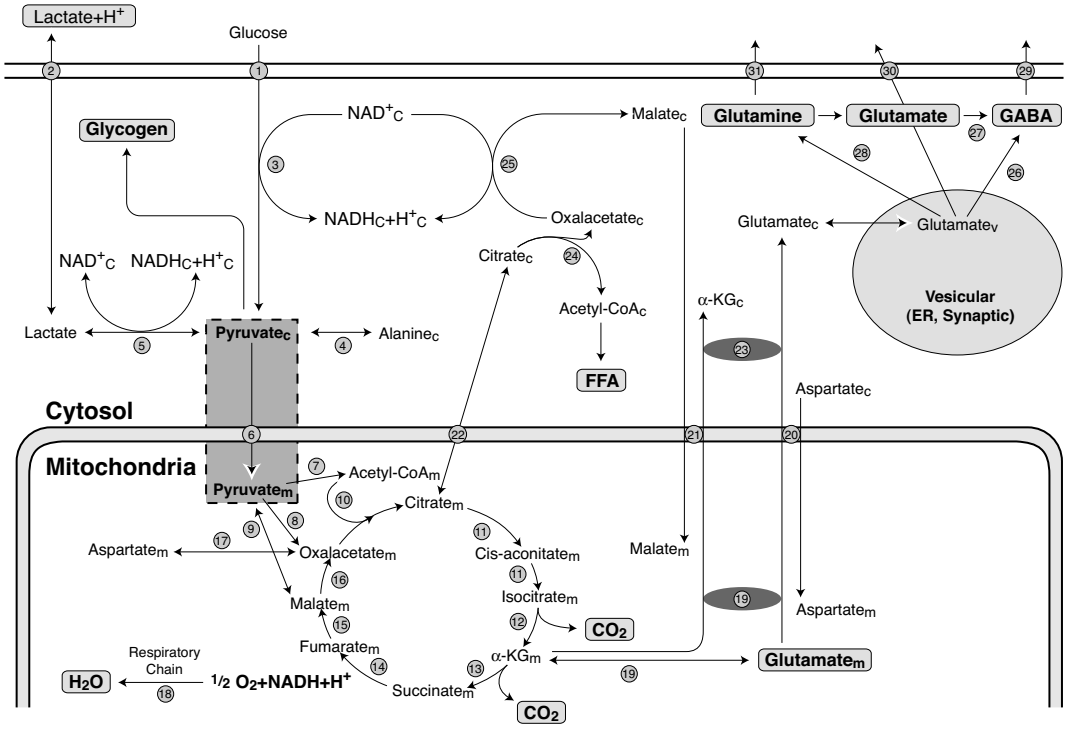

Figure 1.1. Overview of pyruvate oxidation. Intercellular compartmentation is not considered for simplicity. 1: GLUT transporters of the plasma membrane, 2: MCT transporters of the plasma membrane, 3: glycolysis, 4: alanine aminotransferase, 5: lactate dehydrogenase, 6: pyruvate carrier (PyC) of the inner mitochondrial membrane, 7: pyruvate dehydrogenase complex, 8: pyruvate carboxylase, 9: malic enzyme, 10: citrate synthase, 11: aconitase, 12: isocitrate dehydrogenase, 13: α-ketoglutarate dehydrogenase, 14: succinate dehydrogenase, 15: fumarase, 16: malate dehydrogenase, 17: aspartate aminotransferase (mitochondrial), 18: respiratory chain, 19: aspartate aminotransferase + glutamate decarboxylate (mitochondrial), 20: aspartate/glutamate exchanger, 21: α-ketoglutarate/malate exchanger (OGC), 22: tricarboxylate carrier (CIC), 23: aspartate aminotransferase (cytosolic), 24: citrate lyase, 25: malate dehydrogenase (cytosolic), 26: glutamate decarboxylase (vesicular), 27: glutamate decarboxylase (cytosolic), 28: glutamine syntethase, 29: GABA transporters, 30: glutamate transporters, 31: glutamine transporters. Subscripts c, m and v refer to cytosolic, mitochondrial or vesicular (synaptosomal) compartments. FFA: Free Fatty Acids.

or ischemic conditions may preclude the respiratory chain to reoxidize completely the reducing equivalents generated by glycolysis or during TCA cycle activity. This decreases the mitochondrial and cytosolic NAD(P)/NAD(P)H ratio and causes cytosolic pyruvate to be reduced to lactate and extruded (processes 5 and 2) (Bachelard *et al.* 1974). Under these conditions, the oxidative production of ATP is reduced and flux through the glycolytic pathway upregulated, resulting in increased glucose consumption, increased glycerol-3-P levels and increased lactate and alanine productions (Ben-Yoseph *et al.* 1993; Siesjo 1982).

Cerebral pyruvate plays, additionally, other vital roles. Pyruvate is the main precursor for fatty acid synthesis in the CNS (Moore 2001). In this process, intramitochondrial citrate is transported to the cytosol, in exchange for malate (process 22), to produce cytosolic oxalacetate and acetyl-CoA by citrate lyase (process 24) to support fatty acid synthesis (Palmieri 1994; Palmieri 2004). Cytosolic pyruvate can also be produced from mitochondrial TCA cycle intermediates, as malate, through the malic enzyme reaction in the process known as pyruvate recycling (ME, process 9), a NADPH producing pathway thought to support fatty acid synthesis and free-radical scavenging activities of neural cells (Cerdán *et al.* 1990; Cruz *et al.* 1998; Pascual *et al.* 1998). Finally, mitochondrial pyruvate is a crucial precursor for cerebral anaplerosis, helping to replace amino acids and TCA cycle intermediates liberated to the extracellular space during neurotransmission. Anaplerosis involves a net increase in oxalacetate molecules produced through pyruvate carboxylase in astrocytes and, possibly, through the reversal of malic enzyme activity in neurons (process 8 or 9) (Gamberino *et al.* 1997; Hassel 2000). Closely associated to this anaplerotic role, pyruvate (lactate or alanine) may produce glucose and glycogen in astroglial cells, in a similar way to that observed in liver (Dringen *et al.* 1993; Schmoll *et al.* 1995). The following sections address in more detail all these aspects.

3. Transport of Pyruvate and Monocarboxylates Through the Blood Brain Barrier and the Plasma Membrane of Neural Cells

Pyruvate and other monocarboxylates are classically known to pass the BBB through facilitated diffusion (Cremer *et al.* 1979; Crone and Sorensen 1970). Transport of monocarboxylates through the plasma membrane was attributed initially to non ionic diffusion, until it was demonstrated that it could be inhibited by α-cyano-4-hydroxycinamate and organomercurials (Halestrap and Price 1999). This led to the identification of the first member of the family of monocarboxylate-proton cotransporter proteins, MCT1 (Enerson and Drewes 2003). MCTs were shown to operate under near equilibrium conditions, catalyzing the reversible cotransport of the monocarboxylate and one

proton. In the case of pyruvate the following reaction applies,

$$\text{Pyruvate}_{out} + H^{+}_{out} \leftrightarrow \text{Pyruvate}_{in} + H^{+}_{in} \quad [1.1]$$

where the subscripts $_{-in}$ or $_{-out}$ refer to intra- or extracellular concentrations, respectively. A similar reaction can be written for other monocarboxylates including lactate, acetate, acetoacetate, among others. Under near equilibrium conditions the relative concentration of pyruvate molecules in the intra- and extracellular spaces is believed to be dictated by the transmembrane pH gradient,

$$\text{Pyruvate}_{in} / \text{Pyruvate}_{out} = H^{+}_{out} / H^{+}_{in} \quad [1.2]$$

For a physiological pH gradient of 0.1 pH units (acidic inside), the concentration of intracellular monocarboxylates is predicted to be approximately 1.25 times lower than that found in the extracellular space. However, under severe hypoxic or ischemic conditions, when the transmembrane pH gradient may reach one pH unit (alkaline inside), the concentration of intracellular pyruvate or lactate may become one order of magnitude higher than that of the extracellular space. These important changes in monocarboxylate distribution through the plasma membrane reflect the reversibility of MCT transport. Its kinetic parameters are known to be constrained by the Haldane relationship

$$(V_{max}/K_m)_{influx} = (V_{max}/K_m)_{efflux} \quad [1.3]$$

where V_{max} of influx or efflux can be stimulated by either decreasing the pH in the same side of the monocarboxylate or by increasing it in the opposite, respectively (Halestrap and Price 1999).

The MCT proteins are coded by the SCL16 gene family (Halestrap and Meredith 2004). Up to fourteen, relatively homologous, monocarboxylate transporters are coded by this gene family of which only four have been isolated, purified and overexpressed in *Xenopus oocytes*. Although the three dimensional structure of these transmembrane proteins has not been determined, it is possible to infer some of their structural properties, from their resemblance with other receptors. The common topology involves up to twelve transmembrane domains, with both C and N terminus facing the intracellular side. In addition, at least MCT1 and MCT4 (and probably MCT3) require the ancillary protein CD147 for their correct expression in the plasma membrane (Kirk *et al.* 2000). MCT1, MCT2 and MCT4 are heterogeneously expressed in brain (Fayol *et al.* 2004; Rafiki *et al.* 2003). MCT1 is almost ubiquitously expressed, being found in endothelial cells, neurons, astrocytes as well as in glioma cells. Conversely, MCT2 is expressed only in neurons and MCT4 is expressed in the endothelial or glial cells (Mac and Nalecz 2003).

The pattern of expression and the kinetic properties of these transporters support the classical model of vectorial trafficking of monocarboxylates between neurons and astrocytes (Pellerin *et al.*

1998b). The low affinity of astrocytic MCT4 favours lactate extrusion from astrocytes, a situation similar to that found in highly glycolytic tissues such as the white muscle fibers. In contrast, the lower affinity of neuronal MCT2 favours lactate uptake, as found primarily in oxidative tissues as heart and the red muscle fibers (Brooks 2002). Thus, heterogeneous distribution of MCT with different kinetic properties supports astrocytic lactate production and neuronal lactate consumption (Pellerin *et al.* 1998a) (explained with more detail later).

MCT experience important changes in the expression of the different isoforms during ontogenic development (Leino *et al.* 1999; Vannucci and Simpson 2003). Neuronal MCT2 is expressed in most brain areas including hippocampus and cerebellum, being most abundant during the first three weeks after birth and decreasing progressively later. This pattern appears to be complementary to that of the glucose transporters GLUT1, endothelial, and GLUT3, neuronal (Vannucci *et al.* 1997). Both GLUT1 and GLUT3 increase progressively after birth, while MCT2 decreases. In contrast, MCT4 expression is low at birth and increases progressively through development. The temporal pattern of expression of MCTs and GLUT transporters parallel the decrease in lactate utilization and the increase in glucose metabolism observed during cerebral maturation (Clark *et al.* 1994; Clark *et al.* 1993; Dwyer *et al.* 2002; Medina *et al.* 1996; Vannucci *et al.* 1997; Vannucci and Simpson 2003).

4. Cytosolic Metabolism of Pyruvate

Pyruvate is produced in the cytosol of neural cells either from glucose, through the glycolytic pathway, or from extracellular lactate, alanine or pyruvate, after transport and equilibration in the LDH or ATT reactions (cf. Figure 1.1). Cytosolic pyruvate may then be removed to the mitochondrial matrix through the monocarboxylate carriers of the inner mitochondrial membrane, or extruded to the extracellular space as lactate or alanine. Cytosolic pyruvate may also be produced from malate in the malic enzyme reaction. The following paragraphs analyze these aspects.

The glycolytic pathway (Figure 1.2) is the sequence of ten enzyme catalyzed reactions degrading glucose to two molecules of pyruvate

$$\text{Glucose} + 2\text{NAD}^+ + 2\text{ADP} + 2\text{P}_i \rightarrow 2\ \text{Pyruvate} + 2\text{NADH} + 2\text{H}^+ + 2\text{ATP} + 2\text{H}_2\text{O} \quad [1.4]$$

Hexokinase, phosphofructokinase and pyruvate kinase are able to modulate glycolytic flow in most tissues. However, the classical work of Lowry and Saktor showed that in brain, aerobic

glycolysis is regulated primarily at the phosphofructokinase and hexokinase steps (Passonneau and Lowry 1964; Sacktor *et al.* 1966). A schematic description of this pathway is given in Figure 1.2, with maximal activities of the enzymes involved and concentrations of metabolites (Clarke *et al.* 1989). Glycolytic flux *in vivo* represents approximately 5% of the maximal possible flux through the pathway, revealing the important metabolic capacity of this pathway and the need for a strict regulation. The literature on the kinetic properties and structure of the main glycolytic enzymes is large. I will herein focus exclusively in LDH, because of its crucial role for the understanding of some of the developed methodologies.

LDH represents the end point of anaerobic glycolysis, catalyzing the NADH dependent reduction of pyruvate to lactate and NAD^+, in a reversible manner (Everse and Kaplan 1973).

$$\text{Pyruvate} + \text{NADH} + H^+ \leftrightarrow \text{Lactate} + NAD^+ \qquad [1.5]$$

Cerebral LDH appears in five different isoforms, derived from two parental homotetramers and three hybrids. These are: LDH1 (also known as LDH-H or LDH-A, isolated from heart) or LDH5 (also known as LDH-M or LDH-B, isolated from muscle) (Bonavita *et al.* 1964). The remaining isoforms arise from different combinations of H and M subunits (approximately 36 kDa), H4 (LDH1), H3M (LDH2), H2M2 (LDH3), HM3 (LDH4), M4 (LDH5). LDH1 is only

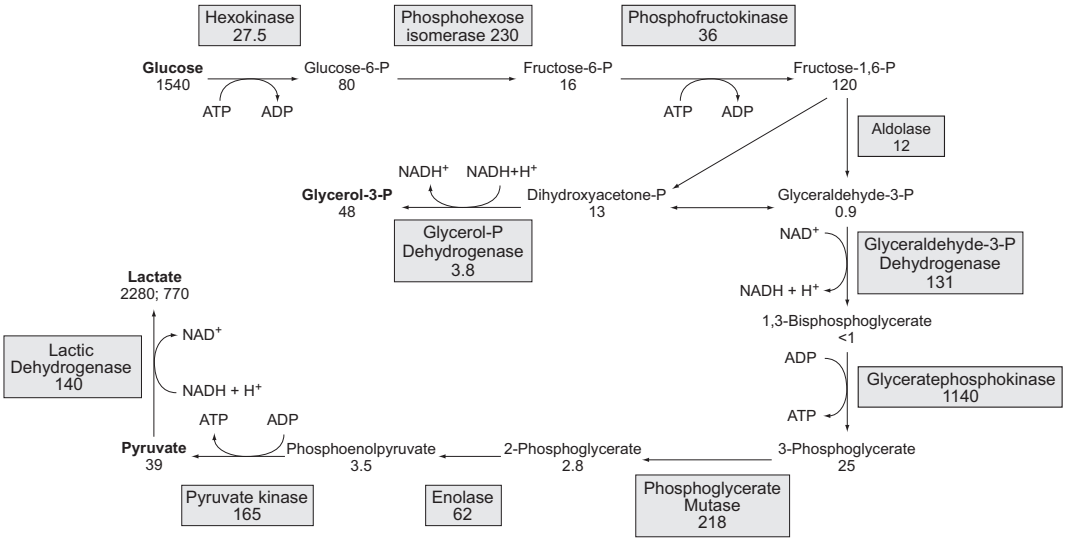

Figure 1.2. The cerebral glycolytic pathway. Numbers below the enzymes and metabolites refer to the maximal velocity ($\mu mol.g^{-1}$ wet weight. min^{-1}) and concentration (nmol. g^{-1} wet weight) as measured in brain homogenates and acid extracts, respectively. Taken from (Clarke et al. 1989). Reproduced with permission of the publisher.

detected in neurons and its kinetic properties favour mainly pyruvate formation (Bittar *et al.* 1996; Laughton *et al.* 2000) while LDH5 is present mainly in astrocytes and its kinetic properties favour lactate formation (Dawson *et al.* 1964; Richard 1963). Thus, the distribution of LDH isoenzymes is also adequate to support the astrocyte to neuron lactate shuttle (Pellerin *et al.* 1998a). Cerebral LDH is believed to be cytosolic in most tissues, with the exception of the testis, where it has a mitochondrial distribution. Nonetheless, recent evidence indicates that at least part of hepatic and cardiac LDH may be mitochondrial (Brooks *et al.* 1999). LDH1 and LDH5 isoenzymes are also heterogeneously distributed within the different cerebral structures, as revealed by *in situ* mRNA hybridization (Laughton *et al.* 2000). LDH also experiences important changes during ontogeny, increasing progressively after birth, in parallel with other glycolytic enzymes and transporters (Medina *et al.* 1996).

5. Mitochondrial Transport - General Characteristics of Mitochondrial Carrier Proteins

Pyruvate and other cytosolic metabolites are transported through the inner mitochondrial membrane by the mitochondrial carrier family of proteins MCF (LaNoue and Schoolwerth 1979; Palmieri 1994; Palmieri 2004; Palmieri *et al.* 1996; Satrustegui *et al.* 2007).

MCF carriers are integral proteins of the inner mitochondrial membrane coded in man by SLC25 genes family (Palmieri 2004). Approximately 35 mRNA transcripts of this family have been observed, although only ten MCFs have been purified, sequenced and reconstituted. The main members of the MCF family include: the ATP translocators (AAC), the phosphate exchanger (PiC), the α-ketoglutarate-malate exchanger (OGC), the dicarboxylate carrier (DIC), the citrate-malate exchanger (CIC), the aspartate-glutamate exchanger (AGC), the carnitine and ornithine carriers (CAC and ORC), the uncoupling proteins (UCP) and the pyruvate carrier (PyC). The primary structure of transmembrane MCF proteins is relatively constant. It depicts a tripartite sequence with three tandemly repeated domains of approximately 100 amino acids in length. Each domain contains two hydrophobic portions, believed to span the membrane as α-helices, separated by hydrophilic regions with the N and C terminals facing the intracellular side. Most isolated MCF proteins have been shown to be homodimer, probably consisting of a total of twelve transmembrane segments, as in the majority of carrier proteins. Figure 1.3 summarizes the operation of different shuttle systems that exchange cytosolic and mitochondrial metabolites related to pyruvate metabolism and the transfer of reducing equivalents.

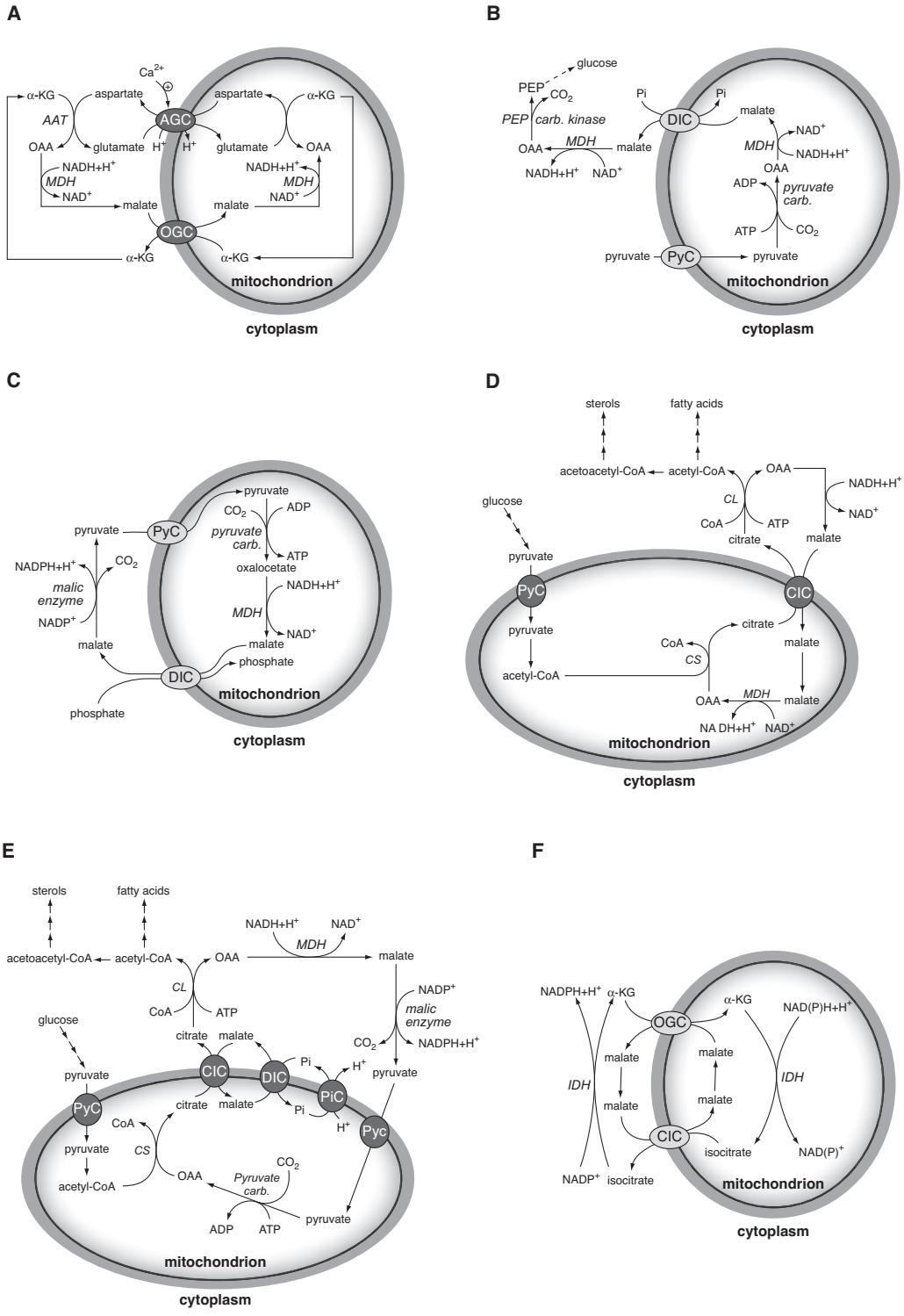
A
α-KG
aspartate
Ca2+
AGC
aspartate
α-KG
AAT
OAA
glutamate
H+
H+
glutamate
OAA
NADH+H+
MDH
NAD+
malate
malate
NADH+H+
MDH
NAD+
OGC
α-KG
α-KG
mitochondrion
cytoplasm
B
glucose
PEP
CO2
PEP carb. kinase
Pi
Pi
DIC
malate
MDH
OAA
malate
NADH+H+
NAD+
NAD+
MDH
NADH+H+
OAA
ADP
pyruvate carb.
ATP
CO2
pyruvate
PyC
pyruvate
mitochondrion
cytoplasm
C
pyruvate
CO2
ADP
pyruvate carb.
pyruvate
PyC
ATP
oxalocetate
NADPH+H+
CO2
NADH+H+
malic enzyme
MDH
NADP+
NAD+
malate
malate
phosphate
DIC
mitochondrion
phosphate
cytoplasm
D
sterols
fatty acids
acetoacetyl-CoA
acetyl-CoA
OAA
NADH+H+
CL
NAD+
glucose
CoA
ATP
citrate
malate
pyruvate
PyC
CIC
pyruvate
citrate
CoA
malate
CS
acetyl-CoA
OAA
MDH
malate
NA DH+H+
NAD+
mitochondrion
cytoplasm
E
sterols
fatty acids
NADH+H+
NAD+
acetoacetyl-CoA
acetyl-CoA
OAA
MDH
malate
CL
NADP+
malic enzyme
glucose
CoA
ATP
CO2
NADPH+H+
citrate
malate
pyruvate
CIC
DIC
Pi
H+
pyruvate
PyC
PiC
citrate
malate
Pi
H+
Pyc
CoA
pyruvate
CS
acetyl-CoA
OAA
CO2
Pyruvate carb.
pyruvate
ADP
ATP
mitochondrion
cytoplasm
F
NADPH+H+
α-KG
α-KG
NAD(P)H+H+
OGC
malate
malate
IDH
malate
IDH
malate
CIC
isocitrate
NAD(P)+
NADP+
isocitrate
mitochondrion
cytoplasm

◄ **Figure 1.3. The mitochondrial transporters present in neural cells and their roles.** The schemes do not show all the mitochondrial transporters nor all the metabolic pathways in which individual carriers are involved. **A:** The malate-aspartate shuttle for the transfer of cytosolic NADH to the mitochondrial matrix. **B:** Extrusion of NADH to the cytosol for gluconeogenesis from pyruvate in astrocytes. **C:** The pyruvate-malate shuttle; extrusion of reducing equivalents (NADPH) to the cytosol. **D:** The citrate-malate shuttle; extrusion of citrate to the cytosol for acetyl-CoA generation and sterols and fatty acid synthesis. **E:** The citrate-pyruvate shuttle; simultaneous extrusion of mitochondrial citrate, NAD^+ and NADPH for cytosolic sterol and fatty acid synthesis. **F:** The α-ketoglutarate-isocitrate shuttle. Extrusion of mitochondrial isocitrate for cytosolic NADPH synthesis. Adapted from (Palmieri 2004). Reproduced with permission of the publisher.

6. Intramitochondrial Pyruvate Oxidation and the Tricarboxylic Acid Cycle

Once transported to the mitochondrial matrix, pyruvate may enter the TCA cycle through the pyruvate dehydrogenase complex (PDHC) or through pyruvate carboxylase (PC).

The TCA cycle plays a central role in cerebral metabolism, providing the main pathway where carbohydrates, fats and amino acids are oxidized to obtain the energy needed to maintain cerebral functions (Dienel 2002; Hertz and Dienel 2002). It fulfils also a fundamental role, providing intermediates for many cerebral biosynthetic processes and neurotransmitters such as glutamate and γ-aminobutyric acid (GABA) (Gruetter 2002; Owen *et al.* 2002). Pioneering work, performed shortly after its discovery in 1937, allowed the understanding of the basic enzymology of the cycle and the principles of its metabolic regulation (Krebs 1964; Krebs 1970; Krebs and Johnson 1937). Later progress has lead to the purification of all the enzymes involved and the elucidation of their primary amino acid sequence and 3D structure. Recently, the sequencing of the mouse and human genomes has allowed the localization of the corresponding genes in specific chromosomes (Consortium 2001; Consortium 2002). Despite these impressive progresses, many aspects of the integrated operation of the TCA cycles in different cellular environments of the *in vivo* brain and their coordinated response to fundamental physiological processes such as cerebral activation, remain today incompletely understood.

A brief historical background will help to gain a more defined perspective over the plurality of TCA cycles in brain and evolution of the classical concepts towards our more recent interpretations. Initial evidences supporting the existence of two kinetically different TCA cycles in brain were obtained in the sixties (Figure 1.4). Soon after the intracerebral administration of ^{14}C acetate, authors measured higher specific radioactivity in glutamine than in its precursor glutamate (Berl 1965; Berl *et al.* 1968; Berl *et al.* 1970). A similar situation was found with $^{14}CO_3H^-$ and butyrate, but not with glucose or glycerol. These findings could only be explained through the

existence of two slowly exchanging pools of glutamate, denoted then as "large" and "small", which exchanged radioactivity with "small" and "large" glutamine pools, respectively. Soon, the "large" and "small" glutamate and glutamine pools were associated to the operation of the "energy" and "synthetic" TCA cycles, proposed to represent the neuronal and glial compartments, respectively (Van den Berg *et al.* 1969; Van den Berg *et al.* 1966). Subsequently, both cycles were connected by

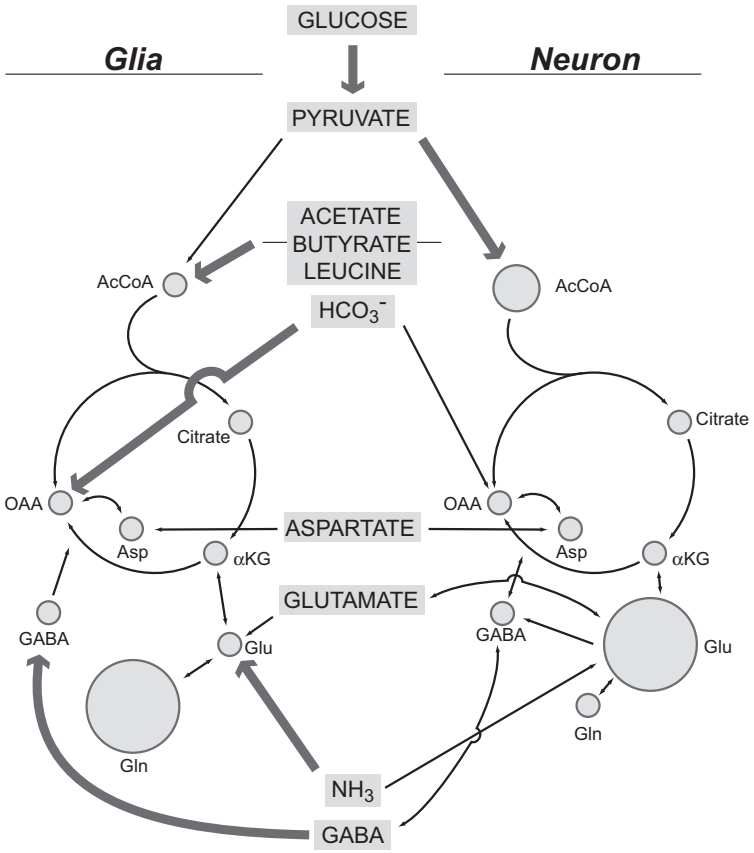

Figure 1.4. The two kinetically different tricarboxylic acid cycles of adult mammalian brain as originally proposed by Berl and Clarke. The metabolic compartmentation concept was proposed to explain the unexpected relationships found between the radioactive specific activities (RSA) of cerebral glutamine to glutamate. The "synthetic cycle", associated to the "large" glutamine pool was assigned to the astrocytes while the "energy cycle", in contact with the "large" glutamate pool was assigned to the neurons. The size of the circles and the thickness of the arrows refer approximately to the pool sizes and preferred compartment for metabolism, respectively. Note the incomplete glutamine cycle with no transfer of glutamine to the neurons and arrow suggesting neuronal pyruvate carboxylation. Adapted from (Berl and Clarke 1969). Reproduced with permission of the publisher.

vectorial transfers of glutamate from the neuronal to the glial cycle, and glutamine in the opposite direction. The "glutamate-glutamine cycle" was conceived then only as a mechanism to replenish small glutamate looses in the neurons during neurotransmission (Garfinkel 1966; Van den Berg and Garfinkel 1971).

Figure 1.5 illustrates the current status of these concepts, emphasizing the aspects that remain incompletely understood. Plasma glucose is taken up by neural cells from the capillaries, mainly by the astrocytic end feet (process 1) and possibly also to some extent by the neurons (process 2). Both neurons and astrocytes contain mitochondria equipped with the enzymatic machinery required for glycolytic (processes 3 and 4) and oxidative glucose metabolism (processes 6 and 7). However, the quantitative contribution of neuronal and glial metabolisms to overall cerebral

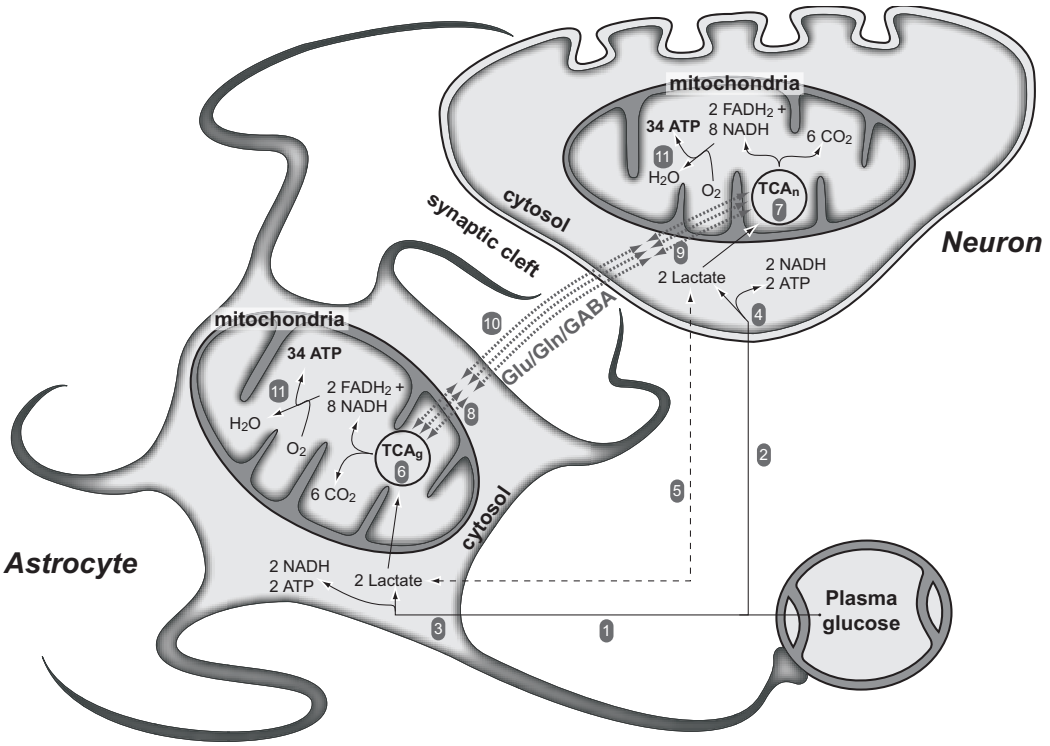

Figure 1.5. Metabolic interactions between oxidative and non oxidative metabolisms in neurons and glia. 1: Glucose uptake by the astrocyte, 2: Glucose uptake by the neuron, 3: Astroglial glycolysis, 4: Neuronal glycolysis, 5: Exchange of lactate between the neurons and glia, 6: Astroglial TCA cycle, 7: Neuronal TCA cycle, 8 and 9: Astrocytic and neuronal mitochondrial transporters allowing exchange of reducing equivalents between mitochondria and cytosol, 10: Intercellular exchange of glutamate, glutamine and GABA, 11: Astrocytic and neuronal respiratory chain.

glycolysis or oxidation *in vivo* remains imprecise. Similarly, it has not been possible to quantify unambiguously the relative proportions of glucose or lactate used to support neuronal oxidative metabolism *in vivo* (process 5). Finally, the operation of the TCA cycle in neural cells, demands the transfer of reducing equivalents from cytosol to mitochondria as well as the exchange of TCA cycle intermediates between these subcellular compartments (processes 8 and 9). The rate at which these processes occur *in vivo* and how subcellular transport may modulate TCA cycle activity in neurons and astrocytes constitute important challenges of modern neurochemistry.

In the following paragraph, I will focus on the operation of the neuronal and glial TCA cycles and their interactions. I begin with an update on the mechanism, regulation and regional distribution of the cerebral TCA cycle, describing later the main methodologies used to investigate the cycle flux. Other recent reviews on the cerebral TCA cycles and neuroenergetics complement appropriately the information presented here (Cruz and Cerdán 1999; García-Espinosa *et al.* 2004; Gruetter 2002; Hertz 2004; Hertz and Dienel 2002; Rothman *et al.* 2003; Shulman *et al.* 2004).

Figure 1.6 and Table 1.1 summarize the individual reactions of the TCA cycle and the main properties of the enzymes involved, respectively. As mentioned above, mitochondrial pyruvate oxidation begins with its decarboxylation to acetyl-CoA by pyruvate dehydrogenase. The pyruvate dehydrogenase complex (PDHC, EC 1.2.4.1) plays a key role in the oxidative metabolism of pyruvate and its regulation, catalyzing the irreversible decarboxylation of pyruvate to CO_2, acetyl-CoA and NADH (Patel and Korotchkina 2001).

The TCA cycle starts by the irreversible condensation of oxaloacetate and acetyl-CoA to produce cytril-CoA, then hydrolyzed to citrate and CoA. This reaction is catalyzed by citrate synthase (EC 2.3.3.1), a homodimer of 52-kDa subunits coded in man by the CS gene, the enzyme being found in the mitochondrial matrix of all cells capable of oxidative metabolism (Goldenthal *et al.* 1998). The synthesis of citrate is a crucial control point of the TCA cycle. Citrate synthase is allosterically inhibited by ATP, through an increase in the K_m for acetyl-CoA. This inhibition is easily reversed by an increase in the ADP concentration, which induces an allosteric stimulation. Concomitantly, high concentrations of NADH and succinyl-CoA also retroinhibit this enzyme (Matsuoka and Srere 1973).

The next step is catalyzed by the 85-kDa monomeric mitochondrial aconitase (EC 4.2.1.3). It is a sequential reaction comprising dehydration and hydration processes. Citrate is isomerized to isocitrate via cis-aconitate. Aconitase is an iron-sulfur protein encoded by the ACO2 gene containing a [4Fe-4S] cluster to which the substrate binds (Mirel *et al.* 1998).

The mitochondrial NAD^+-dependent isocitrate dehydrogenase (EC 1.1.1.41) catalyzes an ordered reaction consisting of the initial oxidation of isocitrate to the unstable β-keto acid oxalosuccinate, followed by decarboxylation to α-ketoglutarate. This constitutes the second rate-limiting step of the TCA cycle, being allosterically activated by increasing intramitochondrial

ADP/ATP ratios and Ca^{2+}. There are additional cytosolic and mitochondrial $NADP^+$ dependent isoenzymes which contribute actively to the $NADP^+$/NADPH dependent detoxification reactions and fatty acid synthesis (Sazanov and Jackson 1994). Both isoenzymes are heterotetramers of two 40-kDa alpha subunits (coded by the IDH3A gene), one 42-kDa beta subunit (IDH3B), and one 43-kDa gamma subunit (IDH3G) (Brenner *et al.* 1997; Kim *et al.* 1995; Kim *et al.* 1999). It is possible that the fate of cytosolic or mitochondrial isocitrate trough the NAD^+ or $NADP^+$ isoenzymes is determined by the availability for corresponding reducing equivalents.

The reaction mechanism of the mitochondrial α-ketoglutarate dehydrogenase complex is analogous to the conversion of pyruvate to acetyl-CoA by PDHC, due to the structural similarity of both complexes (Sheu and Blass 1999). The assembly contains multiple copies of three enzymatic components: α-ketoglutarate dehydrogenase (E1, EC 1.2.4.2, encoded by the OGDH gene, 113 kDa), transsuccinylase (E2, EC 2.3.1.61, encoded by the DLST gene, 49 kDa) and dihydrolipoyl dehydrogenase (E3, EC 1.8.1.4, encoded by the DLD gene, 54 kDa) (Ali *et al.* 1994; Feigenbaum and Robinson 1993; Szabo *et al.* 1994). The α-ketoglutarate dehydrogenase complex requires several cofactors including: lipoamide, thiamine pyrophosphate, CoA, FAD and NAD^+. Succinyl-CoA and NADH inhibit the reaction, providing the third control point of the TCA cycle flux, after citrate synthase and isocitrate dehydrogenase (NAD^+).

Succinyl-CoA synthetase (EC 6.2.1.4) is a mitochondrial enzyme that performs the only substrate-level phosphorylation of the TCA cycle, converting succinyl-CoA into succinate. GDP is phosphorylated to GTP, which then goes on to phosphorylate ADP, resulting in the only ATP molecule directly produced by the TCA cycle. It is a heterodimer of an alpha (35 kDa) and a beta chain (41 kDa), encoded by SUCLG1 and SUCLG2 genes, respectively (James *et al.* 1997; Johnson *et al.* 1998).

The succinate dehydrogenase complex (EC 1.3.5.1) oxidizes succinate to fumarate. It is composed of a 70-kDa flavoprotein (fp), a 27-kDa iron-sulfur protein (ip), and a cytochrome b

►**Figure 1.6. The turnover of carbon and hydrogen in the tricarboxylic acid cycle.** Using (1,2-$^{13}C_2$) acetyl-CoA as substrate, the ^{13}C is incorporated successively in (4,5-$^{13}C_2$) citrate (citrate synthase), (4,5-$^{13}C_2$) cis-aconitate (aconitase), (4,5-$^{13}C_2$) isocitrate (aconitase) and (4,5-$^{13}C_2$) α-ketoglutarate (NAD-isocitrate dehydrogenase). α-ketoglutarate dehydrogenase produces (3,4-$^{13}C_2$) succinyl-CoA and an equimolar mixture of (1,2-$^{13}C_2$) and (3,4-$^{13}C_2$) succinate (succinyl CoA synthetase), followed by the production of (1,2-$^{13}C_2$) or (3,4-$^{13}C_2$) fumarate (succinate dehydrogenase) and (1,2-$^{13}C_2$) or (3,4-$^{13}C_2$) malate or oxaloacetate. Hydrogens from water incorporate in the $H3_{proR}$ and $H3_{proS}$ of isocitrate, α-ketoglutarate and glutamate, the H2 (or H3) of succinate and fumarate and the H3 of oxalacetate and malate. ^{13}C atoms are indicated in red or green (lost by decarboxylation). Hydrogen exchange is considered to start from fumarate on, being indicated in cyan and light blue (H3 and H3' hydrogens of α-ketoglutarate) or white contour (H3 malate or oxalacetate). The same color is maintained in the different intermediates to follow the metabolic history of every carbon or hydrogen.

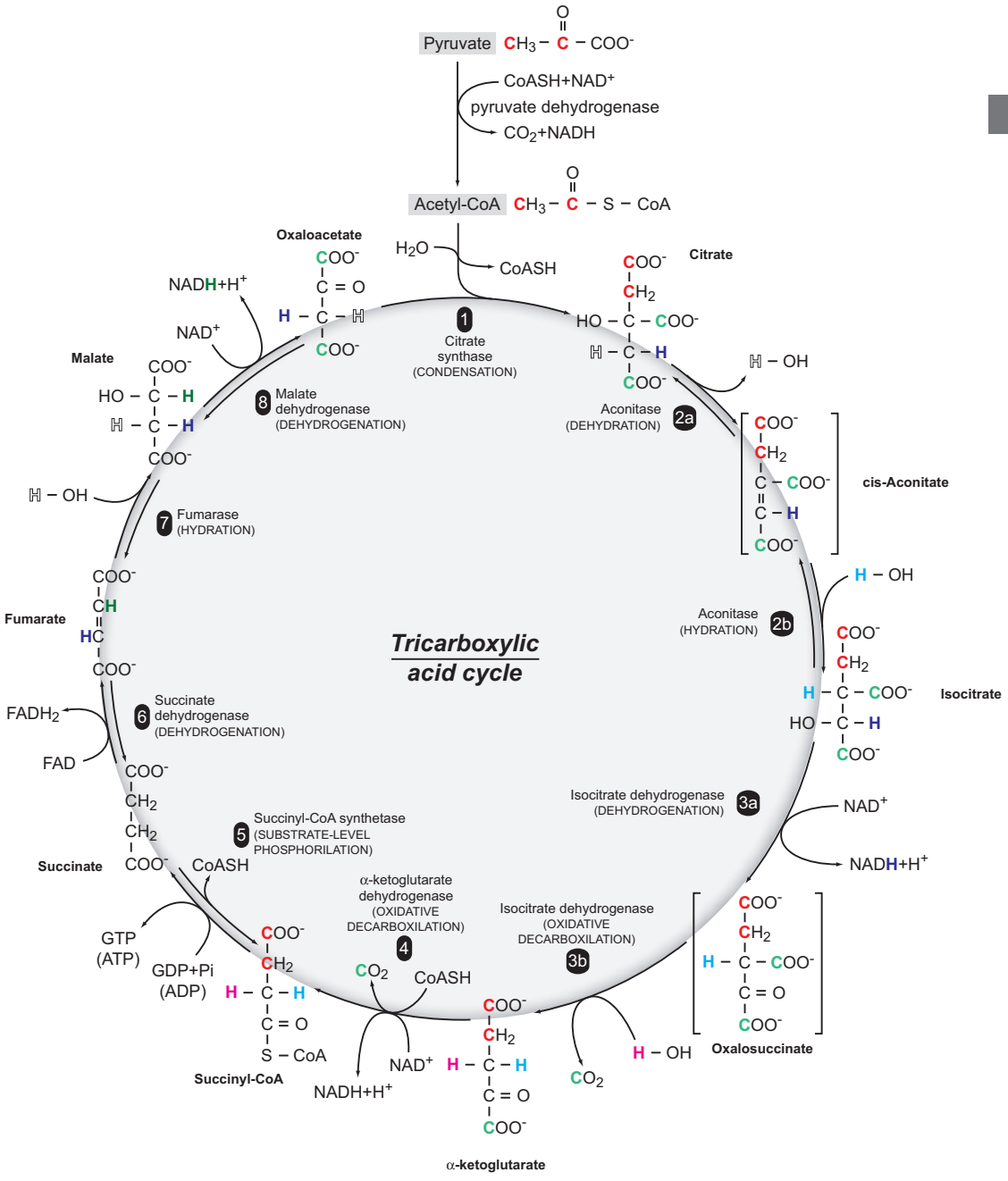
Pyruvate
CoASH+NAD+
pyruvate dehydrogenase
CO2+NADH
Acetyl-CoA
Oxaloacetate
H2O
CoASH
Citrate
1
Citrate synthase
(CONDENSATION)
NADH+H+
NAD+
Malate
8
Malate dehydrogenase
(DEHYDROGENATION)
H – OH
Aconitase
(DEHYDRATION)
2a
cis-Aconitate
H – OH
7
Fumarase
(HYDRATION)
Fumarate
Aconitase
(HYDRATION)
2b
Isocitrate
Tricarboxylic
acid cycle
FADH2
FAD
6
Succinate dehydrogenase
(DEHYDROGENATION)
Isocitrate dehydrogenase
(DEHYDROGENATION)
3a
NAD+
NADH+H+
Succinate
5
Succinyl-CoA synthetase
(SUBSTRATE-LEVEL
PHOSPHORILATION)
CoASH
α-ketoglutarate
dehydrogenase
(OXIDATIVE
DECARBOXILATION)
4
Isocitrate dehydrogenase
(OXIDATIVE
DECARBOXILATION)
3b
GTP
(ATP)
GDP+Pi
(ADP)
CO2
CoASH
Oxalosuccinate
Succinyl-CoA
NAD+
NADH+H+
H – OH
CO2
α-ketoglutarate

composed of two integral membrane proteins, encoded by SDHA, SDHB, SDHC and SDHD genes, respectively (Au *et al.* 1995; Elbehti-Green *et al.* 1998; Hirawake *et al.* 1999; Morris *et al.* 1994). The succinate dehydrogenase complex is the only one among the enzymes of the TCA cycle to be imbedded in the inner mitochondrial membrane. Due to the fact that the free-energy change for this oxidation is not sufficient to reduce NAD^+, FAD is used as the hydrogen acceptor for this reaction (de Gomez-Puyou *et al.* 1972).

The next step is the hydration of fumarate to form L-malate. This stereospecific *trans* addition of H and OH is catalyzed by 55-kDa fumarase (EC 4.2.1.2), a homotetramer that exists both in the mitochondrial and cytosolic compartments of the intact brain and is encoded by the FH gene (Akiba *et al.* 1984; Kinsella and Doonan 1986).

Finally, malate dehydrogenase (EC 1.1.1.37) catalyzes the reversible oxidation of L-malate to

TABLE 1.1. Structural and genomic properties of the tricarboxylic acid cycle enzymes

Enzyme (EC number)	Substrates	Products	Prosthetic group	MW/structure	Genetic sequence /cloned
Citrate synthase (EC: 2.3.3.1)	Oxaloacetate acetyl-CoA	Citrate		52 kDa, homodimer (by similarity)	CS
Aconitase (EC: 4.2.1.3)	Citrate	Isocitrate	Fe–S	85 kDa, monomer (by similarity)	ACO2
NAD^+-dependent isocitrate dehydrogenase (EC: 1.1.1.41)	Isocitrate	α-Ketoglutarate		Heterooligomer of subunits α (40 kDa), β (42 kDa), and γ (43 kDa) in the apparent ratio of 2:1:1 (by similarity)	IDH3A (α), IDH3B (β), IDH3G(γ)
α-Ketoglutarate dehydrogenase complex	α-Ketoglutarate	Succinyl-CoA	Lipoic acid, FAD, TPP	Three enzymatic components: α–ketoglutarate dehydrogenase (E1, EC: 1.2.4.2, 113 kDa), trans-succiylase (E2, EC:2.3.1.61, 49 kDa), and dihydrolipoyl dehydrogenase (E3, EC: 1.8.1.4, 54 kDa)	OGDH (E1), DLST (E2), DLD (E3)
Succinyl-CoA synthetase (EC: 6.2.1.4)	Succinyl-CoA	Succinate		Heterodimer of an α (35 kDa) and a β chain (41 kDa) (by similarity)	SUCLG1(α) SUCLG2 (β)
Succinate dehydrogenase (EC: 1.3.5.1)	Succinate	Fumarate	FAD, Fe–S	Three enzymatic components: a flavoprotein (fp, 70 kDa), an iron protein (ip, 27 kDa), and a cytochrome *b* composed of two integral membrane proteins	SDHA (fp), SDHB (ip), and SDHC and SDHB (integral membrane proteins)
Fumarase (EC: 4.2.1.2)	Fumarate	Malate		55 kDa, homotetramer	FH
Malate dehydrogenase (EC: 1.1.1.37)	Malate	Oxaloacetate		36 kDa, homodimer	MDH2

oxaloacetate. This 36-kDa homodimer is located in the mitochondrial matrix, using the NAD^+/NADH cofactor system. The enzyme is encoded by the MDH2 gene (Benn *et al.* 1977). Moreover, malate dehydrogenase plays a crucial role in the redox coupling between the mitochondrial and the cytosolic compartments, through the malate-aspartate shuttle (Malik *et al.* 1993).

6.1. Regionalization and Subcellular Distribution

Classical studies determined the maximal activities of TCA cycle enzymes both in whole brain and different cerebral regions. Maximal activities of TCA cycle enzymes were, in most cases, higher in rodent than in human brain and higher in the cerebral cortex than in the mid brain, basal ganglia and cerebellum, a finding consistent with the higher oxidative capacity of the cortex.

Concerning the cellular distribution, both neurons and astrocytes in primary culture show TCA cycle activity and therefore contain its complete enzymatic machinery. However, the specific activity of TCA cycle enzymes is much higher in cultures of neurons than in cultures of astrocytes, in agreement with the higher oxidative capacity of the former (Hertz 2004; Hertz and Hertz 2003; Stewart *et al.* 1998). At the subcellular level, the TCA cycle occurs exclusively in the mitochondria. Consistent with this localization, pyruvate dehydrogenase, citrate synthase, succinyl-CoA synthetase activities are found only in this fraction (Almeida and Medina 1997; Almeida and Medina 1998; Lai and Clark 1989). However, many of the remaining enzymes are found also in the cytosol of both neurons and astrocytes. These are the cases of aconitase, isocitrate dehydrogenase and malate dehydrogenase. Interestingly enough, cytosolic fumarase has been reported to be lacking in the brain (Akiba *et al.* 1984). Various reports have proposed the functional organization of TCA cycle enzymes in mitochondrial supramolecular complexes (Robinson and Srere 1985).

6.2. Regulation

The regulation of the TCA cycle demands a close integration with the activities of the upstream glycolytic pathway and the downstream mitochondrial respiratory chain. To this end, the TCA cycle flux is inhibited by NADH and ATP as its products, or activated by NAD^+ and ADP as its substrates (Bachelard *et al.* 1974; Clarke *et al.* 1989; Krebs 1970; McIlwain and Bachelard 1985; Sokoloff 1989). Control by these allosteric effectors occurs mainly at the first irreversible step of pyruvate dehydrogenase, with additional modulations at the citrate synthase, isocitrate dehydrogenase (NAD^+) and α-ketoglutarate dehydrogenase steps (Gibson *et al.* 2000; Patel and Korotchkina 2001). These relatively simple substrate activation or product inhibition mechanisms allow for an effective increase in TCA cycle activity under circumstances of augmented energy demand, or for a decrease in TCA cycle flux when overproduction of NADH or ATP occurs.

The integrated regulation of glycolysis and the TCA cycle activity has a profound impact in cerebral energetics (Bachelard *et al.* 1974; Clarke *et al.* 1989; McIlwain and Bachelard 1985; Siesjo 1982). This process involves a series of highly sophisticated redox and energetic signalling processes that communicate between mitochondrial and cytosolic environments. Under physiological circumstances, tight coupling between TCA cycle and glycolysis relies on the fast exchange between mitochondrial and cytosolic ATP/ADP and NAD^+/NADH ratios, respectively. This occurs through the ATP/ADP exchanger and the various transporters involved in the transfer of reducing equivalents in the inner mitochondrial membrane (Palmieri 2004; Palmieri *et al.* 1996; Palmieri *et al.* 2001). In this way, mitochondrial perturbations in ATP/ADP or NAD/NADH ratios should appear reflected in the corresponding cytosolic ratios and *vice versa*.

The glycolytic pathway is classically known to be modulated in brain, mainly at the phosphofructokinase step, through the balance of positive and negative effectors (Passonneau and Lowry 1964; Sacktor *et al.* 1966). ATP and NADH inhibit phosphofructokinase activity, while citrate, ADP, NAD^+ and NH_4^+ increase it. Under hypoxic conditions, oxygen limitations make difficult the reoxidation of mitochondrial NADH, resulting in a more reduced intramitochondrial NAD^+/NADH ratio which inhibits TCA cycle flux. As a consequence, the mitochondrial and cytosolic ATP/ADP ratios decrease, activating glycolytic flux and net lactate production because cytosolic NADH cannot be completely reoxidized by the respiratory chain. This situation is reversible upon return to physiological oxygen tensions, which normalize intracellular ATP/ADP and NAD^+/NADH ratios, restoring the coupling between glycolysis and the TCA cycle flux (Almeida *et al.* 2004). Finally, it should be mentioned here that even though general properties of the integration between glycolysis and the TCA cycle are sufficiently understood, many aspects concerning the subcellular redox and energetic coupling mechanisms as well as the mitochondrial transporters and shuttles involved in neurons and glia, remain to be quantitatively and kinetically characterized.

7. Methodologies to Investigate Tricarboxylic Acid Cycle Activity

Experimental procedures to investigate the activity of the TCA cycle *in vitro* involved traditionally polarographic measurements of oxygen consumption in suspensions of isolated synaptic or non-synaptic mitochondria from brain. The approach required the preparation of mitochondrial suspensions and the determination of oxygen consumption and ATP/ADP cycling, under different substrate conditions (Barrientos 2002; Rossignol *et al.* 2000). Despite the important

information obtained on the mechanisms of oxidative phosphorylation using these methods, this *in vitro* approach did not allow the investigation of the more complex aspects of TCA cycle regulation and intercellular coupling between astrocytic and neuronal environments, as they occur in the *in vivo* brain. Basically, four different methods have been implemented to address these aspects: Autoradiography, PET, NMR and Dual Photon Fluorescence Confocal Microscopy (Figure 1.7). The following sections describe these in more detail.

7.1. Radioactive Procedures

Autoradiography and PET methods are normally based on the measurement of regional cerebral glucose consumption, after the administration of 2-deoxyglucose, either labeled with ^{14}C or with ^{18}F, respectively (Herholz and Heiss 2004; Sokoloff 1981a; Sokoloff 1981b; Sokoloff 1983a; Sokoloff 1983b; Wienhard 2002). These methodologies determine the regional accumulation of 2-(^{14}C or ^{18}F)-deoxyglucose-6-phosphate, a virtually unmetabolizable analog of glucose 6-phosphate, using autoradiography or PET. Autoradiography was one of the first methods to be proposed. It provided *ex vivo* images of the regional accumulation of radioactive 2-deoxyglucose (or other radioactive substrates as acetate, butyrate, among others), as reflected in photographic plates obtained from sections of fixed brain tissue. PET yielded *in vivo* images of the regional uptake of FDG (or other positron emitters) in different brain sections, as resolved tomographycally by a coronal arrangement of positron selective gamma cameras. Both methods allow the determination of cerebral metabolic rates for glucose (CMR_{glc}) in different brain regions after appropriate modeling of the underlying tracer kinetics (Price 2003). In addition, the use of $^{15}O_2$ as inspired gas or $^{15}OH_2$ as a freely diffusible tracer allow measuring by PET, regional oxygen consumption, cerebral blood volume and blood flow (Hatazawa *et al.* 1995). Both radioactive approaches are limited in resolution and chemical specificity, making it not possible to image single neural cells in the examined area, or to investigate the downstream metabolism of glucose below the phosphofructokinase step.

7.2. Nuclear Magnetic Resonance Methods

Pioneering nuclear Magnetic Resonance approaches to cerebral energetics begun most probably with the application of ^{31}P NMR (Moore *et al.* 1999; Ross and Sachdev 2004). ^{31}P NMR spectra from rodent, cat, dog or human brain, depicted resonances from ATP, phosphocreatine (PCr), inorganic phosphate (P_i), phosphomonoesters (PME, mainly phosphorylethanolamine) and phosphodiesters (PDE, glycerophosphorylcholine) (Gyulai *et al.* 1987; Hilberman *et al.* 1984; Komatsumoto *et al.* 1987; Nioka *et al.* 1991). It was possible to follow non invasively the rates of PCr breakdown and recovery after hypoxic and ischemic episodes. In general, PCr decrease was

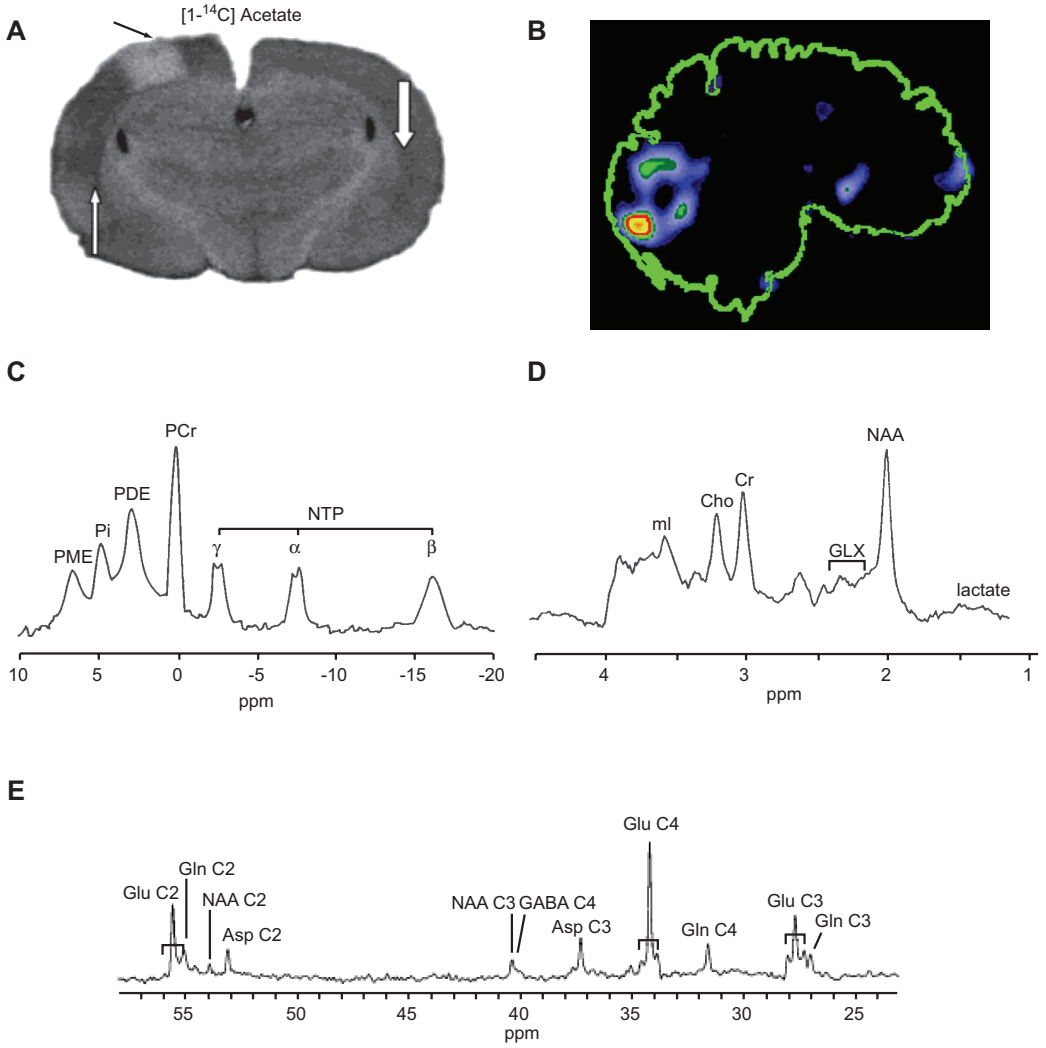

Figure 1.7. Different approaches to measure oxidative capacity in the brain. A: Autoradiography after (1-^{14}C) acetate reflects glial TCA cycle activity during spreading cortical depression (Dienel *et al.* 2001), **B:** A PET scan during the paradigm of "reading words" detects increased ^{18}FDG accumulation in the visual cortex (Mintun *et al.* 2004), **C:** Localized ^{31}P NMR spectra *in vivo* depict resonances from α, β and γ phosphates of nucleotide triphosphates NTP (mainly MgATP), phosphocreatine (PCr), phosphodiesters (PDE), inorganic phosphate (P_i) and phosphomonoesters (PME) (Ross and Sachdev 2004), **D:** Localized ^{1}H NMR spectrum *in vivo* showing resonances from N-acetyl-aspartic acid (NAA), glutamate and glutamine (Glx), creatine and phosphocreatine (Cr), choline derivatives (Cho) and *myo*-inositol (mI) (Ross and Sachdev 2004), **E:** Localized ^{13}C NMR spectroscopy during (1-^{13}C) glucose infusion shows resonances from the C3, C4 and C2 carbons of glutamate (GLU) and glutamine (GLN) and the C3 and C2 carbons of aspartate (Asp) and N-acetyl-aspartate (NAA) (Gruetter *et al.* 2003). Reproduced with permission of the publisher.

the first phenomenon observed, with ATP concentrations remaining initially relatively constant and decreasing eventually after PCr stores had been depleted. The recovery rates of PCr after restoring normal oxygen delivery conditions, reflected directly oxidative phosphorylation and TCA cycle activity *in vivo*. Under these circumstances, the P_i resonance increased and shifted to a more acidic pH. PME increased in the late phases of hypoxia/ischemia, in agreement with increased phospholipase activation and intracellular Ca^{2+} rises due to membrane depolarization.

^{1}H NMR approaches to cerebral competence are probably the most extended today in the clinic (Burtscher and Holtas 2001). ^{1}H NMR spectra from human or rodent brain show resonances from the methyl group of N-acetyl-aspartic acid (NAA), the methyl groups of creatine (Cr) and PCr, the trimethylammonium groups of choline (Cho) containing compounds and the *myo*-inositol (Ino) resonances. NAA and Ino are thought to represent the neuronal or glial contributions to the observed voxel, respectively. Notably, the methyl group of lactate becomes readily observable under hypoxic or ischemic conditions, providing an unambiguous proof of increased net glycolytic flux under these circumstances.

^{13}C NMR approaches constitute probably the most elaborated, chemically specific, tool to trace the metabolic fate of ^{13}C labeled glucose or acetate in the brain, both *in vivo* and *in vitro* (Cerdán 2003; Cruz and Cerdán 1999; de Graaf *et al.* 2003; García-Espinosa *et al.* 2004; Gruetter *et al.* 2003; Rodrigues and Cerdán 2005). The ^{13}C NMR approach is so useful because it makes possible to investigate the activities of the neuronal and glial TCA cycles *in vivo* and *in vitro*, providing direct insight into cerebral metabolic compartmentation. Traditionally, either (^{13}C) glucose, a universal substrate for neurons or glial cells or (^{13}C) acetate, an exclusive substrate for the glia, have been used (Badar-Goffer *et al.* 1990; Cerdán *et al.* 1990; Fitzpatrick *et al.* 1990; Mason *et al.* 1992b). (1-^{13}C) glucose is metabolized to (3-^{13}C) pyruvate which eventually labels (4-^{13}C) glutamate and (4-^{13}C) glutamine. Similarly, (2-^{13}C) or (1,2-$^{13}C_2$) acetate produce (4-^{13}C) or (4,5-$^{13}C_2$) glutamate and glutamine, respectively (see Figure 1.6). Consequently, dynamic or steady state measurements of the turnover and fractional ^{13}C enrichments of glutamate C4 and glutamine C4, as labeled from (^{13}C) glucose or (^{13}C) acetate precursors, have been often interpreted to reflect the neuronal (V_{TCAn}) and glial (V_{TCAg}) TCA cycle fluxes, respectively. These interpretations rely, however, on the assumption that exchange of α-ketoglutarate and glutamate through the cytosolic and mitochondrial aspartate aminotransferases and through the inner mitochondrial membrane (V_x) of both neurons and astrocytes is faster than the TCA cycle rate. This assumption allows considering a single cerebral glutamate pool in both neural cell types and approximating the neuronal and glial TCA cycles by the kinetics (or steady state values) of ^{13}C enrichment in glutamate C4 and glutamine C4, respectively.

Table 1.2 summarizes the values for the TCA cycle flux obtained using different *in vivo* and *in vitro* ^{13}C NMR approaches, as compared to earlier radioactive isotope methods and more recent ^{13}C isotopomer approaches. In general, TCA cycle fluxes calculated for the normoxic adult rat

TABLE 1.2. Tricarboxylic acid cycle and glutamate/glutamine exchange between the neuronal and glial compartments of the adult mammalian brain as calculated with different models and methodologies

Process/model	Garfinkel[a]	Van den Berg and Garfinkel[b]	Kunnecke et al.,[c] Preece and Cerdan[d]	Mason et al.,[e] Sibson et al.,[f,g] Shen et al.,[h] Lebon et al.[i]	Gruetter et al.[j]	Bluml et al.[k]
Total cerebral TCA cycle flux (μmol/min/g)	1.05	1.5	1.4	1.6 or 0.7,[e] 0.6,[f] 1.0-0.2,[g] 0.8[h]	0.6	0.84
Neuronal TCA cycle flux (μmol/min/g)	0.40	1.2	1.0	1.6,[e] 0.6,[f] 1.0-0.2,[g] 0.8[h]	0.6	0.70
Glial TCA cycle flux (μmol/min/g)	0.65	0.3	0.4	0.14[i]		0.14
Size (μmol/g)/turnover (per min) of large glutamate pool	8.8/21.7	7.0/5.7	5.8/5.8	n.a.		n.a.
Size (μmol/g)/turnover (per min) of small glutamate pool	1.7/2.6	1.25/4.16	0.5/1.25	n.d./7.7[l]		n.a.
Net transfer of neuronal glutamate to glial compartment (μmol/min/g)	0.08[m]	0.14	0.1	0.21,[f] 0.40-0.0,[g] 0.32,[h] 0.3[f]	0.3 (0.2)[n]	n.a.
Net transfer of glial glutamine to neuronal compartment (μmol/min/g)	0.45	n.a.	0.1	0.21,[f] 0.40-0.0,[g] 0.32,[h] 0.3[f]	0.3 (0.2)[k,n]	n.a.

[a]Calculated from specific radioactivity measurements in brain extracts obtained after intracranial injections of various radioactive precursors including (U-^{14}C)glutamate, (U-^{14}C) aspartate, $^{14}CO_3H^-$, and $^{15}NH_4$ acetate (Garfinkel, 1966)

[b]Calculated from specific radioactivity measurements in glutamate, glutamine, and aspartate from mouse brain extracts prepared after intraperitoneal injections of ^{14}C-labeled glucose and acetate (van den Berg and Garfinkel, 1971)

[c]Relative flux values were calculated as described in (Kunnecke et al., 1993) and from the relative ^{13}C isotopomer populations in glutamate, glutamine, and GABA measured by highresolution ^{13}C NMR in rat brain extracts after infusion of (1,2-$^{13}C_2$) acetate (Chapa et al., 1995)

[d]Absolute flux values were determined from the relative values described in note c by measuring the absolute rate of GABA accumulation induced by vigabatrin, a selective inhibitor of GABA transaminase (Preece and Cerdan, 1996)

[e]Determined *in vivo* from the kinetics of ^{13}C enrichment in glutamate and glutamine C4 carbons from rat or human brain during infusion of (1-^{13}C) glucose, respectively (Mason et al., 1992a; Mason et al., 1995)

[f]Determined *in vivo* from the kinetics of ^{13}C labeling in glutamate and glutamine C4 (Sibson et al., 1997)

[g]Determined *in vivo* from the kinetics of ^{13}C enrichment in glutamate and glutamine C4, under different conditions of morphine, α-chloralose, and pentobarbital anesthesia (Sibson et al., 1998a)

[h]Determined in the human brain *in vivo* during (1-^{13}C) glucose infusion. Glutamate/glutamine exchange concluded to be stoichiometric 1:1 with CMRglc (Shen et al., 1999)

[i]Determined in the human brain during metabolism of (2-^{13}C) acetate (Lebon et al., 2002)

[j]Determined in the human brain during (1-^{13}C) glucose infusion with a different model than that used in f-i (Gruetter et al., 2001)

[k]Determined in the human brain during (1-^{13}C) acetate metabolism (Bluml et al., 2002)

[l]Determined *in vivo* as the inverse of the rate constant of ^{13}C labeling in cerebral glutamate C4 during (1-^{13}C) glucose infusions (Mason et al., 1992b)

[m]Originally proposed as an α-ketoglutarate exchange between the large and small compartments (Garfinkel, 1966)

[n]Only a fraction of glutamine synthesis considered to be derived from neurotransmitter glutamate. Glutamate/glutamine exchange concluded nonstoichiometric with CMRglc, approaching 0.4 rather than the value of 1 concluded in f-i (Gruetter et al., 2001)

n.a.; not applicable, n.d.; not detectable, Adapted from Cruz and Cerdan (1999). Reproduced with permission of the publisher

or human brain were in the range 0.5 - 1.4 μmol.min^{-1}.g^{-1}. More accurate measurements provide recently values for the neuronal TCA cycle flux in the vicinity of 0.5 μmol. min^{-1}.g^{-1}. This value may decrease to virtually undetectable levels with increasing states of anesthesia (Sibson *et al.* 1998b) or increase by 25-50% with different cerebral activation protocols (Chhina *et al.* 2001; Hyder *et al.* 1996; Hyder *et al.* 1997). TCA cycle fluxes in the glial compartment of rodent or human brain are in the range 0.4-0.14 μmol.min^{-1}.g^{-1}, representing approximately 20% of the total cerebral TCA cycle activity. Table 1.2 also shows sizes and turnover rates of the glutamate compartments associated to the "large" and "small" glutamate pools. No direct measurements exist to our knowledge of these pool sizes. The values shown are based on the assumption that the small glutamate pool accounts for approximately 10% of total cerebral glutamate during (1-^{13}C) glucose metabolism. Recently it has been possible to determine simultaneously the relative labeling of the large and small glutamate pools *ex vivo* using (1-^{13}C) glucose and (2-^{13}C, 2-$^{2}H_3$) acetate as substrates (Chapa *et al.* 2000).

Although there is strong evidence supporting fast α-ketoglutarate/glutamate exchange in the cytosolic and mitochondrial aminotransferases (Erecinska and Silver 1990), there is less information concerning the *in situ* activity of the neuronal or glial dicarboxylate carrier and the glutamate-aspartate exchanger, which are responsible for α-ketoglutarate-glutamate exchange between mitochondria and cytosol in these cells. However, experiments with purified mitochondrial preparations from brain incubated with (U-^{14}C) glutamate, have revealed that the exchange of α-ketoglutarate-glutamate is slower than the TCA cycle flux *in vitro* (Berkich *et al.* 2005). Moreover, hydrogen turnover experiments, as monitored by (^{13}C,^{2}H) NMR, have recently revealed the existence of more than one glutamate pool in the neuronal and glial compartments of the adult rat brain *ex vivo* (Sierra *et al.* 2004). Taken together, these results suggest that α-ketoglutarate-glutamate exchange through the mitochondrial membrane of neural cells is of the same order of magnitude or slightly slower than the TCA cycle flux. The influence of these findings on previous ^{13}C NMR modeling results, which assumed fast α-ketoglutarate-glutamate exchange, remains to be analyzed.

The main advantage of hydrogen turnover experiments over the classical ^{13}C turnover approach is that hydrogen exchange occurs in a much faster time scale than ^{13}C exchange (García-Martín *et al.* 2002). Using (^{13}C,^{2}H) NMR it is possible to monitor faster processes, which could not be monitored with ^{13}C NMR (García-Martín *et al.* 2001). Because most metabolite carbons are attached to one or more hydrogen atoms, ^{13}C NMR additionally could serve as a valuable tool to analyze hydrogen turnover. This is a much faster process than ^{13}C turnover and therefore allows studying faster reactions. Our laboratory has proposed a double labeling strategy to investigate hydrogen turnover. Our approach follows by ^{13}C NMR spectroscopy the exchange of pre-existing ^{1}H by ^{2}H at the steady state, when metabolism occurs in media containing a ^{13}C labeled substrate and $^{2}H_2O$ (Chapa *et al.* 2000; García-Martín *et al.* 2001; García-Martín *et al.* 2002; Hansen 1983; Moldes *et al.* 1994; Rodrigues and Cerdán 2007; Rodrigues *et al.* 2005). This is possible because

high-resolution ^{13}C NMR spectroscopy is well suited to detect complex deuteration patterns in ^{13}C labeled metabolites (Figure 1.8).

The presence of one or more deuterons geminally or vicinally bound to the observed ^{13}C implies the appearance of characteristic ^{2}H isotopic shifts and ^{2}H-^{13}C couplings (Dziembowska *et al.* 2004; García-Martín *et al.* 2001; García-Martín *et al.* 2002; Hansen 1983). Therefore, coupling patterns to ^{2}H may appear as split and/or shifted resonances in relation to the perprotonated ^{13}C resonance. Figure 1.8 depicts this behavior. If one of the protons directly bonded to ^{13}C is substituted by ^{2}H, the original resonance is split into a 1:1:1 triplet ($19.21 < {}^{1}J_{C\text{-}H} < 22$ Hz), inducing a geminal upfield isotopic shift ($-0.25 < \Delta_1 < -0.33$ ppm). Two or three deuterons bound to the same ^{13}C atom would result in additive isotopic shifts and ^{2}H-^{13}C couplings patterns of

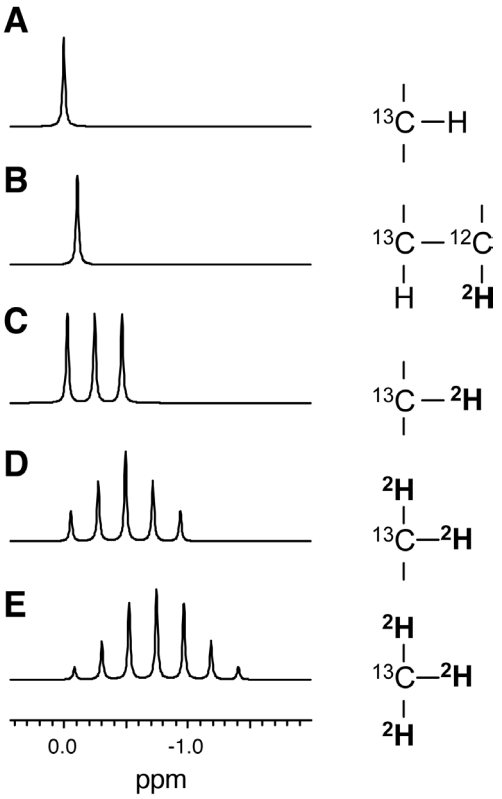

Figure 1.8. ^{2}H-^{13}C multiplets and deuterium induced isotopic shifts in proton decoupled ^{13}C MRS spectra. A: preprotonated carbon, **B:** vicinal deuteration, **C-E:** geminal deuteration by one, two or three deuterons. Simulations were performed with the program WINDAISY using the following parameters: ${}^{1}J_{C\text{-}H} = 20.06$ Hz; geminal isotopic shift, $\Delta_1 = -22.89$ Hz/deuteron; vicinal isotopic shift, $\Delta_2 = -9.89$ Hz/deuteron. Reproduced from (Garcia-Martin et al. 2001) with permission of the publisher.

five or seven line multiplets, shifted by –0.5 or –0.75 ppm respectively. Even a vicinal deuterium substitution induces smaller and additive upfield isotopic shifts ($-0.03 < \Delta_2 < -0.11$ ppm). Vicinal couplings to deuterium are too small to be resolved and resonances shifted vicinally maintain the multiplet structure of their geminal couplings. Thus high-resolution ^{13}C NMR allows determining the number of deuterium replacements, their relative contributions and their geminal or vicinal location with respect to the observed ^{13}C carbon of a specific ^{13}C isotopomers through the analysis of shifted and unshifted (^{1}H,^{2}H)^{13}C multiplets.

This kind of approach makes it possible to develop novel procedures to investigate and resolve in time fast metabolic processes, as long as they involve exchange of hydrogens by deuterons. The exchange of the different hydrogens of glutamate and glutamine molecules by deuterons from heavy water is stereospecific (Cerdán *et al.* 2003). The H2 hydrogen of glutamate is exchanged mainly by aspartate aminotransferase, while the $H3_{proR}$ and $H3_{proS}$ hydrogens are exchanged by aconitase and isocitrate dehydrogenase, respectively. The H4 hydrogens of glutamate are derived from the methyl group of acetyl-CoA and one of them is exchanged during the citrate synthase reaction. This stereospecific exchange is conveniently illustrated by the sequence of exchange of the $H3_{proR}$ and $H3_{proS}$ hydrogens of (2-^{13}C) glutamate by deuterons from the solvent (Figure 1.9).

High-resolution ^{13}C NMR allows distinguishing between perprotonated, monodeuterated and doubly deuterated ^{13}C labeled glutamate and glutamine isotopomers. This is possible because, deuterium substitutions induce readily observable, additive, isotopic shifts in ^{13}C NMR resonances. It has been possible to show, in the perfused liver, that exchange of the H3 hydrogens can be resolved in two different kinetic components (García-Martín *et al.* 2002). A fast exchange of either the $H3_{proR}$ *or* $H3_{proS}$ hydrogens occurs first on pre-existing (2-^{13}C) glutamate or glutamine molecules. This fast process, substitutes *only one* of the H3 hydrogens, in a way that substitution of $H3_{proR}$ precludes substitution of the $H3_{proS}$ and *vice versa*. The fast process may be catalyzed by either cytosolic aconitase or isocitrate dehydrogenases ($NADP^+$). A slower double deuteration of the $H3_{proR}$ *and* $H3_{proS}$ occurs later, but is *only* possible on the (2-^{13}C) glutamate molecules newly synthesized during TCA cycle activity. Thus, the (^{13}C,^{2}H) NMR approach allows resolving the fast turnover of cytosolic (2-^{13}C, 3-^{2}H) glutamate and the slower turnover of (2-^{13}C, 3,3'-$^{2}H_2$) glutamate produced in the TCA cycle. The fact that the fast and slow components of H3 exchange can be resolved by (^{13}C,^{2}H) NMR indicates that the exchange of glutamate across the inner mitochondrial membrane is slow in the H3 hydrogen exchange timescale.

Finally, despite their enormous potential in the evaluation of metabolic pathways *in vivo* and *in vitro*, ^{13}C NMR procedures (and to a smaller extent ^{31}P NMR or ^{1}H NMR) are limited by their low sensitivity and spatial resolution. Unfortunately, *in vivo* and *in vitro* ^{13}C NMR spectra are often obtained from relatively large voxels (up to ca. 50 mL in humans) or extracts prepared from sufficiently large tissue biopsies, respectively. These often include, the weighted contributions from

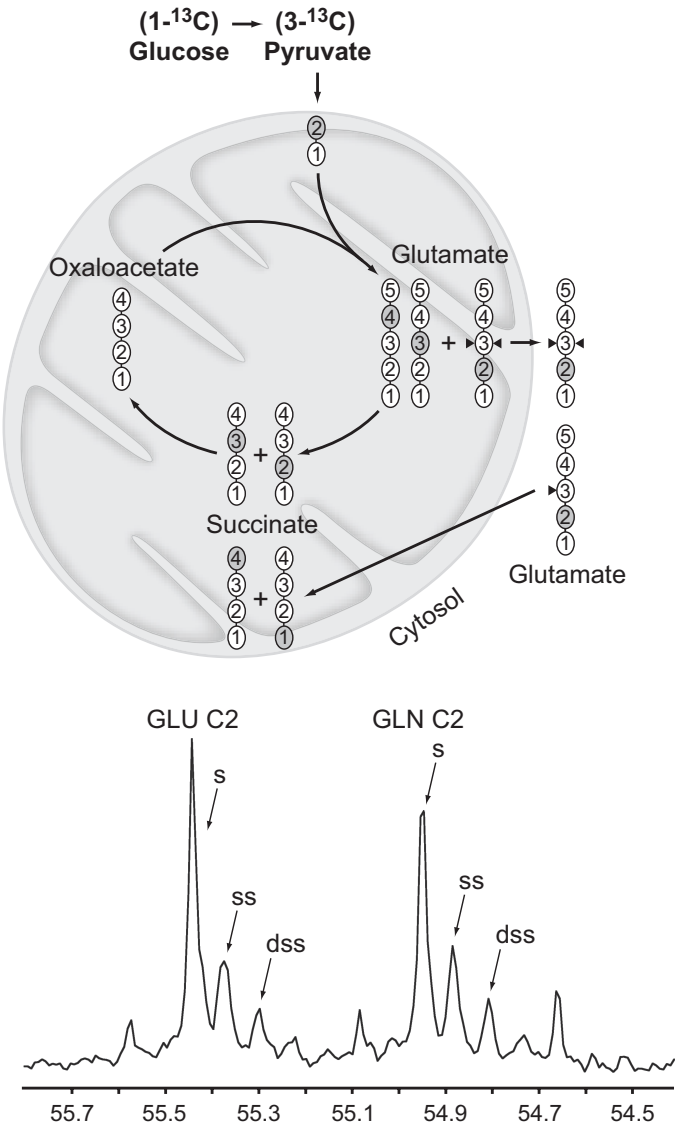

Figure 1.9. The turnover of the H3 hydrogens of cerebral glutamate and glutamine reveals subcellular compartmentation. A fast deuterium exchange occurs in the $H3_{proS}$ *or* $H3_{proR}$ hydrogens of pre-existing molecules of (2-^{13}C) glutamate during the metabolism of (1-^{13}C) glucose, catalyzed by cytosolic isocitrate dehydrogenase ($NADP^+$) or aconitase, respectively. A slower double exchange of the $H3_{proR}$ *and* $H3_{proS}$ occurs only in newly formed (2-^{13}C) glutamate molecules in the TCA cycle (upper panel). Additive isotopic shifts make it possible to distinguish between perprotonated (2-^{13}C) glutamate (GLU C2) or glutamine (GLN C2) (singlets, s), (2-^{13}C, ^{2}H) glutamate or glutamine (shifted singlets, ss) and (2-^{13}C, 3,3'-$^2H_2$) glutamate or glutamine (doubly shifted singlet, dss) by high resolution (^{13}C, ^{2}H) NMR (lower panel). Deuterons are indicated by black triangles. ^{13}C atoms are shown as grey circles.

grey and white matters, as well as from smaller cerebral structures, making it not possible to resolve the metabolism of individual neurons or astrocytes.

7.3. Dual Photon NADH Fluorescence Microscopy

Dual photon fluorescence microscopy is able to provide cellular resolution of fluorescent indicators at moderate tissue depths smaller than 0.5 mm (Gratton *et al.* 2001; Kim and Schwille 2003). The technique is based on classical approaches used previously to measure surface fluorescence (single photon) of NADH (Chance 2004). Dual photon fluorescence microscopy uses pulsed laser excitation with two photons, the emission being detected with confocal optics. Advantages of the technique over classical single photon fluorescence involve deeper penetration (because of the lower wavelength of the excitation pulses), lower "bleaching" and the possibility to use longer examination times because of the lower energy involved. NADH fluorescence is particularly attractive from the point of view of TCA cycle activity measurements. A net increase in glycolytic activity is revealed by increased NADH fluorescence and a net increase in TCA cycle activity is associated to a decrease in NADH fluorescence. Notably, the important limitation of dual photon NADH fluorescence stems from the fact that only net increases or decreases in NADH can be measured. This reveals the net metabolic balance between NADH producing and consuming pathways only, but not the individual activities of glycolysis or the TCA cycle. Thus, it is not appropriate to interpret net NADH changes as revealing exclusively glycolytic or TCA cycle activity, since they could contain opposite contributions from either or both processes.

8. The Cerebral Tricarboxylic Acid Cycles During Cerebral Activation

8.1. The Metabolic Coupling Hypothesis

Figure 1.10 summarizes the main aspects of the Astrocyte to Neuron Lactate Shuttle (ANLS) metabolic coupling hypothesis between neurons and glia during glutamatergic neurotransmission, according the early formulations of Pellerin, Tsacopoulos and Magistretti (Pellerin and Magistretti 1994; Tsacopoulos and Magistretti 1996). Their interpretation was based on pioneering experiments on the honey bee drone retina, demonstrating that these Muller cells released alanine to the medium during photostimulation (Tsacopoulos *et al.* 1994). These results were soon confirmed with preparations of brain astrocytes, showing that these cells liberated lactate (instead of alanine)

to the incubation medium after a glutamate challenge (Pellerin and Magistretti 1994). Together, these findings matched well with earlier evidences on cerebral activation *in vivo* as derived from autoradiography, PET, fMRI and NMR Spectroscopy (Magistretti and Pellerin 1999; Magistretti and Pellerin 2000).

After presynaptic action potential on glutamatergic neurons, glutamate is released to the synaptic cleft and then recaptured by the surrounding astrocytes. Presynaptic glutamate release largely exceeds the amount needed for neurotransmission, making extracellular glutamate levels to increase transiently from approximately 4-5 μM in the resting state, to well over 100 μM just after its release from presynaptic vesicles. These high glutamate concentrations could preclude further neurotransmission events or even become neurotoxic, unless rapidly cleared from the

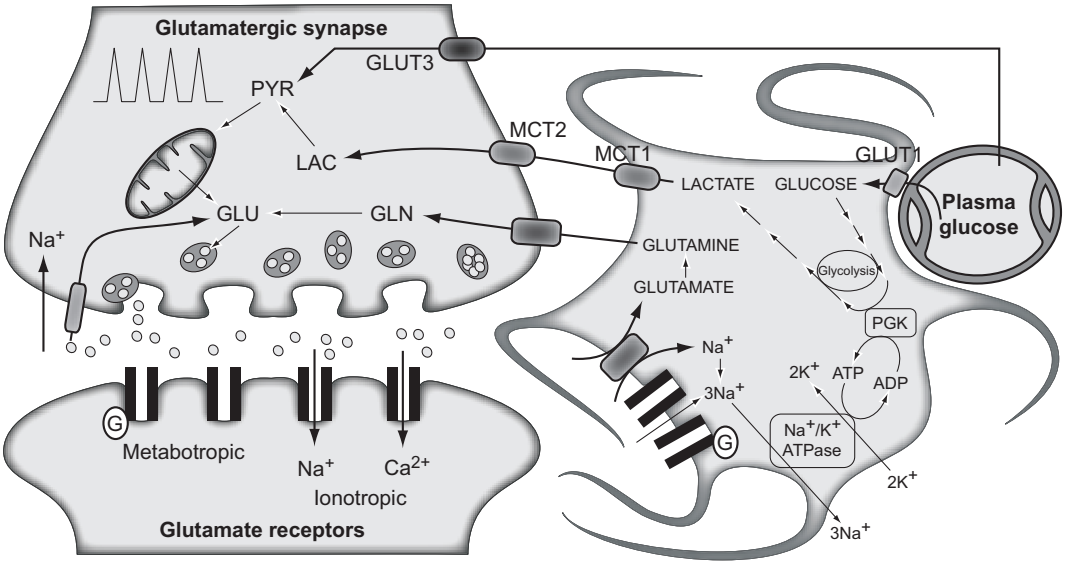

Figure 1.10. The traditional metabolic coupling hypothesis between neurons and glial cells during glutamatergic neurotransmission. Glutamate released to the synaptic cleft during glutamatergic neurotransmission is co-transported with Na^+ to the astrocytes. Astroglial Na^+ is exchanged by extracellular K^+ through the Na^+/K^+ ATPase, consuming one ATP molecule. Astrocytic glutamate produces glutamine through glutamine syntethase, consuming one additional ATP molecule. Lactate produced exclusively in astroglial glycolysis to support these energy demands, is extruded to the extracellular medium, taken up by the surrounding neurons and oxidized as their main metabolic fuel. Note the apparent stoichiometric coupling between glutamate-glutamine cycling and glucose uptake as well as the exclusive *glycolytic* or *oxidative* metabolisms in astrocytes and neurons, respectively. MCT1 and MCT2: monocarboxylate transporters 1 and 2. GLUT 1 and GLUT 3: glucose transporters 1 and 3. PGK: Phosphoglycerate kinase. Adapted with permission from (Tsacopoulos and Magistretti 1996).

synapses. This vital task is performed by the astrocytes surrounding the synapses, which are able to remove the large excess of synaptic glutamate through their highly efficient glutamate transporters. Glutamate is co-transported to the astrocyte together with three Na^+, which need to be returned into the extracellular medium in order to restore the membrane potential. This is thought to involve the activity of the Na^+/K^+ ATPase, at the expense of one ATP molecule. Once in the astrocyte, glutamate is amidated to glutamine by glutamine synthetase, an exclusively astrocytic enzyme consuming one additional ATP molecule. Thus, complete transformation of astrocytic glutamate into glutamine demands two ATP molecules, which were originally proposed to be derived exclusively from the anaerobic metabolism of glucose. According to this proposal, astrocytes would only need the anaerobic degradation of one glucose molecule taken from nearby capillaries to transform one glutamate molecule into glutamine, in a process producing two lactate molecules. Glutamine or lactate released from astrocytes would be taken up by the neurons, to regenerate neurotransmitter glutamate or become oxidized in the neuronal TCA cycle to maintain neuronal energetics, respectively. On these grounds, glutamatergic neurotransmission was proposed to be stoichiometrically coupled to astrocytic glucose uptake and lactate production, the latter becoming the main oxidative fuel for neurons (Magistretti *et al.* 1999; Rothman *et al.* 1999; Shulman *et al.* 2004).

8.2. ^{13}C NMR Evidences and the Neuronal Tricarboxylic Acid Cycle

Early *in vivo* ^{13}C NMR experiments provided support to this hypothesis (Sibson *et al.* 1997; Sibson *et al.* 1998a). Authors infused (1-^{13}C) glucose and followed its brain metabolism using ^{13}C NMR. It was possible to observe the accumulation of ^{13}C label in the C4 carbons of glutamate and glutamine (Figures 1.11-A and 1.11-B). The turnover of the C4 carbon of glutamate was considered to reflect the activity of the neuronal TCA cycle (V_{TCAn}) while the turnover of the glutamine C4 carbon was thought to indicate the turnover of the glutamate-glutamine cycle (V_{cycle}). The results obtained confirmed earlier measurements of the cerebral TCA cycle flux *in vivo* (V_{TCAn} = 0.5-0.6 μmol.min^{-1}.g^{-1}), assuming its predominant neuronal location under these conditions. It was also possible to calculate the flux through glutamine synthetase (0.2 μmol. min^{-1}.g^{-1}), describing that it accounted for a major part of glutamate turnover in the brain. These *in vivo* results were consistent with the stoichiometric coupling of glucose metabolism and glutamate-glutamine cycle. Further experiments monitored dynamically the cerebral metabolism of (1-^{13}C) glucose in rats subjected to increasing degrees of anesthesia obtained with α-chloralose, morphine or pentobarbital (Figure 1.11-C). Quantitative analysis of the time courses of ^{13}C enrichments in glutamate and glutamine C4, with the help of a minimal mathematical model of the neuronal TCA cycle and the glial glutamine synthetase, revealed that the glutamate-glutamine cycle is a major pathway of cerebral metabolism accounting for up to eighty percent of the energy derived from

glucose oxidation in the brain (Rothman *et al.* 2003).

An important aspect of these studies concerned the energetics of glutamatergic neurotransmission. For a TCA cycle flux of 0.6 μmol.min^{-1}.g^{-1} and a glutamate-glutamine cycle flux of 0.2 μmol.min^{-1}.g^{-1}, the cerebral oxidative ATP production capacity approaches 20.4 μmol.min^{-1}.g^{-1}, while the ATP demand for glutamine synthesis is 0.4 μmol.min^{-1}.g^{-1}. Thus, glutamine production and the glutamate-glutamine cycle account only for approximately 2% of the energy produced during glucose oxidation, the rest being invested in the maintenance of presynaptic and postsynaptic resting, action potentials, as well as other processes associated to neurotransmission.

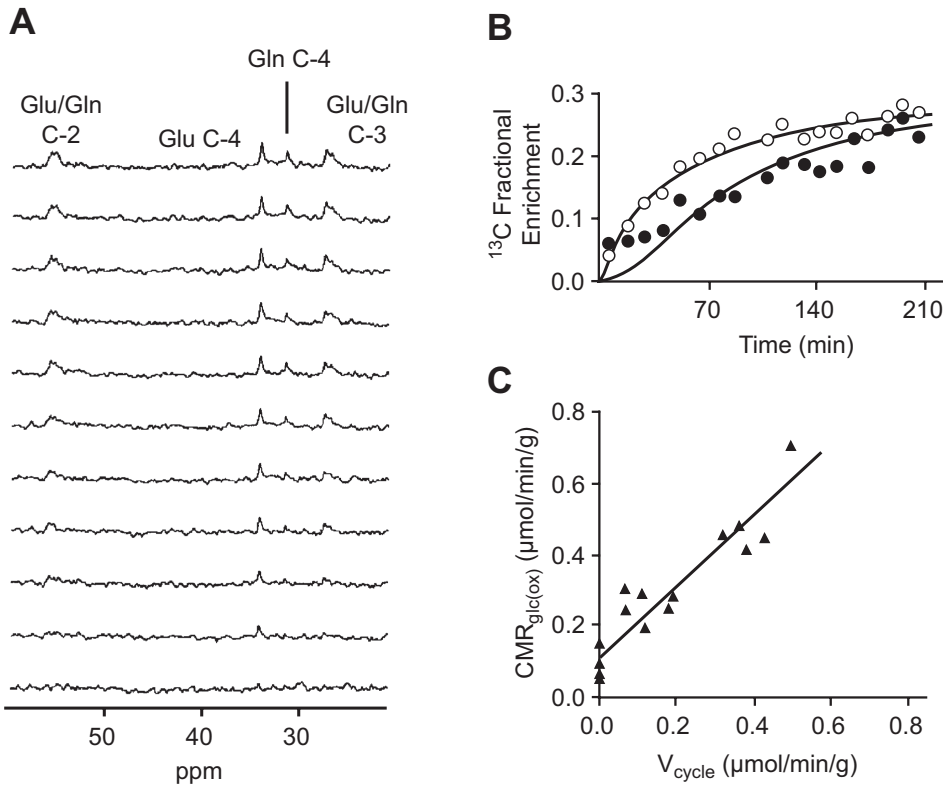

Figure 1.11. The cerebral tricarboxylic acid cycle and glutamatergic neurotransmission as detected by *in vivo* ^{13}C NMR. **A:** Consecutive ^{13}C NMR spectra of rat brain during (1-^{13}C) glucose infusion (Sibson *et al.* 1997). **B:** *In vivo* kinetics of ^{13}C enrichment in cerebral glutamate C4 and glutamine C4 during (1-^{13}C) glucose infusion, thought to represent the neuronal TCA cycle and the glutamine cycle, respectively (Sibson *et al.* 1997). **C:** Apparent stoichiometric relationship between the Cerebral Metabolic Rate for glucose oxidation (CMR$_{glc}$) and the glutamate-glutamine cycle flux (V$_{cycle}$), during the metabolism of (1-^{13}C) glucose in the brain of rats subjected to increasing degrees of anesthesia (Sibson *et al.* 1998a). Reproduced with permission of the publisher.

This balance matches well the calculations of Attwell and Iadecola who proposed an energy budget to interpret the energetics of cerebral activation as observed in fMRI experiments (Atwell and Iadecola 2002). Their conclusions indicated that in rodents, 2% of cerebral energy is dedicated to

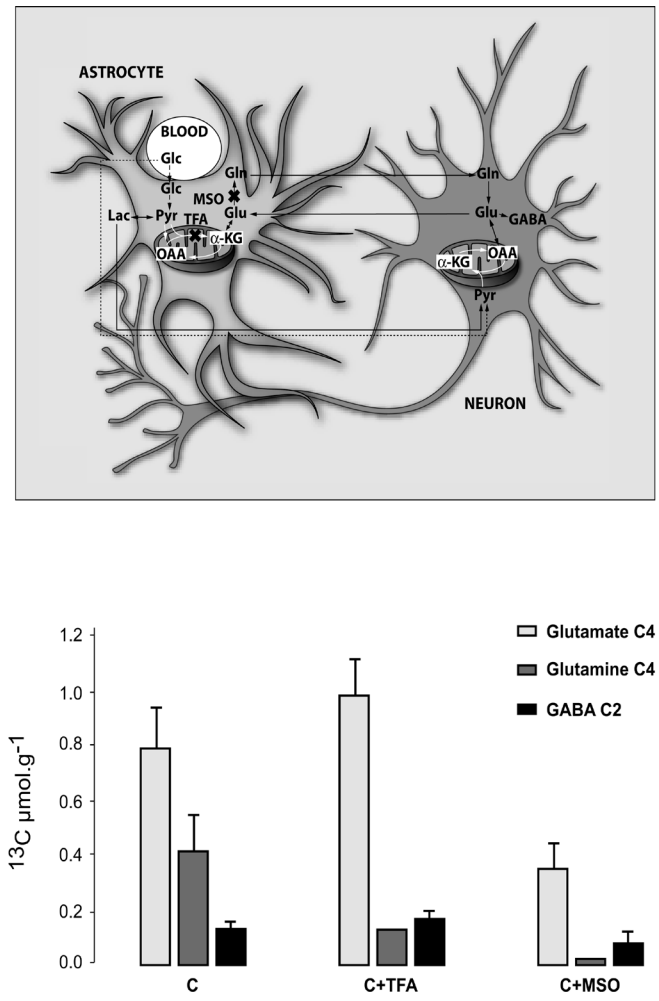

Figure 1.12. Role of the astroglial tricarboxylic acid cycle supporting glutamatergic neurotransmission. Trifluoacetic acid (TFA) or methionine sulfoximine (MSO) strategies to inhibit the astroglial TCA cycle or glutamine syntethase, respectively (upper panel). Effects of TFA or MSO on the steady state labeling of (4-^{13}C) glutamate, (4-^{13}C) glutamine and (2-^{13}C) GABA after (1-^{13}C) glucose infusions (lower panels). Reproduced from (Garcia-Espinosa *et al.* 2003) with permission of the publisher.

maintaining the glutamate-glutamine cycle, the remaining being invested in maintaining the resting membrane potential or presynaptic and postsynaptic action potentials.

8.3. The Astroglial Tricarboxylic Acid Cycle

An important limitation of these interpretations based on fMRI experiments relied on the neglected role of the astroglial TCA cycle during glutamine synthesis and under conditions of cerebral activation. To address this aspect more specifically, other authors infused (1-^{13}C) glucose in the presence and absence of trifluoroacetic acid (TFA), a selective inhibitor of the astroglial TCA cycle or methionine sulfoximine (MSO), a selective inhibitor of glutamine synthetase (García-Espinosa *et al.* 2003). TFA inhibited ca. 60% of glutamine synthesis, revealing a predominant contribution of the glial TCA cycle to the energy used in glutamine synthesis (Figure 1.12). This finding introduced an important modification over pre-existing concepts which considered glutamine synthesis exclusively dependent on glycolytic ATP production (García-Espinosa *et al.* 2004). These results also showed that complete inhibition of glutamine synthesis with MSO did not abort glutamate turnover, as it would be expected for a precise stoichiometric coupling of the glutamate-glutamine cycle. In contrast, the experiments showed that approximately 40% of cerebral glutamate was not derived from astroglial glutamine, suggesting that additional neuronal precursors such as glucose or lactate, should play an important role in its synthesis. Notably, non-stoichiometric coupling of the glutamine cycle with glucose uptake has also been found during (1-^{13}C) glucose metabolism, with very similar data and a different model of cerebral metabolism (Gruetter *et al.* 2001). Taken together these studies disclosed an important role for the astroglial TCA cycle supporting astrocytic energetics and glutamine synthesis, revealing that the coupling mechanisms between neurons and glial cells during glutamatergic neurotransmission were more complex than those initially envisioned.

9. Aim, Scope and Outline of Thesis

This thesis covers mainly pyruvate and lactate metabolism in the neuronal and glial compartments as well as their intercellular interactions. Monocarboxylate exchange and metabolism represent a crucial cross roads of cerebral metabolism, participating in intercellular signalling and coupling processes as well as energetic substrates. The central role of monocarboxylates and their different functions complicate the methods to analyze unambiguously each one of the

contributions to their overall cerebral metabolism. To overcome these limitations I combined in this thesis the classical neurochemical approach with more recent methodologies, including mainly ^{13}C and (^{13}C,^{2}H) NMR strategies. I emphasize an integrative interpretation of previous neuroglial metabolic coupling hypotheses with the results communicated in this work, including the presence of subcellular compartmentation of pyruvate and glutamate and monocarboxylate recycling through the plasma membrane.

The goal of each chapter is to stand as an individual contribution with independence of the others, to facilitate independent reading. In order to present the thesis as a collection of self-standing, and independent chapters, the corresponding methodology, results and reference sections are included in each chapter. Nevertheless, the overall and progressive reading of this thesis will provide the interested reader with a wider coverage and a better understanding of "the entire story".

Chapter 1 contains an introductory section with a fundamental overview to define the state-of-the-art of the general brain functions and metabolism. The main pathways of the brain energetics and the techniques applied for its study are described in detail. In particular, an integrative description of the cerebral metabolism, centered in pyruvate is presented and the NMR methods are explained, in order to allow better analysis and discussion in the following chapters.

Lactate recycling between extracellular space and the cytosolic pools of pyruvate through the monocarboxylate transporters of the plasma membrane and the lactate dehydrogenase isozymes are discussed in **Chapters 2 and 3**. For this purpose, novel (^{13}C,^{2}H) and ^{1}H NMR approaches were developed and implemented to characterize this recycling process. In particular, using (^{13}C,^{2}H) NMR we were able to demonstrate that the deuteration process involved in lactate recycling is redox sensitive.

The results gathered in the previous chapters lead us to propose a novel hypothesis describing the mechanisms underlying the neuroglial coupling in the brain, including the presence of subcellular compartmentation of pyruvate and monocarboxylate recycling through the plasma membrane of both neurons and glial cells. **Chapter 4** is then dedicated to the investigation of the mechanisms underlying this Redox Switch/Redox Coupling hypothesis, as well as its kinetic properties, in primary cultures of cortical neurons and astrocytes from rat brain. Additionally, we also analyzed the current interpretations on the cellular and subcellular compartmentation of TCA cycle during glutamatergic neurotransmission, on the basis of the novel transcellular redox coupling mechanism.

Finally, **Chapter 5** focuses on the interactions between dopaminergic and glutamatergic neurotransmission systems. Despite the neurobiological and clinical relevance of these interactions, the underlying mechanisms remain poorly understood. Our approach, combining ^{13}C NMR spectroscopy, molecular biology and behavioural techniques provided new insight into the mechanisms of interaction between glutamatergic and dopaminergic systems.

10. References

Akiba T, Hiraga K, Tuboi S. 1984. Intracellular distribution of fumarase in various animals. J Biochem (Tokyo) 96(1):189-195.

Ali G, Wasco W, Cai X, Szabo P, Sheu KF, Cooper AJ, Gaston SM, Gusella JF, Tanzi RE, Blass JP. 1994. Isolation, characterization, and mapping of gene encoding dihydrolipoyl succinyltransferase (E2k) of human alpha-ketoglutarate dehydrogenase complex. Somat Cell Mol Genet 20(2):99-105.

Almeida A, Medina JM. 1997. Isolation and characterization of tightly coupled mitochondria from neurons and astrocytes in primary culture. Brain Res 764(1-2):167-172.

Almeida A, Medina JM. 1998. A rapid method for the isolation of metabolically active mitochondria from rat neurons and astrocytes in primary culture. Brain Res Brain Res Protoc 2(3):209-214.

Au HC, Ream-Robinson D, Bellew LA, Broomfield PL, Saghbini M, Scheffler IE. 1995. Structural organization of the gene encoding the human iron-sulfur subunit of succinate dehydrogenase. Gene 159(2):249-253.

Bachelard HS. 1989. Measurement of Carbohydrates and their derivatives in Neuronal Tissues. In: Boulton AA, Baker GB, Butterworth RF, editors. Carbohydrates and Energy Metabolism. Clifton (N.J.): Humana Press. p 133-154.

Bachelard HS, Lewis LD, Ponten U, Siesjo BK. 1974. Mechanisms activating glycolysis in the brain in arterial hypoxia. J Neurochem 22(3):395-401.

Badar-Goffer RS, Bachelard HS, Morris PG. 1990. Cerebral metabolism of acetate and glucose studied by ^{13}C-N.M.R. spectroscopy. A technique for investigating metabolic compartmentation in the brain. Biochem J 266(1):133-139.

Barrientos A. 2002. *In vivo* and *in organello* assessment of OXPHOS activities. Methods 26(4):307-316.

Ben-Yoseph O, Badar-Goffer RS, Morris PG, Bachelard HS. 1993. Glycerol 3-phosphate and lactate as indicators of the cerebral cytoplasmic redox state in severe and mild hypoxia respectively: a ^{13}C- and ^{31}P-N.M.R. study. Biochem J 291 (Pt 3):915-919.

Benn P, Chern CJ, Bruns G, Craig IW, Croce CM. 1977. Assignment of the genes for human beta-glucuronidase and mitochondrial malate dehydrogenase to the region pter leads to q22 of chromosome 7. Cytogenet Cell Genet 19(5):273-280.

Berkich DA, Xu Y, Lanoue KF, Gruetter R, Hutson SM. 2005. Evaluation of brain mitochondrial glutamate and alpha-ketoglutarate transport under physiologic conditions. J Neurosci Res 79(1-2):106-113.

Berl S. 1965. Compartmentation of Glutamic Acid Metabolism in Developing Cerebral Cortex. J Biol Chem 240:2047-2054.

Berl S, Clarke DD. 1969. Compartmentation of amino acid metabolism. In: Lajhta AL, editor. Handbook of Neurochemistry. New York: Plenum Press. p 447-472.

Berl S, Nicklas WJ, Clarke DD. 1968. Compartmentation of glutamic acid metabolism in brain slices. J Neurochem 15(2):131-140.

Berl S, Nicklas WJ, Clarke DD. 1970. Compartmentation of citric acid cycle metabolism in brain: labelling of glutamate, glutamine, aspartate and gaba by several radioactive tracer metabolites. J Neurochem 17(7):1009-1015.

Bittar PG, Charnay Y, Pellerin L, Bouras C, Magistretti PJ. 1996. Selective distribution of lactate dehydrogenase isoenzymes in neurons and astrocytes of human brain. J Cereb Blood Flow Metab 16(6):1079-1089.

Bluml S, Moreno-Torres A, Shic F, Nguy CH, Ross BD. 2002. Tricarboxylic acid cycle of glia in the *in vivo* human brain. NMR Biomed 15(1):1-5.

Bonavita V, Ponte F, Amore G. 1964. Lactate Dehydrogenase Isoenzymes in the Nervous Tissue. IV. An Ontogenetic Study on the Rat Brain. J Neurochem 11:39-47.

Brenner V, Nyakatura G, Rosenthal A, Platzer M. 1997. Genomic organization of two novel genes on human Xq28: compact head to head arrangement of IDH gamma and TRAP delta is conserved in rat and mouse. Genomics 44(1):8-14.

Brooks GA. 2002. Lactate shuttles in nature. Biochem Soc Trans 30(2):258-264.

Brooks GA, Dubouchaud H, Brown M, Sicurello JP, Butz CE. 1999. Role of mitochondrial lactate dehydrogenase and lactate oxidation in the intracellular lactate shuttle. Proc Natl Acad Sci U S A 96(3):1129-1134.

Burtscher IM, Holtas S. 2001. Proton MR spectroscopy in clinical routine. J Magn Reson Imaging 13(4):560-567.

Cerdán S. 2003. ^{13}C NMR and cerebral biochemistry. NMR Biomed 16(6-7):301-302.

Cerdán S, Kunnecke B, Seelig J. 1990. Cerebral metabolism of [1,2-$^{13}C_2$]acetate as detected by *in vivo* and *in vitro* ^{13}C NMR. J Biol Chem 265(22):12916-12926.

Cerdán S, Rodrigues TB, Ballesteros P, Lopez P, Perez-Mayoral E. 2003. The subcellular metabolism of water and its implications for magnetic resonance image contrast. In: Belton PS, Gil AM, Webb GA, Rutledge D, editors. Magnetic Resonance in Food Science. Oxford: Royal Society of Chemistry. p 121-135.

Chance B. 2004. Mitochondrial NADH redox state, monitoring discovery and deployment in tissue. Methods Enzymol 385:361-370.

Chapa F, Cruz F, García-Martín ML, García-Espinosa MA, Cerdán S. 2000. Metabolism of (1-^{13}C) glucose and (2-^{13}C, 2-$^{2}H_3$) acetate in the neuronal and glial compartments of the adult rat brain as detected by [^{13}C, ^{2}H] NMR spectroscopy. Neurochem Int 37(2-3):217-228.

Chapa F, Kunnecke B, Calvo R, Escobar del Rey F, Morreale de Escobar G, Cerdán S. 1995. Adult-onset hypothyroidism and the cerebral metabolism of (1,2-$^{13}C_2$) acetate as detected by ^{13}C nuclear magnetic resonance. Endocrinology 136(1):296-305.

Chhina N, Kuestermann E, Halliday J, Simpson LJ, Macdonald IA, Bachelard HS, Morris PG. 2001. Measurement of human tricarboxylic acid cycle rates during visual activation by ^{13}C magnetic resonance spectroscopy. J Neurosci Res 66(5):737-746.

Clark JB, Bates TE, Almeida A, Cullingford T, Warwick J. 1994. Energy metabolism in the developing mammalian brain. Biochem Soc Trans 22(4):980-983.

Clark JB, Bates TE, Cullingford T, Land JM. 1993. Development of enzymes of energy metabolism in the neonatal mammalian brain. Dev Neurosci 15(3-5):174-180.

Clark JB, Lai JCK. 1989. Glycolytic, tricarboxylic acid cycle and related enzymes in brain. In: Boulton AA, Baker GB, Butterworth RF, editors. Carbohydrates and Energy Metabolism. Clifton (N.J.): Humana Press. p 233-281.

Clarke DD, Lajhta AL, Maker HS. 1989. Intermediary metabolism. In: Siegel G, Agranoff B, Albers RW, Molinoff P, editors. Basic Neurochemistry. New York: Raven Press. p 541-564.

Consortium IHGS. 2001. Initial sequencing and analysis of the human genome. Nature 409:860-921.

Consortium MGS. 2002. Initial sequencing and comparative analysis of the mouse genome. Nature 420:520-562.

Cremer JE, Cunningham VJ, Pardridge WM, Braun LD, Oldendorf WH. 1979. Kinetics of blood-brain barrier transport of pyruvate, lactate and glucose in suckling, weanling and adult rats. J Neurochem 33(2):439-445.

Crone C, Sorensen SC. 1970. The permeability of the blood-brain barrier to lactate and pyruvate. Acta Physiol Scand 80(4):47A.

Cruz F, Cerdán S. 1999. Quantitative ^{13}C NMR studies of metabolic compartmentation in the adult mammalian brain. NMR Biomed 12(7):451-462.

Cruz F, Scott SR, Barroso I, Santisteban P, Cerdán S. 1998. Ontogeny and cellular localization of the pyruvate recycling system in rat brain. J Neurochem 70(6):2613-2619.

Dawson DM, Goodfriend TL, Kaplan NO. 1964. Lactic Dehydrogenases: Functions of the Two Types Rates of Synthesis of the Two Major Forms Can Be Correlated with Metabolic Differentiation. Science 143:929-933.

de Gomez-Puyou MT, Chavez E, Freites D, Gomez-Puyou A. 1972. On the regulation of succinate dehydrogenase in brain mitochondria. FEBS Lett 22(1):57-60.

de Graaf RA, Mason GF, Patel AB, Behar KL, Rothman DL. 2003. *In vivo* ^{1}H-[^{13}C]-NMR spectroscopy of cerebral metabolism. NMR Biomed 16(6-7):339-357.

De Meirleir L. 2002. Defects of pyruvate metabolism and the Krebs cycle. J Child Neurol 17 Suppl 3:3S26-33; discussion 23S33-24.

Denton RM, Halestrap AP. 1979. Regulation of pyruvate metabolism in mammalian tissues. Essays in Biochem 15:37-77.

Desagher S, Glowinski J, Premont J. 1997. Pyruvate protects neurons against hydrogen peroxide-induced toxicity. J Neurosci 17:9060-9067.

Dienel GA. 2002. Energy generation in the Central Nervous System. In: Edvinsson L, Krause DN, editors. Cerebral Blood Flow and Metabolism. Philadelphia: Lippincott Williams & Wilkins. p 141-171.

Dienel GA, Liu K, Cruz NF. 2001. Local uptake of ^{14}C-labeled acetate and butyrate in rat brain *in vivo* during spreading cortical depression. J Neurosci Res 66(5):812-820.

Dringen R, Schmoll D, Cesar M, Hamprecht B. 1993. Incorporation of radioactivity from [^{14}C]lactate into the glycogen of cultured mouse astroglial cells. Evidence for gluconeogenesis in brain cells. Biol Chem Hoppe Seyler 374(5):343-347.

Dwyer DS, Vannucci SJ, Simpson IA. 2002. Expression, regulation, and functional role of glucose transporters (GLUTs) in brain. Int Rev Neurobiol 51:159-188.

Dziembowska T, Hansen PE, Rozwadowski Z. 2004. Studies based on deuterium isotope effect on ^{13}C chemical shifts. Progress in Nuclear Magnetic Resonance Spectroscopy 45:1-29.

Elbehti-Green A, Au HC, Mascarello JT, Ream-Robinson D, Scheffler IE. 1998. Characterization of the human SDHC gene encoding of the integral membrane proteins of succinate-quinone oxidoreductase in mitochondria. Gene 213(1-2):133-140.

Enerson BE, Drewes LR. 2003. Molecular features, regulation, and function of monocarboxylate transporters: implications for drug delivery. J Pharm Sci 92(8):1531-1544.

Erecinska M, Silver IA. 1990. Metabolism and role of glutamate in mammalian brain. Prog Neurobiol 35(4):245-296.

Everse J, Kaplan NO. 1973. Lactate dehydrogenases: structure and function. Adv Enzymol Relat Areas Mol Biol 37:61-133.

Fayol L, Baud O, Monier A, Pellerin L, Magistretti P, Evrard P, Verney C. 2004. Immunocytochemical expression of monocarboxylate transporters in the human visual cortex at midgestation. Brain Res Dev Brain Res 148(1):69-76.

Feigenbaum AS, Robinson BH. 1993. The structure of the human dihydrolipoamide dehydrogenase gene (DLD) and its upstream elements. Genomics 17(2):376-381.

Fitzpatrick SM, Hetherington HP, Behar KL, Shulman RG. 1990. The flux from glucose to glutamate in the rat brain *in vivo* as determined by ^{1}H-observed, ^{13}C-edited NMR spectroscopy. J Cereb Blood Flow Metab 10(2):170-179.

Gamberino WC, Berkich DA, Lynch CJ, Xu B, LaNoue KF. 1997. Role of pyruvate carboxylase in facilitation of synthesis of glutamate and glutamine in cultured astrocytes. J Neurochem 69(6):2312-2325.

García-Espinosa MA, García-Martín ML, Cerdán S. 2003. Role of glial metabolism in diabetic encephalopathy as detected

by high resolution ^{13}C NMR. NMR Biomed 16(6-7):440-449.

García-Espinosa MA, Rodrigues TB, Sierra A, Benito M, Fonseca C, Gray HL, Bartnik BL, García-Martín ML, Ballesteros P, Cerdán S. 2004. Cerebral glucose metabolism and the glutamine cycle as detected by *in vivo* and *in vitro* ^{13}C NMR spectroscopy. Neurochem Int 45(2-3):297-303.

García-Martín ML, Ballesteros P, Cerdán S. 2001. The metabolism of water in cells and tissues as detected by NMR methods. Prog Nucl Mag Res Spectroscopy 39:41-77.

García-Martín ML, Ballesteros P, Cerdán S. 2001. The metabolism of water in cells and tissues as detected by NMR methods. Progress in NMR Spectrosc 39:41-77.

García-Martín ML, García-Espinosa MA, Ballesteros P, Bruix M, Cerdán S. 2002. Hydrogen turnover and subcellular compartmentation of hepatic [2-^{13}C]glutamate and [3-^{13}C]aspartate as detected by ^{13}C NMR. J Biol Chem 277(10):7799-7807.

Garfinkel D. 1966. A simulation study of the metabolism and compartmentation in brain of glutamate, aspartate, the Krebs cycle, and related metabolites. J Biol Chem 241(17):3918-3929.

Gibson GE, Park LC, Sheu KF, Blass JP, Calingasan NY. 2000. The alpha-ketoglutarate dehydrogenase complex in neurodegeneration. Neurochem Int 36(2):97-112.

Goldenthal MJ, Marin-García J, Ananthakrishnan R. 1998. Cloning and molecular analysis of the human citrate synthase gene. Genome 41(5):733-738.

Gratton E, Barry NP, Beretta S, Celli A. 2001. Multiphoton fluorescence microscopy. Methods 25(1):103-110.

Gruetter R. 2002. *In vivo* ^{13}C NMR studies of compartmentalized cerebral carbohydrate metabolism. Neurochem Int 41(2-3):143-154.

Gruetter R, Adriany G, Choi IY, Henry PG, Lei H, Oz G. 2003. Localized *in vivo* ^{13}C NMR spectroscopy of the brain. NMR Biomed 16(6-7):313-338.

Gruetter R, Seaquist ER, Ugurbil K. 2001. A mathematical model of compartmentalized neurotransmitter metabolism in the human brain. Am J Physiol Endocrinol Metab 281(1):E100-112.

Gyulai L, Schnall M, McLaughlin AC, Leigh JS, Jr., Chance B. 1987. Simultaneous ^{31}P- and ^{1}H-nuclear magnetic resonance studies of hypoxia and ischemia in the cat brain. J Cereb Blood Flow Metab 7(5):543-551.

Halestrap AP, Meredith D. 2004. The SLC16 gene family-from monocarboxylate transporters (MCTs) to aromatic amino acid transporters and beyond. Pflugers Arch 447(5):619-628.

Halestrap AP, Price NT. 1999. The proton-linked monocarboxylate transporter (MCT) family: structure, function and regulation. Biochem J 343 Pt 2:281-299.

Hansen PE. 1983. Isotope Effects on Nuclear Shielding. Ann Rep NMR Spectrosc 15:105-234.

Hassel B. 2000. Carboxylation and anaplerosis in neurons and glia. Mol Neurobiol 22(1-3):21-40.

Hatazawa J, Fujita H, Kanno I, Satoh T, Iida H, Miura S, Murakami M, Okudera T, Inugami A, Ogawa T, *et al.* 1995. Regional cerebral blood flow, blood volume, oxygen extraction fraction, and oxygen utilization rate in normal volunteers measured by the autoradiographic technique and the single breath inhalation method. Ann Nucl Med 9(1):15-21.

Heeger DJ, Ress D. 2002. What does fMRI tell us about neuronal activity. Nature Reviews Neuroscience 3:142-151.

Herholz K, Heiss WD. 2004. Positron emission tomography in clinical neurology. Mol Imaging Biol 6(4):239-269.

Hertz L. 2004. Intercellular metabolic compartmentation in the brain: past, present and future. Neurochem Int 45(2-3):285-296.

Hertz L, Dienel GA. 2002. Energy metabolism in the brain. Int Rev Neurobiol 51:1-102.

Hertz L, Hertz E. 2003. Cataplerotic TCA cycle flux determined as glutamate-sustained oxygen consumption in primary cultures of astrocytes. Neurochem Int 43(4-5):355-361.

Hilberman M, Subramanian VH, Haselgrove J, Cone JB, Egan JW, Gyulai L, Chance B. 1984. *In vivo* time-resolved brain phosphorus nuclear magnetic resonance. J Cereb Blood Flow Metab 4(3):334-342.

Hirawake H, Taniwaki M, Tamura A, Amino H, Tomitsuka E, Kita K. 1999. Characterization of the human SDHD gene encoding the small subunit of cytochrome b (cybS) in mitochondrial succinate-ubiquinone oxidoreductase. Biochim Biophys Acta 1412(3):295-300.

Hyder F, Chase JR, Behar KL, Mason GF, Siddeek M, Rothman DL, Shulman RG. 1996. Increased tricarboxylic acid cycle flux in rat brain during forepaw stimulation detected with $^{1}H[^{13}C]$NMR. Proc Natl Acad Sci U S A 93(15):7612-7617.

Hyder F, Rothman DL, Mason GF, Rangarajan A, Behar KL, Shulman RG. 1997. Oxidative glucose metabolism in rat brain during single forepaw stimulation: a spatially localized $^{1}H[^{13}C]$ nuclear magnetic resonance study. J Cereb Blood Flow Metab 17(10):1040-1047.

Izumi Y, Katsuki H, Zorumski CF. 1997. Monocarboxylates (pyruvate and lactate) as alternative energy substrates for the induction of long-term potentiation in rat hippocampal slices. Neurosci Lett 232:17-20.

James M, Man NT, Edwards YH, Morris GE. 1997. The molecular basis for cross-reaction of an anti-dystrophin antibody with alpha-actinin. Biochim Biophys Acta 1360(2):169-176.

Johnson JD, Mehus JG, Tews K, Milavetz BI, Lambeth DO. 1998. Genetic evidence for the expression of ATP- and GTP-specific succinyl-CoA synthetases in multicellular eucaryotes. J Biol Chem 273(42):27580-27586.

Kim SA, Schwille P. 2003. Intracellular applications of fluorescence correlation spectroscopy: prospects for neuroscience. Curr Opin Neurobiol 13(5):583-590.

Kim YO, Oh IU, Park HS, Jeng J, Song BJ, Huh TL. 1995. Characterization of a cDNA clone for human NAD^{+}-specific isocitrate dehydrogenase alpha-subunit and structural comparison with its isoenzymes from different species. Biochem J 308 (Pt 1):63-68.

Kim YO, Park SH, Kang YJ, Koh HJ, Kim SH, Park SY, Sohn U, Huh TL. 1999. Assignment of mitochondrial NAD^{+}-specific isocitrate dehydrogenase beta subunit gene (IDH3B) to human chromosome band 20p13 by *in situ* hybridization and radiation hybrid mapping. Cytogenet Cell Genet 86(3-4):240-241.

Kinsella BT, Doonan S. 1986. Nucleotide sequence of a cDNA coding for mitochondrial fumarase from human liver. Biosci Rep 6(10):921-929.

Kirk P, Wilson MC, Heddle C, Brown MH, Barclay AN, Halestrap AP. 2000. CD147 is tightly associated with lactate transporters MCT1 and MCT4 and facilitates their cell surface expression. Embo J 19(15):3896-3904.

Komatsumoto S, Nioka S, Greenberg JH, Yoshizaki K, Subramanian VH, Chance B, Reivich M. 1987. Cerebral energy metabolism measured *in vivo* by ^{31}P-NMR in middle cerebral artery occlusion in the cat - relation to severity of stroke. J Cereb Blood Flow Metab 7(5):557-562.

Krebs HA. 1964. The citric acid cycle. Nobel Lectures, Physiology or Medicine 1942-1962. Amsterdam: Elsevier. p 399-410.

Krebs HA. 1970. Rate control of the tricarboxylic acid cycle. Adv Enzyme Regul 8:335-353.

Krebs HA, Johnson WA. Metabolism of ketonic acids in animal tissue. 1937. Biochem J 31:645.

Lai CK, Clark JB. 1989. Isolation and characterization of synaptic and nonsynaptic mitochondria from mammalian brain. In: Boulton AA, Baker GB, Butterworth RF, editors. Carbohydrates and Energy Metabolism. Clifton (N.J.): Humana Press. p 43-98.

LaNoue KF, Schoolwerth AC. 1979. Metabolite transport in mitochondria. Annu Rev Biochem 48:871-922.

Laughton JD, Charnay Y, Belloir B, Pellerin L, Magistretti PJ, Bouras C. 2000. Differential messenger RNA distribution of lactate dehydrogenase LDH-1 and LDH-5 isoforms in the rat brain. Neuroscience 96(3):619-625.

Lebon V, Petersen KF, Cline GW, Shen J, Mason GF, Dufour S, Behar KL, Shulman GI, Rothman DL. 2002. Astroglial contribution to brain energy metabolism in humans revealed by ^{13}C nuclear magnetic resonance spectroscopy: elucidation of the dominant pathway for neurotransmitter glutamate repletion and measurement of astrocytic oxidative metabolism. J Neurosci 22(5):1523-1531.

Leino RL, Gerhart DZ, Drewes LR. 1999. Monocarboxylate transporter (MCT1) abundance in brains of suckling and adult rats: a quantitative electron microscopic immunogold study. Brain Res Dev Brain Res 113(1-2):47-54.

Mac M, Nalecz KA. 2003. Expression of monocarboxylic acid transporters (MCT) in brain cells. Implication for branched chain alpha-ketoacids transport in neurons. Neurochem Int 43(4-5):305-309.

Magistretti PJ, Pellerin L. 1999. Cellular mechanisms of brain energy metabolism and their relevance to functional brain imaging. Philos Trans R Soc Lond B Biol Sci 354(1387):1155-1163.

Magistretti PJ, Pellerin L. 2000. The astrocyte-mediated coupling between synaptic activity and energy metabolism operates through volume transmission. Prog Brain Res 125:229-240.

Magistretti PJ, Pellerin L, Rothman DL, Shulman RG. 1999. Energy on demand. Science 283(5401):496-497.

Malik P, McKenna MC, Tildon JT. 1993. Regulation of malate dehydrogenases from neonatal, adolescent, and mature rat brain. Neurochem Res 18(3):247-257.

Mason GF, Behar KL, Rothman DL, Shulman RG. 1992a. NMR determination of intracerebral glucose concentration and transport kinetics in rat brain. J Cereb Blood Flow Metab 12(3):448-455.

Mason GF, Gruetter R, Rothman DL, Behar KL, Shulman RG, Novotny EJ. 1995. Simultaneous determination of the rates of the TCA cycle, glucose utilization, alpha-ketoglutarate/glutamate exchange, and glutamine synthesis in human brain by NMR. J Cereb Blood Flow Metab 15(1):12-25.

Mason GF, Rothman DL, Behar KL, Shulman RG. 1992b. NMR determination of the TCA cycle rate and alpha-ketoglutarate/glutamate exchange rate in rat brain. J Cereb Blood Flow Metab 12(3):434-447.

Matsumoto K, Yamada K, Kohmura E, Kinoshita A, T. H. 1994. Role of pyruvate in ischemia like conditions on cultured neurons. Neurol Res 16:460-464.

Matsuoka Y, Srere PA. 1973. Kinetic studies of citrate synthase from rat kidney and rat brain. J Biol Chem 248(23):8022-8030.

McIlwain H, Bachelard HS. 1985. Biochemistry and the Central Nervoud System. London: Churchill-Livingstone.

Medina JM, Tabernero A, Tovar JA, Martín-Barrientos J. 1996. Metabolic fuel utilization and pyruvate oxidation during the postnatal period. J Inherit Metab Dis 19(4):432-442.

Mintun MA, Vlassenko AG, Rundle MM, Raichle ME. 2004. Increased lactate/pyruvate ratio augments blood flow in physiologically activated human brain. Proc Natl Acad Sci U S A 101(2):659-664.

Mirel DB, Marder K, Graziano J, Freyer G, Zhao Q, Mayeux R, Wilhelmsen KC. 1998. Characterization of the human mitochondrial aconitase gene (ACO2). Gene 213(1-2):205-218.

Moldes M, Cerdán S, Erhard P, Seelig J. 1994. ^{1}H-^{2}H exchange in the perfused rat liver metabolizing [3-^{13}C]alanine and $^{2}H_2O$ as detected by multinuclear NMR spectroscopy. NMR Biomed 7(6):249-262.

Moore CM, Frederick BB, Renshaw PF. 1999. Brain biochemistry using magnetic resonance spectroscopy: relevance to psychiatric illness in the elderly. J Geriatr Psychiatry Neurol 12(3):107-117.

Moore SA. 2001. Polyunsaturated fatty acid synthesis and release by brain-derived cells *in vitro*. J Mol Neurosci 16(2-3):195-200; discussion 215-121.

Morris AA, Farnsworth L, Ackrell BA, Turnbull DM, Birch-Machin MA. 1994. The cDNA sequence of the flavoprotein subunit of human heart succinate dehydrogenase. Biochim Biophys Acta 1185(1):125-128.

Morris P, Bachelard H. 2003. Reflections on the application of ^{13}C-MRS to research on brain metabolism. NMR Biomed 16(6-7):303-312.

Nicholls D. 2007. Bioenergetics. In: Lajhta A, Gibson G, Dienel G, editors. Brain Energetics Integration of Molecular and Cellular Processes. 3rd ed. New York: Springer. p 3-16.

Nioka S, Zaman A, Yoshioka H, Masumura M, Miyake H, Lockard S, Chance B. 1991. ^{31}P magnetic resonance spectroscopy study of cerebral metabolism in developing dog brain and its relationship to neuronal function. Dev Neurosci 13(2):61-68.

Okada Y, Lipton P. 2007. Glucose, Oxidative Energy Metabolism, and Neural Function in Brain Slices—Glycolysis Plays a Key Role in Neural Activity. In: Lajhta A, Gibson G, Dienel G, editors. Brain Energetics Integration of Molecular and Cellular Processes. 3rd ed. New York: Springer. p 17-39.

Owen OE, Kalhan SC, Hanson RW. 2002. The key role of anaplerosis and cataplerosis for citric acid cycle function. J Biol Chem 277(34):30409-30412.

Palmieri F. 1994. Mitochondrial carrier proteins. FEBS Lett 346(1):48-54.

Palmieri F. 2004. The mitochondrial transporter family (SLC25): physiological and pathological implications. Pflugers Arch 447(5):689-709.

Palmieri F, Bisaccia F, Capobianco L, Dolce V, Fiermonte G, Iacobazzi V, Indiveri C, Palmieri L. 1996. Mitochondrial metabolite transporters. Biochim Biophys Acta 1275(1-2):127-132.

Palmieri L, Pardo B, Lasorsa FM, del Arco A, Kobayashi K, Iijima M, Runswick MJ, Walker JE, Saheki T, Satrustegui J, Palmieri F. 2001. Citrin and aralar1 are Ca^{2+}-stimulated aspartate/glutamate transporters in mitochondria. Embo J 20(18):5060-5069.

Pascual JM, Carceller F, Roda JM, Cerdán S. 1998. Glutamate, glutamine, and GABA as substrates for the neuronal and glial compartments after focal cerebral ischemia in rats. Stroke 29(5):1048-1056; discussion 1056-1047.

Passonneau JV, Lowry OH. 1964. The role of phosphofructokinase in metabolic regulation. Adv Enzyme Regul 2:265-274.

Patel MS, Korotchkina LG. 2001. Regulation of mammalian pyruvate dehydrogenase complex by phosphorylation: complexity of multiple phosphorylation sites and kinases. Exp Mol Med 33(4):191-197.

Pellerin L, Magistretti PJ. 1994. Glutamate uptake into astrocytes stimulates aerobic glycolysis: a mechanism coupling neuronal activity to glucose utilization. Proc Natl Acad Sci U S A 91(22):10625-10629.

Pellerin L, Pellegri G, Bittar PG, Charnay Y, Bouras C, Martin JL, Stella N, Magistretti PJ. 1998a. Evidence supporting the existence of an activity-dependent astrocyte-neuron lactate shuttle. Dev Neurosci 20(4-5):291-299.

Pellerin L, Pellegri G, Martin JL, Magistretti PJ. 1998b. Expression of monocarboxylate transporter mRNAs in mouse brain: support for a distinct role of lactate as an energy substrate for the neonatal vs. adult brain. Proc Natl Acad Sci U S A 95(7):3990-3995.

Preece NE, Cerdán S. 1996. Metabolic precursors and compartmentation of cerebral GABA in vigabatrin-treated rats. J Neurochem 67(4):1718-1725.

Price JC. 2003. Principles of tracer kinetic analysis. Neuroimaging Clin N Am 13(4):689-704.

Rafiki A, Boulland JL, Halestrap AP, Ottersen OP, Bergersen L. 2003. Highly differential expression of the monocarboxylate transporters MCT2 and MCT4 in the developing rat brain. Neuroscience 122(3):677-688.

Richard J. 1963. [Lactic Dehydrogenase Isoenzymes in the Nervous System. Actions and Relations to Hydrosoluble

Proteins and Mineral Elements]. Ann Soc R Sci Med Nat Brux 16:185-223.

Robinson JB, Jr., Srere PA. 1985. Organization of Krebs tricarboxylic acid cycle enzymes in mitochondria. J Biol Chem 260(19):10800-10805.

Rodrigues TB, Cerdán S. 2005. ^{13}C MRS: an outstanding tool for metabolic studies. Concepts in Magnetic Resonance, Part A 27A(1):1-16.

Rodrigues TB, Cerdán S. 2007. The cerebral tricarboxylic acid cycles. In: Dienel G, Gibson, G., Lajtha, A., editor. Brain Energetics from Genes to Cells, Integration of Molecular and Cellular Processes. New York: Springer. p 61-93.

Rodrigues TB, Gray HL, Benito M, Garrido S, Sierra A, Geraldes CF, Ballesteros P, Cerdán S. 2005. Futile cycling of lactate through the plasma membrane of C6 glioma cells as detected by (^{13}C, ^{2}H) NMR. J Neurosci Res 79(1-2):119-127.

Ross AJ, Sachdev PS. 2004. Magnetic resonance spectroscopy in cognitive research. Brain Res Brain Res Rev 44(2-3):83-102.

Rossignol R, Letellier T, Malgat M, Rocher C, Mazat JP. 2000. Tissue variation in the control of oxidative phosphorylation: implication for mitochondrial diseases. Biochem J 347 Pt 1:45-53.

Rothman DL, Behar KL, Hyder F, Shulman RG. 2003. *In vivo* NMR studies of the glutamate neurotransmitter flux and neuroenergetics: implications for brain function. Annu Rev Physiol 65:401-427.

Rothman DL, Sibson NR, Hyder F, Shen J, Behar KL, Shulman RG. 1999. *In vivo* nuclear magnetic resonance spectroscopy studies of the relationship between the glutamate-glutamine neurotransmitter cycle and functional neuroenergetics. Philos Trans R Soc Lond B Biol Sci 354(1387):1165-1177.

Sacktor B, Wilson JE, Tiekert CG. 1966. Regulation of glycolysis in brain, *in situ*, during convulsions. J Biol Chem 241(21):5071-5075.

Satrustegui J, Pardo B, Del Arco A. 2007. Mitochondrial transporters as novel targets for intracellular calcium signaling. Physiol Rev 87(1):29-67.

Sazanov LA, Jackson JB. 1994. Proton-translocating transhydrogenase and NAD- and NADP-linked isocitrate dehydrogenases operate in a substrate cycle which contributes to fine regulation of the tricarboxylic acid cycle activity in mitochondria. FEBS Lett 344(2-3):109-116.

Schmoll D, Fuhrmann E, Gebhardt R, Hamprecht B. 1995. Significant amounts of glycogen are synthesized from 3-carbon compounds in astroglial primary cultures from mice with participation of the mitochondrial phosphoenolpyruvate carboxykinase isoenzyme. Eur J Biochem 227(1-2):308-315.

Schurr A. 2002. Lactate, glucose and energy metabolism in the ischemic brain (Review). Int J Mol Med 10(2):131-136.

Shen J, Petersen KF, Behar KL, Brown P, Nixon TW, Mason GF, Petroff OA, Shulman GI, Shulman RG, Rothman DL. 1999. Determination of the rate of the glutamate/glutamine cycle in the human brain by *in vivo* ^{13}C NMR. Proc Natl Acad Sci U S A 96(14):8235-8240.

Sheu KF, Blass JP. 1999. The alpha-ketoglutarate dehydrogenase complex. Ann N Y Acad Sci 893:61-78.

Shulman RG, Rothman DL, Behar KL, Hyder F. 2004. Energetic basis of brain activity: implications for neuroimaging. Trends Neurosci 27(8):489-495.

Sibson NR, Dhankhar A, Mason GF, Behar KL, Rothman DL, Shulman RG. 1997. *In vivo* ^{13}C NMR measurements of cerebral glutamine synthesis as evidence for glutamate-glutamine cycling. Proc Natl Acad Sci U S A 94(6):2699-2704.

Sibson NR, Dhankhar A, Mason GF, Rothman DL, Behar KL, Shulman RG. 1998a. Stoichiometric coupling of brain glucose metabolism and glutamatergic neuronal activity. Proc Natl Acad Sci U S A 95(1):316-321.

Sibson NR, Shen J, Mason GF, Rothman DL, Behar KL, Shulman RG. 1998b. Functional energy metabolism: *in vivo* ^{13}C-NMR spectroscopy evidence for coupling of cerebral glucose consumption and glutamatergic neuronalactivity. Dev Neurosci 20(4-5):321-330.

Sierra A, Lopes da Fonseca L, Ballesteros P, Cerdán S. Quantitative modelling of H3 hydrogen turnover in (2-^{13}C) glutamate and (2-^{13}C) glutamine during (2-^{13}C) acetate metabolism in the adult rat brain; 2004; Copenhagen. p 36.

Siesjo BK. 1982. Lactic acidosis in the brain: occurrence, triggering mechanisms and pathophysiological importance. Ciba Found Symp 87:77-100.

Sokoloff L. 1981a. The deoxyglucose method for the measurement of local glucose utilization and the mapping of local functional activity in the central nervous system. Int Rev Neurobiol 22:287-333.

Sokoloff L. 1981b. Localization of functional activity in the central nervous system by measurement of glucose utilization with radioactive deoxyglucose. J Cereb Blood Flow Metab 1(1):7-36.

Sokoloff L. 1983a. Mapping local functional activity by measurement of local cerebral glucose utilization in the central nervous system of animals and man. Harvey Lect 79:77-143.

Sokoloff L. 1983b. Measurement of local glucose utilization and its use in localization of functional activity in the central nervous system of animals and man. Recent Prog Horm Res 39:75-126.

Sokoloff L. 1989. Circulation and Energy Metabolism of the Brain. In: Siegel G, Agranoff B, Albers RW, Molinoff P, editors. Basic Neurochemistry. New York: Raven Press. p 565-590.

Sokoloff L. 1992. The brain as a chemical machine. Prog Brain Res 94:19-33.

Stewart VC, Land JM, Clark JB, Heales SJ. 1998. Comparison of mitochondrial respiratory chain enzyme activities in rodent astrocytes and neurones and a human astrocytoma cell line. Neurosci Lett 247(2-3):201-203.

Szabo P, Cai X, Ali G, Blass JP. 1994. Localization of the gene (OGDH) coding for the E1k component of the alpha-ketoglutarate dehydrogenase complex to chromosome 7p13-p11.2. Genomics 20(2):324-326.

Tsacopoulos M, Magistretti PJ. 1996. Metabolic coupling between glia and neurons. J Neurosci 16(3):877-885.

Tsacopoulos M, Veuthey AL, Saravelos SG, Perrottet P, Tsoupras G. 1994. Glial cells transform glucose to alanine, which fuels the neurons in the honeybee retina. J Neurosci 14(3 Pt 1):1339-1351.

Van den Berg CJ, Garfinkel D. 1971. A stimulation study of brain compartments. Metabolism of glutamate and related substances in mouse brain. Biochem J 123(2):211-218.

Van den Berg CJ, Krzalic L, Mela P, Waelsch H. 1969. Compartmentation of glutamate metabolism in brain. Evidence for the existence of two different tricarboxylic acid cycles in brain. Biochem J 113(2):281-290.

Van den Berg CJ, Mela P, Waelsch H. 1966. On the contribution of the tricarboxylic acid cycle to the synthesis of glutamate, glutamine and aspartate in brain. Biochem Biophys Res Commun 23(4):479-484.

Vannucci SJ, Maher F, Simpson IA. 1997. Glucose transporter proteins in brain: delivery of glucose to neurons and glia. Glia 21(1):2-21.

Vannucci SJ, Simpson IA. 2003. Developmental switch in brain nutrient transporter expression in the rat. Am J Physiol Endocrinol Metab 285(5):E1127-1134.

Wienhard K. 2002. Measurement of glucose consumption using [^{18}F]fluorodeoxyglucose. Methods 27(3):218-225.

Recycling of Lactate Through the Plasma Membrane of C6 Glioma Cells as Detected by (^{13}C,^{2}H) NMR

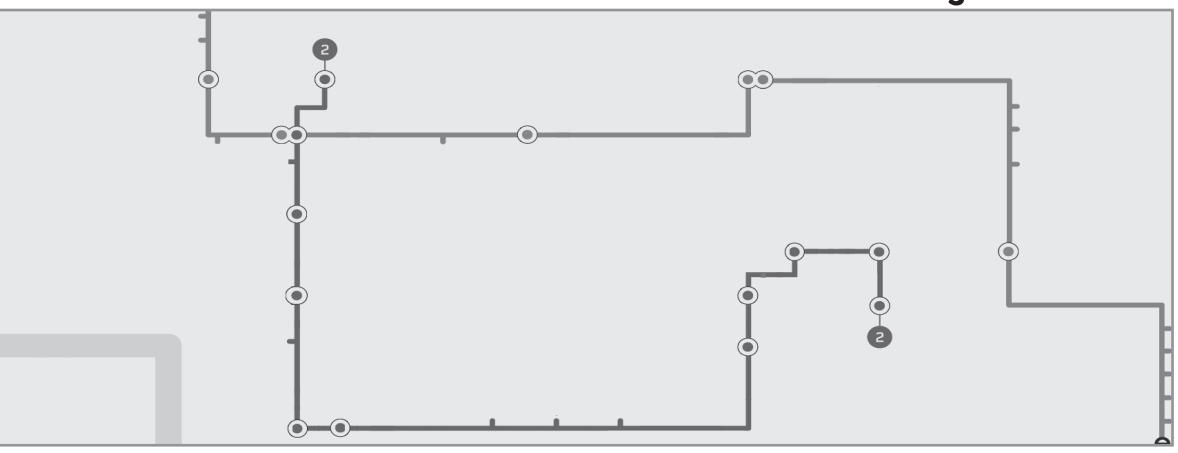

Chapter 2

1. Abstract

We report a novel (^{13}C,^{2}H) Nuclear Magnetic Resonance (NMR) procedure to investigate lactate recycling through the monocarboxylate transporter (MCT) of the plasma membrane of cells in culture. C6 glioma cells were incubated with (3-^{13}C) lactate in Krebs-Henseleit Buffer containing 50% $^{2}H_2O$ (vol/vol) for up to 30 h. ^{13}C NMR analysis of aliquots progressively taken from the medium, showed: (i) a linearly decreasing singlet at ca. 20.85 ppm (-0.119 μmol.mg protein^{-1}.h^{-1}) derived from the methyl carbon of (3-^{13}C) lactate and (ii) an exponentially increasing shifted singlet at ca. 20.74 ppm (0.227 μmol.mg protein^{-1}.h^{-1}) from the methyl carbon of (3-^{13}C, 2-^{2}H) lactate. The shifted singlet appears because during transit through the cytosol, (3-^{13}C) lactate generates (3-^{13}C, 2-^{2}H) lactate in the lactate dehydrogenase (LDH) equilibrium, which may return to the incubation medium through the reversible monocarboxylate carrier. The methyl group of (3-^{13}C, 2-^{2}H) lactate is shifted -0.11 ppm with respect to that of (3-^{13}C) lactate, making it possible to distinguish between both molecules by high-resolution ^{13}C NMR. During incubations with 2.5 mM (1-^{13}C) glucose and 3.98 mM (U-$^{13}C_3$) lactate or with 2.5 mM (1-^{13}C) glucose and 3.93 mM (2-^{13}C) pyruvate, C2-deuterated lactate was produced only from (1-^{13}C) glucose or (U-$^{13}C_3$) lactate, revealing that this deuteration process is redox sensitive. When (1-^{13}C) glucose and (U-$^{13}C_3$) lactate were used as substrates, no significant (3-^{13}C) lactate production from (1-^{13}C) glucose was detected, suggesting that glycolytic lactate production may be stopped under the high lactate concentrations prevailing under mild hypoxic or ischemic episodes or during cerebral activation.

2. Introduction

Lactate is thought to play a central role in cerebral pathophysiology both as an energy substrate for the brain and as a metabolic coupling intermediate between neurons and glial cells (Bouzier-Sore *et al.* 2001; Bouzier-Sore *et al.* 2006; Bouzier-Sore *et al.* 2003; Bouzier *et al.* 1998a; Bouzier *et al.* 1998b; Cater *et al.* 2003; Cerdán *et al.* 2006; Dienel and Hertz 2001; Hertz 2004; Pellerin 2003; Qu *et al.* 2000; Smith *et al.* 2003). In particular, lactate is believed to provide the coupling mechanism between the increased consumption of glucose observed during cerebral activation and the energy demanded by neurons during glutamatergic neurotransmission (Dienel and Cruz 2003; Dienel and Hertz 2001; García-Espinosa *et al.* 2003; García-Espinosa *et al.* 2004; Magistretti and Pellerin 1997; Magistretti and Pellerin 1999; Pellerin *et al.* 2002). Moreover, lactate is thought to serve as a vital substrate for neuronal recovery after hypoxia or ischemia (Cater *et al.* 2003; Muller *et al.* 1994; Schurr 2002; Schurr *et al.* 2001), to contribute primarily to cerebral energetics (Pellerin and Magistretti 2004) and to modulate intra- and extracellular pH (García-Martín *et al.* 2001a; Gillies *et al.* 2004).

Intracellular lactate production is normally small under physiological conditions, increasing significantly in hypoxic or ischemic situations (Cater *et al.* 2003; Schurr 2002; Schurr *et al.* 2001). In these circumstances, the respiratory chain is unable to reoxidize the reducing equivalents produced by glycolysis, causing pyruvate to be reduced to lactate rather than oxidized (Perrin *et al.* 2002). Increased intracellular lactate may then be extruded to the extracellular space through the proton-linked monocarboxylate transport (MCT) (Halestrap and Meredith 2004; Halestrap and Price 1999; Jackson and Halestrap 1996; Pierre and Pellerin 2005; Sierra *et al.* 2007). Reduced oxygen tension and compromised blood flow occurring under hypoxic or ischemic conditions preclude lactate oxidation and removal, resulting in lactate accumulation in the extracellular space. Under these conditions, extracellular lactate may reach concentrations even higher than those found in the intracellular space, eventually returning back to the cytosol, down its concentration gradient through the reversible MCT. Lactate molecules, however, are able to recycle between the extracellular and intracellular compartments, an advantageous situation that makes lactate ubiquitously available. Despite intensive research on lactate metabolism, however, to our knowledge no previous studies have investigated lactate recycling through the plasma membrane. This is due probably to the necessity to distinguish between lactate transport and metabolism and to differentiate those lactate molecules entering the cell from those leaving it, a very difficult aspect for conventional methodologies.

Recently, our laboratory has proposed and implemented hydrogen turnover measurements as alternatives to the classical approaches based on ^{13}C or ^{14}C turnover (Chapa *et al.* 2000; García-

Martín *et al.* 2001b; García-Martín *et al.* 2002; Rodrigues and Cerdán 2005). Our method uses ^{13}C NMR to follow the exchange of preexisting ^{1}H by ^{2}H, when metabolism occurs in media containing a ^{13}C-labeled substrate and $^{2}H_2O$ (García-Martín *et al.* 2002; Hansen 1989; Moldes *et al.* 1994). We herein report on an extension of this approach to monitor lactate recycling in cultures of C6 glioma cells. The method is based on the fact that the H2 hydrogen of lactate is exchanged rapidly by a deuteron in the LDH equilibrium, only in those lactate molecules that have passed through the cytosol.

3. Materials and Methods

3.1 Cell Culture and Incubation Conditions

The experimental protocols used in this study were approved by the appropriate institutional review committees and meet the guidelines of their responsible governmental agency. C6 glioma cells were obtained from a local representative of the American Tissue Culture Collection (LGC Promochem, Barcelona, Spain). Briefly, C6 glioma cells were grown to confluence in Dulbecco's modified Eagle's medium (DMEM) supplemented with 5% fetal bovine serum (FBS), 100 μg/mL streptomycin, 25 μg/mL gentamycin, 100 units/mL of penicillin and fungizone (1% vol/vol). Cells were cultured in sterile Petri dishes (10-cm diameter) maintained in an incubator at 37 °C with a humidified atmosphere containing 5% CO_2 and 95% O_2. For the incubations (3-30h, 37 °C), the culture medium was replaced by Krebs-Henseleit Buffer (KHB) (NaCl, 119 mM; KCl, 4.7 mM; $CaCl_2$, 1.3 mM; $MgSO_4$, 1.2 mM; HEPES, 15 mM and KH_2SO_4, 1.2 mM) containing 50% (vol/vol) $^{2}H_2O$ with the following combinations of ^{13}C-labeled substrates: i) 5 mM (3-^{13}C) lactate, ii) 2.5 mM (1-^{13}C) glucose + 3.98 mM (U-$^{13}C_3$) lactate, (iii) 2.5 mM (1-^{13}C) glucose + 3.93 mM (2-^{13}C) pyruvate, and (iv) 2.5 mM (1-^{13}C) glucose. Aliquots (1 mL) from the medium were collected during the incubation period to measure the rates of substrate utilization and product formation by ^{13}C NMR and conventional spectrophotometric methods.

3.2 (^{13}C,^{2}H) NMR Spectroscopy

Proton-decoupled ^{13}C NMR spectra from 0.5-mL aliquots of the incubation medium were obtained at 11.9 Tesla (125.13 MHz, 25 °C, pH 7.2) with a Bruker AVANCE 500WB NMR spectrometer using a commercial (5-mm) triple resonance probe (^{1}H,^{13}C,^{2}H) optimized for direct ^{13}C NMR detection. Acquisition conditions were: π/3 pulses, 30.0 kHz spectral width, 1.09 s acquisition

time, 64k words data table and 6.0 s recycling time. Proton decoupling was gated on only during the acquisition using a broad band composite pulse decoupling (CPD) sequence that removed the scalar ^{13}C-^{1}H multiplets, maintaining ^{13}C-^{13}C and ^{13}C-^{2}H couplings. Chemical shifts were calibrated with an external reference of dioxane (10% vol/vol, 67.4 ppm). Resonance assignments were based on literature values and on the addition of internal standards (Cerdán *et al.* 1990; Fan 1996). Spectra deconvolution and multiplet structures were analyzed using a PC-based (Intel Centrino Platform) NMR processing program, NUTS™ (Acorn, Freemont, CA, USA).

High-resolution ^{13}C NMR is well suited to detect complex deuteration patterns in ^{13}C-labeled metabolites. This happens because the presence of one or more ^{2}H atoms bound vicinally or geminally to the observed ^{13}C results in the appearance of characteristic ^{2}H-induced isotopic shifts and ^{13}C-^{2}H couplings (Hansen 1983; Hansen 1988). In the case of (3-^{13}C) lactate, the substitution of one of the H3 hydrogens of the methyl group by one deuteron causes the geminal C3 methyl resonance to be: (i) shifted (Δ_1 ca. -0.27 ppm) as well as (ii) split into a 1:1:1 triplet ($^{1}J^{2}_{H-^{13}C}$ = 19.5 Hz). A smaller isotopic shift is also detected in the C3 lactate resonance (Δ_2 = -0.11 ppm), upon deuterium substitution of the vicinal H2 hydrogen by a deuteron. In this case, the singlet multiplicity of the original ^{13}C resonance is maintained because the vicinal coupling constant ^{2}H-^{13}C is too small to be resolved. The isotopic shifts are additive and thus analysis of shifted and unshifted (^{1}H,^{2}H)^{13}C multiplets of the lactate C3 resonance allows one to detect the number of deuterium replacements both in C3 and C2 carbons of (3-^{13}C) lactate (Chapa *et al.* 2000; García-Martín *et al.* 2001a; García-Martín *et al.* 2001b; Moldes *et al.* 1994; Rodrigues and Cerdán 2005).

3.3 Other Determinations

Glucose and lactate concentration in the incubation media were determined spectrophotometrically using classical enzymatic end point methods (Bergmeyer 1983) coupled to the increase or decrease in NAD(P)H absorption at 340 nm. The conventional methods were adapted to become operative using 96-well microplates (0.25 mL) and a vertical microplate reader (Molecular Devices, Spectramax, CA, USA). Protein concentrations were measured using the bicinchoninic acid (BCA) assay (SIGMA Chemical Co., St. Louis, MS, USA). Linear (y=m.x +b) and nonlinear exponential ($y = a\,(1-e^{-bx})$) fittings were carried out using the Sigma Plot program (SPSS Inc., Chicago, IL, USA) as implemented on a Intel Centrino platform.

3.4 Materials

(1-^{13}C) glucose, (U-^{13}C) lactate, (2-^{13}C) pyruvate, (3-^{13}C) lactate (99.9% ^{13}C) and deuterated solvents were obtained from Cambridge Isotope Laboratories (Andover, MA, USA). $^{2}H_2O$ (99.9%

^{2}H) was obtained from Apollo Scientific Ltd. (Stockport, Cheshire, UK). Auxiliary enzymes and cofactors were from Boehringer Mannheim (Germany). FBS and DMEM were purchased from GIBCO BRL (Gent, Belgium). The rest of the reagents were of the highest purity available commercially from SIGMA Chemical Co. (St. Louis, MS, USA).

4. Results

We propose to investigate lactate recycling using the methodology presented in Figure 2.1. Figure 2.1-A illustrates the results of a representative experiment with C6 glioma cells incubated with 5 mM (3-^{13}C) lactate in the presence of KHB containing 50% $^{2}H_2O$ (vol/vol). ^{13}C NMR analysis of aliquots taken from the medium at increasing incubation times showed: (i) a linear decrease in the intensity of the singlet resonance from C3 lactate (ca. 20.85 ppm); and (ii) an exponential increase in the intensity of a vicinally shifted singlet from (3-^{13}C, 2-^{2}H) lactate (ca. 20.74 ppm, arrows). A summary of three similar experiments is shown in Figure 2.1-B. The shifted lactate resonances (Figure 2.1-A, arrows) do not appear in cell-free incubations of KHB (50% $^{2}H_2O$) with (3-^{13}C) lactate, nor during incubations of C6 cells with (3-^{13}C) lactate in undeuterated KHB (not shown). These results indicate that the shifted resonances are derived from the methyl group of (3-^{13}C, 2-^{2}H) lactate as produced by the enzymatic deuteration of intracellular (3-^{13}C) lactate in its C2 carbon. This process necessarily involves the cytosolic LDH equilibrium:

$$\text{Pyruvate} + \text{NAD}(^{2}H) + H^{+} \leftrightarrow (2\text{-}^{2}H)\ \text{Lactate} + \text{NAD}^{+} \qquad [2.1]$$

The sequence of events is illustrated in Figure 2.1-C. Extracellular lactate enters the cytoplasm of the C6 cell through the monocarboxylate transporter MCT1. Once in the cytosol, it loses its H2 hydrogen by exchange with one deuteron from the solvent, as incorporated through the LDH equilibrium (Equation [2.1]). Finally, the cytosolic (3-^{13}C, 2-^{2}H) lactate produced in this way, may eventually abandon the cell (together with a H^{+}) through the reversible MCT1 transporter, becoming detectable by ^{13}C NMR in the incubation medium (Figure 2.1-A arrows, Figure 2.1-B). Intracellular (3-^{13}C) lactate, however, may be either oxidized in the TCA cycle, resulting in the linear decrease of the total signal intensity from (3-^{13}C) lactate, or recycled to the incubation medium, originating the exponential increase of the isotopically shifted singlets shown in Figures 2.1-A and 2.1-B, respectively. In these experiments, it was possible to determine a net (3-^{13}C) lactate consumption of 0.119 ± 0.012 μmol.mg protein^{-1}.h^{-1} and a time constant for lactate extrusion of

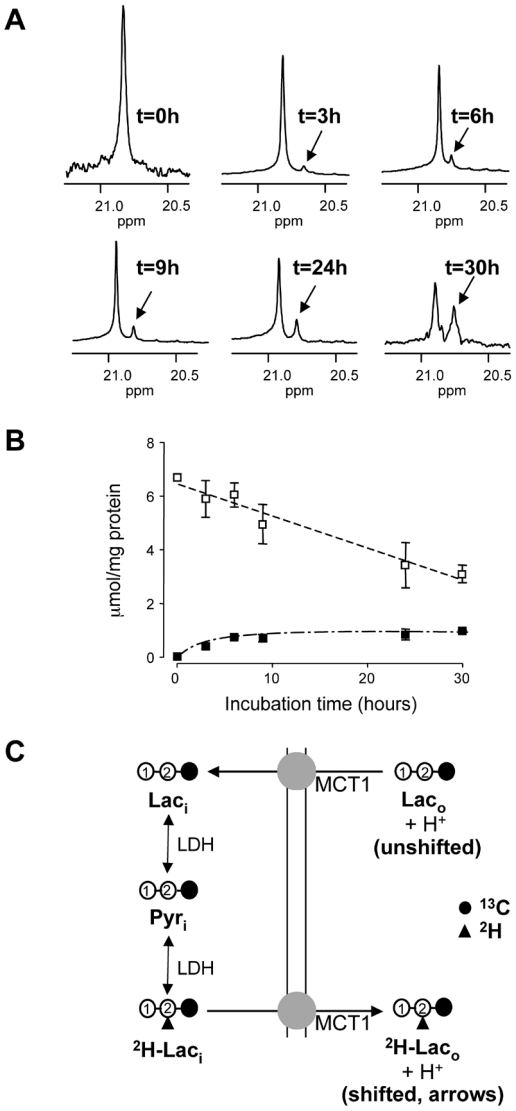

Figure 2.1. Demonstration of lactate recycling by ^{13}C NMR (125.13 MHz, 25 ^{o}C, pH 7.2) in the medium of C6 glioma cells incubated with 5 mM (3-^{13}C) lactate in buffer containing 50% ^2H_2O (vol/vol). A: Representative time course of the ^{13}C resonances from the methyl groups of (3-^{13}C) and (3-^{13}C, 2-^{2}H) lactate (arrows). **B**: Linear (3-^{13}C) lactate consumption (empty squares) and exponential (3-^{13}C, 2-$^2H^2$) lactate production (full squares). **C**: Extracellular (3-^{13}C) lactate (Lac$_o$, unshifted) enters the cytosol (Lac$_i$) through the MCT1 transporter. (3-^{13}C) Lac$_i$ loses its H2 hydrogen and incorporates a deuteron from NAD(^{2}H) in the LDH equilibrium. (3-^{13}C, 2-^{2}H) Lac$_i$ abandons the cell through the reversible MCT1 transporter originating the shifted singlet (^{2}H-Lac$_o$) in the incubation medium detected in Figure 2.1-A (arrows). LDH: lactate dehydrogenase, MCT1: monocarboxylate transporter 1.

0.227 ± 0.031 h^{-1}. For an intracellular lactate concentration of ca. 5 mM, it is possible to calculate a lactate extrusion flux of 1.135 ± 0.155 μmol.mg $protein^{-1}.h^{-1}$ under these conditions. This indicates that lactate equilibration through the MCT is very rapid, occurring approximately ten times faster than the net lactate uptake. At the end of these experiments, the relative ratios of shifted and unshifted areas of the methyl resonances of lactate approached 0.5, suggesting that molecules of (3-^{13}C) lactate deuterated and non deuterated in C2 lactate have virtually reached equilibrium with the ca. 50% deuterated solvent.

Figure 2.2 shows that lactate recycling is also observed in the presence of physiologic concentrations of glucose. In this experiment, C6 cells were incubated with 2.5 mM (1-^{13}C) glucose and 3.98 mM (U-$^{13}C_3$) lactate in KHB containing 50% ^2H_2O (vol/vol). Because the C3 resonance derived from (U-$^{13}C_3$) lactate is a doublet ($^1J_{C2\text{-}C3}$ = 37.0 Hz) whereas the lactate C3 resonance derived from (1-^{13}C) glucose is a singlet, it became possible to follow simultaneously the changes in concentration of the different (^{13}C,^{2}H) isotopomers of lactate derived from (1-^{13}C) glucose or (U-$^{13}C_3$) lactate, respectively. Figure 2.2-A shows that (3-^{13}C) lactate production from (1-^{13}C) glucose was negligible as judged from the virtually unobservable (3-^{13}C) lactate singlet after 9h incubation (dotted arrow). Under these conditions, most of the recycled lactate (full arrows) was the doublet derived from the methyl group of (U-$^{13}C_3$, 2-^{2}H) lactate, as produced from added (U-$^{13}C_3$) lactate. Consumption of glucose (expressed in triose units) and lactate were linear with values of 0.240 ± 0.084 μmol.mg $protein^{-1}.h^{-1}$ and 0.360 ± 0.071 respectively (Figure 2.2-B). Lactate extrusion was exponential, with a time constant of 0.489 ± 0.082 h^{-1}, corresponding for ca. 4 mM lactate, to a recycled lactate efflux of 1.94 ± 0.34 μmol.mg $protein^{-1}.h^{-1}$. Lactate recycling appears therefore to occur, again in this case, significantly faster than glucose or lactate metabolism.

We next investigated the effect of a more oxidized substrate on lactate production and recycling from glucose. C6 cells were incubated with 3.93 mM (2-^{13}C) pyruvate and 2.5 mM (1-^{13}C) glucose in KHB containing 50% ^2H_2O (vol/vol; Figure 2.3-A). Under these conditions, (3-^{13}C) lactate and (3-^{13}C, 2-^{2}H) lactate (full arrow) were produced from glucose in small but approximately equal amounts. Notably, no significant amounts of (2-^{13}C, 2-^{2}H) lactate derived from (2-^{13}C) pyruvate were observed, as revealed by the absence of the corresponding 1:1:1 triplets reflecting geminal ^{13}C-^{2}H coupling of lactate C2 (dotted arrow). Moreover, the lactate C2 resonance depicted a 1:2:1 structure, revealing the additive isotopic shifts (Δ_2 = -0.045 ppm) from a 1:2:1 mixture of vicinally deuterated isotopomers: (2-^{13}C), (2-^{13}C, 3-^{2}H) and (2-^{13}C, 3,3'-$^2H_2$) lactates, respectively. This distribution is consistent with an equilibrium deuteration on the two exchangeable hydrogens of the methyl carbon of (2-^{13}C) lactate, derived from (3-^{13}C, 3-^{2}H) or (3-^{13}C, 3,3'-$^2H_2$) malate in the TCA cycle. (2-^{13}C) lactate produced from (2-^{13}C) pyruvate thus does not appear to incorporate deuterons in H2, whereas (1-^{13}C) glucose produces similar amounts of (3-^{13}C) and (3-^{13}C, 2-^{2}H) lactate. In these experiments, (2-^{13}C) pyruvate consumption was linear only during the first four

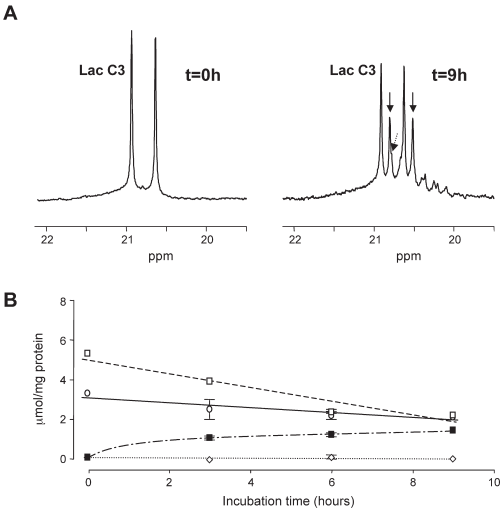

Figure 2.2. Lactate recycling during metabolism of 2.5 mM (1-^{13}C) glucose and 3.98 mM (U-$^{13}C_3$) lactate in buffer containing 50% ^2H_2O (vol/vol) as detected by ^{13}C NMR (125.13 MHz, 25 ^{o}C, pH 7.2). A: Doublet resonances from the methyl groups of (U-$^{13}C_3$) or (U-$^{13}C_3$, 2-^{2}H) lactate (full arrows) at 0 h and 9 h incubation time. Note the reduced intensity of the (3-^{13}C) lactate singlet derived from (1-^{13}C) glucose after 9 h incubation (dotted arrow). **B**: Linear consumption of (U-$^{13}C_3$) lactate (empty squares) and (1-^{13}C) glucose (empty circles). Exponential production of (U-$^{13}C_3$, 2-^{2}H) lactate (full squares). Note the small production of (3-^{13}C) lactate (empty diamonds).

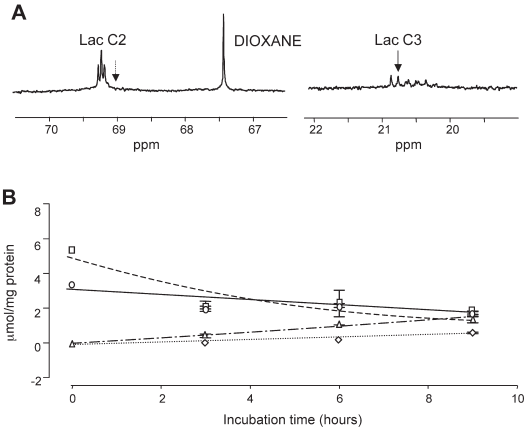

Figure 2.3. Lactate recycling during metabolism of 2.5 mM (1-^{13}C) glucose and 3.93 mM (2-^{13}C) pyruvate in KHB (50% ^2H_2O (vol/vol)) as detected by ^{13}C NMR (125.13 MHz, 25 ^{o}C, pH 7.2). A: Singlet resonances from (2-^{13}C) lactate (69.3 ppm, left panel) and (3-^{13}C) lactate (20.85 ppm, right panel) after 9 h incubation. Note the 1:2:1 distribution of the (2-^{13}C) lactate resonances and the absence of the 1:1:1 triplet of (2-^{13}C, 2-^{2}H) lactate (dotted arrow). Note the 1:1 ratio of shifted (full arrow)/unshifted singlets in (3-^{13}C) lactate. **B**: Consumption of (2-^{13}C) pyruvate (empty squares) or (1-^{13}C) glucose (empty circles) and production of (2-^{13}C) lactate (empty triangles) or (3-^{13}C) lactate (empty diamonds).

hours of the experiment as 1.087 ± 0.110 μmol.mg protein^{-1}.h^{-1}. Glucose consumption remained linear for a longer period, with a value of 0.350 ± 0.110 μmol. mg protein^{-1}.h^{-1} (expressed in triose units); (3-^{13}C) and (2-^{13}C) lactate were produced at rates of 0.063 ± 0.021 and 0.155 ± 0.014 μmol. mg protein^{-1}.h^{-1}, respectively.

Finally, we explored the production of undeuterated and deuterated lactate molecules during the metabolism of (1-^{13}C) glucose. C6 cells were incubated with 2.5 mM (1-^{13}C) glucose and the production of (3-^{13}C) and (3-^{13}C, 2-^{2}H) lactate (arrows) were monitored as indicated in Figure 2.4-A. In this case, (3-^{13}C) and (3-^{13}C, 2-^{2}H) lactate were produced at a very similar rate from the very initial phases of the incubation. This suggests that as expected, the equilibration of lactate C2 deuteration in the LDH step occurs before lactate extrusion to the medium. Because lactate is deuterated before transport to the medium, the experiments with (1-^{13}C) glucose do not allow directly monitoring of lactate recycling through the plasma membrane, but simply the production

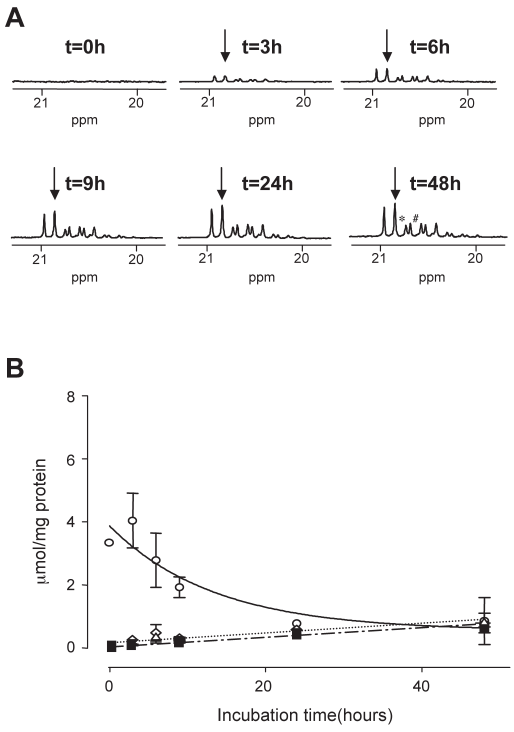

Figure 2.4. Metabolism of (1-^{13}C) glucose in KHB (50% $^{2}H_2O$ (vol/vol)) as detected by ^{13}C NMR (125.13 MHz, 25 ^{o}C, pH 7.2). A: Time course of production of (3-^{13}C) and (3-^{13}C, 2-^{2}H, arrow) lactate. Multiplets at higher field correspond to (3-^{13}C, 3-^{2}H,*) and (3-^{13}C, 3-^{2}H, 2-^{2}H,#) lactate, originated from (3-^{13}C, 3-^{2}H) and (3-^{13}C, 3,3'-$^{2}H_2$) malate in the tricarboxylic acid cycle. **B**: Consumption of (1-^{13}C) glucose (empty circles) and production of (3-^{13}C) and (3-^{13}C, 2-^{2}H) lactates.

of (3-^{13}C) and (3-^{13}C, 2-^{2}H) lactate. (1-^{13}C) glucose consumption (expressed in triose units) was 0.706 ± 0.078 μmol. mg protein^{-1}.h^{-1}, while (3-^{13}C) and (3-^{13}C, 2-^{2}H) lactate production were 0.013 ± 0.004 and 0.015 ± 0.002 μmol. mg protein^{-1}.h^{-1}, respectively. Notably, the similar rates of production of the undeuterated and deuterated species suggest a negligible deuterium kinetic isotopic effect in this process. A summary of the metabolic balances obtained during these experiments is presented in Table 2.1.

TABLE 2.1. Metabolic balances of substrate consumption, product formation, and lactate recycling in C6 cells incubated with different combinations of ^{13}C-labeled substrates in 50% deuterated Krebs-Henseleit buffer*

Incubation conditions	Process investigated					
	Glc consumption[a]	Lac (L) or Pyr (P) consumption	Lac production (from Glc)	Lac recycling	Glc oxidation	Extracellular Lac (L) or Pyr (P) oxidation
5 mM (3-^{13}C)Lac	n.a.	0.119 ± 0.012 (L)	n.a.	0.227 ± 0.031	n.a.	0.119 ± 0.012 (L)
2.5 mM (1-^{13}C)Glc+ 3.98 mM (U-$^{13}C_3$)Lac	0.240 ± 0.084	0.360 ± 0.071 (L)	0.003 ± 0.008	0.489 ± 0.082	0.237 ± 0.092	0.360 ± 0.071 (L)
2.5 mM (1-^{13}C)Glc+ 3.93 mM (2-^{13}C)Pyr	0.350 ± 0.110	0.152 ± 0.060 (P)	0.063 ± 0.021[d] 0.155 ± 0.014[e]	n.d.[b]	0.287 ± 0.131	0.152 ± 0.060 (P)
2.5 mM (1-^{13}C) Glc	0.706 ± 0.078	n.a.	0.028 ± 0.006[c]	n.d.[b]	0.678 ± 0.084	n.d.

*C6 cells were incubated in Krebs-Henseleit buffer containing 50% $^{2}H_2O$ with the specified ^{13}C-labeled substrates. Values are expressed in μmol/mg protein/hr as the mean ± S.D. of at least three replicates. Glc, glucose; Lac, lactate; Pyr, pyruvate; n.a., not applicable; n.d., not detectable.
[a]Expressed in triose units.
[b]Lactate recycling from (2-^{13}C)pyruvate or [1-^{13}C]glucose not detectable.
[c]Includes the addition of (3-^{13}C) and (3-^{13}C, 2-^{2}H) lactates, 0.013±0.004 and 0.015±0.002, respectively.
[d][3-^{13}C]Lactate produced from (1-^{13}C)glucose.
[e][2-^{13}C]Lactate produced from (2-^{13}C)pyruvate.

5. Discussion

Lactate exchange between the intra- and extracellular spaces is thought to be a very fast process occurring in both directions because of the reversible nature of the MCT of the plasma membrane (Halestrap and Meredith 2004; Halestrap and Price 1999; Jackson and Halestrap 1996; Poole and Halestrap 1993). These transporters are believed to operate under near thermodynamic equilibrium conditions, carrying one molecule of lactate and one proton in the inward or outward directions depending on the corresponding transmembrane gradients of lactate and protons (see [2.2]).

$$Lactate_{in} + H^{+}_{in} \leftrightarrow Lactate_{out} + H^{+}_{out} \quad [2.2]$$

Lactate exchange entails important physiological consequences. In particular, it sets the lactate concentration in the intra- and extracellular spaces and determines its subsequent metabolism, coupling it to the transmembrane pH gradient and pH homeostasis. Despite its importance, direct measurements of lactate exchange are complicated because of its relatively fast timescale and the need to discriminate between transport and metabolism and between lactate molecules moving inward or outward. Previous measurements used radioactive isotopes or fluorescence methods to probe extracellular lactate transport to the intracellular space (Jackson and Halestrap 1996; Poole and Halestrap 1993). We are unaware, however, of any previous measurements of direct intracellular lactate transport to the extracellular space through the proton-linked MCT of the plasma membrane.

In this work, we report on a novel procedure to investigate intracellular lactate exchange with the medium in cell cultures. The method is based on the fact that, in deuterium oxide-containing media, perprotonated extracellular lactate molecules entering the cytosol and exchange their H2 proton by a deuteron, in the LDH equilibrium. In the case of (3-^{13}C) lactate, the following cytosolic processes take place (see [2.3] and [2.4]):

$$(3\text{-}^{13}C)\ Lactate + NAD^{+} \leftrightarrow (3\text{-}^{13}C)\ Pyruvate + NADH + H^{+} \quad [2.3]$$

$$(3\text{-}^{13}C)\ Pyruvate + NAD(^{2}H) + H^{+} \leftrightarrow (3\text{-}^{13}C,\ 2\text{-}^{2}H)\ Lactate + NAD^{+} \quad [2.4]$$

The combination of both, results in the net exchange of a deuteron between NAD(^{2}H) and the H2 hydrogen of lactate [2.5]:

$$(3\text{-}^{13}C)\ Lactate + NAD(^{2}H) \leftrightarrow (3\text{-}^{13}C,\ 2\text{-}^{2}H)\ Lactate + NADH \quad [2.5]$$

The (3-^{13}C, 2-^{2}H) lactate originated in this way may return to the incubation medium where it is distinguished easily from (3-^{13}C) lactate by high-resolution ^{13}C NMR, because the methyl group of the deuterated species resonates -0.11 ppm from the methyl group of the perprotonated species.

Deuteration of the C2 carbon of lactate requires the transfer of one deuteron from the heavy water in the solvent to NAD(P)^{2}H. This must involve first one hydration-dehydration reaction (see [2.6]), and second, a redox process of the general type (see [2.7]):

$$AH + {}^{2}H_{2}O \leftrightarrow AH(^{2}H) + {}^{2}HO^{-} \quad [2.6]$$

$$AH(^{2}H) + NAD(P)^{+} \leftrightarrow AH + NAD(P)^{2}H \quad [2.7]$$

where A is the metabolite incorporating the ^2H from ^2H_2O that will be transferred later to $NAD(P)^+$ in the redox process. The combination of reactions in equations [2.6] and [2.7] accounts for the exchange of deuterons between ^2H_2O and $NAD(P)^+$:

$$^2H_2O + NAD(P)^+ \leftrightarrow NAD(P)^2H + {}^2HO^- \quad [2.8]$$

These considerations account for the fact that lactate deuteration is observed easily when (3-^{13}C) lactate or (1-^{13}C) glucose are the substrates, but becomes undetectable when (2-^{13}C) pyruvate is the precursor. Indeed, under the reduced redox conditions prevailing during lactate or glucose and lactate metabolisms, the concentration of $NAD(P)^2H$ is high enough and deuterations derived from it become easily observable. Under the oxidized conditions occurring when glucose and pyruvate are used, however, the concentration of $NAD(P)^2H$ is reduced markedly, concomitantly decreasing the transfers of reducing deuterons. In addition, the much faster pyruvate (ca. 1.07 μmol.mg protein^{-1}.h^{-1}) than lactate uptake could result even faster than the combined hydration-dehydration/redox deuterations, reducing lactate deuteration from ^2H_2O to negligible levels by kinetic constrains.

The present experiments provide also valuable information concerning the redox control of glycolysis. When 2.5 mM (1-^{13}C) glucose is used as the only substrate, glucose consumption and lactate production rates are 0.70 (triose units) and 0.03 μmol. mg protein^{-1}. h^{-1}, respectively. Incubations with 5 mM (3-^{13}C) lactate alone show that C6 cells are able to oxidize lactate at a rate of 0.12 μmol.h^{-1}.mg protein^{-1}. When mixtures of 2.5 mM (1-^{13}C) glucose and 3.98 mM (U-$^{13}C_3$) lactate are used, however, glucose consumption is reduced to 0.240 μmol.mg protein^{-1}.h^{-1} and lactate consumption is increased to 0.36 μmol.mg protein^{-1}.h^{-1}. Notably, no significant (3-^{13}C) lactate production from (1-^{13}C) glucose is observed under these conditions. This indicates that high extracellular lactate concentrations are able to inhibit (3-^{13}C) lactate production from (1-^{13}C) glucose, at the glyceraldehyde-3-phosphate dehydrogenase (GAPDH) step because of the competition between lactate and glycolysis for the severely limited cytosolic pool of NAD^+. Our data also show that lactate can efficiently substitute glucose for oxidation and that the presence of glucose increases lactate uptake under these conditions. Finally, when 2.5 mM (1-^{13}C) glucose and 3.93 mM (2-^{13}C) pyruvate are used, both (2-^{13}C) and (3-^{13}C) lactate are produced, derived from (2-^{13}C) pyruvate and (1-^{13}C) glucose, respectively. This result indicates, as expected, that the oxidized redox state does not inhibit flux through GAPDH. Under these conditions, only (3-^{13}C) lactate molecules are deuterated in C2. Taken together, these findings are consistent with previous reports showing pyruvate compartmentation in C6 cells and other neural cells (Bouzier *et al.* 1998a; Bouzier *et al.* 1998b; Cruz *et al.* 2001; Zwingmann *et al.* 2001).

Figure 2.5 summarizes adequately these and earlier results on pyruvate compartmentation

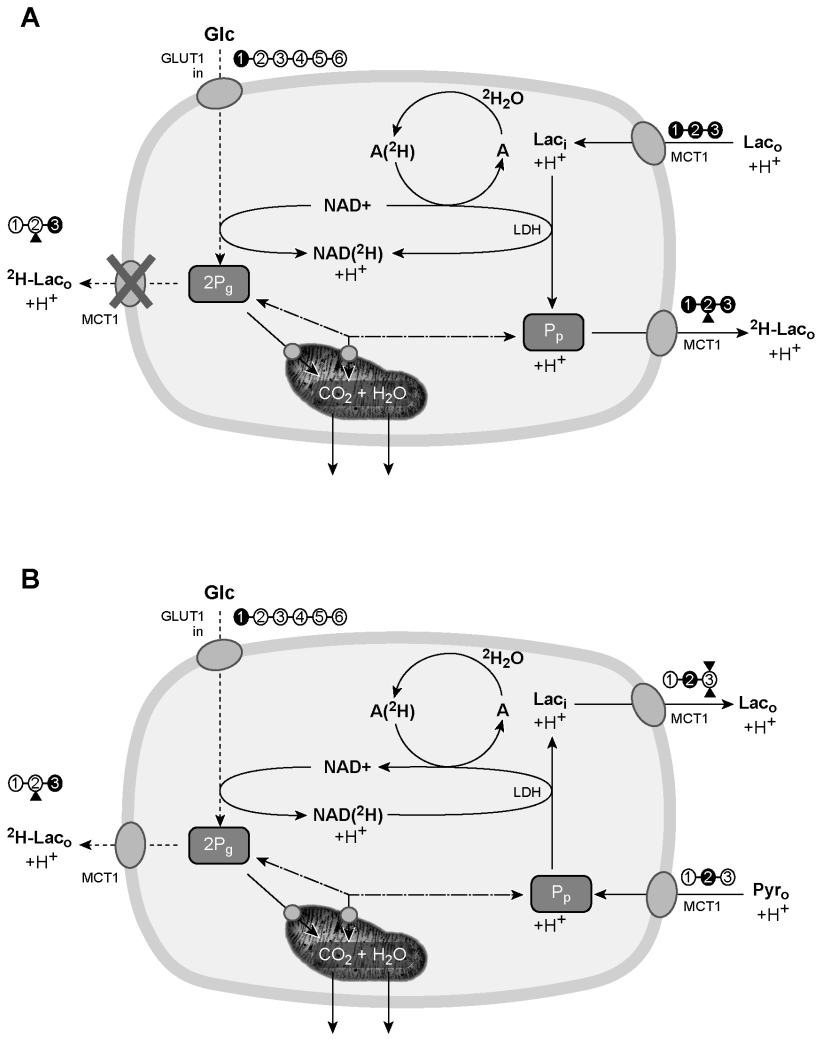

Figure 2.5. Intracellular pyruvate compartmentation and lactate recycling during metabolism of (1-^{13}C) glucose and (U-$^{13}C_3$) lactate (A) or (2-^{13}C) pyruvate (B). Two kinetically different cytosolic pools of pyruvate exist in C6 cells; P_g: Pyruvate pool derived from glucose, P_p: Pyruvate pool derived from extracellular lactate or pyruvate. Coupling of a hydration/dehydration reaction and a redox process allows NAD(^{2}H) to be formed from a solvent deuteron previously incorporated in metabolite A. **A**: Intracellular lactate (Lac_i) competes with glycolysis for NAD$^+$, inhibiting (3-^{13}C) lactate production. Deuteration of the P_p pool in the LDH reaction occurs extensively, extruding large amounts of (U-^{13}C, 2-^{2}H) lactate to the medium but not of (3-^{13}C, 2-^{2}H) lactate (dotted arrow). **B**: Intracellular lactate derived from the P_p pool of (2-^{13}C) pyruvate is formed before H2 deuteration can occur, extruding to the medium mainly (2-^{13}C) lactate. Glycolytic (3-^{13}C) pyruvate is formed significantly slower, allowing (3-^{13}C, 2-^{2}H) lactate to be formed and extruded to the medium. LDH: lactate dehydrogenase, MCT1: monocarboxylate transporter type 1, (●) ^{13}C, (▲) ^{2}H.

(Cruz *et al.* 2001). During the incubations with 2.5 mM (1-^{13}C) glucose and 3.98 mM (U-$^{13}C_3$) lactate (Figure 2.5-A), both substrates compete for the same intracellular pool of NAD^+. (U-$^{13}C_3$) lactate transport and equilibration is significantly faster than is glycolysis, limiting glycolytic flow at the GAPDH step through NAD^+ depletion. Under these conditions, virtually no (3-^{13}C) or (3-^{13}C, 2-^{2}H) lactate are produced from glucose, because NAD(^{2}H) is used much faster in reducing the cytosolic (U-$^{13}C_3$) pyruvate pool originating from lactate P_p than in reducing the cytosolic (3-^{13}C) pyruvate pool originated from (1-^{13}C) glucose P_g. Kinetic compartmentation is also observed in the incubations with 2.5 mM (1-^{13}C) glucose and 3.93 mM (2-^{13}C) pyruvate (Figure 2.5-B). In this case, the fast pyruvate transport and oxidized redox do not allow the production of (2-^{13}C, 2-^{2}H) lactate from the P_p pool. However, the slower glycolytic flow is compatible with the productions of (3-^{13}C) and (3-^{13}C, 2-^{2}H) lactates from the P_g pool.

In summary, using (^{13}C,^{2}H) NMR, we have been able to resolve in time the deuteration of C2 carbon of intracellular lactate by solvent deuterons and its transport to the extracellular medium. C2 deuteration of lactate is extensive when (3-^{13}C) lactate or combinations of (3-^{13}C) lactate and (1-^{13}C) glucose are the substrates. It becomes negligible, however, when (2-^{13}C) pyruvate is used as substrate. We also show that increased (U-$^{13}C_3$) lactate concentrations in the incubation medium, such as those commonly found during neuronal excitation or during mild hypoxic or ischemic conditions, inhibit (3-^{13}C) lactate production from (1-^{13}C) glucose, suggesting that under these conditions, lactate could become a preferred substrate to glucose.

Finally, the present methodology to evaluate lactate exchange through the plasma membrane can be extended easily to other neural cells in culture (Fonseca *et al.* 2004) or to other metabolites as long as they present exchangeable hydrogens becoming deuterated during the pass of the metabolite through the intracellular space.

6. References

Bergmeyer HU. 1983. Methods of Enzymatic Analysis: Weinheim: Verlag Chemie.

Bouzier-Sore AK, Canioni P, Merle M. 2001. Effect of exogenous lactate on rat glioma metabolism. Journal of Neuroscience Research 65(6):543-548.

Bouzier-Sore AK, Voisin P, Bouchaud V, Bezancon E, Franconi JM, Pellerin L. 2006. Competition between glucose and lactate as oxidative energy substrates in both neurons and astrocytes: a comparative NMR study. Eur J Neurosci 24(6):1687-1694.

Bouzier-Sore AK, Voisin P, Canioni P, Magistretti TJ, Pellerin T. 2003. Lactate is a preferential oxidative energy substrate

over glucose for neurons in culture. Journal of Cerebral Blood Flow and Metabolism 23(11):1298-1306.

Bouzier AK, Goodwin R, de Gannes FMP, Valeins H, Voisin P, Canioni P, Merle M. 1998a. Compartmentation of lactate and glucose metabolism in C6 glioma cells - A C-13 and H-1 NMR study. Journal of Biological Chemistry 273(42):27162-27169.

Bouzier AK, Voisin P, Goodwin R, Canioni P, Merle M. 1998b. Glucose and lactate metabolism in C6 glioma cells: Evidence for the preferential utilization of lactate for cell oxidative metabolism. Developmental Neuroscience 20(4-5):331-338.

Cater HL, Chandratheva A, Benham CD, Morrison B, Sundstrom LE. 2003. Lactate and glucose as energy substrates during, and after, oxygen deprivation in rat hippocampal acute and cultured slices. Journal of Neurochemistry 87(6):1381-1390.

Cerdán S, Kunnecke B, Seelig J. 1990. Cerebral metabolism of [1,2-$^{13}C_2$]acetate as detected by *in vivo* and *in vitro* ^{13}C NMR. J Biol Chem 265(22):12916-12926.

Cerdán S, Rodrigues TB, Sierra A, Benito M, Fonseca LL, Fonseca CP, García-Martín ML. 2006. The redox switch/redox coupling hypothesis. Neurochem Int 48(6-7):523-530.

Chapa F, Cruz F, García-Martín ML, García-Espinosa MA, Cerdán S. 2000. Metabolism of (1-^{13}C) glucose and (2-^{13}C, 2-$^{2}H_3$) acetate in the neuronal and glial compartments of the adult rat brain as detected by [^{13}C, ^{2}H] NMR spectroscopy. Neurochem Int 37(2-3):217-228.

Cruz F, Villalba M, García-Espinosa MA, Ballesteros P, Bogonez E, Satrustegui J, Cerdán S. 2001. Intracellular compartmentation of pyruvate in primary cultures of cortical neurons as detected by ^{13}C NMR spectroscopy with multiple ^{13}C labels. J Neurosci Res 66(5):771-781.

Dienel GA, Cruz NF. 2003. Neighborly interactions of metabolically-activated astrocytes *in vivo*. Neurochemistry International 43(4-5):339-354.

Dienel GA, Hertz L. 2001. Glucose and lactate metabolism during brain activation. Journal of Neuroscience Research 66(5):824-838.

Fan TWM. 1996. Metabolite profiling by one- and two-dimensional NMR analysis of complex mixtures. Progress in NMR Spectrosc 28(2):161-219.

Fonseca LL, Sierra A, Santos H, Cerdán S. Lactate Recycling In Primary Cultures of Astrocytes and Neurons Studied by (^{2}H)^{13}C-NMR Spectroscopy; 2004; Heraklion, Crete, Greece. p 48.

García-Espinosa MA, García-Martín ML, Cerdán S. 2003. Role of glial metabolism in diabetic encephalopathy as detected by high resolution ^{13}C NMR. NMR Biomed 16(6-7):440-449.

García-Espinosa MA, Rodrigues TB, Sierra A, Benito M, Fonseca C, Gray HL, Bartnik BL, García-Martín ML, Ballesteros P, Cerdán S. 2004. Cerebral glucose metabolism and the glutamine cycle as detected by *in vivo* and *in vitro* ^{13}C NMR spectroscopy. Neurochem Int 45(2-3):297-303.

García-Martín M-L, Herigault G, Remy C, Farion R, Ballesteros P, Coles JA, Cerdán S, Ziegler A. 2001a. Mapping extracellular pH in rat brain gliomas *in vivo* by ^{1}H magnetic resonance spectroscopic imaging: comparison with maps of metabolites. Cancer Res 61(17):6524-6531.

García-Martín ML, Ballesteros P, Cerdán S. 2001b. The metabolism of water in cells and tissues as detected by NMR methods. Prog Nucl Mag Res Spectroscopy 39:41-77.

García-Martín ML, García-Espinosa MA, Ballesteros P, Bruix M, Cerdán S. 2002. Hydrogen turnover and subcellular compartmentation of hepatic [2-^{13}C]glutamate and [3-^{13}C]aspartate as detected by ^{13}C NMR. J Biol Chem 277(10):7799-7807.

Gillies RJ, Raghunand N, García-Martín ML, Gatenby RA. 2004. pH imaging. A review of pH measurement methods and applications in cancers. IEEE Eng Med Biol Mag 23(5):57-64.

Halestrap AP, Meredith D. 2004. The SLC16 gene family-from monocarboxylate transporters (MCTs) to aromatic amino acid transporters and beyond. Pflugers Arch 447(5):619-628.

Halestrap AP, Price NT. 1999. The proton-linked monocarboxylate transporter (MCT) family: structure, function and regulation. Biochem J 343 Pt 2:281-299.

Hansen PE. 1983. Isotope Effects on Nuclear Shielding. Ann Rep NMR Spectrosc 15:105-234.

Hansen PE. 1988. Deuterium Isotope Effects on Nuclear Shielding. Progress in NMR Spectrosc 20:207-257.

Hansen PE. 1989. Isotope effects on nuclear shielding. Ann Rep NMR Spectrosc 15:105-234.

Hertz L. 2004. The astrocyte-neuron lactate shuttle: a challenge of a challenge. J Cereb Blood Flow Metab 24(11):1241-1248.

Jackson VN, Halestrap AP. 1996. The kinetics, substrate, and inhibitor specificity of the monocarboxylate (lactate) transporter of rat liver cells determined using the fluorescent intracellular pH indicator, 2',7'-bis(carboxyethyl)-5(6)-carboxyfluorescein. J Biol Chem 271(2):861-868.

Magistretti PJ, Pellerin L. 1997. The cellular bases of functional brain imaging: Evidence for astrocyte-neuron metabolic coupling. Neuroscientist 3(6):361-365.

Magistretti PJ, Pellerin L. 1999. Astrocytes couple synaptic activity to glucose utilization in the brain. News in Physiological Sciences 14:177-182.

Moldes M, Cerdán S, Erhard P, Seelig J. 1994. ^{1}H-^{2}H exchange in the perfused rat liver metabolizing [3-^{13}C]alanine and $^{2}H_2O$ as detected by multinuclear NMR spectroscopy. NMR Biomed 7(6):249-262.

Muller TB, Sonnewald U, Westergaard N, Schousboe A, Petersen SB, Unsgard G. 1994. C-13 Nmr-Spectroscopy Study of Cortical Nerve-Cell Cultures Exposed to Hypoxia. Journal of Neuroscience Research 38(3):319-326.

Pellerin L. 2003. Lactate as a pivotal element in neuron-glia metabolic cooperation. Neurochemistry International 43(4-5):331-338.

Pellerin L, Bonvento G, Chatton JY, Pierre K, Magistretti PJ. 2002. Role of neuron-glia interaction in the regulation of brain glucose utilization. Diabetes Nutrition & Metabolism 15(5):268-273.

Pellerin L, Magistretti PJ. 2004. Neuroenergetics: Calling upon astrocytes to satisfy hungry neurons. Neuroscientist 10(1):53-62.

Perrin A, Roudier E, Duborjal H, Bachelet C, Riva-Lavieille C, Leverve X, Massarelli R. 2002. Pyruvate reverses metabolic effects produced by hypoxia in glioma and hepatoma cell cultures. Biochimie 84(10):1003-1011.

Pierre K, Pellerin L. 2005. Monocarboxylate transporters in the central nervous system: distribution, regulation and function. J Neurochem 94(1):1-14.

Poole RC, Halestrap AP. 1993. Transport of Lactate and Other Monocarboxylates across Mammalian Plasma-Membranes. American Journal of Physiology 264(4):C761-C782.

Qu H, Haberg A, Haraldseth O, Unsgard G, Sonnewald U. 2000. C-13 MR spectroscopy study of lactate as substrate for rat brain. Developmental Neuroscience 22(5-6):429-436.

Rodrigues TB, Cerdán S. 2005. ^{13}C MRS: an outstanding tool for metabolic studies. Concepts in Magnetic Resonance, Part A 27A(1):1-16.

Schurr A. 2002. Energy metabolism, stress hormones and neural recovery from cerebral ischemia/hypoxia. Neurochemistry International 41(1):1-8.

Schurr A, Payne RS, Miller JJ, Tseng MT. 2001. Preischemic hyperglycemia-aggravated damage: Evidence that lactate

utilization is beneficial and glucose-induced corticosterone release is detrimental. Journal of Neuroscience Research 66(5):782-789.

Sierra A, Rodrigues TB, Benito M, Ballesteros P, García-Espinosa MA, García-Martín ML, Cerdán S. 2007. Pyruvate Oxidation and Mitochondrial Substrate Transport in the Central Nervous System. In: Lajhta A, Gruetter R, editors. Neural Metabolism *in Vivo*. New York: Springer.

Smith D, Pernet A, Hallett WA, Bingham E, Marsden PK, Amiel SA. 2003. Lactate: A preferred fuel for human brain metabolism *in vivo*. Journal of Cerebral Blood Flow and Metabolism 23(6):658-664.

Zwingmann C, Richter-Landsberg C, Leibfritz D. 2001. ^{13}C isotopomer analysis of glucose and alanine metabolism reveals cytosolic pyruvate compartmentation as part of energy metabolism in astrocytes. Glia 34(3):200-212.

Fast and Robust ^{1}H NMR Methods to Measure the Turnover of the H2 Hydrogen of Lactate

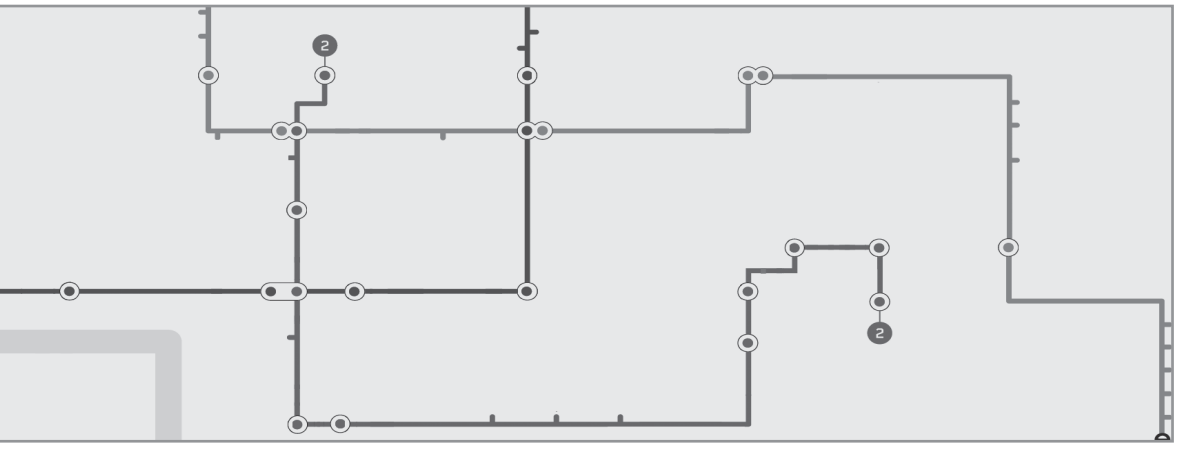

Chapter 3

1. Abstract

Two fast and sensitive procedures to determine the turnover of the H2 hydrogen of lactate and quantify its ^{2}H-enrichment by ^{1}H NMR are illustrated using C6 cells metabolizing lactate in 50% $^{2}H_2O$ (vol/vol). The first one is based on the fact that ^{2}H substitution of the lactate H2 hydrogen results in two easily detectable transformations of the vicinal H3 doublet resonance: (i) the formation of an H3 singlet due to the disappearance of the homonuclear coupling to H2 ($^{3}J_{\beta H-\alpha H}$ = 6.9 Hz) and (ii) an upfield isotopic shift derived from the vicinal ^{2}H2 substitution (Δ_3 = -0.007 ppm). Only those lactate molecules that have passed through the cell cytosol experience these effects, since H2 deuteration involves lactate dehydrogenase (LDH) activity and NAD(^{2}H). Thus, analysis of the observed shifted and unshifted H3 lactate resonances from the incubation medium allows the discrimination of the perprotonated lactate added as substrate, and the lactate recycled to the incubation medium after passage through the cytosol. The second approach discriminates between non-deuterated and deuterated H2 lactate molecules through the use of a specific lactate editing sequence. The experiment involves two separate acquisitions using a regular spin echo sequence with an appropriate echo time to produce a phase-modulation of 180 degrees on the H2 and H3 resonances of lactate. By applying a selective decoupling pulse on the H2 resonance of lactate in the first acquisition, we destroyed the phase-modulation. Adding both spectra obtained in these two subsequent acquisitions, non-deuterated lactate resonances are canceled out whereas non-modulated resonances' intensities are effectively added, including the H3 singlet of H2 deuterated lactate.

2. Introduction

Lactate is considered to play a pivotal role in cerebral metabolism, both as an intracellular energy substrate for oxidation in neural cells and as a shuttle intermediate for the transcellular metabolic coupling between neurons and astrocytes (Bouzier-Sore *et al.* 2003a; Bouzier-Sore *et al.* 2003b; Cerdán *et al.* 2006; Dienel and Hertz 2001; Qu *et al.* 2000; Smith *et al.* 2003). In particular, the classical Astrocyte to Neuron Lactate Shuttle (ANLS) hypothesis proposed a flux of lactate from astrocytes to neurons, to support the energy demand occurring during glutamatergic neurotransmission (Dienel and Hertz 2001; Pellerin and Magistretti 1994). Under the reduced vascular clearance conditions occurring in cerebral excitation, ischemic episodes or even in tumors, lactate has also been proposed to play a crucial role in cellular survival, approaching more the nature of a vital substrate than that of a lethal product (Cater *et al.* 2003; Muller *et al.* 1994; Schurr *et al.* 2001). These lactate molecules have been reported to accumulate in the extracellular space reaching concentrations that exceed those found in the cell cytosol (Cater *et al.* 2003; Schurr *et al.* 2001). In these situations, extracellular lactate molecules may return to the cytosol through the reversible MCT, located in the plasma membrane of all normal and transformed cells (Halestrap and Meredith 2004; Halestrap and Price 1999). This lactate recycling through the plasma membrane, driven by the concentration of lactate inside and outside the cell and the pH gradient, remains as a difficult process to investigate, given the identical nature of recycled and non-recycled lactate molecules hindering their unambiguous identification.

We previously proposed several hydrogen turnover methods to investigate trafficking of various (^{13}C,^{2}H) labeled isotopomers, including lactate (see Chapter 2), between different compartments in cell cultures, perfused liver, and brain (Chapa *et al.* 2000; García-Martín *et al.* 2002; Rodrigues *et al.* 2005). These methods are able to monitor, by ^{13}C NMR, the incorporation of deuterium into ^{13}C-labeled metabolites, because covalent binding of ^{2}H results in characteristic ^{13}C-^{2}H heteronuclear couplings and geminal or vicinal isotopic shifts of the corresponding ^{13}C resonances (García-Martín *et al.* 2001; Hansen 1989). The methodology combines the inherent advantage of detecting deuterium incorporation with the positional selectivity and increased sensitivity of ^{13}C NMR, as compared to the direct ^{2}H NMR detection (Perdigoto *et al.* 2003; Vianello *et al.* 1997). It requires, however, the use of relatively expensive ^{13}C labeled substrates as well as sufficiently long ^{13}C NMR acquisitions.

Figure 3.1 illustrates the process of lactate recycling through the plasma membrane of a representative tumor cell. Once lactate molecules reach the cytosolic space, they participate in the LDH equilibrium, incorporating one deuteron in their methine carbon and eventually returning to the extracellular space. This circumstance is observed by ^{1}H NMR because of the vicinal

isotopic effect of ^{2}H2 on the chemical shifts of the methyl resonance of lactate in the incubation medium. This makes it possible to discriminate lactate molecules that have passed through the cell cytosol from those that have not, because only the former become deuterated by cytosolic LDH in incubation media containing $^{2}H_2O$. Notably, the proposed methodologies allow the detection of H2 deuteration with the increased sensitivity of ^{1}H NMR, and thus avoid the necessity of using ^{13}C-labeled substrates. Even if these are used, however, our methods allow the turnover of the H2 hydrogen in both ^{13}C-labeled and ^{12}C lactate molecules to be measured simultaneously, and thus provide robust methods to investigate ^{2}H and ^{13}C isotopic effects simultaneously on lactate turnover.

In this chapter, we describe two new rapid and robust methods for ^{1}H NMR spectroscopy discrimination between non-deuterated and H2 deuterated lactate molecules. The first one is a conventional non-edited ^{1}H NMR spectroscopy and the second approach is based on the use of a specific lactate editing sequence (Choi *et al.* 2006; Rothman *et al.* 1984b).

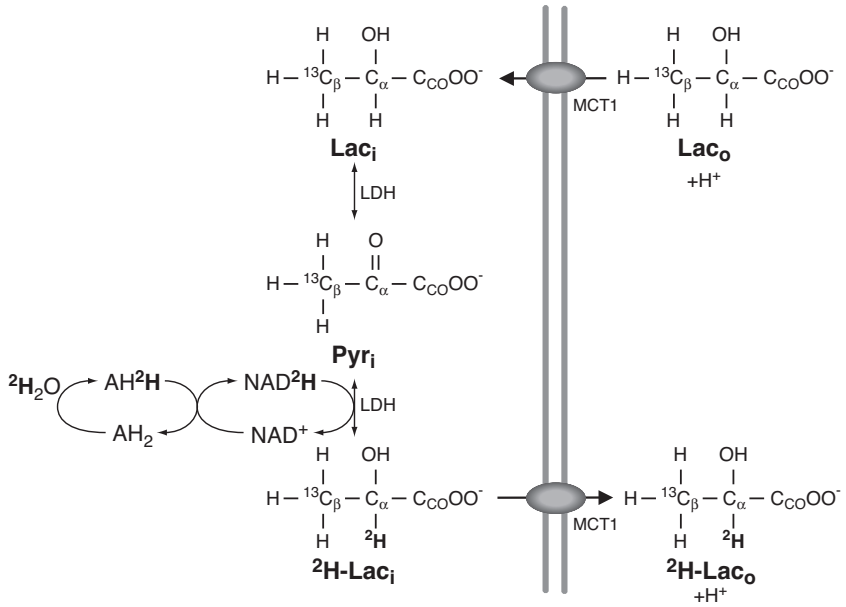

Figure 3.1. Mechanism of lactate recycling during metabolism of 5 mM (3-^{13}C) lactate in Krebs-Henseleit Buffer containing 50% $^{2}H_2O$ (vol/vol). Extracellular (3-^{13}C) lactate (Lac$_o$, unshifted) enters the cytosol (Lac$_i$) through the MCT1 transporter. (3-^{13}C) Lac$_i$ loses its H2 hydrogen and incorporates a deuteron from NAD(^{2}H) in the cytosolic LDH equilibrium. (3-^{13}C, 2-^{2}H) Lac$_i$ abandons the cell through the reversible MCT1 transporter originating the shifted singlet (^{2}H-Lac$_o$) in the incubation medium (cf. Figures 3.2 and 3.3). Deuterons are transferred to NAD^{+} through a combination of hydration-dehydration (formation of A^{2}H) and red-ox reactions (formation of NAD^{2}H). Lac: lactate, LDH: lactate dehydrogenase, MCT1: monocarboxylate transporter type 1, Pyr: pyruvate.

Both protocols may be easily extendable to other molecules and exchange pathways between intra- and extracellular spaces, where a deuterium exchange site is present only in the intracellular milieu.

3. Materials and Methods

3.1 Cell Culture and Preparation

C6 glioma cells were purchased from the local representative of the American Tissue Culture Collection (LGC Promochem, Barcelona, Spain). Briefly, C6 glioma cells were grown to confluence in Dulbecco's modified Eagle's medium (DMEM) supplemented with fetal bovine serum (5%) (FBS), 100 μg/mL streptomycin, 25 μg/mL gentamycin, 100 U/mL of penicillin and fungizone (1% vol/vol), in sterile Petri dishes (10-cm diameter) at 37 °C in a humidified atmosphere containing 5% CO_2-95% O_2. Nine independent cultures of C6 cells were used. When cells reached a confluent appearance, five cultures were incubated (3-30 h, 37 ºC) in Krebs-Henseleit Buffer (KHB) (NaCl, 119 mM; KCl, 4.7 mM; $CaCl_2$, 1.3 mM; $MgSO_4$, 1.2 mM; HEPES, 15 mM and KH_2SO_4, 1.2 mM) containing 50% (vol/vol) ^2H_2O with 5 mM (3-^{13}C) lactate. Other five confluent cultures were incubated in the same conditions for the development of the edited ^{1}H NMR spectroscopy approach, except by the fact that the lactate used was unlabeled. In both cases, aliquots from the medium (0.5 mL) were collected for increasing incubation periods, lyophilized and ressuspended in 0.5 mL ^2H_2O (99.9% ^{2}H) prior to high-resolution ^{1}H NMR analysis. Appropriate control experiments were carried out with cell free incubations or incubations carried out under similar cellular conditions (one culture) in the absence of ^2H_2O.

3.2 Non-Edited ^{1}H NMR Spectroscopy

^{1}H NMR spectra from 0.5-mL samples of the incubation medium were obtained at 11.7 Tesla (500.130 MHz, 25 ºC, pH 7.2) with a Bruker AVANCE 500WB NMR spectrometer using a commercial (5-mm) triple resonance probe (^{1}H,^{13}C,^{2}H). Acquisition conditions were: $\pi/3$ pulses, 10.3 kHz spectral width, 3.17 s acquisition time, 64 k words data table and an interpulse delay of 3.0 s, resulting in a repetition time of 6.17 s. Fully-relaxed ^{1}H NMR spectra were acquired under the same conditions using $\pi/3$ flip angle and a relaxation delay of 20 s. T_1 measurements were obtained and analyzed with the Bruker analysis software (Bruker BioSpin GmbH, Rheinstetten, Germany), being calculated from inversion recovery experiments with at least 15 different τ values. The T_1

values of the (3-^{13}C) and (3-^{12}C) lactate methyl multiplets ranged from 114 to 128 ms, indicating an almost complete relaxation in our acquisition protocol. Under these conditions it is not necessary to introduce correction factors to account for partial saturation of any multiplet resonance.

The ^{1}H spectra were line-broadened (0.2 Hz), zero-filled, Fourier-transformed, phased, and referenced to external TSP (0.0 ppm). Selectively ^{13}C-decoupled ^{1}H NMR spectra of the methyl resonance of lactate were obtained with low power single-frequency irradiation over the ^{13}C3 lactate resonance (20.9 ppm), using the GARP technique (Globally optimized Alternating-phase Rectangular Pulses) (Shaka *et al.* 1985). Simulated spectra were generated with program NUTS™ (Acorn, Freemont, CA, USA) to investigate the isotopic shifts and quantify relative resonance areas.

The ^{1}H NMR time courses $M_{(t)}$ were fitted to single exponentials of the type $M_{(t)} = M_{(\infty)}$ (1-exp(-k.t)) to obtain the values of the rate constant k and the asymptote $M_{(\infty)}$. For this purpose we used the nonlinear least-squares routines of the Sigma Plot program (SPSS Inc., Chicago, IL, USA) as implemented on an Intel PC platform. Statistical significance in the comparisons of values of k and $M_{(\infty)}$ was assessed using the Student's *t*-test.

3.3 Edited ^{1}H NMR Spectroscopy

High-resolution ^{1}H NMR spectra from 0.5-mL aliquots of the incubation medium were obtained at 11.7 Tesla (500.130 MHz, 4 ºC, pH 7.2) with a Bruker AVANCE 500WB NMR spectrometer using a commercial (5-mm) triple resonance probe (^{1}H,^{13}C,^{2}H). As indicated above, the non-edited ^{1}H NMR spectra of these samples are relatively complex, mainly because H3 proton resonances from both H2 non-deuterated and deuterated lactate molecules overlap at 1.31 ppm (Rodrigues and Cerdán 2005). To resolve this overlap, we implemented the lactate editing method previously described to isolate lactate from lipids (Rothman *et al.* 1984a; Rothman *et al.* 1984b). Briefly, the experiment comprises two separate acquisitions using a regular spin echo sequence with an echo time of 144 ms (1/*J*), which produces a phase-modulation (*J*-modulation) of 180 degrees on the H2 and H3 resonances of lactate. In the first acquisition a selective decoupling pulse is applied on the H2 resonance of lactate that destroys the phase modulation. The second spectrum is acquired in the absence of the decoupling pulse and hence lactate resonances appear with a phase modulation of 180 degrees. The summation of the two spectra cancels out the non-deuterated lactate resonances (modulated) whereas it adds the resonance intensities of the other resonances (non-modulated), including the H3 singlet of H2 deuterated lactate.

The ^{1}H spectra were line-broadened (0.3 Hz), zero-filled, Fourier-transformed, phased, and referenced to internal TSP (0.0 ppm) at a concentration of 1 mM. Comparing the TSP area with the ones obtained in the edited spectra, we were able to easily quantify the time course of (2-^{2}H)

lactate concentration. The program NUTS™ (Acorn, Freemont, CA, USA) was used to analyze the isotopic shifts and quantify the relative areas of shifted and non shifted resonances.

Finally, the ^{1}H NMR time course of H2 deuteration as detected with our editing sequence $C_{(t)}$ was fitted to a single exponential of the type $C_{(t)} = C_{(\infty)}$ (1-exp(-k.t)) to obtain the values of the rate constant k and the asymptote $C_{(\infty)}$. For this purpose, we also used the non linear least squares routines of the Sigma Plot program (SPSS Inc., Chicago, IL, USA).

3.4 Determination of Lactate Concentration

The lactate concentration in the incubation media was determined spectrophotometrically using classical enzymatic end-point methods coupled to the increase in NADH absorption at 340 nm. Conventional methods were adapted to become operative using 96-well microplates (0.25 mL) and a vertical microplate reader (Molecular Devices, Spectramax, Sunnyvale, CA, USA).

3.5 Materials

(3-^{13}C) lactate (98% ^{13}C) and deuterated solvents were obtained from Cambridge Isotope Laboratories (Andover, MA, USA). $^{2}H_2O$ (99.9% ^{2}H) was obtained from Apollo Scientific Ltd. (Stockport, Cheshire, UK). Auxiliary enzymes and cofactors were from Boehringer Mannheim (Germany). FBS and DMEM were purchased from GIBCO BRL (Gent, Belgium). Other items were of the highest purity available commercially from SIGMA Chemical Co. (St. Louis, MS, USA).

4. Results and Discussion

4.1 Non-Edited ^{1}H NMR Spectroscopy

Figures 3.2-A and 3.2-B show the ^{1}H NMR resonances of the methyl group of (3-^{13}C) and (3-^{12}C) lactate from the incubation medium of C6 cells, immediately after the addition of (3-^{13}C) lactate in KHB containing 50% $^{2}H_2O$ (vol/vol) (Figure 3.2-A), or 30 h later (Figure 3.2-B). At the beginning of the incubation (Figure 3.2-A), the ^{1}H NMR multiplet from the methyl group of lactate consists of six resonances: (i) a central doublet originated from the vicinal homonuclear coupling $J_{\beta H\text{-}\alpha H}$ (6.9 Hz) of the methyl group from (3-^{12}C) lactate molecules (Figure 3.2-A: resonances c-c´) and (ii) a doublet of doublets derived from the combination of the larger geminal heteronuclear coupling

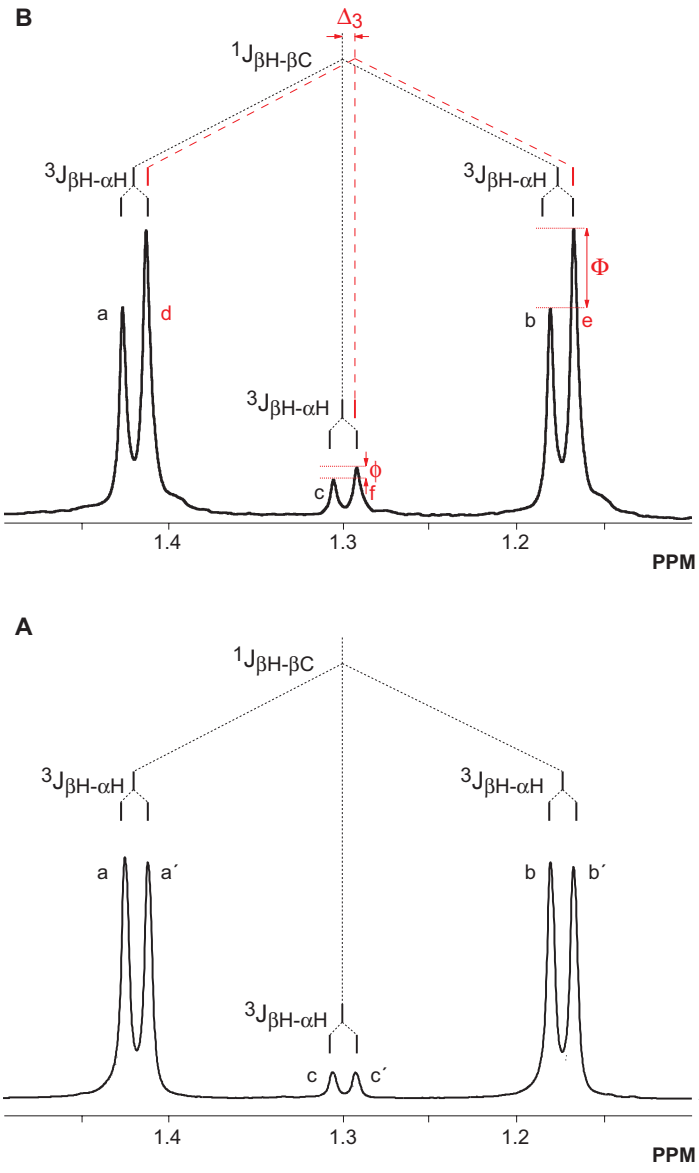

Figure 3.2. ^{1}H NMR resonances (500.13 MHz, 25 °C, pH 7.2) of the methyl signals of lactate from the medium of C6 glioma cells incubated with 5 mM (3-^{13}C) lactate in Krebs-Henseleit Buffer containing 50% $^{2}H_2O$ (vol/vol). A: immediately after the addition of the ^{13}C label. (3-^{13}C) and (3-^{12}C) lactate originate an isointense doublet of doublets a,a´-b,b´ ($^{1}J_{\beta H-\beta C}$ = 128.0 Hz + $^{3}J_{\beta H-\alpha H}$ = 6.9 Hz) and a doublet c,c´ ($^{3}J_{\beta H-\alpha H}$ = 6.9 Hz), respectively. **B:** 30 h later, (3-^{13}C, 2-^{2}H) and (3-^{12}C, 2-^{2}H) originate an isotopically shifted doublet (Δ_3 = -0.007 ppm, $^{1}J_{\beta H-\beta C}$ = 128.0 Hz) and a singlet (Δ_3 = -0.007 ppm), respectively. The shifted resonances are superimposed over those of the perprotonated multiplet, originating an asymmetric increase in the intensity of the upfield transitions of the multiplets d,e (Φ) and f (ϕ).

$J_{\beta H\text{-}\beta C}$ (128.0 Hz) (Figure 3.2-A: a-b, a´-b´) with the smaller vicinal homonuclear $J_{\beta H\text{-}\alpha H}$ coupling (6.9 Hz) (Figure 3.2-A: a-a´, b-b´) from the methyl group of (3-^{13}C) lactate molecules. The ratio of intensities of the external doublet of doublets to the internal doublet allows the determination of the fractional ^{13}C enrichment in the lactate C3 carbon (Rothman *et al.* 1985).

The substitution of the H2 hydrogen of (3-^{13}C) lactate by one deuteron introduces remarkable changes in the multiplet structure of the H3 resonance: (i) the transformation of the original doublet of doublets into an apparent doublet, because of the disappearance of the homonuclear vicinal $J_{\beta H\text{-}\alpha H}$ coupling (6.9 Hz) and (ii) the upfield shift of this doublet caused by the vicinal heavy atom isotope effect (Δ_3 = -0.007 ppm). This upfield isotopic shift has a very similar value to ½ $J_{\beta H\text{-}\alpha H}$ coupling constant, a situation that results in the superposition of the shifted doublet over the higher-field components of the doublet of doublets, causing an apparent doublet of doublets with dissymmetric intensities (Figure 3.2-B, dotted lines, e-b = Φ).

Similar effects of H2 deuteration are observed in the central (3-^{12}C) lactate doublet, which loses the vicinal, $J_{\beta H\text{-}\alpha H}$ coupling (6.9 Hz) to originate a vicinal and isotopically shifted singlet (Figure 3.2-B: f) that superimposes on the high-field component of the doublet. This superposition causes a difference in intensity between the otherwise isointense transitions of the (3-^{12}C) lactate doublet (see c-c´ in Figure 3.2-A), the imbalance being due to superposition of the (3-^{12}C, 2-^{2}H) singlet over the high-field component of the doublet (Figure 3.2-B: dotted lines, f-c = ϕ). Notably, H2 deuteration of lactate was not observed in the same experimental time when cell-free incubations with (3-^{13}C) lactate in KHB containing 50% $^{2}H_2O$ (vol/vol) were used, revealing the intracellular origin of the deuteration process.

Figure 3.3 illustrates these changes in more detail by showing the simulated deconvolution of the heteronuclear multiplet from the methyl group of (3-^{13}C) lactate in the corresponding components. Figure 3.3-A depicts the structure of the doublet of doublets derived from (3-^{13}C) lactate. Figure 3.3-B shows the methyl resonance from (3-^{13}C, 2-^{2}H) lactate, in which the vicinal homonuclear $J_{\beta H\text{-}\alpha H}$ coupling (6.9 Hz) is lost because of the ^{2}H2 substitution. A residual heteronuclear coupling $J_{\beta H\text{-}\alpha^{2}H}$ remains resolved (ca. 1.07 Hz) in the simulation. This residual doublet is approximately 6.25 times smaller than the corresponding doublet derived from homonuclear coupling (ca. 7 Hz in Figure 3.3-A), as would be expected from the 6.25 smaller value of the gyromagnetic ratios of ^{2}H *vs.* ^{1}H (Evans 1995). Unfortunately, the small vicinal heteronuclear ^{1}H-^{2}H scalar coupling constant (ca. 1.07 Hz) observed in the simulation is smaller than the natural linewidth of the H3 proton doublet in extracts or *in vivo*, which makes this heteronuclear $J_{\beta H\text{-}\alpha^{2}H}$ coupling virtually unobservable experimentally. Figure 3.3-C shows the combined multiplet structure of the methyl resonances from a mixture of (3-^{13}C) and (3-^{13}C, 2-^{2}H) lactate isotopomers, after the linewidth of the latter is increased to the natural linewidths observed in extracts (2-2.5 Hz). The same effect occurs in (3-^{12}C) lactate (not shown). In this case, ^{2}H binding to C2 transforms and shifts the doublet resonance

from the methyl group of (3-^{12}C) lactate into an apparent singlet, which appears superimposed on the high-field portion of the doublet, resulting in an increase in intensity that depends on the amount of ^{2}H incorporated (c.f. Figure 3.2-A, central multiplet).

Therefore, analysis of the structure of the ^{1}H NMR multiplets from (3-^{13}C) and (3-^{12}C) lactate allows the determination of the relative amounts of (3-^{13}C) and (3-^{12}C) lactate *vs.* (3-^{13}C, 2-^{2}H) and (3-^{12}C, 2-^{2}H) lactate, respectively. The differences in multiplet structure of the methyl resonances (3-^{13}C) and (3-^{12}C) lactate and those of (3-^{13}C, 2-^{2}H) and (3-^{12}C, 2-^{2}H) lactate allow

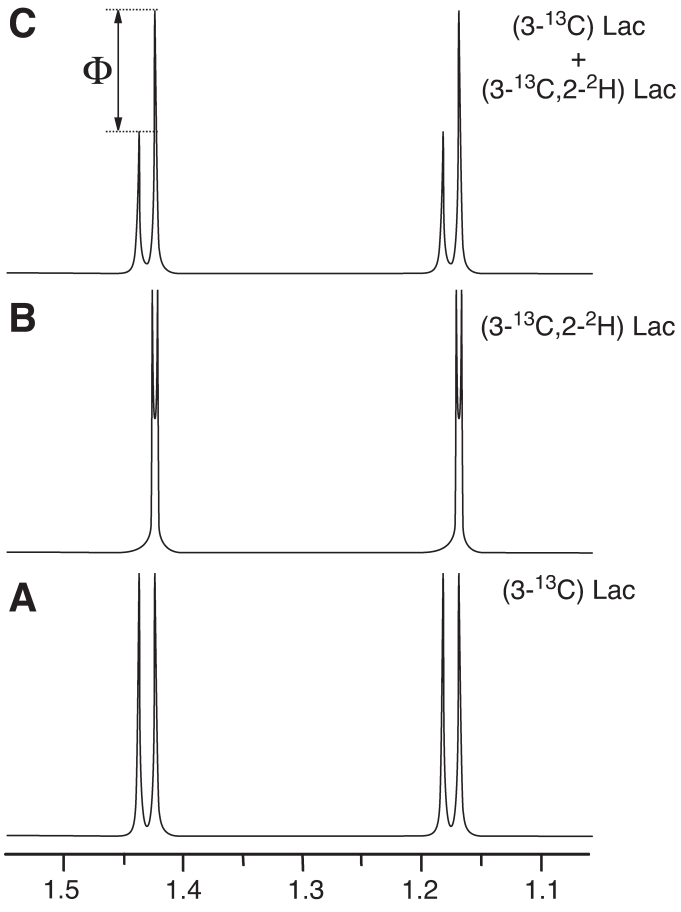

Figure 3.3. Representative ^{1}H NMR simulations of the methyl resonances of: A: (3-^{13}C) lactate ($^{1}J_{\beta H\text{-}\beta C}$ = 128.0 Hz, $^{3}J_{\beta H\text{-}\alpha H}$ = 6.9 Hz), **B**: (3-^{13}C, 2-^{2}H) lactate ($^{1}J_{\beta H\text{-}\beta C}$ = 128.0 Hz, $^{1}J_{\beta H\text{-}\alpha^{2}H}$ = 1.07 Hz; Δ_{3} = -0.007 ppm) and **C**: a mixture of (3-^{13}C, 66%) and (3-^{13}C, 2-^{2}H, 33%) lactate with natural linewidth of 2.0 Hz. Simulations were performed with the NUTS™ program. Φ: increase in intensity due to the appearance of (3-^{13}C, 2-^{2}H) lactate.

the determination of the fractional deuterium enrichment in H2 of (3-^{13}C) and (3-^{12}C) lactate, as indicated by equations. [3.1] and [3.2], respectively:

$$\text{Fractional } ^2\text{H2 enrichment in (3 - } ^{13}\text{C) lactate} = \frac{[^2\text{H2}]}{([^2\text{H2}] + [^1\text{H2}])} = \frac{(d + e) - (a + b)}{a + b + d + e} = \frac{2\,\Phi}{a + b + c + d} \qquad [3.1]$$

$$\text{Fractional } ^2\text{H2 enrichment in (3 - } ^{13}\text{C) lactate} = \frac{[^2\text{H2}]}{([^2\text{H2}] + [^1\text{H2}])} = \frac{f - c}{c + f} = \frac{\phi}{c + f} \qquad [3.2]$$

The intensities of resonances *a*, *b*, *c*, *d*, *e* and *f* are those illustrated in Figure 3.2-B.

Figure 3.4 depicts the time dependence of the H2 deuteration process as detected by the changes in the structure of the methyl multiplets of (3-^{13}C) and (3-^{12}C) lactate, during a 30 h incubation

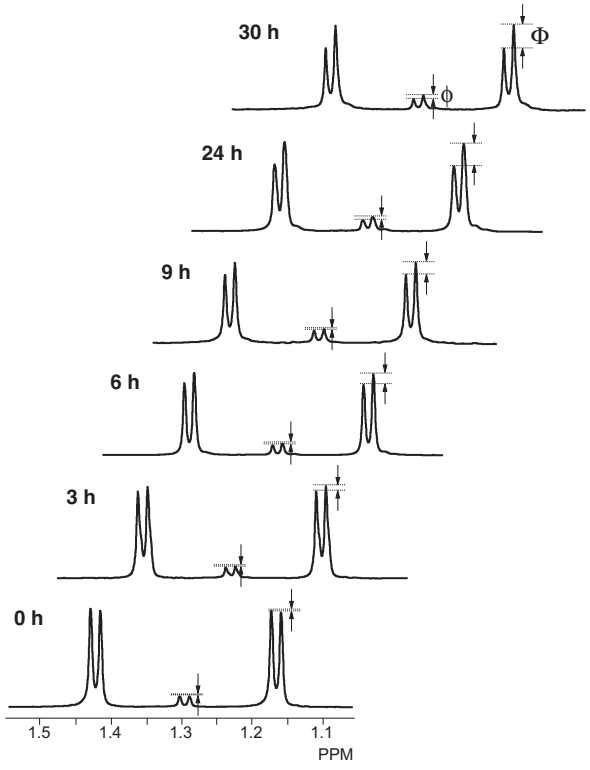

Figure 3.4. Representative time course of H2 deuteration as detected by the changes in the relative intensities of the multiplet resonances from the methyl groups of (3-^{13}C) and (3-^{12}C) lactate. C6 glioma cells were incubated for 30 h with 5 mM (3-^{13}C) lactate in Krebs-Henseleit Buffer containing 50% ^2H_2O (vol/vol). Deuteration can be easily followed through the asymmetric increase in the intensity of the upper field transitions reflecting the increase in concentration of (3-^{13}C, 2-^{2}H) lactate (Φ) or (3-^{12}C, 2-^{2}H) lactate (ϕ).

of C6 cells with (3-^{13}C) lactate in KHB containing 50% $^{2}H_2O$ (vol/vol). During this period, total lactate concentrations in the incubation medium decreased from 4.2 ± 0.6 mM at the beginning of the incubation to 3.3 ± 1.2 mM at the end. An exponential increase in the deuterared portion of the (3-^{13}C) and (3-^{12}C) multiplets was detected (arrows). These modifications are not observed in cell free incubations of KHB (50% $^{2}H_2O$, vol/vol) with (3-^{13}C) lactate, or in during incubations of C6 cells with (3-^{13}C) lactate in undeuterated KHB (data not shown), confirming that the described modifications are indeed derived from *de novo* enzymatic production of (3-^{13}C, 2-^{2}H) lactate. In addition, Figure 3.4 also shows that it is possible to analyze the deuteration of (3-^{13}C) and (3-^{12}C) lactate molecules simultaneously, allowing the evaluation of the kinetics of H2 deuteration both in (3-^{13}C) and (3-^{12}C) lactate, as indicated in Figure 3.5.

Figure 3.5 shows the time course of H2 deuteration in (3-^{13}C) and (3-^{12}C) lactate, as obtained from three experiments with different cultures of C6 cells. The kinetics were fitted to a single exponential and gave values for the rate constants k (n = 3, mean ± S.D.) of 0.06 ± 0.02 h^{-1} and 0.15 ± 0.05 h^{-1}, for the production of (3-^{13}C, 2-^{2}H) lactate and (3-^{12}C, 2-^{2}H) lactate, respectively.

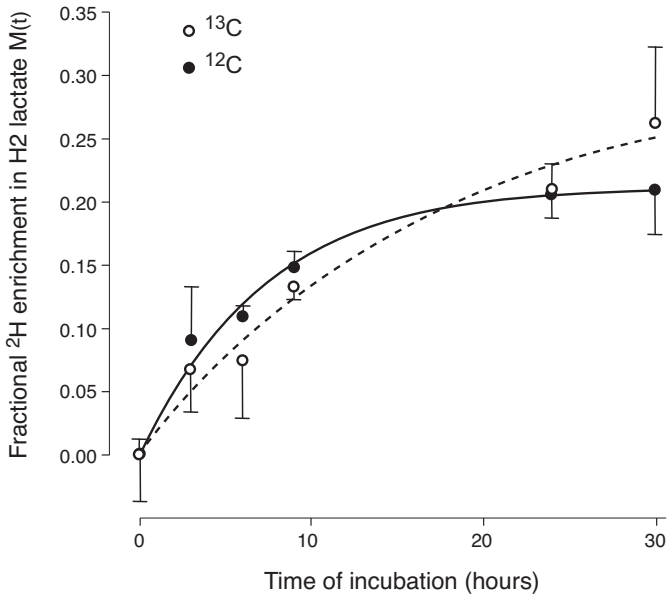

Figure 3.5. Turnover of the H2 hydrogen from (3-^{13}C) lactate (empty circles, dotted line) and (3-^{12}C) lactate (filled circles, full line) during incubations with 5 mM (3-^{13}C) lactate in Krebs-Henseleit Buffer containing 50% $^{2}H_2O$ (vol/vol). Fractional ^{2}H enrichments in H2 lactate for each time point were determined as described in the text. The experimental points $M_{(t)}$ were fitted to a single exponential of the type $M_{(t)} = M_{(\infty)}$ (1-exp(-k.t)) to determine $M_{(\infty)}$ and k. Results are shown as the mean ± S.D. of three independent experiments with different cell cultures.

Similarly, the asymptote values $M_{(\infty)}$ were 0.30 ± 0.05 and 0.21 ± 0.02 for (3-^{13}C, 2-^{2}H) lactate and (3-^{12}C, 2-^{2}H) lactate, respectively. The differences found between the average rate constants and asymptote values were not statistically significant as revealed by the Student *t* test (P=0.12 for k and P = 0.14 for $M_{(\infty)}$).

4.2 Edited ^{1}H NMR Spectroscopy

Figure 3.6 depicts representative ^{1}H NMR (500.130 MHz, 4 ºC, pH 7.2) non-modulated (1), modulated (2) and edited (1+2) spectra, obtained from the incubation medium of C6 glioma cells, 30 h after the addition of lactate to the incubation buffer. At the beginning of the incubation,

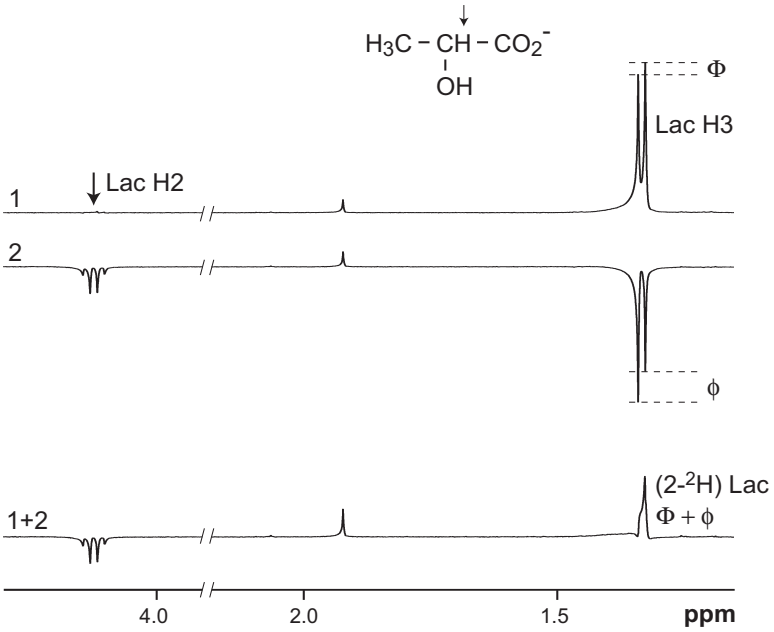

Figure 3.6. Representative ^{1}H NMR spectra (500.130 MHz, 4 ºC, pH 7.2) non-modulated (1), modulated (2) and edited (1+2) from the medium of C6 glioma cells incubated during 30 hours with 10 mM lactate in Krebs-Henseleit buffer containing 50% $^{2}H_2O$ (vol/vol). The lactate H3 resonance doublet ($^{3}J_{\beta H\text{-}\alpha H}$ = 6.9 Hz) is observed at 1.31 ppm in spectrum 1. Note that the upfield moiety of the lactate doublet shows higher intensity (Φ) because of the overlap with the isotopically shifted methyl resonance of ^{2}H2 lactate. The arrow symbolizes the selective decoupling pulse applied on the H2 proton resonance at 4.08 ppm (not observable because of the saturation caused by the decoupling pulse). An echo time of 144 ms results in a 180 degrees phase modulation on the non-deuterated lactate H2 and H3 resonances (inverted peaks in spectrum 2), which is not present in the non-modulated spectrum (1). Note that the upfield moiety of the lactate doublet depicts now lower intensity (ϕ). By adding spectra 1 and 2, we can readily observe a peak that represents the double of the concentration of (2-^{2}H) lactate (δ ≈ 1.3 ppm, Φ + ϕ).

the edited lactate resonance from the lactate methyl group is virtually zero (not shown). The subsequent substitution of the lactate hydrogen of the H2 proton by one deuteron gives rise to an upfield shifted singlet in the H3 resonance, which can be clearly isolated and resolved in the edited spectrum. When the same experimental design was used in the cell-free incubations, this deuteration was not observed (data not shown), confirming that the observed deuteration process is necessarily intracellular.

Figure 3.7 shows the time course of H2 deuteration in lactate, as detected with this edition protocol in five experiments with different cultures of C6 cells. Since we used 1 mM TSP as an internal reference, it became possible to calculate quantitatively the increase in deuterated lactate concentration. The kinetics for the production of (2-^{2}H) lactate were fitted to a single exponential, providing a value for the rate constant k of 0.09 ± 0.01 h^{-1}, and an asymptote value $C_{(\infty)}$ of 1.59 ± 0.07 mM (mean ± S.E.M.). These values are similar to those obtained by non-edited ^{1}H NMR (Rodrigues and Cerdán 2005).

Finally, the present study shows that it is possible to distinguish lactate molecules that are moving from the cytosol to the incubation medium because they become labeled with ^{2}H in the LDH equilibrium (c.f. Figure 3.1, equation [3.3]).

$$\text{Pyruvate} + \text{NAD}(^{2}\text{H}) + \text{H}^{+} \leftrightarrow (2\text{-}^{2}\text{H})\ \text{Lactate} + \text{NAD}^{+} \qquad [3.3]$$

The required NAD(^{2}H) for this process may be derived from the sequential combination of a hydration-dehydration reaction (equation [3.4]) and a redox process (equation [3.5]) as follows,

$$\text{AH}_{2} + {}^{2}\text{H}_{2}\text{O} \leftrightarrow \text{AH}(^{2}\text{H}) + (^{2}\text{H})\text{HO} \qquad [3.4]$$

$$\text{AH}(^{2}\text{H}) + \text{NAD}^{+} + \text{H}^{+} \leftrightarrow \text{AH}_{2} + \text{NAD}(^{2}\text{H}) \qquad [3.5]$$

$$\text{Total} \qquad {}^{2}\text{H}_{2}\text{O} + \text{NAD}^{+} + \text{H}^{+} \leftrightarrow \text{H}(^{2}\text{H})\text{O} + \text{NAD}(^{2}\text{H}), \qquad [3.6]$$

where A is the metabolite incorporating the ^{2}H from $^{2}H_{2}O$ that will be transferred later to NAD^{+} in the redox process. Both reactions are stereospecific and only deuterons incorporated through malic enzyme or isocitrate dehydrogenase activities produce the correct stereochemistry in NAD(^{2}H) to become a cofactor in the LDH equilibrium (García-Martín *et al.* 2001). Therefore, cytosolic deuteration of lactate in H2 is a complex process involving several enzymes. The rate limiting step of this process is currently under investigation in our laboratory.

In conclusion, the present report shows how to distinguish nondeuterated lactate from the (2-^{2}H) lactate. For this purpose, we developed two simple, robust and sensitive ^{1}H NMR approaches for the measurement of the turnover of the H2 hydrogen of lactate, one of them based on a

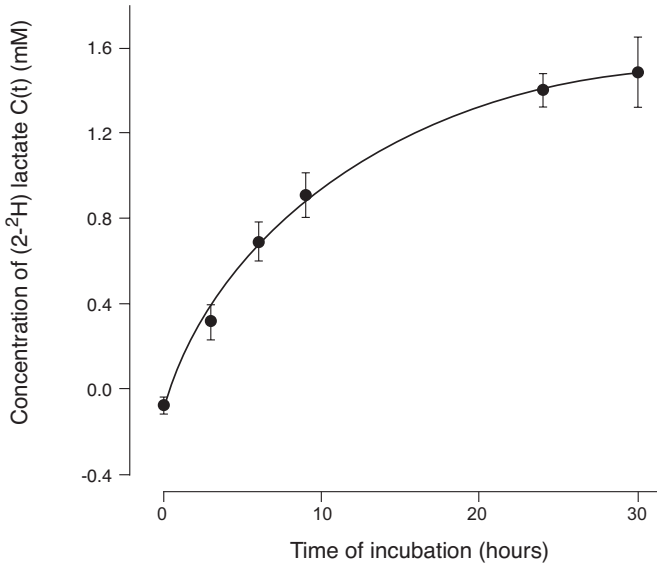

Figure 3.7. Turnover of the lactate H2 during incubations with 5 mM lactate in Krebs-Henseleit buffer containing 50% ^2H_2O (vol/vol). Concentrations of (2-^{2}H) lactate for each time point were determined as described in the text. The experimental points $C_{(t)}$ were fitted to a single exponential $C_{(t)} = C_{(\infty)}$ (1-exp(-k.t)) in order to determine the optimized $C_{(\infty)}$ and k parameter values. Results are the mean ± SEM of five experiments with different cell cultures.

lactate editing protocol.

Both methods are faster than previous ^{13}C NMR approaches and can be easily implemented virtually in all NMR apparatus. It is important to remark that while the measurement of perdeuteration was done in ^{13}C-labeled lactate in the non-edited ^{1}H NMR approach, with all the demonstrated benefits, it is also applicable to lactate in the absence of ^{13}C labeling.

Using the lactate editing sequence, we were able to eliminate the spectral overlap in the H3 lactate doublet, allowing the H2 deuteration measurement with greater accuracy than possible with non-edited ^{1}H NMR. This edited ^{1}H NMR method may be of potential interest for *in vivo* studies of lactate turnover, where other available methodologies, like ^{13}C NMR spectroscopy, are not only more expensive, but also much more difficult to implement.

5. References

Bouzier-Sore AK, Serres S, Canioni P, Merle M. 2003a. Lactate involvement in neuron-glia metabolic interaction: ^{13}C-NMR spectroscopy contribution. Biochimie 85(9):841-848.

Bouzier-Sore AK, Voisin P, Canioni P, Magistretti PJ, Pellerin L. 2003b. Lactate is a preferential oxidative energy substrate over glucose for neurons in culture. J Cereb Blood Flow Metab 23(11):1298-1306.

Cater HL, Chandratheva A, Benham CD, Morrison B, Sundstrom LE. 2003. Lactate and glucose as energy substrates during, and after, oxygen deprivation in rat hippocampal acute and cultured slices. J Neurochem 87(6):1381-1390.

Cerdán S, Rodrigues TB, Sierra A, Benito M, Fonseca LL, Fonseca CP, García-Martín ML. 2006. The redox switch/redox coupling hypothesis. Neurochem Int 48(6-7):523-530.

Chapa F, Cruz F, García-Martín ML, García-Espinosa MA, Cerdán S. 2000. Metabolism of (1-^{13}C) glucose and (2-^{13}C, 2-$^{2}H_3$) acetate in the neuronal and glial compartments of the adult rat brain as detected by [^{13}C, ^{2}H] NMR spectroscopy. Neurochem Int 37(2-3):217-228.

Choi C, Coupland NJ, Kalra S, Bhardwaj PP, Malykhin N, Allen PS. 2006. Proton spectral editing for discrimination of lactate and threonine 1.31 ppm resonances in human brain *in vivo*. Magn Reson Med 56(3):660-665.

Dienel GA, Hertz L. 2001. Glucose and lactate metabolism during brain activation. J Neurosci Res 66(5):824-838.

Evans JNS. 1995. Biomolecular NMR Spectroscopy. Oxford, U.K.: Oxford University Press.

García-Martín ML, Ballesteros P, Cerdán S. 2001. The metabolism of water in cells and tissues as detected by NMR methods. Progress in NMR Spectrosc 39:41-77.

García-Martín ML, García-Espinosa MA, Ballesteros P, Bruix M, Cerdán S. 2002. Hydrogen turnover and subcellular compartmentation of hepatic [2-^{13}C]glutamate and [3-^{13}C]aspartate as detected by ^{13}C NMR. J Biol Chem 277(10):7799-7807.

Halestrap AP, Meredith D. 2004. The SLC16 gene family-from monocarboxylate transporters (MCTs) to aromatic amino acid transporters and beyond. Pflugers Arch 447(5):619-628.

Halestrap AP, Price NT. 1999. The proton-linked monocarboxylate transporter (MCT) family: structure, function and regulation. Biochem J 343 Pt 2:281-299.

Hansen PE. 1989. Isotope effects on nuclear shielding. Ann Rep NMR Spectrosc 15:105-234.

Muller TB, Sonnewald U, Westergaard N, Schousboe A, Petersen SB, Unsgard G. 1994. C-13 Nmr-Spectroscopy Study of Cortical Nerve-Cell Cultures Exposed to Hypoxia. J Neurosci Res 38(3):319-326.

Pellerin L, Magistretti PJ. 1994. Glutamate uptake into astrocytes stimulates aerobic glycolysis: a mechanism coupling neuronal activity to glucose utilization. Proc Natl Acad Sci U S A 91(22):10625-10629.

Perdigoto R, Rodrigues TB, Furtado AL, Porto A, Geraldes CF, Jones JG. 2003. Integration of [U-$_{13}$C]glucose and $^{2}H_2O$ for quantification of hepatic glucose production and gluconeogenesis. NMR Biomed 16(4):189-198.

Qu H, Haberg A, Haraldseth O, Unsgard G, Sonnewald U. 2000. ^{13}C MR spectroscopy study of lactate as substrate for rat brain. Dev Neurosci 22(5-6):429-436.

Rodrigues TB, Cerdán S. 2005. A fast and sensitive ^{1}H NMR method to measure the turnover of the H2 hydrogen of lactate. Magn Reson Med 54(4):1014-1019.

Rodrigues TB, Gray HL, Benito M, Garrido S, Sierra A, Geraldes CF, Ballesteros P, Cerdán S. 2005. Futile cycling of lactate through the plasma membrane of C6 glioma cells as detected by (^{13}C, ^{2}H) NMR. J Neurosci Res 79(1-2):119-127.

Rothman DL, Arias-Mendonza F, Shulman GI, Shulman RG. 1984a. A pulse sequence for symplifying hydrogen NMR spectra of biological tissues. J Magn Reson 60:430-436.

Rothman DL, Behar KL, Hetherington HP, den Hollander JA, Bendall MR, Petroff OA, Shulman RG. 1985. ^{1}H-Observe/^{13}C-decouple spectroscopic measurements of lactate and glutamate in the rat brain *in vivo*. Proc Natl Acad Sci U S A 82(6):1633-1637.

Rothman DL, Behar KL, Hetherington HP, Shulman RG. 1984b. Homonuclear 1H double-resonance difference spectroscopy of the rat brain *in vivo*. Proc Natl Acad Sci U S A 81(20):6330-6334.

Schurr A, Payne RS, Miller JJ, Tseng MT. 2001. Preischemic hyperglycemia-aggravated damage: Evidence that lactate utilization is beneficial and glucose-induced corticosterone release is detrimental. J Neurosci Res 66(5):782-789.

Shaka AJ, Barker PB, Freeman R. 1985. Computer-optimized decoupling scheme for wideband applications and low-level operation. J Magn Reson 64(3):547-552.

Smith D, Pernet A, Hallett WA, Bingham E, Marsden PK, Amiel SA. 2003. Lactate: a preferred fuel for human brain metabolism *in vivo*. J Cereb Blood Flow Metab 23(6):658-664.

Vianello F, Scarpa M, Viglino P, Rigo A. 1997. Deuterium distribution in lactate as tracer of metabolic pathways. Biochem Biophys Res Commun 237(3):650-652.

The Redox Switch/Redox Coupling Hypothesis and its Kinetic Properties

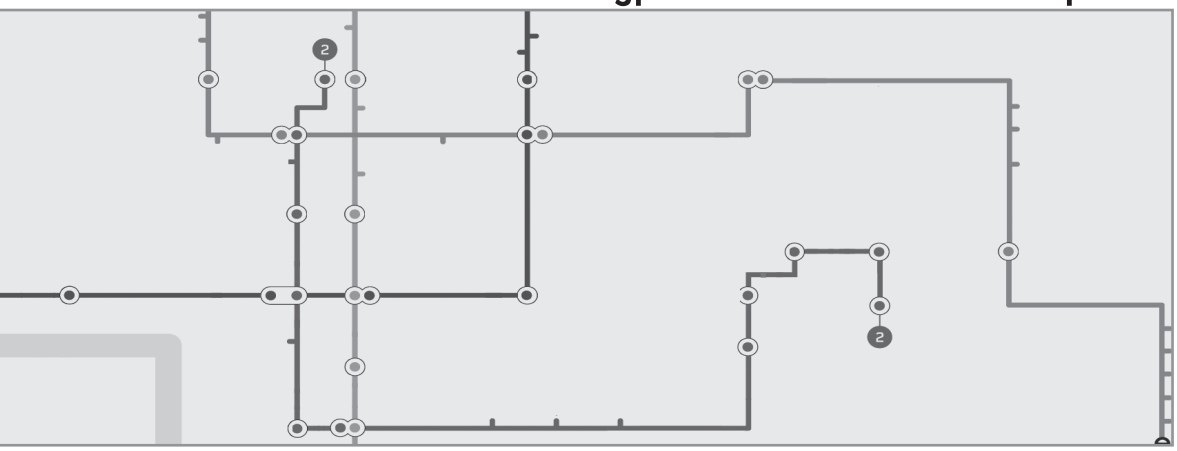

Chapter 4

1. Abstract

We provide an integrative interpretation of neuroglial metabolic coupling including the presence of subcellular compartmentation of pyruvate and monocarboxylate recycling through the plasma membrane of both neurons and glial cells. The subcellular compartmentation of pyruvate allows neurons and astrocytes to select between glucose and lactate as alternative substrates, depending on their relative extracellular concentration and the operation of a redox switch. This mechanism is based on the inhibition of glycolysis at glyceraldehyde 3-phosphate dehydrogenase level by NAD^+ limitation, under sufficiently reduced cytosolic NAD^+/NADH redox conditions. Lactate and pyruvate recycling through the plasma membrane allows the return to the extracellular medium of cytosolic monocarboxylates enabling their transcellular, reversible, exchange between neurons and astrocytes. Together, intracellular pyruvate compartmentation and monocarboxylate recycling result in an effective transcellular coupling between the cytosolic NAD^+/NADH redox states of both neurons and glial cells. Following glutamatergic neurotransmission, increased glutamate uptake by the astrocytes is proposed to augment glycolysis and TCA cycle activity, balancing to a reduced cytosolic NAD^+/NADH in the glia. Reducing equivalents are then transferred to the neuron resulting in a reduced neuronal NAD^+/NADH redox state. This may eventually switch off neuronal glycolysis, favoring the oxidation of extracellular lactate in the LDH equilibrium and in the neuronal TCA cycles. Finally, pyruvate derived from neuronal lactate oxidation, may return to the extracellular space and to the astrocyte, restoring the basal redox state and beginning a new loop of the lactate/pyruvate transcellular coupling cycle. Transcellular redox coupling operates through MCTs at the plasma membrane, similarly to the intracellular redox shuttles coupling the cytosolic and mitochondrial redox states through the transporters of the inner mitochondrial membrane.

Additionally, we investigate the kinetic mechanisms underlying this Redox Switch/Redox Coupling hypothesis by characterizing the competitive consumption of glucose or lactate and the kinetics of pyruvate production in primary cultures of cortical neurons and astrocytes from rat brain. Glucose consumption was determined in neuronal cultures incubated in Krebs-Ringer bicarbonate buffer containing 0.25-5 mM glucose, in the presence and absence of 5 mM lactate as an alternative substrate. Lactate consumption was measured in neuronal cultures incubated with 1-15 mM lactate, in the presence and absence of 1 mM glucose. In both cases, the alternative substrate increased the K_m (mM) values for glucose consumption (from 2.2 ± 0.2 to 3.6 ± 0.1) or lactate consumption (from 7.8 ± 0.1 to 8.5 ± 0.1) without significant changes on the corresponding V_{max}. This is consistent with a competitive inhibition between simultaneous consumption of glucose and lactate. When cultures of neurons or astrocytes were incubated with increasing lactate concentrations 1-20 mM, pyruvate production was observed with K_m (mM) and V_{max} ($nmols.mg^{-1}.h^{-1}$) values of 1.0 ± 0.1 and

109 ± 4 in neurons, or 0.28 ± 0.1 and 342 ± 54 in astrocytes. Thus, astrocytes or neurons are able to return to the incubation medium as pyruvate, a significant part of the consumed lactate. Present results support the reversible exchange of reducing equivalents between neurons and astrocytes in the form of lactate or pyruvate. Monocarboxylate exchange is envisioned to operate under near equilibrium, with the transcellular flux directed thermodynamically towards the more oxidized intracellular redox environment. Transcellular redox coupling mechanisms may couple glycolytic and oxidative zones in other heterogeneous tissues including muscle and tumors.

2. Introduction

Metabolism of the monocarboxylates lactate and pyruvate plays a central role in cerebral energetics, providing a crucial link between glycolytic and oxidative metabolisms in the brain (Gruetter 2002; Hertz and Dienel 2002; Pellerin 2003; Rodrigues and Cerdán 2007; Sierra *et al.* 2007). Lactate and pyruvate metabolism in neural cells involves necessarily the activity of the MCTs of the plasma membrane and the cytosolic LDH isoenzymes. It has been described that neurons and astrocytes are equipped with different isoforms of these proteins, namely MCT1 and MCT2 or LDH1 and LDH5, respectively (Bittar *et al.* 1996; Laughton *et al.* 2000; Pellerin *et al.* 2005; Pierre and Pellerin 2005). This selective distribution of MCTs and LDH isozymes is thought to be consistent with a unidirectional flux of lactate from astrocytes to neurons, as proposed in the classical Astrocyte to Neuron Lactate Shuttle (ANLS) metabolic coupling hypothesis (Magistretti 2000; Magistretti and Pellerin 2000; Pellerin and Magistretti 1994; Tsacopoulos and Magistretti 1996). Additionally, the flow of carbon skeletons from glucose to CO_2, in neurons and astrocytes, during cerebral activation is currently understood to proceed as outlined by this hypothesis (Magistretti *et al.* 1999; Pellerin and Magistretti 1994; Tsacopoulos and Magistretti 1996). During the past decades much attention has been given to this flow of carbon skeletons and their relationship to cerebral energetics and neurotransmission (Cruz and Cerdán 1999; Rothman *et al.* 2003). However, the pathways for the transfer of reducing equivalents to O_2 and H_2O remained much less explored. In particular, the highly heterogeneous cellular composition of the cerebral tissue led to considerable uncertainties concerning the roles, relative contributions, subcellular compartmentation and coordination of the metabolisms of carbon skeletons and reducing equivalents, in neurons and glial cells.

Pyruvate and lactate transport through the MCTs is known to be reversible and driven by concentration gradients of monocarboxylate and protons (Halestrap and Meredith 2004; Halestrap and Price 1999; Hertz and Dienel 2005). Similarly, LDH is classically known to operate in the cytosol reversibly and close to thermodynamic equilibrium conditions (Veech 1991; Ward and Winzor 1983). Together, these concepts support the presence of reversible, rather than unidirectional, exchanges of lactate or pyruvate through plasma membrane of neurons and astrocytes, respectively. In this respect, intracellular compartmentation of lactate and pyruvate pools has been described both in neurons and astrocytes (Cruz *et al.* 2001; Sonnewald *et al.* 1993; Waagepetersen *et al.* 2001; Zwingmann *et al.* 2001), as well as in glioma cells (Bouzier *et al.* 1998). Two different intracellular pyruvate pools were characterized: one thought to operate in fast kinetic exchange with extracellular lactate or pyruvate (the P_p pool), the other proposed to be derived from the slower glycolytic degradation of glucose (the P_g pool) (Cruz *et al.* 2001). Earlier descriptions of neuroglial coupling did not consider these aspects. Thus, this reversibility of the LDH isozymes and MCT of neurons

and astrocytes allows these neural cells to produce and consume lactate or pyruvate, resulting in recycling of carbon and reducing equivalents through the corresponding plasma membranes (Rodrigues and Cerdán 2005b; Rodrigues *et al.* 2005). Moreover, because both lactate and pyruvate can exchange reversibly between cytosol of each cell and extracellular space, it follows that these metabolites can also be exchanged transcellular between both cells in a lactate/pyruvate shuttle, an aspect previously not envisioned. The competitive metabolism of glucose or lactate in neurons and astrocytes and the transcellular exchange of the monocarboxylates lactate and pyruvate between neurons and astrocytes, provided the basis for the Redox Switch/Redox Coupling hypothesis (Cerdán *et al.* 2006). However, despite a number of studies on the consumption of pyruvate by neurons and astrocytes (Cruz *et al.* 2001; Desagher *et al.* 1997; Matsumoto *et al.* 1994; Zwingmann and Leibfritz 2003), no evidence had been presented to our knowledge on the crucial aspect of pyruvate production by these cells.

In this chapter we provide a novel interpretation of neuroglial coupling that accounts for the proposals mentioned above. We begin summarizing the classical concepts of metabolic coupling, we continue our approach by analyzing the evidences of metabolic compartmentation of pyruvate and lactate, and then the presence of lactate recycling and the redox switch. In this chapter, we explore also the kinetics of the Redox Switch/Redox Coupling mechanisms by investigating the consumption of glucose and lactate in primary cultures of cortical neurons and demonstrate that pyruvate can be produced from lactate, both by neurons and astrocytes. Our results show that lactate and glucose are consumed competitively and simultaneously, the dominant substrate being determined by their relative extracellular concentrations, the specific kinetic constants for substrate consumption and the cytosolic redox states. In addition, we were also able to demonstrate that pyruvate is produced from lactate in primary cultures of neurons and glial cells, establishing a crucial link for the operation of the redox coupling mechanism. We conclude by describing the Redox Switch/Redox Coupling hypothesis as an integrative interpretation of neuroglial coupling.

2.1 The Astrocyte to Neuron Lactate Shuttle Hypothesis

In the section 8.1 of the first chapter of this thesis, and more particularly in Figure 1.10, we introduced the main aspects of the astrocyte to neuron lactate shuttle (ANLS) hypothesis (Magistretti 2000; Magistretti and Pellerin 2000; Pellerin 2003; Pellerin and Magistretti 1994; Tsacopoulos 2002; Tsacopoulos and Magistretti 1996; Tsacopoulos *et al.* 1998). Briefly, in this proposal, astrocytes are thought to play a central role in cerebral bioenergetics by coupling glucose consumption to neuronal activation. In summary, Pellerin and Magistretti suggested that the uptake of glutamate by astrocytes increases intracellular Na^+ activating Na^+/K^+ ATPase, which in turn reduces the levels of ATP that stimulates glycolytic activity, initiating production and release of lactate from

astrocytes. This enhanced lactate production is proposed to support neural metabolism during neurotransmission. In addition, calculated fluxes though the cerebral TCA cycle and the glutamate-glutamine cycle during (1-^{13}C) glucose metabolism, provided additional support to this hypothesis (Magistretti *et al.* 1999; Rothman *et al.* 1999; Shulman *et al.* 2001).

Since then, considerable experimental evidences have accumulated revealing that a major portion of the energy used to synthesize glutamine is derived from the astroglial TCA cycle rather than from glycolysis (García-Espinosa *et al.* 2003), that up to 40% of cerebral glutamate is obtained from alternative sources to glutamine (García-Espinosa *et al.* 2003) and that the glutamate-glutamine cycle may not present a 1:1 stoichiometry (Gruetter *et al.* 2001). Moreover, it was shown that different kinetic pools of pyruvate and lactate exist in neurons and astrocytes and that part of the lactate consumed by the neuron could be recycled back to the medium during the lactate recycling process (Cruz *et al.* 2001; Fonseca *et al.* 2004; Rodrigues and Cerdán 2005b; Rodrigues *et al.* 2005; Zwingmann *et al.* 2001). Finally, independent studies from several laboratories found that glutamate was significantly oxidized by astrocyte preparations and that increased glutamate concentrations resulted in a decrease of glucose consumption by these cells (Hertz 2004a; Peng *et al.* 2001; Sonnewald *et al.* 1997). Together, these findings suggested that the coupling mechanisms between neuronal and glial metabolisms during glutamatergic neurotransmission were more complex than initially envisioned. The following sections provide a more detailed analysis of these concepts.

2.2 Monocarboxylate Compartmentation in Neural Cells and the Redox Switch Hypothesis

Figure 4.1 illustrates the existence of two different intracellular pools of pyruvate in primary cultures of neurons and astrocytes (Cruz *et al.* 2001; García-Espinosa *et al.* 2004). Neurons incubated with mixtures containing 1 mM (1,2-$^{13}C_2$) glucose and increasing (3-^{13}C) pyruvate concentrations produced exclusively (3-^{13}C) lactate, rather than the corresponding mixtures of (3-^{13}C) and (2,3-$^{13}C_2$) lactate. This indicated that the cytosolic pools of (3-^{13}C) and (2,3-$^{13}C_2$) pyruvates derived from (3-^{13}C) pyruvate and (1,2-$^{13}C_2$) glucose, did not equilibrate rapidly in the neuronal cytosol. In contrast, data suggested that one pyruvate pool (the P_p pool) was derived from extracellular pyruvate (or other monocarboxylates as lactate) while the other (the P_g pool) was produced by glycolysis from extracellular glucose.

The detection of two intracellular pyruvate pools disclosed the mechanism by which neurons could select glucose or lactate as fuels to support neurotransmission. Indeed, both substrates are available in the extracellular fluid and could be, simultaneously or alternatively, consumed by neurons. A redox switch mechanism was proposed then to coordinate the subcellular compartmentation of the pyruvate pools and regulate glucose and monocarboxylate metabolism in neural cells. This

mechanism allowed neurons (and astrocytes) to switch between glucose and lactate as substrates for oxidation, depending on their relative availability in the extracellular space (García-Espinosa *et al.* 2004).

Briefly, fast monocarboxylate transport through the neuronal plasma membrane made the high lactate concentration in extracellular space derived from astrocytic glycolysis, to result rapidly, in augmented cytosolic lactate concentration in the neurons. Increased neuronal lactate in cytosol could switch off glycolysis in these cells by competition for NAD^+ between glyceraldehyde-3-phosphate dehydrogenase (GAPDH) and LDH systems (Figure 4.1-A). Under these conditions,

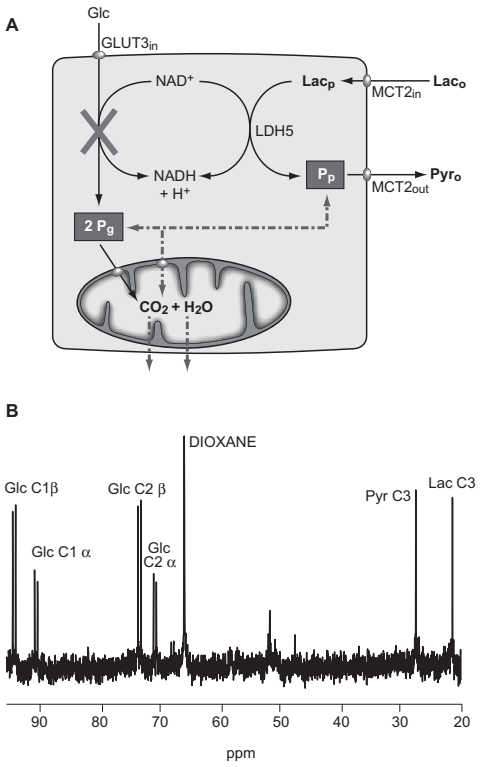

Figure 4.1. Intracellular compartmentation of pyruvate in primary cultures of neurons. A: ^{13}C NMR spectrum of neurons medium after incubation with 1 mM (1,2-$^{13}C_2$) glucose and 1 mM (3-^{13}C) pyruvate. Note that only (3-^{13}C) lactate is produced, as derived from (3-^{13}C) pyruvate. No (2,3-$^{13}C_2$) lactate is produced from (1,2-$^{13}C_2$) glucose. **B:** Two kinetically different pyruvate pools exist in neurons. The fast turnover P_p pool is derived from extracellular lactate or pyruvate while the slow turnover P_g pool is derived from glucose. In the presence of high lactate concentrations, glycolytic flow may be reduced or stopped by competition with lactate dehydrogenase for cytosolic NAD^+. Glc, glucose; Pyr, pyruvate; Lac, lactate. Adapted from (Cruz *et al.* 2001) with permission of the publisher.

glucose metabolism in neurons is reduced and lactate is oxidized in the TCA cycle until its concentration decreases to preactivation levels, restoring then normal neuronal glycolysis and TCA cycle activity.

Recently, dual photon NADH fluorescence confocal microscopy has been able to resolve in time the NADH balances occurring in neurons and astrocytes during glutamatergic activation (Figure 4.2) (Kasischke *et al.* 2004). Using cerebral cortex slices stimulated electrically, authors first found a transient decrease in NADH fluorescence colocalized with neuronal markers and sensitive to postsynaptic receptor inhibitors. Following this fast neuronal NADH depression, it was observed a sustained and more pronounced increase in NADH fluorescence, which colocalized with astrocytic markers. The transient decrease of neuronal NADH fluorescence could be due to net aerobic oxidation of glucose in the neuronal respiratory chain, while the increase in astrocytic NADH fluorescence could be attributed to anaerobic net lactate production in the astrocytes. NADH fluorescence results show that the (^{18}F)-2-deoxyglucose (FDG) accumulation observed

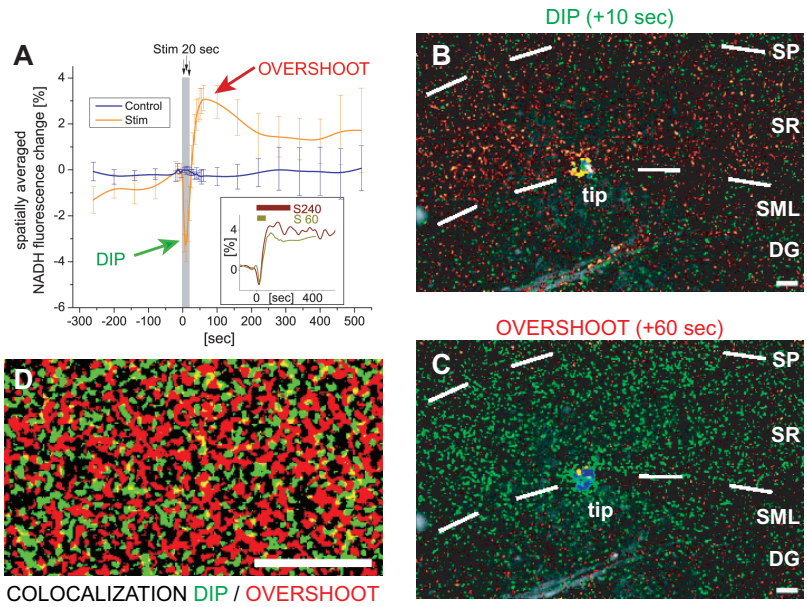

Figure 4.2. Confocal dual photon NADH fluorescence of neurons and glial cells *ex vivo* during electrical stimulation of cerebral cortex slices. A: Biphasic response after activation (orange) as compared to the resting state (blue). An initial NADH fluorescence dip is followed by an NADH fluorescence overshoot (orange). **B:** The NADH-dip colocalizes with neurons (green). **C:** The NADH-overshoot colocalizes with astrocytes (red). **D:** Binary image of NADH-dip and NADH-overshoot showing anticolocalization of both phases. Reproduced from (Kasischke *et al.* 2004) with permission of the publisher.

in vivo by PET techniques during cerebral activation occurs in the astrocytes, rather than in the neurons (Kasischke *et al.* 2004; Raichle 1998). Nevertheless, it should be noted here that the detected changes in NADH fluorescence in neurons and astrocytes, represent only the net balance between NADH production and consumption processes, rather than their absolute oxidative or glycolytic capacities in these cells (discussed later). Therefore, these findings are also consistent with the significant oxidative capacity described in astrocytes as well as with the considerable glycolytic capacity available to neurons, as long as the net balance between both processes favors neuronal oxidation or astrocytic glycolysis in the early or late phases of cerebral activation, respectively.

2.3 Lactate Recycling

Recently developed NMR methods (chapters 2 and 3) have allowed the demonstration of lactate recycling through the plasma membrane of glioma cell lines and primary cultures of neurons and astrocytes (Fonseca *et al.* 2004; Rodrigues and Cerdán 2005b; Rodrigues *et al.* 2005). A relevant consequence of the lactate recycling process in the ANLS hypothesis is that part of the neuronal lactate may return to the extracellular fluid rather than being metabolized intracellularly and that part of astrocytic lactate may recycle back from the extracellular fluid to the astrocyte cytosol. Lactate recycling could thus account in part for a non-stoichiometric relationship between glucose consumption and glutamate-glutamine cycling. A similar recycling situation may be found with pyruvate, suggesting that reversible exchange of lactate and pyruvate with the extracellular space occurs both in neurons and in astrocytes. Indeed, both neurons and astrocytes are known to be able to consume pyruvate (Cruz *et al.* 2001; Sharma *et al.* 2003; Zwingmann and Leibfritz 2003). In general, the exchange of reducing equivalents between neurons and astrocytes mimics, at the transcellular level, the intracellular exchange of reducing equivalents in the redox shuttles of the inner mitochondrial membrane (Palmieri 2004), providing the background for the transcellular redox coupling hypothesis proposed here.

3. Materials and Methods

3.1 Preparation and Characterization of Primary Cultures from Neural Cells and Incubation Conditions

Primary cultures of cortical neurons were prepared from embryos of Wistar rats with 17 days of gestation, essentially as described previously (Cruz *et al.* 2001). Briefly, the brains were isolated

from the embryos, the meninges removed, and the cortical areas collected in a PBS solution with 6 mM glucose and 1% BSA. Then, the cerebral tissue was minced and resuspended with a pipette. The suspension was then passed through a 80 μm filter and the cells seeded at 1.3×10^6 cells/mL in poly-lysine coated 8 cm plates with 10 mL of culture medium (DMEM with 15 mM HEPES, 2.5 μg/mL of fungizone, 100 U/mL of penicillin/streptomycin, 5 ng/mL Na_2SeO_4, 5 μg/mL insulin, 5 μg/mL transferrin, 6.3 ng/mL progesterone and 100 μM putrescine) with 5% FBS, 5% HS. Plates were maintained in a humidified incubator chamber at 37 ºC with 5% CO_2. After 24 hours, the cells were transferred to culture medium without serum and maintained for 6 more days in culture. 48 hours before the experiments, 10 μM cytosine β-D-arabinofuranoside was added to the culture medium.

On the day of the experiment, the DMEM medium was removed and substituted by Krebs-Ringer bicarbonate buffer containing increasing glucose concentrations of 0.25, 0.5, 1, 2.5 and 5 mM in the absence and presence of 5 mM lactate, or increasing lactate concentrations of 1, 2.5, 5, 10 and 15 mM in the absence and presence of 1 mM glucose. The concentrations of the competing substrates used were chosen from pilot sensitivity tests of glucose and lactate consumption to the presence of lactate and glucose, respectively. Two aliquots from the incubation medium (0.5 mL each) were withdrawn after three and six hours of incubation to determine glucose or lactate consumption and investigate the kinetic constants of these processes. An independent set of experiments was performed to evaluate neuronal pyruvate production from lactate. Primary cultures of neurons, prepared as described above, were incubated in Krebs Ringer bicarbonate buffer containing increasing lactate concentrations in the same range. In some experiments, the neuronal cultures were incubated with (3-^{13}C) lactate, to monitor (3-^{13}C) pyruvate production by ^{13}C NMR. Two aliquots (0.5 mL) from the incubation medium were withdrawn at three and six hours and the pyruvate concentration determined spectrophotometrically. The incubation was continued up to 24 hours, the medium collected and concentrated for high-resolution ^{13}C NMR analysis. At least three primary cultures from neurons prepared from foetuses derived from different animals were used for every experimental condition.

Primary cultures of cortical astrocytes were prepared from newborn (up to 2-day-old) Wistar rats. Briefly, the cortices were removed and cleaned from the meninges. Cerebral tissue was then minced, resuspended with a pipette and vortexed for 1 minute. The resulting suspension was passed through a 80 μm filter and the cells seeded in poly-lysine coated 8 cm plate with 10 mL DMEM with 10% FBS, 10% HS, 10 mM HEPES, 2.5 μg/mL of fungizone and 100 U/mL of penicillin/streptomycin. Plates were maintained in a humidified incubator chamber at 37ºC with 5% CO_2. After one week in culture cells were transferred to DMEM with 5% FBS, 5% HS, 10 mM HEPES, 2.5 μg/mL of fungizone and 100 U/mL of penicillin/streptomycin. Confluent cultures were obtained and used for experiments after two weeks in culture. In the day of the experiment,

the DMEM medium was removed and substituted by Krebs-Ringer bicarbonate buffer containing increasing concentrations of lactate in the range 1-15 mM in the absence and presence of 1 mM glucose. In some experiments, astrocyte cultures were incubated with (3-^{13}C) lactate to evaluate (3-^{13}C) pyruvate production under similar conditions to those described above for neurons. At least three primary astrocyte cultures prepared from different animals were used for every experimental condition.

Cell culture purity was assessed using standard immunolabeling techniques. Cells were washed three times with PBS for 10 minutes, fixed in 4% (weight/vol) paraformaldehyde in PBS for 5 min and permeabilized with 0.2% (vol/vol) Triton in PBS. Neurons were visualized (negative staining) using rabbit anti-Glial Fibrillary Acidic Protein (GFAP, 1:200) and (positive staining) rat anti-β-III-tubulin (1:200) as primary antibodies and biotin conjugated anti-rat Immuno gamma Globulin (IgG,1:200), Streptavidin Alexa Fluor® 488 (1:2000) and Alexa Fluor® 594 goat anti-rabbit IgG (1:2000) as secondary antibodies. Astrocytes were visualised with rabbit anti-GFAP (1:200) and Alexa Fluor® 594 goat anti-rabbit IgG (1:2000). Cellular nuclei were labeled with 4'-6-diamidino-2-phenylindol (DAPI). The purities of neuron or astrocyte cultures determined in this way were higher than 95%.

3.2 Analytical Determinations

Glucose, lactate or pyruvate in the incubation medium of neurons or astrocytes, were determined spectrophotometrically (340 nm, 37 ºC) using a vertical spectrophotometer (Molecular Devices Spectramax TM 340 PC, Sunnyvale, CA, U.S.A.) in 96-well polypropylene plates. To this end, we adapted conventional enzymatic end point methods coupled to NAD(P)H production or consumption (Bergemeyer 1983). Briefly, glucose was determined through the NADPH production by hexokinase and glucose-6-phosphate dehydrogenase, lactate and pyruvate through NADH production or consumption by lactate dehydrogenase. Total protein was determined in cell pellets obtained after the incubation using the Bradford assay (Bradford 1976).

3.3 Determination of Kinetic Constants

The apparent K_m and V_{max} values for glucose consumption in the absence and presence of lactate, lactate consumption in the presence and absence of glucose and pyruvate production, were determined by non-linear least squares fit of the measured rates to the Michaelis-Menten expression $v = V_{max}\,[S]/\,K_m + [S]$ where v or [S] represent the initial rates of substrate consumption or the initial concentrations of substrate and K_m and V_{max}, the corresponding apparent kinetic constants. The apparent inhibition constant K_i was determined using the expression for competitive inhibition

$K_{mI} = K_m + (1 + [I]/ K_i)$ where K_{mI} and K_m represent the K_m values in the presence and absence of the inhibitor and [I] the inhibitor concentration. Non-linear fits were performed using the Mathematica v4.0 software (Wolfram Research, Champaign, IL, USA) as implemented in an Intel Centrino Pentium M 1.5 GHz platform.

3.4 ^{13}C NMR Spectroscopy

High-resolution ^{13}C NMR spectra (4 ºC, pH = 7.2) from aliquots of the incubation medium after incubation with (3-^{13}C) lactate were acquired in a Bruker AVANCE 500 WB NMR spectrometer using a commercial 5-mm high resolution triple probe (^{13}C,^{1}H,^{2}H). Conditions were: $\pi/3$ pulses, 1.09 s acquisition time, 7.0 s recycle time, 30 kHz sweep width, 64k points zero-filled to 256k points prior to Fourier transformation and 20.000 scans. Broad band proton decoupling was gated on only during acquisition. Chemical shifts were measured with respect to the resonance of a 10% dioxane solution in water at 67.4 ppm, placed in a coaxial capillary. Assignments were performed using literature values and confirmed through the addition of the authentic compounds (Cruz and Cerdán 1999; Rodrigues and Cerdán 2005a).

3.5 Statistics

Kinetic constants obtained under different incubation conditions were compared using the Student *t* test, as implemented in the SAS package (Statistical Analysis System, Cary, NC, USA) running on an Intel Centrino Pentium M 1.5 GHz Platform. Comparisons with $P < 0.05$ were considered statistically significant.

3.6 Materials

Dulbecco's modified Eagle's medium (DMEM), foetal bovine serum (FBS), horse serum (HS) and phosphate-buffered saline (PBS) were purchased from GIBCO (Glasgow, Scotland, U.K.). Kits for analytical determinations of glucose, lactate and pyruvate were from Roche (Mannheim, Germany). Sodium (3-^{13}C) L-lactate (99% ^{13}C) was purchased from Cambridge Isotope Laboratories, Inc. (Andover, MA, USA). $^{2}H_2O$ (99.9 % ^{2}H) was purchased from Apollo Scientific (Bradbury, Stockport, UK). All other chemicals were of the purest grade available from commercial sources.

4. Results

4.1 Competitive Consumption of Glucose and Lactate

Table 4.1 summarizes the kinetic constants for glucose consumption in the absence and presence of 5 mM lactate or those for lactate consumption in the presence and absence of 1 mM glucose. Aliquots withdrawn at three and six hours of incubation showed a linear decrease in the initial glucose or lactate concentrations allowing the determination of the initial rates. Glucose or lactate consumption rates depicted a clear hyperbolic pattern, consistent with Michaelis-Menten kinetics. These experiments were reproduced with neuronal cultures from foetuses of three different litters and the combined results fitted to the Michaelis-Menten expression to determine the apparent K_m and V_{max} values. The K_m for glucose consumption increased from 2.2 ± 0.2 mM in the absence of lactate, to 3.6 ± 0.1 mM ($P < 0.001$) in the presence of 5 mM lactate, with no significant effects on the V_{max} value. This is consistent with a competitive inhibition mechanism, with a K_i value of 3.6 mM for the inhibition of glucose consumption by extracellular lactate. The K_m and V_{max} values for lactate consumption increased from 7.8 ± 0.1 mM and 440 ± 3 nmols. min^{-1}. h^{-1} in the absence of glucose to 8.5 ± 0.1 and 451 ± 3 nmols. min^{-1}. h^{-1} ($P < 0.05$) in the presence of 1 mM glucose, also consistent with a competitive inhibition mechanism with a K_i value of 11.1 mM.

To evaluate the effects of the competing substrates over the full range of substrate and inhibitor concentrations, 0.25-5 mM glucose and 1-15 mM lactate, we generated 3D plots of glucose (Figure 4.3-A) or lactate (Figure 4.3-B) consumption rates, as a function of concentration variations of the competing substrate. To this end, we used the expression for hyperbolic competitive inhibition

TABLE 4.1. Apparent kinetic constants of glucose and lactate consumption in primary cultures of cortical neurons in the absence and presence of the corresponding competitive substrate

Process	Incubation condition	K_m (mM)[a]	V_{max} (nmol/mg/hr)[a]	K_i (mM)[b]
Glucose consumption	Glucose 0.25–5 mM	2.2 ± 0.2	600 ± 65	n.a.
Glucose consumption in the presence of lactate	Glucose 0.25–5 mM and 5 mM lactate	3.6 ± 0.1	674 ± 54	3.6
Lactate consumption	Lactate 1–15 mM	7.8 ± 0.1	440 ± 3	n.a.
Lactate consumption in the presence of glucose	Lactate 1–15 mM and 1 mM glucose	8.5 ± 0.1	451 ± 3	11.1

[a]Apparent kinetic constants were obtained from non-linear fits of substrate consumption curves to the Michaelis-Menten equation as described in Materials and Methods.

[b]Apparent K_i values were obtained as described in Materials and Methods from the expression $K'_m = K_m (1 + [I]/K_i)$ where K'_m is the K_m in the presence concentration of inhibitor [I] and K_m the value obtained in the absence of inhibitor. n.a., not applicable.

$v = V_{max}$ [S]/ (K_m (1 + [I]/K_i) + [S]) for the consumption of glucose or lactate in the presence and absence of one competitive inhibitor. Our results revealed that at resting glucose and lactate concentrations of ca. 1 mM in the extracellular fluid, primary cultures of neurons consumed 81% glucose and 19% lactate. However, when the extracellular glucose concentration was maintained at 1 mM and the extracellular lactate concentration increased to 2 mM and 5 mM, the relative lactate consumption rate increased to 30% and 60%, respectively.

4.2 Pyruvate Production

We continued by investigating the reversible exchange of monocarboxylate reducing equivalents between astrocytes and neurons. This process involves necessarily not only the reversible transfer of reduced substrates such as lactate between neurons and astrocytes, but the transfer of oxidized equivalents in the form of pyruvate, in the opposite direction. Figure 4.4 illustrates the kinetics of pyruvate production in the medium of primary cultures of astrocytes (Figure 4.4-A) or neurons (Figure 4.4-B) incubated with increasing concentrations of lactate in the range 1-20 mM. Pyruvate production showed hyperbolic kinetics in both cell types. However, neurons were able to release pyruvate with K_m and V_{max} values of 1.0 ± 0.2 mM and 109 ± 4.4 nmol.mg^{-1}.h^{-1}, while astrocytes incubated under similar conditions released pyruvate to the medium with K_m and V_{max} values of 0.3 ± 0.1 mM and 341 ± 53.7 nmol. mg^{-1}.h^{-1}, respectively.

Finally, we investigated if pyruvate produced by primary cultures of neurons or astrocytes during incubation with (3-^{13}C) lactate could be detected by ^{13}C NMR in the incubation medium.

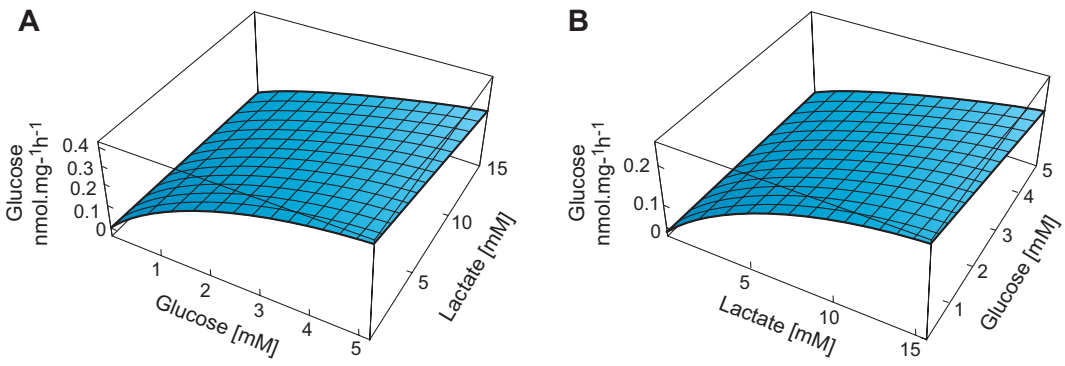

Figure 4.3. 3D simulations of (A) glucose consumption (nmol.mg^{-1}.h^{-1}) for the range 0.25-5 mM glucose and 1-15 mM lactate and (B) lactate consumption (nmol.mg^{-1}.h^{-1}) for the range 1-15 mM lactate and 0.25-5 mM glucose. 3D Simulations were performed with the Mathematica v4.0 software package, using the kinetic constants of Table 4.1.

Figure 4.4-C shows a representative ^{13}C NMR spectrum from astrocytes incubation medium incubated for 24 h with 5 mM (3-^{13}C) lactate. After extensive concentration of the 8 ml medium to dryness and resuspension in 0.5 ml of $^{2}H_2O$, it was possible to observe the resonance of (3-^{13}C) pyruvate at 27.4 ppm, together with other additional resonances derived from the (3-^{13}C) lactate (20.9 ppm) used as substrate. The lower capacity of pyruvate production by neurons made it not possible to detect the corresponding (3-^{13}C) pyruvate resonance in their incubation media after similar incubation conditions and concentration steps (not shown).

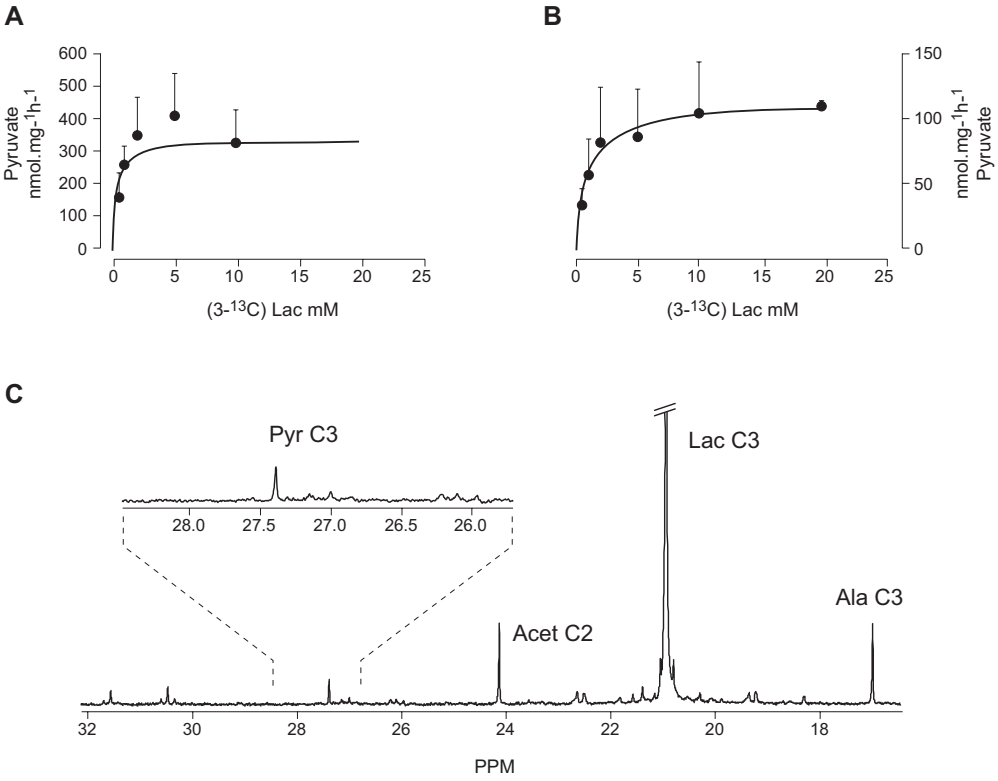

Figure 4.4. Kinetics of pyruvate production in primary cultures of cortical astrocytes (A) and neurons (B). Initial rates of pyruvate consumption were determined spectrophotometrically in the incubation media of neuronal and glial cultures containing lactate concentrations in the range 1-20 mM. ^{13}C NMR spectra of the media of cortical astrocytes incubated with 5 mM (3-^{13}C) lactate for 24 h (**C**).

5. Discussion

5.1 Simultaneous and Competitive Consumption of Glucose and Lactate

The competition between glucose and lactate as neuronal oxidative substrates has been previously addressed a number of times, both *in vitro* and *in vivo* (Bouzier-Sore *et al.* 2006; Bouzier-Sore *et al.* 2003; Dienel and Hertz 2001; Waagepetersen *et al.* 1998). *In vitro* studies used primary cultures of neurons or astrocytes and combinations of ^{13}C labeled glucose or lactate in the presence of the unlabeled competitor whereas *in vivo* studies infused different combinations of labeled and unlabeled glucose and lactate (Bouzier-Sore *et al.* 2006; Bouzier-Sore *et al.* 2003). The *in vitro* results revealed a preferential oxidation of lactate by neurons as shown by increased ^{13}C labeling of the amino acids glutamate and glutamine. Similarly, the *in vivo* data were consistent with a preferential oxidation of lactate in a compartment devoid of pyruvate carboxylase activity, presumably the neuronal environment (Bouzier *et al.* 2000).

In contrast, the inhibitory effects of glucose or lactate on the consumption of each other received less attention and no kinetic studies are available to our knowledge. Primary cultures of cortical neurons incubated with glucose or lactate only, consumed preferentially glucose because of its more favorable kinetic constants K_m and V_{max}. Lactate increased the K_m for glucose consumption without a significant effect on V_{max} and glucose increased the K_m for lactate consumption, without apparent effects on V_{max}. These results showed that glucose and lactate are consumed competitively and simultaneously, rather than alternatively as thought previously. Moreover, the kinetics for glucose and lactate consumption in the presence of each other are consistent with a one-site inhibition by the competing substrate in both cases. We hypothesize that the common inhibition site occurs at the GADPH step, the inhibition mechanism relying in the competition for cytosolic NAD^+ between glycolysis and lactate oxidation (Cruz *et al.* 2001; García-Espinosa *et al.* 2004). The apparent K_i values indicate that relatively high lactate concentrations (ca. 3.6 mM) are required to inhibit by 50% glucose consumption. This concentration is in the range of the high K_m value of the dominant LDH activity of synaptosol (O'Brien *et al.* 2007), suggesting that this isoform is the main participant in the regulation of the redox switch.

The relevance of these results to the *in vivo* situation in the adult brain remains difficult to evaluate at present. Lactate concentrations in the *in vivo* brain have been measured previously by ^1H NMR spectroscopy and *in vivo* microdialysis methods, with values in the range of 0.5 $\mu mol.g^{-1}$ or 0.4 mM, respectively (Darbin *et al.* 2006; Gruetter *et al.* 1998). Moderate increases ranging 50-150% have been reported on cerebral activation (Giove *et al.* 2003). These concentrations seem to be too small to elicit a significant inhibition of glucose consumption or an important relative rate of lactate consumption, in our cultures. Under these *in vivo* conditions, present results indicate that

neurons would consume preferentially glucose. This conclusion agrees with the *in vivo* accumulation of fluorescently labeled deoxyglucose observed in neurons from the hippocampus or cerebellar Purkinje cells (Itoh *et al.* 2004). It is also possible that the actual concentrations of lactate in the highly constrained space of the synaptic cleft are significantly higher than the average concentrations measured by NMR over larger volumes or determined by microdialysis in the extracellular spaces. Under these conditions, synaptic lactate could operate effectively the redox switch, provided that its concentration approaches or exceeds significantly the K_i value. Extracellular lactate can also approach a complete switch off of glycolysis under hypoxic or ischemic conditions, when lactate concentrations reach the 10-15 mM range. This confirms previous proposals of lactate becoming a predominant substrate under ischemic conditions (Schurr 2006; Schurr *et al.* 1988).

In addition to these considerations, it should be noted that cerebral activation can induce changes in the rates of lactate production and consumption by the neuronal and glial compartments *in vivo* (Serres *et al.* 2004; Serres *et al.* 2005; Serres *et al.* 2003). Increased glutamate concentrations obtained during activation have been shown to increase the uptake of fluorescently labeled glucose by astrocytes and reduce it in neurons (Loaiza *et al.* 2003; Porras *et al.* 2004). Together, this evidence indicates that the cerebral activation process *in vivo* could involve changes in the kinetic parameters investigated in this study for primary cultures of neurons or astrocytes under resting conditions. In summary, our results suggest that glucose and lactate can be consumed simultaneously, the consumption of one substituting partially the need for the other. This is a useful bioenergetic circumstance because both substrates appear to be equally effective energizing activity dependent synaptic vesicle turnover (Morgenthaler *et al.* 2006).

Importantly, it should be noted that the kinetics of relative glucose or lactate consumption reported here are different from the relative glucose or lactate oxidation rates described previously (Bouzier-Sore *et al.* 2006; Bouzier-Sore *et al.* 2003). For the combination of 1 mM glucose and 1 mM lactate, it was previously calculated that lactate contributed with 75% of the carbons oxidized in the neuronal cycle, whereas lactate consumption values reported here would indicate that lactate consumption represents only 20% of the glucose consumed. Together, these results indicate that even though lactate consumption may be smaller than glucose consumption, the lactate consumed may be preferentially oxidized. This situation is consistent with our previous findings of two kinetically different pyruvate pools in neurons, one derived from glucose (P_g) pool and the other from monocarboxylates (P_p) pool, able to be oxidized preferentially under different substrate and redox conditions (Cruz *et al.* 2001; García-Espinosa *et al.* 2004). Thus, glucose or lactate consumption rates may not be linearly correlated to the respective oxidation rates.

5.2 The Transcellular Monocarboxylate Redox Shuttle

A number of studies have reported previously lactate and pyruvate consumption by primary

cultures of neural cells (Bouzier-Sore *et al.* 2006; Cruz *et al.* 2001; Dienel and Hertz 2001; Zwingmann and Leibfritz 2003). In addition, the presence of pyruvate in the extracellular fluid has been classically described in a variety of microdialysis experiments (Ronne-Engstrom *et al.* 1995; Valtysson *et al.* 1998). The origin of the cerebral pyruvate present in the extracellular fluid and its consumption by neural cells has not, however, been sufficiently addressed. The present study provides an advance in this direction by showing pyruvate production and its kinetics in primary cultures of neurons and glial cells. Interestingly, our results indicate that both neural cells are able to produce pyruvate from lactate but with different kinetics. For the same extracellular lactate concentration, astrocytes present a larger capacity of pyruvate production than neurons. This occurs, most probably, because of different kinetic properties of the LDH isozymes present in both cells (O'Brien *et al.* 2007). Although both neurons and astrocytes have been shown recently to contain the five isoforms of LDH, the muscle LDH5 isoenzyme seems to be predominant in astrocytes whereas the heart LDH1 isoenzyme in neurons (Bittar *et al.* 1996; Pellerin *et al.* 1998). The kinetic constants of LDH5 favor lactate production whereas those LDH1 favor pyruvate formation. The fact that from the same amount of lactate neurons produce less pyruvate than astrocytes indicates that the pyruvate produced by neurons may be, as expected, preferentially oxidized rather than exported to the extracellular medium. It should be noted that the capacity for pyruvate production in neurons may account for a very large proportion of the consumed lactate. Considering the kinetic constants of lactate consumption (Table 4.1) and pyruvate production for a 1 mM extracellular lactate concentration, it can be calculated that both lactate and pyruvate can be consumed and produced virtually at the same rate of 50 $nmols.mg^{-1}.h^{-1}$. This represents an important observation because many previous studies considered that all lactate consumed by neural cells was completely oxidized. On this basis, our results suggest that the rates of lactate oxidation reported previously, based on metabolic balances not considering pyruvate production, could be overestimated.

5.3 The Redox Switch/Redox Coupling Hypothesis

The results described above, and in particular the demonstration of pyruvate production by neurons and astrocytes, entail considerable implications for the traditional interpretations of metabolic coupling between neurons and glial cells during glutamatergic neurotransmission. In particular, it is now known that oxidative metabolism in the neurons and astrocytes can switch between glucose or lactate as alternative substrates, depending on their relative availability in the extracellular fluid (García-Espinosa *et al.* 2004). This is possible because of the kinetic compartmentation of the intracellular pyruvate pools, mentioned above. Thus, the relative extracellular concentrations of lactate, pyruvate and glucose determine, by operating the redox switch, the final oxidation of

the P_p or P_g pyruvate pools, respectively (Cruz *et al.* 2001). In addition, the exchange of cytosolic lactate and pyruvate with the extracellular milieu in neurons and astrocytes has been shown to be reversible, rather than unidirectional. This supports the reversible exchange of reducing equivalents between neurons and astrocytes, driven by the transcellular redox gradient, rather than the traditional vectorial transfer of a single metabolite as lactate. Although lactate release from primary cultures of neurons and astrocytes is well documented, no information is available to our knowledge on pyruvate release by these cells. Furthermore, numerous evidences have reported previously the presence of pyruvate in the extracellular fluid of the adult rat and human brain as well as alterations in the extracellular lactate/pyruvate ratio following ischemic episodes, seizures or other physiopathological events (Darbin *et al.* 2005; Nilsson *et al.* 1990). These findings support pyruvate production and release to the extracellular fluid in the adult brain. In summary, these findings imply that changes in cytosolic NAD^+/NADH redox state of astrocytes can be efficiently transferred to the extracellular space and to the neurons and *vice versa*, following the concentration gradients of extracellular glucose, lactate, pyruvate and oxygen. In addition to pyruvate, glutamate, glutamine and GABA have also been shown to be compartmented intracellularly (Hertz 2004b; Waagepetersen *et al.* 2006; Waagepetersen *et al.* 2001; Waagepetersen *et al.* 1999; Waagepetersen *et al.* 2003).

Taken together, present evidences suggest that intracellular monocarboxylate and glutamate compartmentation as well as the Redox Switch/Redox Coupling processes play a fundamental role in the integration of the oxidative and non-oxidative metabolisms of neurons and glial cells during glutamatergic neurotransmission. More concretely, the Redox Switch/Redox Coupling hypothesis proposed here supports the following sequence of events (Figure 4.5). Following presynaptic glutamate release, astrocytic transporters incorporate glutamate and three Na^+ to the astrocytic cytosol, which are later removed through the plasma membrane Na^+/K^+ ATPase. Increased activity of the Na^+/K^+ ATPase in the astrocytes decreases their cytosolic ATP/ADP concentrations, stimulating *both* glycolysis and the TCA cycle in these cells. Astrocytic glycolysis and the TCA cycle contribute together with the ATP necessary for glutamine synthesis, with a predominant contribution of the oxidative sources of ATP during resting conditions and the non-oxidative sources during stimulated conditions. This is so because the energy demands in the astrocyte during glutamatergic neurotransmission may exceed the glial TCA cycle capacity, resulting in a net activation of the glycolytic flux and a net production of lactate and pyruvate. Both metabolites are rapidly extruded to the extracellular space which reflects, under these conditions, the reduced NAD^+/NADH redox of the astrocytic cytosol. Extracellular lactate and pyruvate are then taken up rapidly by neurons, reducing their cytosolic redox which then, reflects the extracellular (and astrocytic) lactate/pyruvate ratio. Neuronal NAD^+/NADH redox state may become reduced to a point where glycolysis is reduced or even switched off at the GAPDH step. The same inhibition

of glycolysis, by redox switching under high extracellular lactate concentrations, may occur also in astrocytes. Under these conditions, extracellular lactate and pyruvate will be mainly consumed by oxidation both in neurons and astrocytes, until their extracellular concentration decreases to preactivation levels, setting up the stage for a new glutamatergic event. In this way, the present proposal accounts for the simultaneous operation of both neuronal and glial TCA cycles during activation, a situation now firmly established (Cruz *et al.* 2005; Dienel and Hertz 2005). Neuroglial coupling is most probably achieved through a reversible exchange of reducing equivalents between neurons and astrocytes in the form of lactate and pyruvate, rather than from the unidirectional transfer of lactate molecules. Thus, the operation of this transcellular redox coupling mechanism appears to relay ultimately in the regulation of the intracellular redox states of neurons and astrocytes and, consequently, is determined by the activity of the intracellular redox shuttles through the inner mitochondrial membrane (Arco and Satrustegui 2005; McKenna *et al.* 2006) and also the bioenergetic requirements of both cells. Under these strong redox coupling conditions, neurons and glial cells behave effectively as a "single neural cell", containing one anaerobic (astrocytic or cytosolic) and one aerobic (neuronal or mitochondrial) compartment, which exchange NADH reducing equivalents through very potent transcellular and intracellular shuttle mechanisms.

The transcellular exchange of reducing equivalents underlies most probably the biphasic changes in NADH fluorescence observed in hippocampal slice preparations (Kasischke *et al.* 2004) or the extracellular lactate dynamics calculated during activation (Aubert and Costalat 2005; Aubert *et al.* 2005). Following stimulation, the dynamics of NADH fluorescence and extracellular lactate concentration follow a biphasic time course with an initial dip followed by a pronounced overshoot. Dip and overshoot kinetics have been interpreted to reflect the initial neuronal oxidation of lactate followed by an increase in its glycolytic delivery from astrocytes. Present results suggest that the decrease in neuronal NADH fluorescence, or in the extracellular lactate concentration, may not necessarily reflect neuronal lactate oxidation. In fact, both processes could well be due to an increase in the transcellular transfer of neuronal pyruvate to the astrocyte, a process resulting also in neuronal NADH oxidation and reduced extracellular lactate levels. Similarly, the overshoot in NADH fluorescence in astrocytes or the increase in extracellular lactate concentrations may not simply reflect lactate production and its stoichiometric oxidation in the neurons. These processes reveal the net balance between lactate produced and oxidized in the astrocyte, lactate and pyruvate transferred to the neuron and the balance between lactate oxidized in neurons and returned to astrocytes in the transcellular redox shuttle.

An interesting implication of the present proposal is that the coupling between neuronal and glial metabolisms could be monitored *in vivo*, in addition to the NADH fluorescence approach, by following non-invasively changes in extracellular and intracellular pH. This is so because the reversible NAD^+/NADH redox exchange involves proton production for NAD^+ reductions and

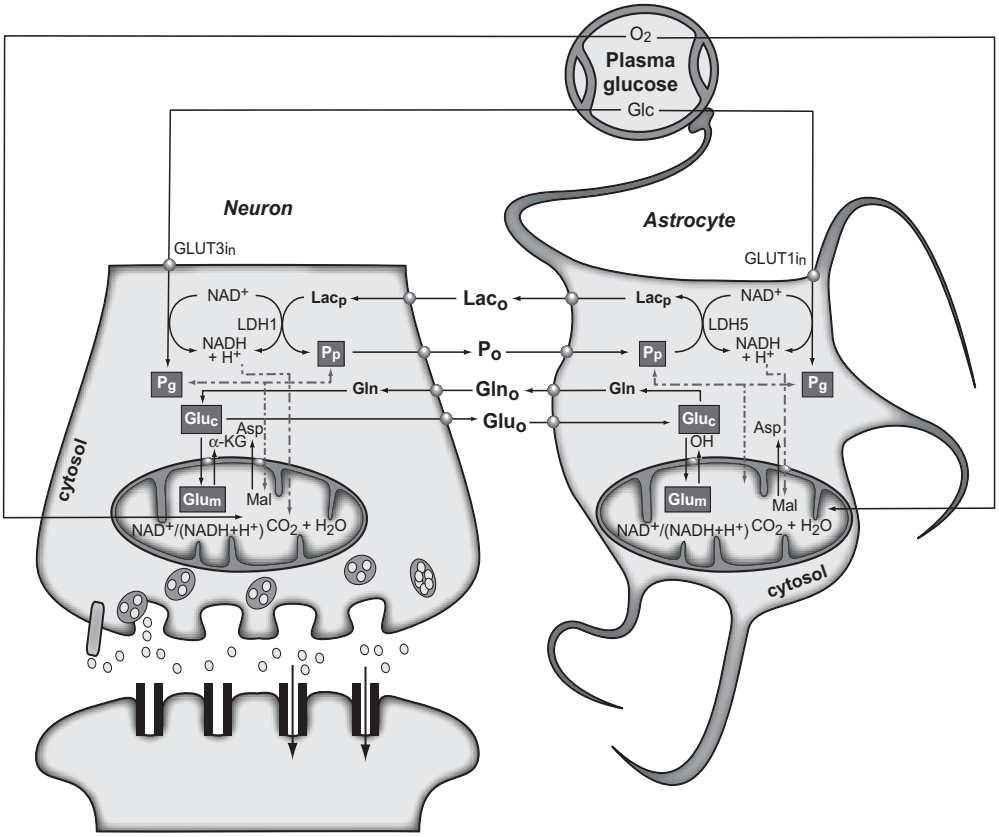

Figure 4.5. The redox switch/redox coupling hypothesis and the subcellular compartmentation of pyruvate and glutamate in neurons and astrocytes. Two pools of pyruvate exist in neurons and astrocytes derived from extracellular monocarboxylates (P_p) or glucose (P_g). A lactate/pyruvate redox shuttle is able to transfer continuously lactate from astrocytes to neurons, taking advantage of the kinetics of plasma membrane transporters and lactate dehydrogenase isoenzymes. High cytosolic lactate inhibits neuronal glycolysis at the GAPDH step by competition with cytosolic NAD^+, favoring the oxidation of extracellular lactate. Neuronal pyruvate (from the P_p pool) is then transferred to the astrocytes to close the redox loop and restart a new redox transfer process. Two α-ketoglutarate/glutamate pools exist in neurons and astrocytes, associated to cytosolic and mitochondrial compartments, respectively. Exchange of α-ketoglutarate/glutamate between mitochondria and cytosol is slow and dependent of the cytosolic and mitochondrial $NAD(P)^+/NAD(P)H$ ratios, as determined by the malate-aspartate shuttle. Both glycolysis and oxidative astrocytic metabolism contribute energy for glutamine production in the astrocytes. Asp, aspartate; Glc, glucose; Gln, glutamine; Glu, glutamate; GLUT1 and GLUT3, glutamate transporters 1 and 3; α-KG, α-ketoglutarate; Lac, lactate; LDH1 and LDH5, lactate dehydrogenase 1 and 5; Mal, malate.

proton consumption for NADH oxidations. Lactate and protons are cotransported through the MCTs [4.1] and the LDH redox equilibrium is dependent of the proton concentration [4.2],

$$Lac_i + H_i^+ \leftrightarrow Lac_o + H_o^+ \quad [4.1]$$

$$Lac + NAD^+ \leftrightarrow Pyr + NADH + H^+ \quad [4.2]$$

Consequently, the transcellular redox shuttle seems to be intimately related to intra- and extracellular pH regulation and, because of the proton involvement in many monovalent and divalent cation transport processes, linked to the overall ionic homeostasis. In this context, the transcellular monocarboxylate shuttle investigated in this study is envisioned to play a central role in the integration of redox processes, pH regulation, and ion homeostasis in the CNS. Redox shuttles based on monocarboxylate exchange may present a more general biological significance, coupling hypoxic and oxidative environments in many other heterogeneous tissues including muscle and tumors.

A variety of NMR methods have become available to determine intra- and extracellular pH that potentially make it possible to investigate the operation of the redox shuttle *in vivo* and *in vitro* (García-Martín *et al.* 2001; Gillies *et al.* 2004).

Glutamate and glutamine compartmentation are also taken into account in our hypothesis. The recently proposed slow exchange of α-ketoglutarate/glutamate through the inner mitochondrial membrane may result in cytosolic and mitochondrial glutamate pools (Berkich *et al.* 2005). We propose here that only the cytosolic (and vesicular) pools of glutamate or glutamine are involved in glutamate-glutamine cycling and neurotransmission.

In summary, we delineated a revised interpretation of the mechanisms underlying metabolic coupling between neurons and astrocytes. Our mechanism is compatible with the subcellular compartmentations of pyruvate, lactate and glutamate, with the redox switch and with monocarboxylate recycling through the plasma membrane. Finally, the present proposal may not be restricted to the coupling of neurons and glial cells in the nervous system. It could well be extended to other heterogeneous tissues where oxidative and glycolytic environments coexist, such as muscle and tumors (Brooks 2002; Henderson *et al.* 2004). In all these cases, redox shuttles could couple the activity of glycolytic and oxidative environments, providing a general mechanism of intra- and intercellular coupling supporting metabolic heterogeneity in cells and tissues.

6. References

Arco AD, Satrustegui J. 2005. New mitochondrial carriers: an overview. Cell Mol Life Sci 62(19-20):2204-2227.

Aubert A, Costalat R. 2005. Interaction between astrocytes and neurons studied using a mathematical model of compartmentalized energy metabolism. J Cereb Blood Flow Metab 25(11):1476-1490.

Aubert A, Costalat R, Magistretti PJ, Pellerin L. 2005. Brain lactate kinetics: Modeling evidence for neuronal lactate uptake upon activation. Proc Natl Acad Sci U S A 102(45):16448-16453.

Bergemeyer HU. 1983. Methods of Enzymatic Analysis. Weinheim: Verlag Chemie.

Berkich DA, Xu Y, LaNoue KF, Gruetter R, Hutson SM. 2005. Evaluation of brain mitochondrial glutamate and alpha-ketoglutarate transport under physiologic conditions. J Neurosci Res 79(1-2):106-113.

Bittar PG, Charnay Y, Pellerin L, Bouras C, Magistretti PJ. 1996. Selective distribution of lactate dehydrogenase isoenzymes in neurons and astrocytes of human brain. J Cereb Blood Flow Metab 16(6):1079-1089.

Bouzier-Sore AK, Voisin P, Bouchaud V, Bezancon E, Franconi JM, Pellerin L. 2006. Competition between glucose and lactate as oxidative energy substrates in both neurons and astrocytes: a comparative NMR study. Eur J Neurosci 24(6):1687-1694.

Bouzier-Sore AK, Voisin P, Canioni P, Magistretti PJ, Pellerin L. 2003. Lactate is a preferential oxidative energy substrate over glucose for neurons in culture. J Cereb Blood Flow Metab 23(11):1298-1306.

Bouzier AK, Goodwin R, de Gannes FM, Valeins H, Voisin P, Canioni P, Merle M. 1998. Compartmentation of lactate and glucose metabolism in C6 glioma cells. A ^{13}C and ^{1}H NMR study. J Biol Chem 273(42):27162-27169.

Bouzier AK, Thiaudiere E, Biran M, Rouland R, Canioni P, Merle M. 2000. The metabolism of [3-^{13}C]lactate in the rat brain is specific of a pyruvate carboxylase-deprived compartment. J Neurochem 75(2):480-486.

Bradford MM. 1976. A rapid and sensitive method for the quantitation of microgram quantities of protein utilizing the principle of protein-dye binding. Anal Biochem 72:248-254.

Brooks GA. 2002. Lactate shuttles in nature. Biochem Soc Trans 30(2):258-264.

Cerdán S, Rodrigues TB, Sierra A, Benito M, Fonseca LL, Fonseca CP, García-Martín ML. 2006. The redox switch/redox coupling hypothesis. Neurochem Int 48(6-7):523-530.

Cruz F, Cerdán S. 1999. Quantitative ^{13}C NMR studies of metabolic compartmentation in the adult mammalian brain. NMR Biomed 12(7):451-462.

Cruz F, Villalba M, García-Espinosa MA, Ballesteros P, Bogonez E, Satrustegui J, Cerdán S. 2001. Intracellular compartmentation of pyruvate in primary cultures of cortical neurons as detected by ^{13}C NMR spectroscopy with multiple ^{13}C labels. J Neurosci Res 66(5):771-781.

Cruz NF, Lasater A, Zielke HR, Dienel GA. 2005. Activation of astrocytes in brain of conscious rats during acoustic stimulation: acetate utilization in working brain. J Neurochem 92(4):934-947.

Darbin O, Carre E, Naritoku D, Risso JJ, Lonjon M, Patrylo PR. 2006. Glucose metabolites in the striatum of freely behaving rats following infusion of elevated potassium. Brain Res 1116(1):127-131.

Darbin O, Risso JJ, Carre E, Lonjon M, Naritoku DK. 2005. Metabolic changes in rat striatum following convulsive seizures. Brain Res 1050(1-2):124-129.

Desagher S, Glowinski J, Premont J. 1997. Pyruvate protects neurons against hydrogen peroxide-induced toxicity.

J Neurosci 17:9060-9067.

Dienel GA, Hertz L. 2001. Glucose and lactate metabolism during brain activation. J Neurosci Res 66(5):824-838.

Dienel GA, Hertz L. 2005. Astrocytic contributions to bioenergetics of cerebral ischemia. Glia 50(4):362-388.

Fonseca LL, Sierra A, Santos H, Cerdán S. Lactate recycling in primary cultures of astrocytes and neurons studied by (^{2}H)^{13}C-NMR spectroscopy.; 2004; Heraklion, Crete, Greece. p 48.

García-Espinosa MA, García-Martín ML, Cerdán S. 2003. Role of glial metabolism in diabetic encephalopathy as detected by high resolution ^{13}C NMR. NMR Biomed 16(6-7):440-449.

García-Espinosa MA, Rodrigues TB, Sierra A, Benito M, Fonseca C, Gray HL, Bartnik BL, García-Martín ML, Ballesteros P, Cerdán S. 2004. Cerebral glucose metabolism and the glutamine cycle as detected by *in vivo* and *in vitro* ^{13}C NMR spectroscopy. Neurochem Int 45(2-3):297-303.

García-Martín ML, Herigault G, Remy C, Farion R, Ballesteros P, Coles JA, Cerdán S, Ziegler A. 2001. Mapping extracellular pH in rat brain gliomas *in vivo* by ^{1}H magnetic resonance spectroscopic imaging: comparison with maps of metabolites. Cancer Res 61(17):6524-6531.

Gillies RJ, Raghunand N, García-Martín ML, Gatenby RA. 2004. pH imaging. A review of pH measurement methods and applications in cancers. IEEE Eng Med Biol Mag 23(5):57-64.

Giove F, Mangia S, Bianciardi M, Garreffa G, Di Salle F, Morrone R, Maraviglia B. 2003. The physiology and metabolism of neuronal activation: *in vivo* studies by NMR and other methods. Magn Reson Imaging 21(10):1283-1293.

Gruetter R. 2002. *In vivo* ^{13}C NMR studies of compartmentalized cerebral carbohydrate metabolism. Neurochem Int 41(2-3):143-154.

Gruetter R, Seaquist ER, Kim S, Ugurbil K. 1998. Localized *in vivo* ^{13}C-NMR of glutamate metabolism in the human brain: initial results at 4 tesla. Dev Neurosci 20(4-5):380-388.

Gruetter R, Seaquist ER, Ugurbil K. 2001. A mathematical model of compartmentalized neurotransmitter metabolism in the human brain. Am J Physiol Endocrinol Metab 281(1):E100-112.

Halestrap AP, Meredith D. 2004. The SLC16 gene family-from monocarboxylate transporters (MCTs) to aromatic amino acid transporters and beyond. Pflugers Arch 447(5):619-628.

Halestrap AP, Price NT. 1999. The proton-linked monocarboxylate transporter (MCT) family: structure, function and regulation. Biochem J 343 Pt 2:281-299.

Henderson GC, Horning MA, Lehman SL, Wolfel EE, Bergman BC, Brooks GA. 2004. Pyruvate shuttling during rest and exercise before and after endurance training in men. J Appl Physiol 97(1):317-325.

Hertz L. 2004a. The astrocyte-neuron lactate shuttle: a challenge of a challenge. J Cereb Blood Flow Metab 24(11):1241-1248.

Hertz L. 2004b. Intercellular metabolic compartmentation in the brain: past, present and future. Neurochem Int 45 (2-3):285-296.

Hertz L, Dienel GA. 2002. Energy metabolism in the brain. Int Rev Neurobiol 51:1-102.

Hertz L, Dienel GA. 2005. Lactate transport and transporters: general principles and functional roles in brain cells. J Neurosci Res 79(1-2):11-18.

Itoh Y, Abe T, Takaoka R, Tanahashi N. 2004. Fluorometric determination of glucose utilization in neurons *in vitro* and *in vivo*. J Cereb Blood Flow Metab 24(9):993-1003.

Kasischke KA, Vishwasrao HD, Fisher PJ, Zipfel WR, Webb WW. 2004. Neural activity triggers neuronal oxidative metabolism followed by astrocytic glycolysis. Science 305(5680):99-103.

Laughton JD, Charnay Y, Belloir B, Pellerin L, Magistretti PJ, Bouras C. 2000. Differential messenger RNA distribution of

lactate dehydrogenase LDH-1 and LDH-5 isoforms in the rat brain. Neuroscience 96(3):619-625.

Loaiza A, Porras OH, Barros LF. 2003. Glutamate triggers rapid glucose transport stimulation in astrocytes as evidenced by real-time confocal microscopy. J Neurosci 23(19):7337-7342.

Magistretti PJ. 2000. Cellular bases of functional brain imaging: insights from neuron-glia metabolic coupling. Brain Res 886(1-2):108-112.

Magistretti PJ, Pellerin L. 2000. The astrocyte-mediated coupling between synaptic activity and energy metabolism operates through volume transmission. Prog Brain Res 125:229-240.

Magistretti PJ, Pellerin L, Rothman DL, Shulman RG. 1999. Energy on demand. Science 283(5401):496-497.

Matsumoto K, Yamada K, Kohmura E, Kinoshita A, Hayakawa T. 1994. Role of pyruvate in ischaemia-like conditions on cultured neurons. Neurol Res 16(6):460-464.

McKenna MC, Waagepetersen HS, Schousboe A, Sonnewald U. 2006. Neuronal and astrocytic shuttle mechanisms for cytosolic-mitochondrial transfer of reducing equivalents: current evidence and pharmacological tools. Biochem Pharmacol 71(4):399-407.

Morgenthaler FD, Kraftsik R, Catsicas S, Magistretti PJ, Chatton JY. 2006. Glucose and lactate are equally effective in energizing activity-dependent synaptic vesicle turnover in purified cortical neurons. Neuroscience 141(1):157-165.

Nilsson P, Hillered L, Ponten U, Ungerstedt U. 1990. Changes in cortical extracellular levels of energy-related metabolites and amino acids following concussive brain injury in rats. J Cereb Blood Flow Metab 10(5):631-637.

O'Brien J, Kla KM, Hopkins IB, Malecki EA, McKenna MC. 2007. Kinetic parameters and lactate dehydrogenase isozyme activities support possible lactate utilization by neurons. Neurochem Res 32(4-5):597-607.

Palmieri F. 2004. The mitochondrial transporter family (SLC25): physiological and pathological implications. Pflugers Arch 447(5):689-709.

Pellerin L. 2003. Lactate as a pivotal element in neuron-glia metabolic cooperation. Neurochem Int 43(4-5):331-338.

Pellerin L, Bergersen LH, Halestrap AP, Pierre K. 2005. Cellular and subcellular distribution of monocarboxylate transporters in cultured brain cells and in the adult brain. J Neurosci Res 79(1-2):55-64.

Pellerin L, Magistretti PJ. 1994. Glutamate uptake into astrocytes stimulates aerobic glycolysis: a mechanism coupling neuronal activity to glucose utilization. Proc Natl Acad Sci U S A 91(22):10625-10629.

Pellerin L, Pellegri G, Bittar PG, Charnay Y, Bouras C, Martin JL, Stella N, Magistretti PJ. 1998. Evidence supporting the existence of an activity-dependent astrocyte-neuron lactate shuttle. Dev Neurosci 20(4-5):291-299.

Peng L, Swanson RA, Hertz L. 2001. Effects of L-glutamate, D-aspartate, and monensin on glycolytic and oxidative glucose metabolism in mouse astrocyte cultures: further evidence that glutamate uptake is metabolically driven by oxidative metabolism. Neurochem Int 38(5):437-443.

Pierre K, Pellerin L. 2005. Monocarboxylate transporters in the central nervous system: distribution, regulation and function. J Neurochem 94(1):1-14.

Porras OH, Loaiza A, Barros LF. 2004. Glutamate mediates acute glucose transport inhibition in hippocampal neurons. J Neurosci 24(43):9669-9673.

Raichle ME. 1998. Behind the scenes of functional brain imaging: a historical and physiological perspective. Proc Natl Acad Sci U S A 95(3):765-772.

Rodrigues TB, Cerdán S. 2005a. ^{13}C MRS: An outstanding tool for metabolic studies. Concepts in Magnetic Resonance Part A 27A:1-16.

Rodrigues TB, Cerdán S. 2005b. A fast and sensitive ^{1}H NMR method to measure the turnover of the H2 hydrogen of

lactate. Magn Reson Med 54(4):1014-1019.

Rodrigues TB, Cerdán S. 2007. The cerebral tricarboxylic acid cycles. In: Dienel G, Gibson, G., Lajtha, A., editor. Brain Energetics from Genes to Cells, Integration of Molecular and Cellular Processes. New York: Springer. p 61-93.

Rodrigues TB, Gray HL, Benito M, Garrido S, Sierra A, Geraldes CF, Ballesteros P, Cerdán S. 2005. Futile cycling of lactate through the plasma membrane of C6 glioma cells as detected by (^{13}C, ^{2}H) NMR. J Neurosci Res 79(1-2):119-127.

Ronne-Engstrom E, Carlson H, Liu Y, Ungerstedt U, Hillered L. 1995. Influence of perfusate glucose concentration on dialysate lactate, pyruvate, aspartate, and glutamate levels under basal and hypoxic conditions: a microdialysis study in rat brain. J Neurochem 65(1):257-262.

Rothman DL, Behar KL, Hyder F, Shulman RG. 2003. *In vivo* NMR studies of the glutamate neurotransmitter flux and neuroenergetics: implications for brain function. Annu Rev Physiol 65:401-427.

Rothman DL, Sibson NR, Hyder F, Shen J, Behar KL, Shulman RG. 1999. *In vivo* nuclear magnetic resonance spectroscopy studies of the relationship between the glutamate-glutamine neurotransmitter cycle and functional neuroenergetics. Philos Trans R Soc Lond B Biol Sci 354(1387):1165-1177.

Schurr A. 2006. Lactate: the ultimate cerebral oxidative energy substrate? J Cereb Blood Flow Metab 26(1):142-152.

Schurr A, West CA, Rigor BM. 1988. Lactate-supported synaptic function in the rat hippocampal slice preparation. Science 240(4857):1326-1328.

Serres S, Bezancon E, Franconi JM, Merle M. 2004. *Ex vivo* analysis of lactate and glucose metabolism in the rat brain under different states of depressed activity. J Biol Chem 279(46):47881-47889.

Serres S, Bezancon E, Franconi JM, Merle M. 2005. *Ex vivo* NMR study of lactate metabolism in rat brain under various depressed states. J Neurosci Res 79(1-2):19-25.

Serres S, Bouyer JJ, Bezancon E, Canioni P, Merle M. 2003. Involvement of brain lactate in neuronal metabolism. NMR Biomed 16(6-7):430-439.

Sharma P, Karian J, Sharma S, Liu S, Mongan PD. 2003. Pyruvate ameliorates post ischemic injury of rat astrocytes and protects them against PARP mediated cell death. Brain Res 992(1):104-113.

Shulman RG, Hyder F, Rothman DL. 2001. Lactate efflux and the neuroenergetic basis of brain function. NMR Biomed 14(7-8):389-396.

Sierra A, Rodrigues TB, Benito M, Ballesteros P, García-Espinosa MA, García-Martín ML, Cerdán S. 2007. Pyruvate Oxidation and Mitochondrial Substrate Transport in the Central Nervous System. In: Lajhta A, Gruetter R, editors. Neural Metabolism *in Vivo*. New York: Springer.

Sonnewald U, Westergaard N, Hassel B, Muller TB, Unsgard G, Fonnum F, Hertz L, Schousboe A, Petersen SB. 1993. NMR spectroscopic studies of ^{13}C acetate and ^{13}C glucose metabolism in neocortical astrocytes: evidence for mitochondrial heterogeneity. Dev Neurosci 15(3-5):351-358.

Sonnewald U, Westergaard N, Schousboe A. 1997. Glutamate transport and metabolism in astrocytes. Glia 21(1):56-63.

Tsacopoulos M. 2002. Metabolic signaling between neurons and glial cells: a short review. J Physiol Paris 96(3-4):283-288.

Tsacopoulos M, Magistretti PJ. 1996. Metabolic coupling between glia and neurons. J Neurosci 16(3):877-885.

Tsacopoulos M, Poitry-Yamate CL, MacLeish PR, Poitry S. 1998. Trafficking of molecules and metabolic signals in the retina. Prog Retin Eye Res 17(3):429-442.

Valtysson J, Persson L, Hillered L. 1998. Extracellular ischaemia markers in repeated global ischaemia and secondary hypoxaemia monitored by microdialysis in rat brain. Acta Neurochir (Wien) 140(4):387-395.

Veech RL. 1991. The metabolism of lactate. NMR Biomed 4(2):53-58.

Waagepetersen HS, Bakken IJ, Larsson OM, Sonnewald U, Schousboe A. 1998. Comparison of lactate and glucose metabolism in cultured neocortical neurons and astrocytes using ^{13}C-NMR spectroscopy. Dev Neurosci 20(4-5):310-320.

Waagepetersen HS, Hansen GH, Fenger K, Lindsay JG, Gibson G, Schousboe A. 2006. Cellular mitochondrial heterogeneity in cultured astrocytes as demonstrated by immunogold labeling of alpha-ketoglutarate dehydrogenase. Glia 53(2):225-231.

Waagepetersen HS, Sonnewald U, Larsson OM, Schousboe A. 2001. Multiple compartments with different metabolic characteristics are involved in biosynthesis of intracellular and released glutamine and citrate in astrocytes. Glia 35(3):246-252.

Waagepetersen HS, Sonnewald U, Qu H, Schousboe A. 1999. Mitochondrial compartmentation at the cellular level: astrocytes and neurons. Ann N Y Acad Sci 893:421-425.

Waagepetersen HS, Sonnewald U, Schousboe A. 2003. Compartmentation of glutamine, glutamate, and GABA metabolism in neurons and astrocytes: functional implications. Neuroscientist 9(5):398-403.

Ward LD, Winzor DJ. 1983. Thermodynamic studies of the activation of rabbit muscle lactate dehydrogenase by phosphate. Biochem J 215(3):685-691.

Zwingmann C, Leibfritz D. 2003. Regulation of glial metabolism studied by ^{13}C-NMR. NMR Biomed 16(6-7):370-399.

Zwingmann C, Richter-Landsberg C, Leibfritz D. 2001. ^{13}C isotopomer analysis of glucose and alanine metabolism reveals cytosolic pyruvate compartmentation as part of energy metabolism in astrocytes. Glia 34(3):200-212.

The Metabolic Interactions Between Glutamatergic and Dopaminergic Neurotransmitter Systems are Mediated Through D_1 Dopamine Receptors

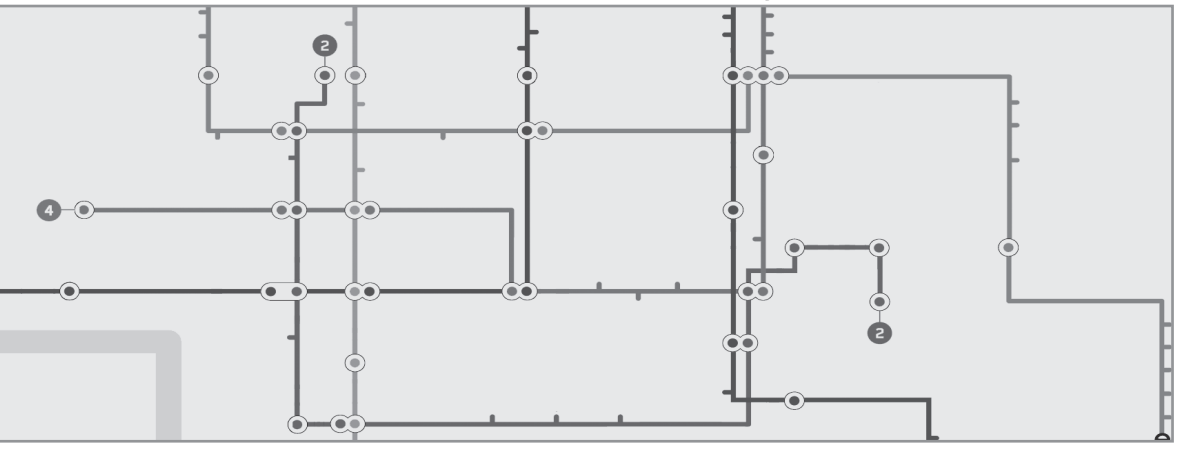

Chapter 5

1. Abstract

The interactions between the dopaminergic and glutamatergic neurotransmission systems were investigated in the adult brain of wild type and transgenic mice lacking the dopamine D_1 or D_2 receptor subtypes. Activity of the glutamine cycle was evaluated by using ^{13}C NMR spectroscopy, and striatal activity was assessed by c-Fos expression and motor coordination. Brain extracts from (1,2-$^{13}C_2$) acetate-infused mice were prepared and analyzed by ^{13}C NMR to determine the incorporation of the label into the C4 and C5 carbons of glutamate and glutamine. $D_1R^{-/-}$ mice showed a significantly higher concentration of cerebral (4,5-$^{13}C_2$) glutamine, consistent with an increased activity of the glutamate-glutamine cycle and of glutamatergic neurotransmission. Conversely, $D_2R^{-/-}$ mice did not show significant changes in (4,5-$^{13}C_2$) glutamate or (4,5-$^{13}C_2$) glutamine, suggesting that alterations in glutamine metabolism are mediated through D_1 receptors. This was confirmed using $D_1R^{-/-}$ and wild type mice treated with reserpine, a dopamine-depleting drug, or with reserpine followed by L-DOPA, a dopamine precursor. Exposure to reserpine increased (4,5-$^{13}C_2$) glutamine in wild type to levels similar to those found in untreated $D_1R^{-/-}$ mice. These values were the same as those reached in the reserpine-treated $D_1R^{-/-}$ mice. Treatment of wild type animals with L-DOPA returned (4,5-$^{13}C_2$) glutamine levels to normal, but this was not verified in $D_1R^{-/-}$ animals. Reserpine impaired motor coordination and decreased c-Fos expression, whereas L-DOPA restored both variables to normal values in wild type but not in $D_1R^{-/-}$. Together, our results reveal novel neurometabolic interactions between glutamatergic and dopaminergic systems that are mediated through the D_1, but not the D_2, dopamine receptor subtype.

2. Introduction

Precise integration of the different neurotransmitter signalling pathways is necessary to provide efficient and coordinated responses to internal and external stimuli in the Central Nervous System (CNS). Glutamate is the principal neurotransmitter in the excitatory circuits of the CNS, participating in many neuronal activities (Conn 2003; Lipsky and Goldman 2003; Malenka 2003). Similarly, dopamine is implicated in motor control, cognition, motivation, and emotional processing. Notably, indirect pharmacological and behavioural evidences revealed that glutamatergic neurotransmission is altered in several pathological disorders traditionally associated with abnormal dopamine signalling (Coyle 2006; Kalivas *et al.* 2003; Sanacora *et al.* 2003; Tamminga *et al.* 2003). These findings indicate the existence of interactions between dopaminergic and glutamatergic neurotransmission. Such interactions may underlie not only the adaptive and plastic responses to pathophysiological states such as Parkinson's disease (Chase and Oh 2000; Lange *et al.* 1997), schizophrenia (de Bartolomeis *et al.* 2005), drug abuse (Lapish *et al.* 2006) and personality disorders (Karasawa *et al.* 2006), but also the operation of the normal brain under physiological conditions (Lee *et al.* 2002; Pei *et al.* 2004; Salter 2003; Sesack *et al.* 2003; West *et al.* 2003). However, despite the neurobiological and clinical relevance of these interactions, the underlying mechanisms remain poorly understood (Abekawa *et al.* 2000; David and Abraini 2001). In particular, the dopamine receptor subtype that mediates communication between glutamatergic and dopaminergic systems has not been identified.

The use of ^{13}C NMR and the ^{13}C-enriched precursors ^{13}C glucose or ^{13}C acetate has provided extensive information on glutamate metabolism in neurons and glia as well as the interactions between these cell types through glutamate-glutamine cycling and glutamatergic neurotransmission (Rodrigues and Cerdán 2005; Rothman *et al.* 2003). This approach can be used to reveal glutamate turnover, and it is sensitive to perturbations at the glutamate receptor and transport levels as well as in the transport of glucose or acetate precursors (García-Espinosa *et al.* 2004; Waagepetersen *et al.* 2001). On the other hand, transgenic animals also provide an excellent tool for investigating the effects of gene and protein ablation on their function *in vivo* (Chen and Zhuang 2003).

On these grounds, we employed ^{13}C NMR (Rodrigues and Cerdán 2005; Rothman *et al.* 2003), to investigate the metabolism of glutamate and glutamine in the brain of wild type (WT) and transgenic mice that lack dopamine D_1 or D_2 receptors (Baik *et al.* 1995; Kelly *et al.* 1998; Xu *et al.* 1994). We confirmed these results using a complementary pharmacological approach. Accordingly, WT and $D_1R^{-/-}$ mice were treated with reserpine, a dopamine-depleting drug (Graybiel *et al.* 1990; Slattery *et al.* 2004), and also with reserpine and L-DOPA, an acute antiparkinsonian treatment (Carlsson *et al.* 1957; Hornykiewicz 2002; Pavon *et al.* 2006; Schildkraut *et al.* 1965), to investigate the effects of these drugs on the glutamate-glutamine cycle and on glutamatergic neurotransmission.

Finally, we correlated the information obtained by ^{13}C NMR with tests of motor coordination and with the expression of the c-Fos protein, a marker of dopaminergic activity in neurons. Together, our results indicate that the interactions observed between glutamatergic and dopaminergic neurotransmitter systems are mediated through the D_1 but not the D_2 dopamine receptors and that the lack of dopamine or lack of D_1 receptors results in an increase in glutamatergic activity.

3. Materials and Methods

3.1 Animals, Drug Treatments, and Infusion Techniques

The experimental protocols used in this study were approved by the appropriate institutional review committees and met the guidelines of the appropriate government agency. All efforts were made to minimize animal suffering. Experiments were carried out in male dopamine D_1 and D_2 receptor knock out ($D_1R^{-/-}$, $D_2R^{-/-}$) mice (Baik *et al.* 1995; Kelly *et al.* 1998) as well as in their heterozygous (+/-) and wild type (+/+) littermates. Mice were used at 2-3 months of age, and the genotype of each mouse was determined by genomic Southern blot analysis as described previously (Chen *et al.* 1999). The mice were housed at the Cajal Institute, in a humidity- and temperature-controlled room on a 12-h light/dark cycle, receiving water and food *ad libitum*.

In the first series of experiments, two groups of mice were used without any kind of pharmacological intervention: group 1 included $D_1R^{+/+}$, $D_1R^{-/+}$ and $D_1R^{-/-}$ mice; group 2 included $D_2R^{+/+}$, $D_2R^{-/-}$ mice (n = 6 per genotype). The involvement of D_1 receptors was further investigated by analyzing the effects of dopamine depletion in WT and $D_1R^{-/-}$ mice (n = 12 for each genotype). Half of these animals (n = 6 per genotype) were given the dopamine depleting drug reserpine (5 mg/kg, i.p.) 18 h before the infusion of the ^{13}C label (group 3). The other half (n = 6 per genotype) also received an intraperitoneal injection of L-DOPA (50 mg/kg) combined with benserazide-HCl (20 mg/kg), a DOPA-decarboxylase inhibitor, 18 h after reserpine administration and 60 min before the infusion of the ^{13}C label (group 4). This reserpine treatment protocol has previously been shown to lower striatal dopamine content by 81-96% and to produce changes in behaviour and in IEG expression (Day *et al.* 2006; Graybiel *et al.* 1990; LaHoste and Marshall 1992; Moratalla *et al.* 1996b). Before the infusion of the ^{13}C label, the animals were deeply anesthetised by administering 1-2% of isoflurane in 1 liter/min O_2 through a nose cap. Body temperature was maintained at approximately 37 ºC using a thermostatic blanket and a temperature-regulated circulating water bath, and it was measured with a rectal probe (Panlab, Barcelona, Spain). The physiological state of the animal was monitored by a Biotrig physiological monitor (Bruker Medical Gmbh, Ettlingen,

Germany), measuring the respiratory rate and the body temperature. The right jugular vein was dissected and cannulated, and (1,2-$^{13}C_2$) acetate (0.24 μmol min^{-1} g^{-1}) was infused for 60 min. At the end of this infusion, the head of the animal was funnel-frozen, and perchloric acid extracts of the brain, excluding the cerebellum, were prepared as described previously prior to high-resolution ^{13}C NMR spectroscopy (Cerdán *et al.* 1990; Chapa *et al.* 1995)

3.2 ^{13}C NMR Spectroscopy

High-resolution proton-decoupled ^{13}C NMR spectra of brain extracts were obtained at 11.9 Tesla (125.13 MHz, 25 ºC, pH 7.2) with a Bruker AVANCE 500WB NMR spectrometer using a commercial (5 mm) triple-resonance probe (^1H,^{13}C,^2H) optimized for direct ^{13}C NMR detection. The acquisition conditions were: π/3 pulses; 30.0 kHz spectral width; 1.09 s acquisition time; 64k words data table; and 6.0 s recycling time. Proton decoupling was only gated during the acquisition using a broad-band composite pulse decoupling (CPD) sequence, and chemical shifts were calibrated with an external reference of dioxane (10% vol/vol, 67.4 ppm). Resonance assignments were based on literature values and on the addition of internal standards (Cerdán *et al.* 1990). Spectra deconvolution and multiplet structures were analyzed using the PC-based (Intel Centrino Platform) NMR program, NUTS™ (Acorn, Freemont, CA, USA). All ^{13}C NMR resonance areas were normalized relative to the unchanged *myo*-inositol resonance areas of the corresponding perchloric acid extracts. This was possible because *myo*-inositol had a low turnover and did not becoming enriched after the 60-min (1,2-$^{13}C_2$) acetate infusion, providing a robust internal reference from which all ^{13}C resonances can be derived (Bouzier *et al.* 1998).

3.3 Behavioural Experiments (Motor Coordination, Rota-rod)

Motor coordination was measured using an accelerating rota-rod apparatus (Hugo Basile, Rome, Italy). Two groups of adult mice were used, $D_1R^{-/-}$ and $D_1R^{+/+}$ mice (n = 6 per group). On the first day, the mice were subjected to a practice trial, placing the animal on the rota-rod without rotation for 60 seconds, followed by a 1-min period during which the rod rotated at a constant speed of 4 r.p.m. After this, the mice were returned to their cages and 20 min later they were trained to use the rota-rod with six sessions of 5 min at a constant acceleration and with an interval of 20 min between trials. The following day, mice were tested on the accelerated rota-rod and the time to fall from the rod was measured, with a cut off time established at 5 min. Animals were tested in basal conditions or 3 days after administration of reserpine (5 mg/kg) or 30 minutes after L-DOPA administration (20 mg/kg) given 3 days after the reserpine.

3.4 c-Fos Immunocytochemical Staining and Quantification Experiments

At the end of the experiments, animals were anaesthetized with pentobarbital and transcardially perfused with 4% paraformaldehyde in 0.1% phosphate buffer (PB), pH 7.4. After perfusion, the brains were dissected out and immersed overnight in the same fixative solution. The brains were then cryoprotected in a solution of 30% sucrose for one day. Coronal brain sections (30 μm) throughout the striatal area were obtained on a slicing microtome (Leica, Madrid, Spain) and they were kept in PB solution at 4 ºC until use. Immunostaining was carried out on free-floating sections with a standard avidin-biotin immunocytochemical protocol previously described (Grande *et al.* 2004; Pavon *et al.* 2006; Rivera *et al.* 2002). Striatal sections were incubated overnight with specific c-Fos antisera (Chemicon, Temecula, CA, USA) and after three washes, the sections were incubated for two hours with the secondary antisera at room temperature. Peroxidase reactions were developed with 0.06% of diaminobenzidine (DAB) in PB buffer containing 1% nickel ammonium sulphate and 5 μl of H_2O_2, and the reaction was monitored every 5 min using an optical microscope. After being washed, the sections were mounted on gelatin-coated slides, air dried and dehydrated in ascending series of ethanol, cleared with xylene, and coverslipped with Permount. Quantification of c-Fos striatal expression was performed with the aid of an image analysis system (AIS, Imaging Research Inc., Linton, England) using a ×10 lens. Before counting, a standardized threshold was established in the images at the gray-scale level, empirically determined by two different observers, to permit the detection of stained nuclei of low to high intensity and to suppress the very lightly stained nuclei. Thus, the number of positive nuclei for c-Fos was determined and expressed as number of positive nuclei per μm. Counting was performed on five sections from each animal and on three different mice.

3.5 Statistical Analysis

Statistical analysis was performed using the SPSS package (SAS Institute Inc., Cary, NC, USA). The results are expressed as means ± standard deviation. When indicated, the statistical significance of the differences was assessed using the Student's *t*-test. Statistical analysis for gene expression and motor coordination between mice of different genotypes and drug treatments were performed by two-way ANOVA, followed by post-hoc Tukey's test. The threshold for statistical significance was set at $P < 0.05$.

3.6 Materials

Reserpine, L-DOPA, benserazide-HCl and d-amphetamine sulphate were obtained from Sigma-Aldrich (Madrid, Spain). (1,2-$^{13}C_2$) acetate (99.9% ^{13}C) was obtained from Cambridge Isotope

Laboratories (Andover, MA, USA). $^{2}H_2O$ (99.9% ^{2}H) was obtained from Apollo Scientific Ltd. (Stockport, Cheshire, USA). All the other items were of the highest purity available commercially from Sigma-Aldrich (Madrid, Spain).

4. Results

4.1 ^{13}C NMR Spectroscopy

High-resolution ^{13}C NMR spectra from perchloric acid brain extracts from a homozygous mutant mouse ($D_1R^{-/-}$, Figure 5.1-A) and from a wild type ($D_1R^{+/+}$, Figure 5.1-B) were obtained

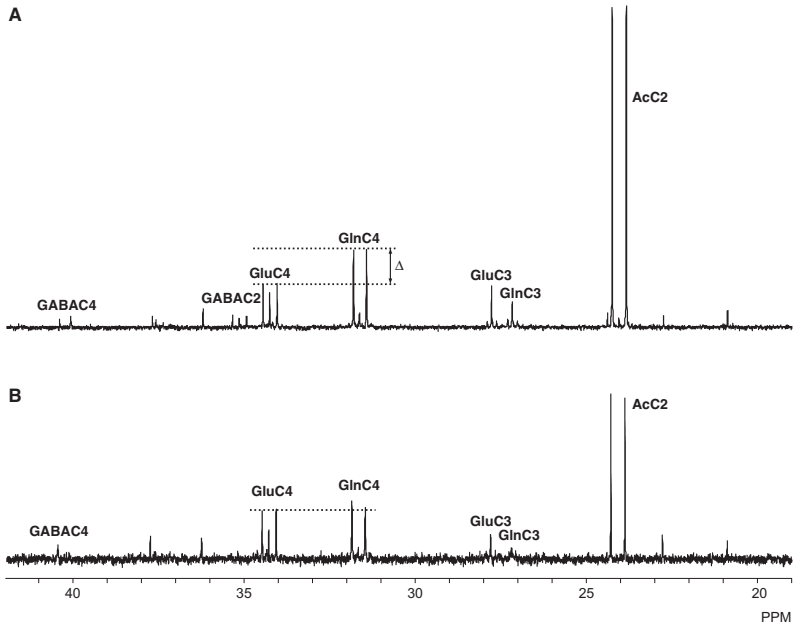

Figure 5.1. **Representative proton-decoupled ^{13}C NMR spectra (125.13 MHz, 25 ^{o}C, pH 7.2) of neutralized perchloric acid brain extracts from $D_1R^{-/-}$ (A) and $D_1R^{+/+}$ (B) mice infused with (1,2-$^{13}C_2$) acetate**. Only the 20-40 ppm region is shown. Ac: acetate (C2: 24.2 ppm); GABA: γ-aminobutyric acid (C2: 35.1 ppm; C4: 40.4 ppm); Glu: glutamate (C3: 27.7 ppm; C4: 34.2 ppm); Gln: glutamine (C3: 27.0 ppm; C4: 32.4 ppm); PPM: parts per million.

sixty minutes after infusion of (1,2-$^{13}C_2$) acetate. The spectra display different characteristics, indicating that the loss of D_1 receptor has significant consequences on acetate metabolism in the brain. After (1,2-$^{13}C_2$) acetate infusion, glutamate, glutamine and GABA are labeled in different carbon positions depending on the metabolic pathways connecting these intermediates (Cerdán *et al.* 1990; Rodrigues and Cerdán 2005). Glutamate and glutamine (Glx) are both labeled contiguously at C-4 and C-5 during the first turn of the cycle, because these carbons are derived directly from a (1,2-$^{13}C_2$) acetyl-CoA precursor. It is readily apparent that mice lacking D_1 dopamine receptors were characterized by a significant increase in ^{13}C incorporation into the cerebral glutamine C4 resonance doublet when compared to the glutamate precursor C4 (dotted lines).

The incorporation of ^{13}C into the resonance doublet for cerebral glutamate C4 and glutamine C4 in the four different groups examined in our experiments and relative to the natural abundance of ^{13}C inositol C1-C3 resonance is summarized in Figure 5.2. There were no detectable changes in glutamate C4 labeling, when both D_1 and D_2 receptor expression was genetically deleted. However, glutamine C4 labeling increased significantly in $D_1R^{-/-}$ mice compared with the values obtained from the WT and heterozygous counterparts (group 1). In contrast, complete ablation of D_2 receptors appeared to provoke only a small increase in the incorporation of ^{13}C in glutamine C4, although when both groups of animals were compared this difference was not statistically significant. Interestingly, heterozygous $D_1R^{+/-}$ mice exhibited ^{13}C labeling patterns very similar to

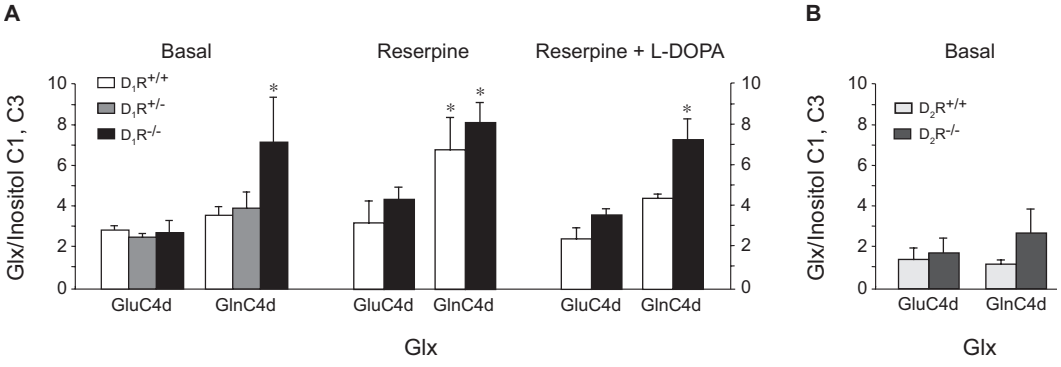

Figure 5.2. Inactivation of dopamine D_1 receptors or dopamine depletion increases the incorporation of ^{13}C from (1,2-$^{13}C_2$) acetate in (4,5-$^{13}C_2$) glutamine. Relative ^{13}C incorporation in the doublet resonances of cerebral glutamine C4 (GlnC4d) and glutamate C4 (GluC4d) in **(A)** $D_1R^{+/+}$, heterozygous $D_1R^{+/-}$ and $D_1R^{-/-}$ mice, under basal conditions or after treatment with reserpine (5 mg/kg), with or without subsequent exposure to L-DOPA (50 mg/kg) and **(B)** in $D_2R^{+/+}$ and $D_2R^{-/-}$ mice in basal conditions. Values represent the mean ± SD, n = 6 animals per group. * Significantly different from basal $D_1R^{+/+}$ and heterozygous $D_1R^{+/-}$, $P < 0.003$. Glx: Glutamate or glutamine.

those observed in WT mice. This indicates that, at least, only half of the D_1 receptors are sufficient to account for a complete physiological response. To avoid uncertainties derived from incomplete receptor ablation, we restricted the rest of the study to WT and $D_1R^{-/-}$ mice only. To confirm these results, we adopted a complementary pharmacological approach using WT and $D_1R^{-/-}$ mice. Hence, a third group of animals (group 3) was given reserpine, a dopamine-depleting drug, 18 h prior to infusion of (1,2-$^{13}C_2$) acetate. This treatment resulted in an increase in glutamine C4 labeling in WT mice but not in glutamine C4 labeling in $D_1R^{-/-}$ mice. Indeed, both reserpine-treated WT and $D_1R^{-/-}$ mice have values of glutamine C4 labeling similar to those observed in $D_1R^{-/-}$ animals in basal conditions. The reserpine treatment in group 4 was supplemented with L-DOPA, administered in combination with benserazide, a DOPA-decarboylase inhibitor. With these conditions, we observed a reversion of the effect of reserpine on the pattern of glutamine C4 labeling. Thus, WT mice exhibited values of glutamine C4 labeling very similar to those obtained in untreated animals. In contrast, mice lacking the D_1 dopamine receptor did not show significant differences in glutamine C4 labeling following reserpine-plus-L-DOPA treatment when compared to the untreated $D_1R^{-/-}$ animals or those treated with reserpine alone. Together, these results indicate that the effect of genetic ablation of the D_1 receptor can be mimicked by treatment with reserpine and reversed by L-DOPA.

4.2 Implication of Dopamine and D_1 Receptors in Motor Coordination

To test the influence of dopaminergic activity through dopamine D_1 receptors on motor coordination and to correlate this with our previous ^{13}C NMR results, we used a rota-rod apparatus to analyze the behaviour of the animals under the same conditions. Under basal conditions, WT mice quickly adapted to the accelerating rod, and most of the mice reached the cutoff time (300 s) on the rod (Figure 5.3). However, the $D_1R^{-/-}$ mice were unable to remain on the rod, and achieved an average latency time of only 162 s. Reserpine administration significantly reduced the time on the rod for both genotypes with an average permanence time of 32.1 and 34.5 s for WT and $D_1R^{-/-}$, respectively ($P < 0.001$ *vs.* basal conditions). This reduction highlighted the relevance of dopaminergic activity in motor coordination. Finally, administration of L-DOPA (20 mg/kg i.p.) reverted the effects of reserpine in WT animals, increasing the latency time to normal values. However, while L-DOPA increased the latency time on the rod for $D_1R^{-/-}$ animals (from 34 to 128 s), this increase did not completely restore motor coordination to the level of WT mice. Indeed, the average time on the rod of 128 s for $D_1R^{-/-}$ animals after L-DOPA treatment was similar to the latency time obtained under basal condition (average 162 s, Figure 5.3). These results indicate that dopamine is necessary for proper motor coordination but that it is not sufficient, insofar the integrity of dopamine D_1 receptors is critical for a complete motor function.

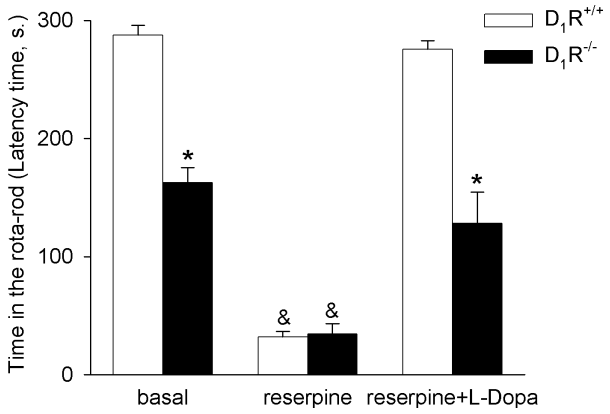

Figure 5.3. Inactivation of dopamine D_1 receptors or dopamine depletion impairs motor coordination. Histograms illustrating how the lack of dopamine or the ablation of D_1R decreases the latency time of mice on an accelerating rota-rod. Animals were tested in basal conditions or 3 days after 5 mg/kg of reserpine, or 30 min after 20 mg/kg of L-DOPA administered 3 days after reserpine. Note that reserpine impairs motor coordination and that L-DOPA restores this impairment in WT but not in $D_1R^{-/-}$ mice. * $P < 0.005$ compared to WT and & $P < 0.001$ compared to basal or reserpine plus L-DOPA treatment, Post-hoc Tukey's test, n = 6.

4.3 Implication of Dopamine and D_1 Receptor in Neuronal Activity as Demonstrated by c-Fos Induction

To investigate dopaminergic function in the basal ganglia further and its correlation with the ^{13}C NMR parameters determined in the present study, we used c-Fos expression in the striatum as a readout of neuronal activity (Hiroi *et al.* 2002; Moratalla *et al.* 1996a; Pavon *et al.* 2006). The c-Fos transcription factor is constitutively expressed in the basal ganglia, and it has been shown to be activated after dopaminergic stimulation (Grande *et al.* 2004; Pavon *et al.* 2006). Under basal conditions, WT mice displayed a low level of c-Fos expression in the striatum and c-Fos-positive nuclei were homogeneously yet sparsely distributed throughout the caudoputamen. Inactivation of dopamine D_1 receptors caused a significant decrease of c-Fos expression in the striatum ($P \leq 0.001$, WT *vs.* $D_1R^{-/-}$, Figure 5.4). Reserpine treatment significantly diminished c-Fos expression in the caudoputamen of WT mice but did not alter the already weak expression in $D_1R^{-/-}$ mice. This loss of c-Fos in WT mice was mainly observed in the middle of the caudoputamen. However, administering L-DOPA after reserpine treatment resulted in a significant increase in c-Fos expression in WT but not in $D_1R^{-/-}$ mice, in which the level of c-Fos expression was similar to those found in basal conditions, ($P < 0,001$, WT *vs.* $D_1R^{-/-}$ mice, Figure 5.4, Table 5.1). These results indicate that the constitutive c-Fos gene expression found in the caudoputamen of WT mice was due to dopaminergic activity via D_1 receptor activation, insofar as the absence of dopamine or

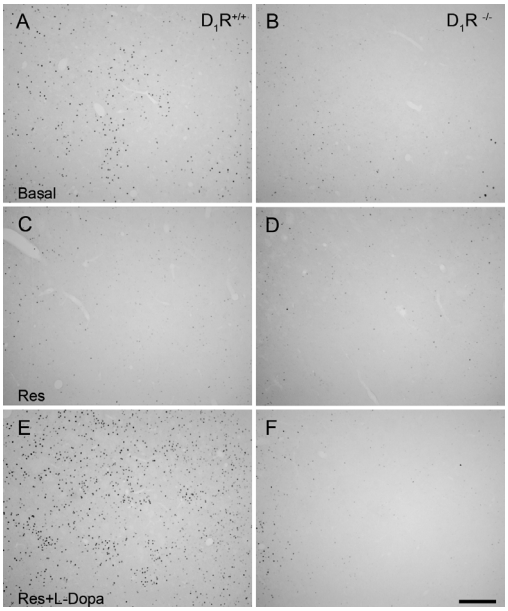

Figure 5.4. Inactivation of dopamine D_1 receptors or dopamine depletion results in a drastic reduction of c-Fos expression in the striatum. Photomicrographs of coronal sections from the striatum of $D_1R^{+/+}$ and $D_1R^{-/-}$ mice illustrating c-Fos expression under basal conditions **(A, B)**, after treatment with 5 mg/kg of reserpine **(C, D)** and reserpine plus 20 mg/kg of L-DOPA **(E, F)**. Note the constitutive expression of c-Fos nuclei in $D_1R^{+/+}$ mice in basal conditions compared to $D_1R^{-/-}$. Treatment with reserpine diminishes c-Fos expression and treatment with L-DOPA restores c-Fos expression in the WT, but not in $D_1R^{-/-}$ animals. Bar represents 200 microns; Res: reserpine.

TABLE 5.1. Quantification of c-Fos-positive nuclei expression per square millimeter†

	Number of positive nucleus c-Fos	
	WT	$D_1R^{-/-}$
Basal conditions	83.16 ± 10.56	3.11 ± 1.18**
Reserpine	15.86 ± 4.26***	13.71 ± 3.12*
Reserpine + L-DOPA	292.33 ± 24.61****	9.92 ± 2.97**

†Immunostained cell nuclei were counted in striatal sections from 3 different animals per group, 5 sections each. Data are expressed as mean of c-fos-positive nuclei per mm^2 (mean ± SEM).
*$P < 0.05$ compared with basal condition in $D_1R^{-/-}$.
**$P < 0.001$ compared with WT mice.
***$P < 0.001$ compared with basal conditions in WT mice.
****$P < 0.001$ compared with reserpine and basal conditions in WT mice; post hoc Tukey test.

dopamine D_1 receptors significantly reduced c-Fos expression. In summary, the decrease in c-Fos expression revealed diminished dopaminergic activity, and this correlated well with the increase in the (4,5-$^{13}C_2$) glutamine labeling and glutamatergic activity detected by ^{13}C NMR.

5. Discussion

Our results confirm that an interaction exists between the dopaminergic and glutamatergic neurotransmission systems, demonstrating that functional D_1 dopamine receptors are required for adequate glutamatergic neurotransmission. Based on the data presented in this study regarding the metabolism of (1,2-$^{13}C_2$) acetate, we present an overview of the neurometabolic interactions between the dopaminergic and glutamatergic or GABAergic systems (see Figure 5.5). In brain metabolism, (1,2-$^{13}C_2$) acetate is incorporated mainly through the glial compartment (Cruz and Cerdán 1999; Lebon *et al.* 2002; Waniewski and Martin 1998). The (4,5-$^{13}C_2$) glutamine produced by glutamine synthase, an enzyme exclusively found in glia, is exported to glutamatergic neurons. It is in these neurons that the neurotransmitter glutamate is stored in vesicles and eventually released to the synaptic cleft during the action potential. Synaptic glutamate is recaptured by the astrocytes and transformed into glutamine, completing the glutamate-glutamine cycle that supports glutamatergic neurotransmission. In GABAergic neurons, glial glutamate is transformed into GABA by the GABA decarboxylase isozymes, and it is eventually released following GABAergic stimulation. Released GABA is recaptured by astrocytes and inactivated through GABA transaminase and semialdehyde succinic dehydrogenase isozymes. Thus, astrocytic glutamate and glutamine play a crucial role during glutamatergic or GABAergic neurotransmission, providing a common metabolic precursor that supports both neurotransmission systems.

The present study shows that the supporting role of astrocytes can be further extended to the dopaminergic system, to which no direct metabolic links are immediately apparent to our knowledge. Dopaminergic neurons release dopamine to the synaptic cleft and this dopamine eventually binds to the postsynaptic dopamine D_1 or D_2 receptors. Our results show that $D_1R^{-/-}$ mice display significant increases in (4,5-$^{13}C_2$) glutamine, revealing an increase in glutamine synthetase activity. Therefore, the question that arises is how a metabolic signal originating from the dopaminergic system, or the lack of it, may trigger an astrocytic response involving the glutamatergic system or *vice versa*. There is evidence that dopamine D_1 receptors are coexpressed with ionotropic and metabotropic NMDA receptors in the striatum (Landwehrmeyer *et al.* 1995). Moreover, functional protein-protein interactions between D_1 and glutamate receptors have also been described. In

this environment, dopamine D_1 receptors can physically interact with the NR_1 or NR_2A subunits of NMDA receptors, modulating their activity (Lee *et al.* 2002; Pei *et al.* 2004; Salter 2003). The coactivation of these two receptors stimulates protein synthesis, up-regulates the expression of the $GluR_1$ receptor subunit, and increases the surface expression of the $GluR_1$ subunit of AMPA receptors at synaptic sites (Smith *et al.* 2005). In addition, we have also demonstrated that the integrity of D_1 receptors is required for corticostriatal and hippocampal LTP (Centonze *et al.* 2003; Granado *et al.* in press), a phenomenon known to be dependent on glutamate receptors. Therefore, these two classes of receptors could interact with each other to modulate glutamatergic or dopaminergic neurotransmission. In agreement with previous *in vivo* microdialysis studies, adaptive changes in

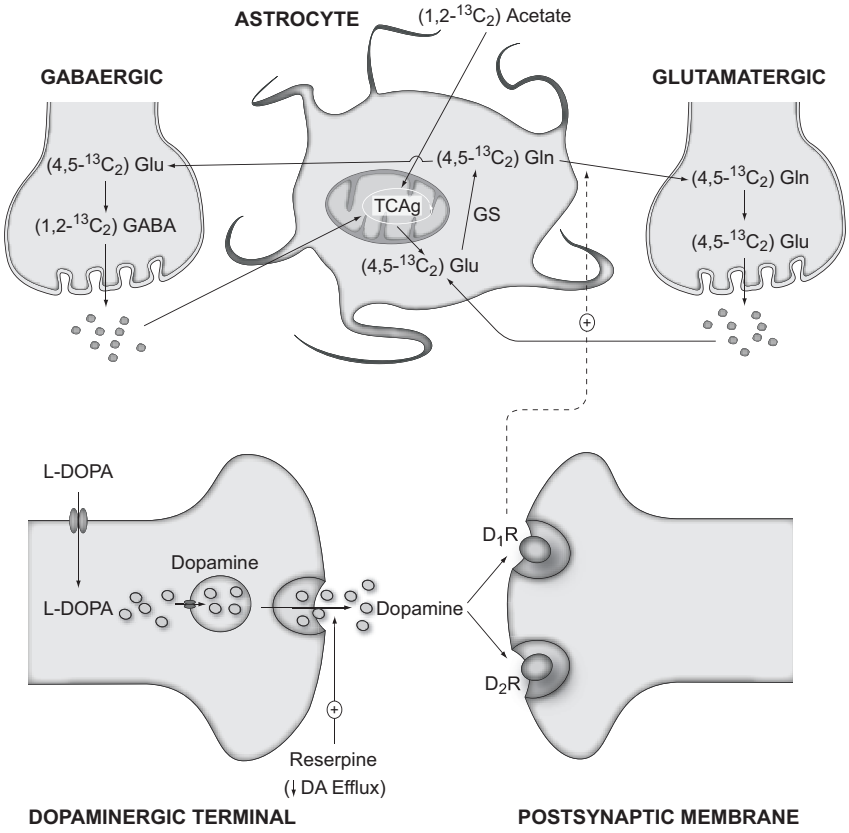

Figure 5.5. Neurometabolic interactions between glial cells and the glutamatergic, the GABAergic and the dopaminergic systems. Note that the interactions between the glutamatergic and GABAergic systems appear to involve transport and metabolism of glutamate and GABA, whereas the dopaminergic interaction with the glutamatergic system is transmitted through D_1 dopamine receptors. GABA: γ-aminobutyric acid; Gln: Glutamine; GS: Glutamine Synthase; Glu: Glutamate; TCAg: glial tricarboxylic acid cycle.

the glutamatergic system have been observed in rats and in reserpinized mice, as in the present study, probably as a feedback mechanism to increase synaptic activity after lesion (Day *et al.* 2006; Jonkers *et al.* 2002; Meshul *et al.* 1999). Moreover, decreases in the level of cerebral glutamate have been reported following dopaminergic treatments (Yamamoto and Davy 1992). In summary, the simultaneous presence of dopamine D_1 receptors in glutamatergic neurons in the cortex, or the coexpression of D_1 and glutamate receptors in the caudoputamen opens the possibility that these two neurotransmitter systems interact and influence each other. Thus, pathologic disturbances or genetic ablation of either of these partners can induce an increase in the activity of the other in an attempt to reestablish normal synaptic activity.

In the present study, we also correlated the *in vivo* neuronal glutamatergic activity defined in ^{13}C labeling studies, with motor coordination and the expression of markers of neuronal activity in selected brain regions in wild-type mice, dopamine-depleted animals, and dopamine $D_1R^{-/-}$ mice. Our results show that dopamine depletion or inactivation of dopamine D_1 receptors in mice augments the activity of the glutamine cycle, producing impairment in motor coordination and a significant decrease in c-Fos expression in the striatum. Replacing dopamine in animals treated with reserpine by administering L-DOPA normalizes glutamatergic activity, motor coordination, and c-Fos activity in the striatum of WT but not $D_1R^{-/-}$ mice. All these results suggest that the increase in glutamatergic activity that we found in dopamine-depleted animals or in $D_1R^{-/-}$ mice is inversely correlated with c-Fos expression and with motor coordination. Thus, we think that the increase in (4,5-$^{13}C_2$) glutamine, consistent with an increase in the activity of the glutamine cycle, is the result of a compensatory mechanism in the glutamatergic system to cope with the loss of dopamine or D_1R function. However, this increase in glutamatergic activity appears not to be sufficient to restore normal motor coordination, as revealed by the rota-rod experiments, or normal c-Fos expression. On the other hand, we have found repeatedly over the years that $D_1R^{-/-}$ mice have enhanced horizontal motor activity (Centonze *et al.* 2003; Granado *et al.* in press.; Xu *et al.* 1994), a result that could reflect the increased glutamatergic activity we report here. In addition, our results also show that the reduction in motor coordination observed in $D_1R^{-/-}$ mice further decreased after exposure to reserpine and it was restored by L-DOPA administration. These data clearly indicate that components of the dopaminergic system besides D_1 dopamine receptors are implicated in motor coordination. Among the components potentially implicated in this effect, the dopamine D_2 receptor appears most likely to be involved, because the lack of D_2 receptors in the mutant mice impairs motor activity (Baik et al, 1995; Kelly et al, 1998). Thus, the present results disclose novel implications of the ^{13}C NMR labeling patterns, revealing motor coordination or localized c-Fos expression.

The results of the present study invoke additional circumstances to be able to interpret the ^{13}C NMR spectra of brain metabolism *in vivo* and *in vitro*. A variety of ^{13}C NMR studies have revealed

significant alterations in glutamate and glutamine metabolism during neurodegenerative diseases, ischemia, or psychiatric disorders (Krystal *et al.* 2002; Lin *et al.* 2003; Pascual *et al.* 1998; Ross *et al.* 2003). Our work indicates that these alterations may include, embedded, the contributions of altered dopaminergic neurotransmission. Moreover, current therapeutic protocols for Parkinson's disease are mainly based on substitution therapies with dopamine analogues or precursors such as L-DOPA. Present results indicate that more adequate therapeutic regimes should also be considered, including the use of inhibitors of glutamatergic neurotransmission.

Finally, it is possible that the neurometabolic interactions of the glutamatergic neurotransmission system not only involve the dopaminergic system, as disclosed in the present study, but additional neurotransmitters such as the cholinergic or serotoninergic systems. More experiments in this direction will be necessary, but it could be envisioned now, that strong coupling mechanisms may exist between the different neurotransmission systems and glial cells to ensure a coordinated response of the brain under physiological or pathological conditions.

6. References

Abekawa T, Ohmori T, Ito K, Koyama T. 2000. D1 dopamine receptor activation reduces extracellular glutamate and GABA concentrations in the medial prefrontal cortex. Brain Res 867:250-254.

Baik JH, Picetti R, Saiardi A, Thiriet G, Dierich A, Depaulis A, Le Meur M, Borrelli E. 1995. Parkinsonian-like locomotor impairment in mice lacking dopamine D2 receptors. Nature 377:424-428.

Bouzier AK, Goodwin R, de Gannes FM, Valeins H, Voisin P, Canioni P, Merle M. 1998. Compartmentation of lactate and glucose metabolism in C6 glioma cells. A ^{13}C and ^{1}H NMR study. J Biol Chem 273:27162-27169.

Carlsson A, Lindqvist M, Magnusson T. 1957. 3,4-Dihydroxyphenylalanine and 5-hydroxytryptophan as reserpine antagonists. Nature 180:1200.

Centonze D, Grande C, Saulle E, Martin AB, Gubellini P, Pavon N, Pisani A, Bernardi G, Moratalla R, Calabresi P. 2003. Distinct roles of D1 and D5 dopamine receptors in motor activity and striatal synaptic plasticity. J Neurosci 23:8506-8512.

Cerdán S, Kunnecke B, Seelig J. 1990. Cerebral metabolism of [1,2-$^{13}C_2$]acetate as detected by *in vivo* and *in vitro* ^{13}C NMR. J Biol Chem 265:12916-12926.

Chapa F, Kunnecke B, Calvo R, Escobar del Rey F, Morreale de Escobar G, Cerdán S. 1995. Adult-onset hypothyroidism and the cerebral metabolism of (1,2-$^{13}C_2$) acetate as detected by ^{13}C nuclear magnetic resonance. Endocrinology 136:296-305.

Chase TN, Oh JD. 2000. Striatal dopamine- and glutamate-mediated dysregulation in experimental parkinsonism. Trends Neurosci 23:S86-91.

Chen JF, Huang Z, Ma J, Zhu J, Moratalla R, Standaert D, Moskowitz MA, Fink JS, Schwarzschild MA. 1999. A(2A) adenosine receptor deficiency attenuates brain injury induced by transient focal ischemia in mice. J Neurosci 19:9192-9200.

Chen L, Zhuang X. 2003. Transgenic mouse models of dopamine deficiency. Ann Neurol 54:S91-102.

Conn PJ. 2003. Physiological roles and therapeutic potential of metabotropic glutamate receptors. Ann N Y Acad Sci 1003:12-21.

Coyle JT. 2006. Glutamate and Schizophrenia: Beyond the Dopamine Hypothesis. Cell Mol Neurobiol 26:363-382.

Cruz F, Cerdán S. 1999. Quantitative ^{13}C NMR studies of metabolic compartmentation in the adult mammalian brain. NMR Biomed 12:451-462.

David HN, Abraini JH. 2001. The group I metabotropic glutamate receptor antagonist S-4-CPG modulates the locomotor response produced by the activation of D1-like, but not D2-like, dopamine receptors in the rat nucleus accumbens. Eur J Neurosci 13:2157-2164.

Day M, Wang Z, Ding J, An X, Ingham CA, Shering AF, Wokosin D, Ilijic E, Sun Z, Sampson AR, Mugnaini E, Deutch AY, Sesack SR, Arbuthnott GW, Surmeier DJ. 2006. Selective elimination of glutamatergic synapses on striatopallidal neurons in Parkinson disease models. Nat Neurosci 9:251-259.

de Bartolomeis A, Fiore G, Iasevoli F. 2005. Dopamine-glutamate interaction and antipsychotics mechanism of action: implication for new pharmacological strategies in psychosis. Curr Pharm Des 11:3561-3594.

García-Espinosa MA, Rodrigues TB, Sierra A, Benito M, Fonseca C, Gray HL, Bartnik BL, García-Martín ML, Ballesteros P, Cerdán S. 2004. Cerebral glucose metabolism and the glutamine cycle as detected by *in vivo* and *in vitro* ^{13}C NMR spectroscopy. Neurochem Int 45:297-303.

Granado N, Ortiz O, Suaréz LM, Martin ED, Ceña V, Solís JM, Moratalla R. in press. D1 but not D5 dopamine receptors are critical for LTP, spatial learning and LTP-induced arc and zif268 expression in the hippocampus. Cerebral Cortex.

Grande C, Zhu H, Martín AB, Lee M, Ortiz O, Hiroi N, Moratalla R. 2004. Chronic treatment with atypical neuroleptics induces striosomal FosB/DeltaFosB expression in rats. Biol Psychiatry 55:457-463.

Graybiel AM, Moratalla R, Robertson HA. 1990. Amphetamine and cocaine induce drug-specific activation of the c-fos gene in striosome-matrix compartments and limbic subdivisions of the striatum. Proc Natl Acad Sci U S A 87:6912-6916.

Hiroi N, Martín AB, Grande C, Alberti I, Rivera A, Moratalla R. 2002. Molecular dissection of dopamine receptor signaling. J Chem Neuroanat 23(4):237-242.

Hornykiewicz O. 2002. L-DOPA: from a biologically inactive amino acid to a successful therapeutic agent. Amino Acids 23:65-70.

Jonkers N, Sarre S, Ebinger G, Michotte Y. 2002. MK801 suppresses the L-DOPA-induced increase of glutamate in striatum of hemi-Parkinson rats. Brain Res 926:149-155.

Kalivas PW, McFarland K, Bowers S, Szumlinski K, Xi ZX, Baker D. 2003. Glutamate transmission and addiction to cocaine. Ann N Y Acad Sci 1003:169-175.

Karasawa J, Yoshimizu T, Chaki S. 2006. A metabotropic glutamate 2/3 receptor antagonist, MGS0039, increases extracellular dopamine levels in the nucleus accumbens shell. Neurosci Lett 393:127-130.

Kelly MA, Rubinstein M, Phillips TJ, Lessov CN, Burkhart-Kasch S, Zhang G, Bunzow JR, Fang Y, Gerhardt GA, Grandy DK, Low MJ. 1998. Locomotor activity in D2 dopamine receptor-deficient mice is determined by gene dosage, genetic background, and developmental adaptations. J Neurosci 18:3470-3479.

Krystal JH, Sanacora G, Blumberg H, Anand A, Charney DS, Marek G, Epperson CN, Goddard A, Mason GF. 2002. Glutamate and GABA systems as targets for novel antidepressant and mood-stabilizing treatments. Mol Psychiatry 7:S71-80.

LaHoste GJ, Marshall JF. 1992. Dopamine supersensitivity and D1/D2 synergism are unrelated to changes in striatal

receptor density. Synapse 12:14-26.

Landwehrmeyer GB, Standaert DG, Testa CM, Penney JB, Jr., Young AB. 1995. NMDA receptor subunit mRNA expression by projection neurons and interneurons in rat striatum. J Neurosci 15:5297-5307.

Lange KW, Kornhuber J, Riederer P. 1997. Dopamine/glutamate interactions in Parkinson's disease. Neurosci Biobehav Rev 21:393-400.

Lapish CC, Seamans JK, Judson Chandler L. 2006. Glutamate-dopamine cotransmission and reward processing in addiction. Alcohol Clin Exp Res 30:1451-1465.

Lebon V, Petersen KF, Cline GW, Shen J, Mason GF, Dufour S, Behar KL, Shulman GI, Rothman DL. 2002. Astroglial contribution to brain energy metabolism in humans revealed by ^{13}C nuclear magnetic resonance spectroscopy: elucidation of the dominant pathway for neurotransmitter glutamate repletion and measurement of astrocytic oxidative metabolism. J Neurosci 22:1523-1531.

Lee FJ, Xue S, Pei L, Vukusic B, Chery N, Wang Y, Wang YT, Niznik HB, Yu XM, Liu F. 2002. Dual regulation of NMDA receptor functions by direct protein-protein interactions with the dopamine D1 receptor. Cell 111:219-230.

Lin AP, Shic F, Enriquez C, Ross BD. 2003. Reduced glutamate neurotransmission in patients with Alzheimer's disease - an *in vivo* ^{13}C magnetic resonance spectroscopy study. Magma 16:29-42.

Lipsky RH, Goldman D. 2003. Genomics and variation of ionotropic glutamate receptors. Ann N Y Acad Sci 1003:22-35.

Malenka RC. 2003. Synaptic plasticity and AMPA receptor trafficking. Ann N Y Acad Sci 1003:1-11.

Meshul CK, Emre N, Nakamura CM, Allen C, Donohue MK, Buckman JF. 1999. Time-dependent changes in striatal glutamate synapses following a 6-hydroxydopamine lesion. Neuroscience 88:1-16.

Moratalla R, Elibol B, Vallejo M, Graybiel AM. 1996a. Network-level changes in expression of inducible Fos-Jun proteins in the striatum during chronic cocaine treatment and withdrawal. Neuron 17:147-156.

Moratalla R, Xu M, Tonegawa S, Graybiel AM. 1996b. Cellular responses to psychomotor stimulant and neuroleptic drugs are abnormal in mice lacking the D1 dopamine receptor. Proc Natl Acad Sci U S A 93:14928-14933.

Pascual JM, Carceller F, Roda JM, Cerdán S. 1998. Glutamate, glutamine, and GABA as substrates for the neuronal and glial compartments after focal cerebral ischemia in rats. Stroke 29:1048-1056; discussion 1056-1047.

Pavon N, Martín AB, Mendialdua A, Moratalla R. 2006. ERK phosphorylation and FosB expression are associated with L-DOPA-induced dyskinesia in hemiparkinsonian mice. Biol Psychiatry 59:64-74.

Pei L, Lee FJ, Moszczynska A, Vukusic B, Liu F. 2004. Regulation of dopamine D1 receptor function by physical interaction with the NMDA receptors. J Neurosci 24:1149-1158.

Rivera A, Cuellar B, Giron FJ, Grandy DK, de la Calle A, Moratalla R. 2002. Dopamine D4 receptors are heterogeneously distributed in the striosomes/matrix compartments of the striatum. J Neurochem 80:219-229.

Rodrigues TB, Cerdán S. 2005. ^{13}C MRS: an outstanding tool for metabolic studies. Concepts in Magnetic Resonance, Part A 27A:1-16.

Ross B, Lin A, Harris K, Bhattacharya P, Schweinsburg B. 2003. Clinical experience with 13C MRS *in vivo*. NMR Biomed 16:358-369.

Rothman DL, Behar KL, Hyder F, Shulman RG. 2003. *In vivo* NMR studies of the glutamate neurotransmitter flux and neuroenergetics: implications for brain function. Annu Rev Physiol 65:401-427.

Salter MW. 2003. D1 and NMDA receptors hook up: expanding on an emerging theme. Trends Neurosci 26:235-237.

Sanacora G, Rothman DL, Mason G, Krystal JH. 2003. Clinical studies implementing glutamate neurotransmission in mood disorders. Ann N Y Acad Sci 1003:292-308.

Schildkraut JJ, Gordon EK, Durell J. 1965. Catecholamine metabolism in affective disorders. I. Normetanephrine and VMA excretion in depressed patients treated with imipramine. J Psychiatr Res 3:213-228.

Sesack SR, Carr DB, Omelchenko N, Pinto A. 2003. Anatomical substrates for glutamate-dopamine interactions: evidence for specificity of connections and extrasynaptic actions. Ann N Y Acad Sci 1003:36-52.

Slattery DA, Hudson AL, Nutt DJ. 2004. Invited review: the evolution of antidepressant mechanisms. Fundam Clin Pharmacol 18:1-21.

Smith WB, Starck SR, Roberts RW, Schuman EM. 2005. Dopaminergic stimulation of local protein synthesis enhances surface expression of GluR1 and synaptic transmission in hippocampal neurons. Neuron 45:765-779.

Tamminga CA, Lahti AC, Medoff DR, Gao XM, Holcomb HH. 2003. Evaluating glutamatergic transmission in schizophrenia. Ann N Y Acad Sci 1003:113-118.

Waagepetersen HS, Sonnewald U, Larsson OM, Schousboe A. 2001. Multiple compartments with different metabolic characteristics are involved in biosynthesis of intracellular and released glutamine and citrate in astrocytes. Glia 35:246-252.

Waniewski RA, Martin DL. 1998. Preferential utilization of acetate by astrocytes is attributable to transport. J Neurosci 18:5225-5233.

West AR, Floresco SB, Charara A, Rosenkranz JA, Grace AA. 2003. Electrophysiological interactions between striatal glutamatergic and dopaminergic systems. Ann N Y Acad Sci 1003:53-74.

Xu M, Moratalla R, Gold LH, Hiroi N, Koob GF, Graybiel AM, Tonegawa S. 1994. Dopamine D1 receptor mutant mice are deficient in striatal expression of dynorphin and in dopamine-mediated behavioral responses. Cell 79:729-742.

Yamamoto BK, Davy S. 1992. Dopaminergic modulation of glutamate release in striatum as measured by microdialysis. J Neurochem 58:1736-1742.

Concluding Remarks

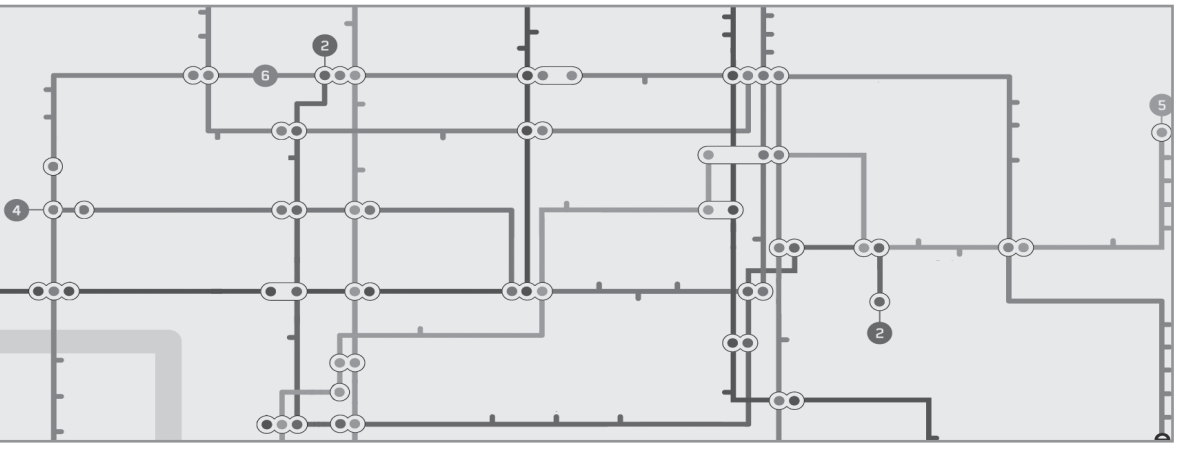

Chapter 6

1. Concluding Remarks

This thesis provides a novel interpretation of cerebral metabolism and energetics based on the transcellular exchange of monocarboxilates and reducing equivalents. I address the intra- and intercellular metabolism of pyruvate and lactate, the subcellular compartmentation of the monocarboxylate pool and its interactions with the neuronal and glial TCA cycles or with glutamatergic neurotransmission. To investigate these topics appropriately, we implemented and validated a variety of novel NMR approaches. Our experiments revealed that:

i) It is possible to investigate lactate recycling through the reversible LDH isozymes and monocarboxylate transporter of the plasma membrane of C6 cells in culture using a novel (^{13}C,^{2}H) NMR approach. Our methodology relies on the fact that the H2 hydrogen of intracellular lactate, in incubation media containing deuterium oxide, is rapidly exchanged by a deuteron in the LDH equilibrium, only in those lactate molecules that have passed through the cytosol. The methodology can be easily extended to other metabolites recycling between the intra- and extracellular spaces, as long as they present exchangeable hydrogens becoming deuterated only in one of these spaces.

ii) Using different combinations of glucose, lactate and pyruvate, we investigated the redox control of glycolysis. Incubations with different proportions of glucose and lactate revealed a competition between both substrates for the same intracellular pool of NAD^+. Lactate transport and equilibration is significantly faster than glycolysis, limiting glycolytic flow at the GAPDH step through NAD^+ depletion. Therefore, under conditions of relative excess of lactate over glucose concentration in the extracellular fluid, lactate could become the preferred substrate. Our results revealed also the existence of two kinetically different cytosolic pools of pyruvate, one derived from glucose and the other from extracellular monocarboxylates.

iii) Our novel ^{1}H NMR approaches allow the investigation of the turnover of the H2 hydrogen of lactate. The advantages rely on the increased sensitivity as compared to ^{13}C NMR and the possibility to avoid the use of relatively expensive ^{13}C labeled substrates. Even if the ^{13}C labeled substrates are used, our method allows the simultaneous measurement of the turnover of the H2 hydrogen in ^{13}C labeled and in ^{12}C lactate molecules. This favourable circumstance provides a unique and robust method to investigate simultaneously ^{2}H and ^{13}C isotopic effects on lactate turnover. In our hands, the presence of ^{13}C did not alter the

kinetics of the deuteration process. The edited ^{1}H NMR method described herein, may be of potential interest for *in vivo* studies of lactate turnover, once it is relatively inexpensive and easy to implement.

iv) The fact that part of the neuronal lactate may return to the extracellular fluid rather than being metabolized, and that astrocytic lactate may recycle back from the extracellular fluid to the astrocyte cytosol, could account in part for the transcellular exchange of reducing equivalents and the non-stoichiometric relationship between glucose consumption and glutamate-glutamine cycling.

v) We investigated the kinetics of glucose or lactate consumption and pyruvate production using primary cultures of cortical neurons or astrocytes from rat brain. Glucose and lactate are demonstrated to be consumed competitively, the dominant substrate being determined by their relative extracellular concentrations, the corresponding kinetic constant and the relevant cytosolic redox states. In addition, our data also demonstrated that pyruvate is produced from lactate both in primary cultures of neurons or glial cells, establishing a crucial link for the operation of the redox coupling mechanism.

vi) Taken together, our conclusions provided the basis for a revised interpretation of the mechanisms underlying neuroglial coupling during glutamatergic neurotransmission, the Redox Switch/Redox Coupling hypothesis. Neuroglial coupling is achieved through a reversible exchange of reducing equivalents between neurons and astrocytes in the form of lactate and pyruvate, rather than from the unidirectional transfer of lactate molecules. The operation of this transcellular redox coupling mechanism appears to rely ultimately in the regulation of the intracellular redox states of neurons and astrocytes and, consequently, being determined by the activity of the corresponding intracellular redox shuttles through the inner mitochondrial membrane. Our proposal could well be extended to other heterogeneous tissues where oxidative and glycolytic environments coexist, such as muscle or tumors.

vii) Using ^{13}C NMR spectroscopy of brain extracts of D_1- or D_2-deficient mice, we established that the interaction between the dopaminergic and glutamatergic neurotransmission systems is mediated by the D_1 dopamine receptors. Using a complementary pharmacological approach, consisting in the administration of reserpine and L-DOPA to D_1- deficient and wild type mice, we show that: 1) reserpine-induced dopamine depletion increases the activity of glutamate-glutamine cycle, yielding similar results to those obtained in $D_1R^{-/-}$ mice, and 2)

L-DOPA restored to normal values the glutamate-glutamine cycle. Furthermore, our results show that dopamine depletion or inactivation of dopamine D_1 receptors in mice produced impairment in motor coordination and a significant decrease in c-Fos expression in the striatum.

viii) Present results indicate that more adequate therapeutic regimes for Parkinson's disease should include inhibitors of glutamatergic neurotransmission. Moreover, the possibility exists that the neurometabolic interactions of the glutamatergic neurotransmission system not only involve the dopaminergic system, but additional neurotransmitter systems such as the cholinergic or serotoninergic systems. In this context, it is now clearly envisioned that strong coupling mechanisms exist between the various neurotransmitter systems and glial cells, ensuring a coordinated response of the brain under physiological or pathological conditions.

In summary, our work clarifies some concepts of current neurochemical knowledge. It emphasizes the operation of transcellular pyruvate and lactate shuttling, the neuronal and glial TCA cycles, and glutamatergic activity and their respective bilateral and multilateral interactions. Multinuclear NMR Spectroscopy is demonstrated to be a useful and effective tool to investigate cerebral metabolism, revealing unique aspects not accessible to other more conventional techniques and opening new frontiers in the understanding of cerebral metabolism and energetics.

Ackowledgments/Agradecim(i)entos

"É tão bom uma amizade assim
Ai, faz tão bem saber com quem contar
Eu quero ir ver quem me quer assim
É bom pra mim, e é bom pra quem tão bem me quer"

Letra da música "É tão bom",
Albúm "Os Amigos de Gaspar",
Sérgio Godinho, 1988

Sinto que é inevitável olhar atentamente e de forma cuidada para trás, para todo este tempo de gestação. Tomar consciência real que esta minha empreitada profissional, e vital, esteve recheada e ladeada de inúmeros momentos colectivos, faz-me entender com veemência o quão decisivos foram estes contributos, reafirmando-se a minha vontade de expressar os meus enérgicos agradecimentos. Em todo o caso, e sabendo que se quisesse agradecer a todos os que me ajudaram, teria de preparar uma adenda importante a esta tese, deixo aqui somente umas quantas notas, suplementadas seguramente com oportunos agradecimentos *in loco*.

Mi primer agradecimiento va, como es natural, para el Doctor Sebastián Cerdán. Querría expresar mi admiración y mi reconocimiento por toda su trayectoria y trabajo realizado. Subrayo, de un modo más particular, sus enseñanzas, su apoyo y la total confianza que fue depositando en mí a lo largo de todo este tiempo de convivencia.

Para o Professor Doutor Carlos Geraldes vai a minha elevada gratidão, admiração e estima. Reconhecido, recordo e evidencio a sempre constante dedicação, disponibilidade e proximidade, assim como a amizade que senti ser depositário. Sem dúvida, já desde os tempos da licenciatura sinto que o Professor Geraldes ilustra a tão almejada universalidade da Universidade, naquilo que ela tem de melhor.

À Professora Doutora Margarida Castro agradeço, além da sua amizade, o legado que deixa em todos aqueles que temos a sorte de nos inspirarmos na sua força e sabedoria. Os seus conselhos ajudaram também a viabilizar esta tese. Muito Obrigado por tudo!

To Drs. A. Dean Sherry and Craig Malloy, my gratitude for receiving me in their laboratories, in the preamble of this doctoral period. Some of the discussions we had were of central importance to my understanding that my Ph.D. period should be an exciting phase of my life.

To Dr. John G. Jones, I want to thank him for allowing me to join the *adventure* that represented the first clinical studies of his group in Coimbra.

Quero também agradecer a todos os grupos de investigação com quem tive a oportunidade

de colaborar durante estes últimos anos, e que me permitiram diversificar e aumentar os meus conhecimentos. Registo com agrado esses momentos.

Ainda que de forma mais abstracta, queria neste espaço deixar uma menção muito especial a todos os meus professores que contribuíram activamente para o meu desenvolvimento pessoal e científico. Agradeço, em particular, ao Professor Doutor Luís Martinho do Rosário a sua confiança e amizade.

Las instituciones son entidades que, por definición, perduran más allá que las personas. Pero son exactamente estas *efímeras* personas las que me hacen sentir tan afortunado y orgulloso de formar parte del Instituto de Investigaciones Biomédicas "Alberto Sols". Como protagonistas intensos de este trabajo, con papeles inspiradores e *intervencionistas* centrales en el mismo, mi cariño más sincero va para mis compañeros y amigos del laboratorio durante mi periodo predoctoral. ¡Que días los de aquellos años!, pensaré seguramente en el futuro. No me gustaría plasmar aquí mis agradecimientos personificados para cada uno de ellos, por lo que apostaré por hacerlo personalmente. Resalto, de forma más acentuada por su participación próxima en algunos de estos trabajos y por su apoyo y amistad constantes, la colaboración con las Doctoras Pilar López-Larrubia y María Luisa García-Martín, así como con Susana Garrido y Patricia Sánchez. Además, me gustaría dejar aquí algunos nombres más como reconocimiento público de mi más profunda admiración: Teresa Navarro, Jesús, Inês, Rui, Teresa Delgado, Marina, Sandra, Vanessa, Alejandra, Valeria, Pascual, Ruth, Luís, Rosa, Laura, ... Quiero también dejar aquí reflejada mi profunda gratitud a algunos amigos del Instituto que se caracterizaron por su proximidad, amistad y nobleza: Susana, María, Antonio, Sita, Mariana, Merche, Edel, Jimena, Pablo y Maxy. Muchas otras personas se cruzaron en mi camino, teniendo claramente un papel importante en que la rutina del laboratorio se tornara amena y placentera. En especial, mi agradecimiento a todo el personal de los servicios y administración del Instituto, que siempre me *cuidaron* con una amabilidad exquisita.

Mi agradecimiento a la Profesora Paloma Ballesteros y a su grupo, por todos los momentos compartidos a lo largo de todos estos años. Sin duda, nuestros grupos se complementan de forma muy especial.

Aos bons amigos que vão marcando tão indelevelmente a minha vida. São eles que fazem tão especial dizer que sou de Paredes de Coura, que sou quase de Moledo, que estudei em Braga e que me *formei* em Coimbra. Em Coimbra, alguns destes amigos povoavam sítios tão únicos como os Emiratos Aracônídeos, o Solar do 44, o CUMN ou a Real República do Bota-Abaixo, onde a felicidade e o compromisso faziam com que a Alta de Coimbra fosse algo verdadeiramente único e excepcional. Entretanto, a *gaiola* abriu-se e eles andam por aí, a espalhar esse calor tão especial no ser e no estar. A todos eles, o meu melhor abraço de agradecimento por também serem parte de mim.

Aos meus pais, de forma especial, pela forma que estão, e são, tão próximos e presentes. Agradecer-lhes também por, juntamente com o meu irmão João, serem sempre a minha pedra basilar, lugar tão nosso e tão cúmplice. *Oubrigado, Dius bos lo pague, miu armano burriqueiro,* por seres tão único. Também para o resto da minha família, e principalmente para os meus avós Marília, Narcisa e Bento, vai o meu maior carinho e gratidão, por me fazerem sentir realmente especial.

Para a Patrícia, minha sempre companheira, pelo seu amor vigilante e carinhoso, toda a minha gratidão por me ter mostrado que um outro mundo é verdadeiramente possível. Ainda está por conquistar boa parte da *Banheira de Ulisses*, sonho que partilhamos com cumplicidade.

Curriculum Vitæ

Tiago B. Rodrigues was born on June 3, 1977 in Braga, Portugal. After completion of his basic education in Paredes de Coura, he ventured in 1992 to Braga to spend his three last years of secondary school. His universitarian career started in 1995, when he initiated his Biochemistry studies at the University of Coimbra. For his final B.Sc. thesis, he left Portugal to carry out a one year project in the Biomedical Research Institute "Alberto Sols" in Madrid, Spain, working under the supervision of Prof. Dr. Sebastián Cerdán. During this period, he started his commitment with Nuclear Magnetic Resonance and its use for metabolic studies. Having completed his university degree he returned to the NMR Unit of the University of Coimbra, where he worked about a year in pre-clinical pilot studies related with liver metabolism, under the supervision of Prof. Dr. Carlos F.G.C. Geraldes and Dr. John G. Jones. In 2001, he visited the Mary Nell and Ralph B. Rogers Magnetic Resonance Center at the University of Texas Southwestern Medical Center at Dallas, U.S.A., where he developed some work related with ^{13}C isotopomer kinetic analysis applied to heart metabolism, under the supervision of Prof. Dr. A. Dean Sherry and Prof. Dr. Craig Malloy. Afterwards, and continuing his passion for science, he returned to Madrid where he worked from 2003 to 2007 on his Ph.D. project, under the supervision of Prof. Dr. Sebastián Cerdán and Prof. Dr. Carlos F.G.C. Geraldes. His project was mainly dedicated to the study of cerebral intermediary metabolism, using Nuclear Magnetic Resonance as the "golden technique". Particularly, his research was focused on double isotope labeled Nuclear Magnetic Resonance studies applied to neurochemistry and he was deeply interested in understanding how neurodegenerative diseases and cancer altered the physiological metabolism of the cerebral tissue. He had the opportunity to collaborate with several world-recognized groups, and some of the results of his work have been published in this thesis, as well as in several peer-reviewed papers in international journals and book series. His research activity during this time was sponsored by the Portuguese Foundation for Science and Technology, having additional funding from several sources for the attendance to international scientific meetings, where he has been presenting regularly his novel results. As of July 2007, Tiago B. Rodrigues continues in Madrid, projecting to move to another laboratory in order to continue his scientific formation.

List of Publications

1. Jones JG, Perdigoto R, **Rodrigues TB**, Geraldes CFGC. *Quantitation of absolute ^{2}H enrichment of plasma glucose by ^{2}H NMR analysis of its monoacetone derivative.* Magn Reson Med 48:535-539. **2002.**

2. Perdigoto R, Furtado AL, Porto A, **Rodrigues TB**, Geraldes CFGC, Jones JG. *Sources of glucose production in cirrhosis by $^{2}H_2O$ ingestion and ^{2}H NMR analysis of plasma glucose.* Biochim Biophys Acta 1637:156-163. **2003.**

3. Perdigoto R, **Rodrigues TB**, Furtado AL, Porto A, Geraldes CFGC, Jones JG. *Integration of [U-^{13}C]glucose and $^{2}H_2O$ for quantification of hepatic glucose production and gluconeogenesis.* NMR Biomed 16:189-198. **2003.**

4. Cerdán S, **Rodrigues TB**, Ballesteros P, López P, Perez-Mayoral E. *The subcellular metabolism of water and its implications for magnetic resonance image contrast.* In: Belton PS, Gil AM, Webb GA, Rutledge D, editors. Magnetic Resonance in Food Science. Oxford: Royal Society of Chemistry. p 121-135. **2003.**

5. Carvalho RA, **Rodrigues TB**, Zhao P, Jeffrey FM, Malloy CR, Sherry AD. *A ^{13}C isotopomer kinetic analysis of cardiac metabolism: influence of altered cytosolic redox and $[Ca^{2+}]_o$.* Am J Physiol Heart Circ Physiol 287:H889-895. **2004.**

6. García-Espinosa MA, **Rodrigues TB**, Sierra A, Benito M, Fonseca C, Gray HL, Bartnik BL, García-Martín ML, Ballesteros P, Cerdán S. *Cerebral glucose metabolism and the glutamine cycle as detected by in vivo and in vitro ^{13}C NMR spectroscopy.* Neurochem Int 45:297-303. **2004.**

7. **Rodrigues TB**, Gray HL, Benito M, Garrido S, Sierra A, Geraldes CFGC, Ballesteros P, Cerdán S. *Futile cycling of lactate through the plasma membrane of C6 glioma cells as detected by (^{13}C, ^{2}H) NMR.* J Neurosci Res 79:119-127. **2005.**

8. **Rodrigues TB**, Cerdan S. *^{13}C MRS: an outstanding tool for metabolic studies.* Concepts in Magnetic Resonance, Part A 27A:1-16. **2005.**

9. **Rodrigues TB**, Cerdán S. *A fast and sensitive ^{1}H NMR method to measure the turnover of the H2 hydrogen of lactate.* Magn Reson Med 54:1014-1019. **2005.**

10. Cerdán S, **Rodrigues TB**, Sierra A, Benito M, Fonseca LL, Fonseca CP, García-Martín ML. *The redox switch/redox coupling hypothesis.* Neurochem Int 48:523-530. **2006.**

11. Prata MI, Santos AC, Torres S, André JP, Martins JA, Neves M, García-Martín ML, **Rodrigues TB**, López-Larrubia P, Cerdán S, Geraldes CFCG. *Targeting of lanthanide(III) chelates of DOTA-type glycoconjugates to the hepatic asialoglycoprotein receptor: cell internalization and animal imaging studies.*

Contrast Media Mol Imaging 1:246-258. **2006.**

12. Torija P, Vicente JJ, **Rodrigues TB**, Robles A, Cerdán S, Sastre L, Calvo RM, Escalante R. *Functional genomics in Dictyostelium: MidA, a new conserved protein, is required for mitochondrial function and development.* J Cell Sci 119:1154-1164. **2006.**

13. **Rodrigues TB**, Cerdán S. *The cerebral tricarboxylic acid cycles.* In: Dienel G, Gibson, G., Lajtha, A., editors. Handbook of Neurochemistry and Molecular Neurobiology: Brain Energetics from Genes to Cells, Integration of Molecular and Cellular Processes. New York: Springer. p 61-93. **2007.**

14. Ramírez BG, **Rodrigues TB**, Violante IR, Cruz F, Fonseca LL, Ballesteros P, Castro MMCA, García-Martín ML, Cerdán S. *Kinetic properties of the redox switch/redox coupling mechanism as determined in primary cultures of cortical neurons and astrocytes from rat brain.* J Neurosci Res. **In Press 2007.**

15. **Rodrigues TB**, Granado N, Ortiz O, Cerdán S, Moratalla R. *Metabolic interactions between glutamatergic and dopaminergic neurotransmitter systems are mediated through D_1 dopamine receptors.* J Neurosci Res. **In Press 2007.**

16. Torres S, Prata MI, Santos AC, André JP, Martins JA, Helm L, Tóth É, García-Martín ML, **Rodrigues TB**, López-Larrubia P, Cerdán S, Geraldes CFCG. *Gd(III)-EPTPAC$_{16}$, a new self-assembling potential liver MRI contrast agent: in vitro characterization and in vivo animal imaging studies.* NMR Biomed. **In Press 2007.**

17. Cauli O, López-Larrubia P, **Rodrigues TB**, Cerdán S, Felipo V. *Magnetic resonance analysis of the effects of acute ammonia intoxication on rat brain. Role of NMDA receptors.* J Neurochem. **In Press 2007.**

18. **Rodrigues TB**, Cerdán S, García-Martín ML. *A method to measure lactate recycling by edited ^{1}H NMR spectroscopy***.** Anal Biochem. **In Press 2007.**

19. Sierra A, **Rodrigues TB**, Benito M, Ballesteros P, García-Espinosa M.A., García-Martín ML, Cerdán S. *Pyruvate Oxidation and Mitochondrial Substrate Transport in the Central Nervous System.* In: Gruetter R, Choi IY, Lajhta A, editors. Handbook of Neurochemistry and Molecular Neurobiology: Neural Metabolism *in Vivo*. New York: Springer. **In Press 2007.**